UNIVERSIDAD CARLOS III DE MADRID

ESCUELA POLITÉCNICA SUPERIOR

DEPARTAMENTO DE MECÁNICA DE MEDIOS CONTINUOS Y TEORÍA DE ESTRUCTURAS

INGENIERÍA INDUSTRIAL

PROYECTO FIN DE CARRERA

NUMERICAL ANALYSIS OF IMPACT BEHAVIOUR ON AERONAUTICAL COMPOSITE PROTECTIONS

AUTOR:

ALBERTO PORTILLA BULLIDO

TUTOR:

LUIS BENÍTEZ MONTAÑÉS

Septiembre 2011

AKNOWLEDGMENTS

I would like to thank to all my colleagues of the department of *Structural Dynamics and Aeroelasticity* at Airbus Military (EADS-CASA) for their support and help during my internship and for being such a good people. Mainly, thanks to Luis Benítez, without his advice, help and dedication to this project, it would not have been possible. Also thanks to Ángel Arias for his help during the first and last steps of this project.

I want mention too my university friends, for all the time we spent together, working together to get through the exams and the degree. My colleagues from the swimming pool, which whom I had very tough afternoons training, but even though more good afternoons; and to all my friends from school, my friends since I can remember.

Finally, but not less important, I would like to thank my family, mi parents and my brother for such an unconditional support they gave me during all this years. And to Carlota, for supporting me always for such a long time.

Thank you all very much.

ABSTRACT

In this project, a complete study of impacts against protection composite materials is presented, taking into account all parameters involved in the process: from the organic fibre that is part of the composite, to the projectile impacting on the protection panels. The project was done during an internship in the department of *Structural Dynamics and Aeroelasticity* at Airbus Military (EADS-CASA), therefore most of the impacts studied here are typical from aeronautics industry.

During the impact event, there are two main components: protection panels and projectiles.

- ***Protection panels*** studied are manufactured with composite materials, made of organic fibres, which have good behaviour under impact and are light, an important aspect when integrating these protections into an aircraft. In this project, two types of organic fibres are studied:
    - Aramids.
    - Polyethylenes.

- ***Projectiles (or impactors)*** studied here are mainly two:
    - Impacts of gas turbine fragments due to uncontained engine rotor failure.
    - Impacts of ice due to propeller ice release.

The impact study has been done considering several approaches. First of all, a study of semi-analytical models is done to know performance and behaviour of protection laminates and to determine the principal parameters involved in protection design.

Then, an impact research with numerical simulations is presented. The non-linear commercial explicit code called PamCrash has been used. It was necessary to develop numerical models of protection materials using validation information based on available bibliography.

With these material models, some numerical simulations for sizing protections impacted by small metallic fragments due to uncontained engine rotor failure and ice fragments to ensure aircraft security are presented. Finally, some sensitivity studies: to the angle of impact and boundary conditions.

It is important to note that simulations done during this project are preliminary, because a set of impact test campaigns are programmed within Airbus Military (EADS-CASA) Research Activities. These tests campaigns would check and validate the numerical models prepared during this work.

RESUMEN

En este proyecto se realiza un estudio completo de impactos sobre materiales compuestos de protección teniendo en cuenta todos los parámetros que influyen en el proceso: desde la fibra orgánica que forma parte del material compuesto, hasta el proyectil que impacta sobre los paneles de protección. El trabajo se ha realizado mediante una beca en el departamento de *Dinámica Estructural y Aeroelasticidad* en Airbus Military (EADS-CASA), por lo que la mayor parte de los impactos estudiados son característicos de la industria aeronáutica.

Durante un proceso de impacto, los dos componentes principales son: los paneles de protección y los proyectiles.

- Los ***paneles de protección*** estudiados están hechos de materiales compuestos de fibras orgánicas, los cuales presentan buena resistencia frente a impacto y son muy ligeros, aspecto muy importante a la hora de integrarlos en un avión. En este proyecto se estudiarán principalmente dos tipos de fibras orgánicas:
    - Aramidas.
    - Polietilenos.

- Los ***proyectiles (o impactores)*** que se han estudiado son principalmente dos:
    - Impactos de fragmentos de turbina por fallos de motor.
    - Impactos de hielo por desprendimiento de las hélices del motor.

El estudio de los impactos se ha realizado mediante varias aproximaciones. En primer lugar, un estudio de diversos modelos semi-analíticos, que nos servirán para conocer el rendimiento y el comportamiento de laminados de protección, así como para poder hacer un pre-dimensionado de las protecciones para poder detener los proyectiles frente a los que están diseñadas.

A continuación se presenta un estudio de los impactos mediante simulación numérica. Para ello se utiliza un código comercial no lineal y explícito, PamCrash. La primera actividad de simulación ha sido desarrollar unos modelos numéricos de material adecuados, que se han validado con información encontrada en la bibliografía.

Mediante los modelos numéricos de material se presenta un dimensionado final de las protecciones y se estudia cómo afectan el cambio de parámetros relevantes como es el ángulo de incidencia del impactor o las condiciones de contorno de cómo estén fijados los paneles de protección.

Cabe destacar que las simulaciones hechas en este proyecto son simulaciones pre-test, ya que hay programado una campaña de ensayos de impacto contra protecciones de materiales compuestos, gracias a las cuales será posible comparar y ajustar los resultados obtenidos en este trabajo.

OBJECTIVES

The objectives of this project are three and are clearly defined:

1. **Study of semi-analytical models.** These models are a useful tool for design purposes of protection panels. Several models are studied and one is presented as the best choice for the type of impacts and materials analysed.

2. **Develop some numerical models of protection materials.** Using explicit code PamCrash and based on bibliographic research, two material models of organic fibres were validated: one for aramid laminates and other for polyethylene.

3. **Design of protections for two types of aeronautical impacts with numerical simulation**. With material models developed previously several protection panels are designed for two types of aeronautical impacts to stop two types of impactors: gas turbine fragments and ice.

INDEX

INTRODUCTION.....1

CHAPTER I. IMPACTS IN AERONAUTICS.....3
1.1. General impacts in aeronautics.....4
1.1.1. Introduction.....4
1.1.2. Gas turbine fragments from Uncontained Engine Rotor Failure.....5
1.1.3. Ice impact.....7
1.2. Protection concepts in aeronautics.....9

CHAPTER II. IMPACTS ON COMPOSITES.....11
2.1. Introduction.....12
2.2. Composite materials for impact protection.....12
2.2.1. Introduction.....13
2.2.2. Fibres.....13
2.2.2.1. Aramid.....15
2.2.2.2. Ultra High Molecular Weight Polyethylene (UHWM-PE).....18
2.2.2.3. Glass.....19
2.2.2.4. Carbon.....19
2.2.2.5. PBO.....20
2.2.2.6. M5.....20
2.2.3. Matrix.....20
2.2.3.1. Vinylester.....20
2.2.3.2. Polyvinyl butyral.....21
2.2.3.3. Polyethylene.....21
2.2.4. Configurations for shield design with organic fibres materials.....21
2.2.4.1. Woven fabrics.....21
2.2.4.2. Non-woven fabrics.....23
2.3. Material response to impact.....25
2.3.1. Key parameters of impact behaviour in composites.....29
2.4. Bullets and fragments.....33
2.4.1. Full Metal Jacket bullet.....33
2.4.2. Fragment Simulating Projectiles.....34
2.5. Standards and specifications.....35
2.6. Semi-analytical models. Predicting penetration and ballistic limit.....36
2.6.1. Lambert and Jonas model.....36
2.6.2. Navarro model.....38
2.6.3. Chocron *et al.* model.....39
2.6.4. Bless and Hartman model.....40
2.6.5. Caprino *et al.* model.....41
2.6.6. Jacobs and Van Dingenen model.....42
2.6.7. Van Gorp *et al.* model.....44
2.6.8. Wen model.....45
2.6.9. Song and Egglestone model.....46

CHAPTER III. NUMERICAL SIMUALTIONS 49
3.1. Introduction 50
3.2. Numerical models of protection laminates 50
3.2.1. Types of models 50
3.2.2. Isotropic homogeneous model 52
3.2.3. Orthotropic homogeneous model 55
3.3. Validation activities 56
3.3.1. Comparison with experimental and numerical results from Colakoglu *et al.* work 57
3.3.1.1. Penetration tests 59
3.3.1.2. Deformation tests 66
3.3.2. Comparison with experimental and numerical results from Silva *et al.* work 72
3.4. Numerical models proposed for protections materials using PamCrash 74

CHAPTER IV. APPLICATIONS 76
4.1. Introduction 77
4.2. Design of protections with analytical models for small metallic and ice impactors 78
4.2.1. Aramid fibres 80
4.2.2. Polyethylene fibres 83
4.2.3. Conclusions extracted from design of protections with semi-analytical models 89
4.3. Design of protections with numerical models for small metallic impactors 90
4.3.1. Impactors 90
4.3.2. Protection panels 91
4.3.3. Curves of design 92
4.3.4. Sensitivity analysis 102
4.3.4.1. Sensitivity to impact angle 102
4.3.4.2. Sensitivity to boundary conditions 107
4.4. Design of protections with numerical models for ice impactors 110
4.4.1. Impactor 110
4.4.2. Protection panels 112
4.4.3. Curves of design 113
4.4.4. Sensitivity analysis 119
4.4.4.1. Sensitivity to impact angle 119
4.4.4.2. Sensitivity to boundary conditions 124

CONCLUSIONS 127

BIBLIOGRAPHIC REFERENCES 130

APPENDIX 135
A1. Project budget 136
A2. Design of protections with semi-analytical models. Complete calculation 138

LIST OF FIGURES

Figure 1.1. Damage in aircraft due to uncontained engine rotor failure 5
Figure 1.2. Typical fragments generated by UERF 6
Figure 1.3. Estimated path of fragments 7
Figure 1.4. Ice formed on fan blades and on engine spinner 8
Figure 1.5. Propeller blade release trajectory analysis 8
Figure 1.6. Ice impact sequence 9
Figure 1.7. Stand alone protection (in red) 9
Figure 1.8. Protection attached to structure (in red) 10
Figure 1.9. Hybrid armour configuration 10

Figure 2.1. Fibre Reinforced Polymers = fibre + matrix 13
Figure 2.2. Ballistic limit for different high performance fibres 14
Figure 2.3. Kevlar crystallographic structure 15
Figure 2.4. Hydrolytic stability of Kevlar at 154 ºC 17
Figure 2.5. Effect of elevated temperatures on tensile strength of Kevlar 29 17
Figure 2.6. Scheme of gel spinning process 18
Figure 2.7. Warp (1) and weft (2) directions on a woven fabric 22
Figure 2.8. Two different woven fabrics: plain weave (left) and basket weave 4x4 (right) 22
Figure 2.9. Two different woven fabrics: twill weave (left) and 5-harness satin weave (right) 23
Figure 2.10. Examples of polyethylene felt 23
Figure 2.11. Scheme of Dyneema UD 24
Figure 2.12. Scheme of Spectra Shield 24
Figure 2.13. Schematic representation of impact response under high velocity impact and low velocity impact 25
Figure 2.14. Failure modes in laminated composites resulting from various impact velocities 26
Figure 2.15. Schematic description of two types of matrix cracks seen in laminated composites 27
Figure 2.16. Shear plugging 28
Figure 2.17. Hole expansion 28
Figure 2.18. Hole friction 29
Figure 2.19. High performance polymeric fibres 30
Figure 2.20. Stress - strain curves at different strain rates for different composite materials 31
Figure 2.21. Stress - strain curves of Twaron yarns at various strain rates 32
Figure 2.22. 9 mm Full Metal Jacket Bullets 33
Figure 2.23. Fragment Simulating Projectiles: real image (left) and scheme (right) 34
Figure 2.24. Scheme of a projectile impacting in a single fibre 38
Figure 2.25. Sketch of the impact of a projectile onto a fabric 39
Figure 2.26. Normalised energy absorption versus areal density 42
Figure 2.27. Conical nosed projectile geometry 45
Figure 2.28. Ogival nosed projectile geometry 46
Figure 2.29. Ballistic limit versus areal density with an FSP 1.1g impactor 47

Figure 3.1. Isotropic material (left) and orthotropic material (right) 51
Figure 3.2. Ply model 51
Figure 3.3. Fibre-matrix model 51
Figure 3.4. Stress versus strain. Scheme of composite materials properties 53
Figure 3.5. Tensile test of Kevlar 29: MAT 16 (left) and MAT 30 (right) 54
Figure 3.6. Flexion test of Kevlar 29: MAT 16 (left) and MAT 30 (right) 54
Figure 3.7. Uniaxial static tension test 55
Figure 3.8. Projectile models used in numerical simulations:
FMJ bullet (a) and FSP 1.1g (b) 58
Figure 3.9. Mesh detail of plate central zone 58
Figure 3.10. Plate mesh isometric view (8 mm thickness plate) 59
Figure 3.11. Plate mesh view in plan XY (left) and central region detail (right) 59
Figure 3.12. Fragment Simulating Projectiles 1.1g mesh at different views 60
Figure 3.13. Residual velocity versus strike velocity. 8 mm thickness Kevlar 29 plate
with different material models 62
Figure 3.14. Penetration test sequence for an initial velocity of 600 m/s (left) and 800 m/s (right) with Kevlar 29 composite modelled with isotropic material type 16 63
Figure 3.15. Residual velocity versus strike velocity. 5.6 mm thickness Dyneema HB2 plate with different material models 64
Figure 3.16. Penetration test sequence for an initial velocity of 400 m/s (left) and 600 m/s (right) with Dyneema HB2 composite modelled with isotropic material type 16 65
Figure 3.17. FMJ bullet mesh at different views 67
Figure 3.18. Backface deformation of Kevlar 29 versus initial striker speed 68
Figure 3.19. Backface deformation of Dyneema HB2 versus initial striker speed 69
Figure 3.20. Deformation test sequence for an initial velocity of 352 m/s with Kevlar 29 (left) and with Dyneema HB2 (right) modelled with isotropic material type 16 70
Figure 3.21. Vertical displacement in mm. Contour plot of deformation test sequence for an initial velocity of 352 m/s with Kevlar 29 71
Figure 3.22. Data point used to determine ballistic limit 72
Figure 3.23. Residual velocity versus strike velocity. 2 mm thickness Kevlar 29 plate
with different material models 73
Figure 3.24. Maximum vertical displacement for shell material model (left)
and for solid material model (right) 75
Figure 3.25. Plastic strain for shell material model (left) and for solid
material model (right) 75

Figure 4.1. Scheme of calculation procedure for sizing protection materials
with semi-analytical models 79
Figure 4.2. FSP used to evaluate the armour system 84
Figure 4.3. 1.1g FSP according to NATO STANAG 2920 87
Figure 4.4. Geometry and mesh of low size impactor 90
Figure 4.5. Geometry and mesh of high size impactor 90
Figure 4.6. Plate mesh isometric view (12 mm thickness plate) 91
Figure 4.7. Plate mesh view in plan XY (left) and central region detail (right) 91
Figure 4.8. Impact sequence for small metallic 8g impactor against 12 mm thickness protection made of Kevlar 29 (left) and for small metallic 74g impactor against 12 mm thickness protection made of Dyneema HB2 (right) 93
Figure 4.9. Residual velocity versus strike velocity at various thicknesses
for an small metallic impactor of 8g and Kevlar 29 target 94

Figure 4.10. Residual velocity versus strike velocity at various thicknesses for an small metallic impactor of 8g and Dyneema HB2 target 94
Figure 4.11. Plastic strain contours: impact sequence for small metallic 8g impactor (left) and for small metallic 74g impactor (right) against protection made of Kevlar 29 at nominal conditions 95
Figure 4.12. Residual velocity versus strike velocity at various thicknesses for an small metallic impactor of 74g and Kevlar 29 target 96
Figure 4.13. Residual velocity versus strike velocity at various thicknesses for an small metallic impactor of 74g and Dyneema HB2 target 96
Figure 4.14. Plastic strain contours: impact sequence for small metallic 8g impactor (left) and for small metallic 74g impactor (right) against protection made of Dyneema HB2 97
Figure 4.15. Ballistic limit calculated for Kevlar 29 and small metallic 8g impactor at three different thicknesses 100
Figure 4.16. Ballistic limit calculated for Dyneema HB2 and small metallic 8g impactor at three different thicknesses 100
Figure 4.17. Ballistic limit calculated for Kevlar 29 and small metallic 74g impactor at three different thicknesses 101
Figure 4.18. Ballistic limit calculated for Dyneema HB2 and small metallic 74g impactor at three different thicknesses 101
Figure 4.19. Ballistic limit at different angles of impact 103
Figure 4.20. Impact scheme with impact angle 103
Figure 4.21. Impact sequence of small metallic 74g impactor with an impact angle of 30º at 840 m/s impacting on Kevlar 29 (left) and small metallic 74g impactor with an impact angle of 45º at 700 m/s impacting on Dyneema HB2 (right) 105
Figure 4.22. Impact sequence of small metallic 8g impactor with an impact angle of 60º at 800 m/s impacting on Kevlar 29 (left) and small metallic 8g impactor with an impact angle of 75º at 640 m/s impacting on Dyneema HB2 (right) 106
Figure 4.23. Scheme of boundary conditions with 2 edge fixed (left) and 4 edge fixed (right) 107
Figure 4.24. Sensitivity to boundary conditions. small metallic 8g impactor and Kevlar 29 8 mm thickness plate 108
Figure 4.25. Sensitivity to boundary conditions. small metallic 8g impactor and Dyneema HB2 11 mm thickness plate 108
Figure 4.26. Sensitivity to boundary conditions. small metallic 74g impactor and Kevlar 29 21 mm thickness plate 109
Figure 4.27. Sensitivity to boundary conditions. small metallic 8g impactor and Dyneema HB2 30 mm thickness plate 109
Figure 4.28. SPH model of ice impactor 110
Figure 4.29. SPH main control parameters 111
Figure 4.30. Shell plate mesh isometric view 112
Figure 4.31. Plate mesh view in plan XY (left) and central region detail (right) 112
Figure 4.32. Initial configuration: ice impactor and composite plate 113
Figure 4.33. Residual velocity versus strike velocity at various thicknesses for an ice impactor of 35g and Kevlar 29 target 114
Figure 4.34. Residual velocity versus strike velocity at various thicknesses for an ice impactor of 35g and Dyneema HB2 target 114
Figure 4.35. Ice impact sequence for 1.1 mm thickness Kevlar 29 protection at 150 m/s (left) and at 300 m/s (right) 115
Figure 4.36. Ice impact sequence for 1.6 mm thickness Dyneema HB2 protection at 150 m/s (left) and at 500 m/s (right) 116

Figure 4.37. Final mark (plastic strain contours) for 1.1 mm thickness Kevlar 29 at 150 m/s (left) and at 300 m/s (right) 117
Figure 4.38. Final mark (plastic strain contours) for 1.6 mm thickness Dyneema HB2 at 150 m/s (left) and at 500 m/s (right) 117
Figure 4.39. Ice impactor rotated to axis X (left) and to axis Y (right) 120
Figure 4.40. Ballistic limit depending on impact angle 120
Figure 4.41. Ice impact sequence for 1.6 mm thickness Dyneema HB2 protection at 550 m/s with impact angle of 30º (left) and at 540 m/s with impact angle of 45º (right) 122
Figure 4.42. Ice impact sequence for 1.6 mm thickness Dyneema HB2 protection at 460 m/s with impact angle of 60º (left) and at 360 m/s with impact angle of 75º (right) ... 123
Figure 4.43. Scheme of fixing 2 edge of axis X (left) and 2 edge of axis Y (right) 124
Figure 4.44. Sensitivity to boundary conditions. Ice impactor 35g and Kevlar 29 1.1 mm thickness plate 124
Figure 4.45 Sensitivity to boundary conditions. Ice impactor 35g and Dyneema HB2 1.6 mm thickness plate 125
Figure 4.46. Ice impact sequence at 150 m/s for 1.6 mm thickness Kevlar 29 protection with 2 edges fixed of axis X (left) and for 1.6 mm thickness Dyneema HB2 protection with 2 edges fixed of axis Y (right) 126

Figure A1.1. Budget graphic with main costs 137

LIST OF TABLES

Table 1.1. General impacts in aeronautics 4

Table 2.1. Main properties of typical high performance fibres....14
Table 2.2. Typical mechanical and thermal properties of Kevlar 29 and Kevlar 49 16
Table 2.3 Mechanical properties of a polyethylene fibre (Spectra 1000) for different weight per length 19
Table 2.4. Different types of FSP....34
Table 2.5. List of the most utilized ballistic standards....35
Table 2.6. Values of the constants α and K for some materials 41
Table 2.7. Values of constants for different fibre reinforcements and resin systems 47
Table 2.8. Summary of some semi-analytical models 48

Table 3.1. Mechanical properties of composites....52
Table 3.2. Input PamCrash parameters for material type 16....53
Table 3.3. Input PamCrash parameters for material type 30....54
Table 3.4. EMI's orthotropic elastic properties....55
Table 3.5. Input PamCrash parameters for material type 30....56
Table 3.6. Initial models prepared before validation tests 56
Table 3.7. Input PamCrash parameters for isotropic homogeneous Kevlar 29 with material type 16....60
Table 3.8. Input PamCrash parameters (up) and damage law (down) for isotropic homogeneous Kevlar 29 with material type 30 61
Table 3.9. Input PamCrash parameters (up) and damage law (down) for orthotropic homogeneous Kevlar 29 with material type 30 61
Table 3.10. Input PamCrash parameters for isotropic homogeneous Dyneema HB2 with material type 16....64
Table 3.11. Input PamCrash parameters (up) and damage law (down) for isotropic homogeneous Dyneema HB2 with material type 30 64
Table 3.12. Input parameters for brass Johnson-Cook model....66
Table 3.13. Input parameters for steel 4340 Johnson-Cook model....73
Table 3.14. Properties of final numerical models adopted with solid elements....74
Table 3.15. Properties of final numerical models adopted with shell elements....75

Table 4.1. Material constants values calculated for Kevlar 29 80
Table 4.2. Semi-analytical models. Protection design of Kevlar 29 for low size metallic impactor....80
Table 4.3. Semi-analytical models. Protection design of Kevlar 29 for high size metallic impactor 81
Table 4.4. Semi-analytical models. Protection design of Kevlar 29 for ice impactor 81
Table 4.5. Properties of fibres, matrix and final laminate of Kevlar 129....81
Table 4.6. Material constants values calculated for Kevlar 129 82
Table 4.7. Semi-analytical models. Protection design of Kevlar 129 for low size metallic impactor....82
Table 4.8. Semi-analytical models. Protection design of Kevlar 129 for high size metallic impactor 83
Table 4.9. Semi-analytical models. Protection design of Kevlar 129 for ice impactor 83

Table 4.10. Material constants values calculated for Spectra 900 with vynilester and polyurethane 85
Table 4.11. Semi-analytical models. Protection design of Spectra 900 for low size metallic impactor 85
Table 4.12. Semi-analytical models. Protection design of Spectra 900 for high size metallic impactor 86
Table 4.13. Semi-analytical models. Protection design of Spectra 900 for ice impactor 86
Table 4.14. Material constants values calculated for Dyneema HB2 87
Table 4.15. Semi-analytical models. Protection design of Dyneema HB2 for low size metallic impactor 88
Table 4.16. Semi-analytical models. Protection design of Dyneema HB2 for high size metallic impactor 88
Table 4.17. Semi-analytical models. Protection design of Dyneema HB2 for ice impactor ... 88
Table 4.18. Properties of steel for small metallic impactors 90
Table 4.19. Minimum thickness necessary to stop impactors for both materials (in red) 92
Table 4.20. Material constant for Kevlar 29 98
Table 4.21. Material constant for Dyneema HB2 99
Table 4.22. Comparison of ballistic limit calculated with numerical simulations and with analytical expression 99
Table 4.23. Comparison of ballistic limit calculated with numerical simulations and with analytical expression 101
Table 4.24. Ballistic limit at different angles of impact 102
Table 4.25. Coefficients of impact angle for both impactors (up) and coefficient average and deviation (down) 104
Table 4.26. Maximum vertical displacements for both materials at two different velocities 118
Table 4.27. Material constant for Kevlar 29 118
Table 4.28. Material constant for Dyneema HB2 118
Table 4.29. Ballistic limit depending on impact angle 120
Table 4.30. Coefficients of impact angles 121

INTRODUCTION

Throughout the years, aeronautical industry has been to the vanguard of the technology in different aspects. One of them is the development of lightweight structures made of composite materials. However, an aircraft structure does not only have to resist structural loads, furthermore there are some environmental threats and fragments that may impact against the aircraft structure. Therefore, the aircraft structure design has to consider not only resistance aspects but also impact requirements which minimize hazards to the aircraft.

The principal scope of the current project is to analyze specific materials to protect aircraft structure from impacts. The shields should meet two main requirements:

- *Good impact behaviour* in order to protect aircraft structure from external threats.

- *Low weight*, which is the classical driver of any aeronautical design due to direct implications on operational costs.

Considering the aspects mentioned above, all the protection materials studied during this project are composite materials made of high performance organic fibres, such as: aramid, polyethylene, PBO… This type of materials has good properties that fulfil all the requirements: high stiffness, high ultimate strength and low density.

The study of protection materials have been considering a research of experimental test and analytical models found in bibliography, complemented with numerical simulations in proposed models for polyethylene and aramid monolithic laminates. The numerical models were validated with published impact tests. The scope of these models is to represent properly ballistic limits of monolithic laminates made of polyethylene and aramids.

This project is divided into four main chapters. In the first one, typical impacts in aeronautics are presented, with more emphasis in the two kind of impact studied in this project: small fragment from engine failure and ice impacts. In the second one, different composite materials and their behaviour due to impact are studied, in order to understand the characteristics of this type of materials. In addition, some semi-analytical models to predict the ballistic limit are presented. Chapter III presents two numerical models of organic fibre laminates and validated tests from bibliography. In the forth chapter, semi-analytical and numerical models are used to design protection panels against high speed fragments from engine failure and ice impact from propeller release.

This project has been developed within an internal scholarship at the department of *Structural Dynamics and Aeroelasticity* in Airbus Military (EADS-CASA).

CHAPTER I. IMPACTS IN AERONAUTICS

1.1. General impacts in aeronautics

1.1.1. Introduction

In aeronautics there are different types of impacts against the aircraft structure. In civil aviation the most common impacts are bird strike, ice impact and small fragments from engine failure. A typical situation of small fragment impact is Uncontained Engine Rotor Failure (UERF). In military aviation, besides the previous situations, impacts coming from external aggressions have relevance.

General impacts in aeronautics can be classified depending on impact velocity and the kind of threat as shown in Table 1.1

Threat	Velocity (m/s)	
Hailstones	5 - 30	**LOW VELOCITY**
Bird strike	100 - 250	
Ice impact	150 - 400	
Gas turbine fragments	300 - 1500	**HIGH VELOCITY**
Small arms	500 - 1200	
Light armour	500 - 1200	
Heavy armour	500 - 2000	
Simulated bomb fragments	1000 – 2000	
Space debris	5000 - 11000	

Table 1.1. *General impacts in aeronautics [1]*

The main differences between low and high velocity impact are the structural response and damage in the material. At **low velocity impacts** the structural response is of utmost importance because the projectile has enough time to transfer and spread its energy through a large area of the target. In this case, most of the energy is absorbed elastically and boundary conditions have a significant relevance. At low velocity impacts, composite materials may have delamination and matrix cracking [1].

On the other hand, at **high velocity impacts**, the structure response is local due to the characteristic short time scales. Stress waves propagate throughout the material and boundary conditions effects are negligible. At high velocity impacts, composite material may have penetration and induced fibre breaking [1].

Within the framework of current research activities of Airbus Military (EADS-CASA), two types of impacts are studied in this project: impacts of high speed metallic fragments coming from uncontained engine rotor failure and propeller ice release.

1.1.2. Gas turbine fragments from Uncontained Engine Rotor Failure (UERF)

Uncontained failure of a gas turbine engine is any failure which results in the escape of rotor fragments from the engine that could result in a hazard. Rotor failures which are concern are those where released fragments have enough energy to create a hazard to the aircraft [2].

A real situation of engine failure occurred recently in an Australian airline with an Airbus A380 aircraft. Few minutes after takeoff, the aircraft did an emergency landing due to an engine failure, causing it extensive damages [3].

Figure 1.1. *Damage in aircraft due to uncontained engine rotor failure [4]*

Airworthiness regulations [2] classify four types of fragments in an uncontained engine rotor failure event:

- Single one-third disc fragment: disc fragment with its maximum dimension corresponding to the one-third of the disc with one-third blade height and a fragment spread angle of 3º. Where energy considerations are relevant, the mass should be assumed to be one-third of the bladed disc mass and its energy, the translational energy of the sector travelling at the speed of its centre of gravity.

- Intermediate fragment: the intermediate fragment has a maximum dimension corresponding to one-third of the bladed disc radius and a fragment spread angle of 5º. Where energy considerations are relevant, the mass should be assumed to be 1/30 of the bladed disc mass and its energy, the translational energy of the piece travelling at rim speed.

- Small fragments: small fragments range in size up to a maximum dimension corresponding to the tip half of the blade airfoil and a fragment spread angle of 15º. Where energy considerations are relevant, it should be assumed that the mass will correspond to the one-half of the airfoil fragment dimensions and that it has a translational energy level of one percent of the total rotational energy of the original rotor stage.

- Fan blade fragment: fan blade fragment has a maximum dimension corresponding to the blade tip with one-third blade airfoil height and a fragment spread angle of 15º. Where energy considerations are relevant the mass should be assumed to be corresponding to the one-third of the airfoil including any part span shroud and the transitional energy of the fragment travelling at the speed of its centre of gravity.

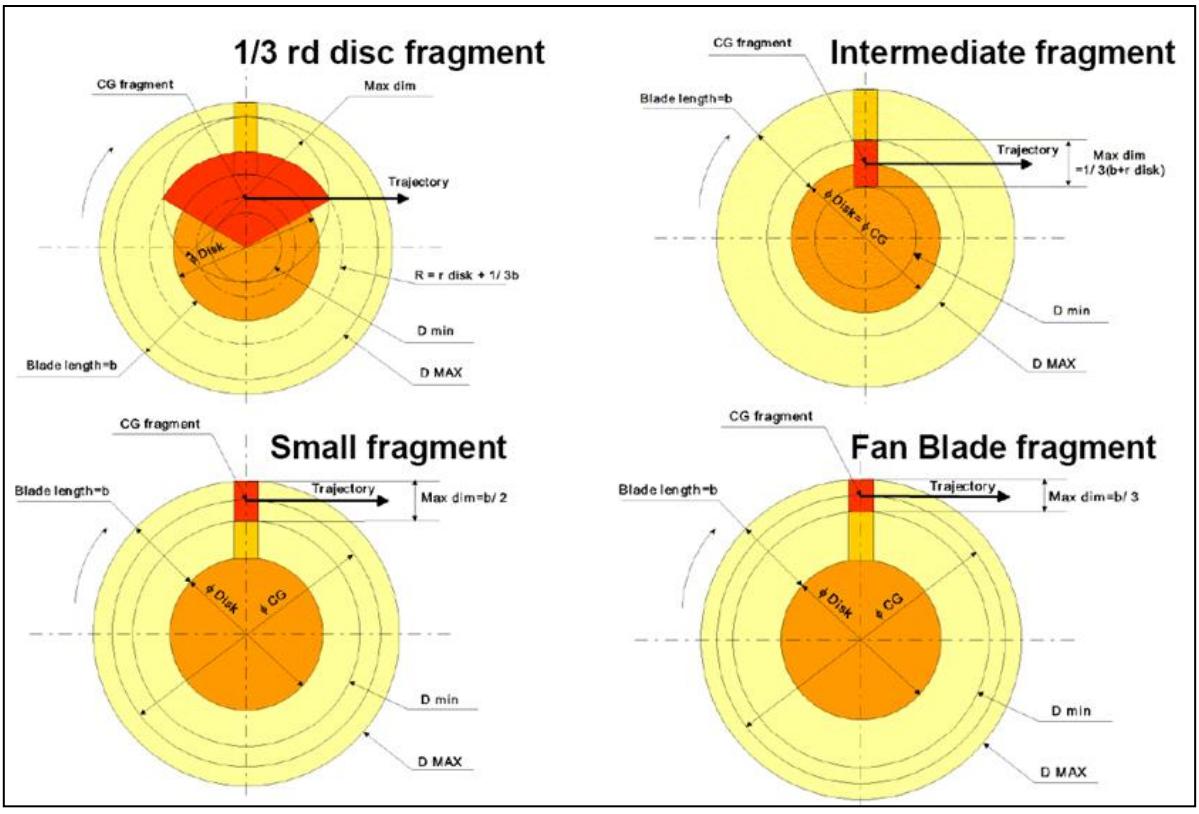

Figure 1.2. *Typical fragments generated by UERF [4]*

The main components of a gas turbine are made of materials with a very high stiffness like steel or titanium. Hence, fragments generated by engine failure have also very high stiffness travelling at high speed. The typical velocity range of gas turbine fragments goes from 350 m/s up to 1500 m/s [1]. Due to its high stiffness and velocity, this kind of fragments might be dangerous for the aircraft structure.

Considering the estimated path of fragments (Figure 1.3), it is assumed that zones where is more likely that gas turbine fragments impact are in fuselage zones near to engines and in the wings of the aircraft where the gas turbines are installed.

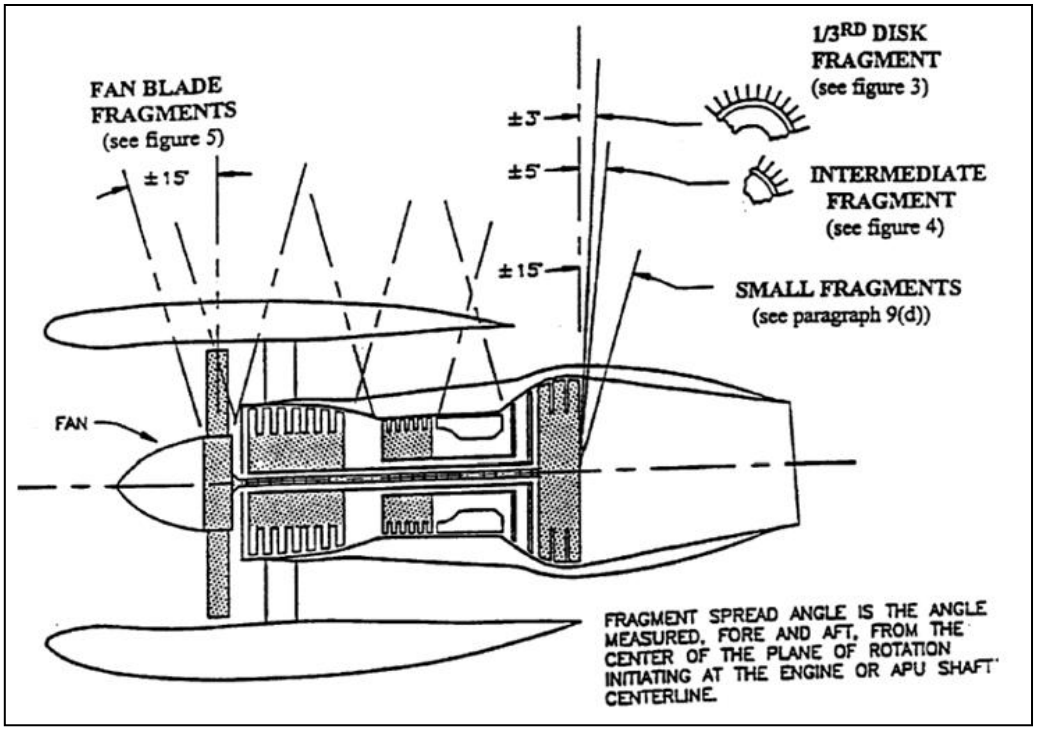

Figure 1.3. *Estimated path of fragments [2]*

Engine failure is an unexpected event and it may happen during takeoff, landing or even during the flight, so the operational conditions of the designed protection panels must take into account that the atmospheric conditions (pressure, radiation, temperature and humidity) may change significantly. During the flight, temperatures are low and radiation is higher than at lower altitudes.

1.1.3. Ice impact

During aircraft operation it is likely that ice may be formed at lifting surfaces, leading edges, propeller blades and engine intakes. That makes quite common impacts on aircraft structure due to ice shedding. This phenomena is well known in propeller aircrafts when flying in adverse atmospheric conditions. Therefore, it is necessary to take into account risks due to this type of impacts, and to protect the aircraft structure in consequence.

Figure 1.4. *Ice formed on fan blades (left) and on engine spinner (right) [5]*

Ice fragments are completely different from fragments coming from an engine failure. Ice stiffness is much lower than steel. The maximum measured ice hardness was 60MPa, measured by Vickers indenter. This corresponds to a Vickers Hardness of about 6 HV. For comparison, a mild steel has hardness around 120-150 HV, whereas a hardened blade steel is up around 800-900 HV [6]. The density of both fragments is also different. The normal steel density is 7850 kg/m^3, whereas ice density is about 917 kg/m^3.

Speed range for ice impact goes from 150 m/s up to 400 m/s [1]. Ice impact event is typical in propeller aircrafts. A geometrical analysis of the trajectory reveals that there are two regions of the fuselage which may be impacted. Figure 1.5 shows propeller tip points from where ice release may impact the fuselage and fuselage regions which can receive the impact. The angle of impact between the blade trajectory and fuselage may vary from 0 to 90 degrees [7].

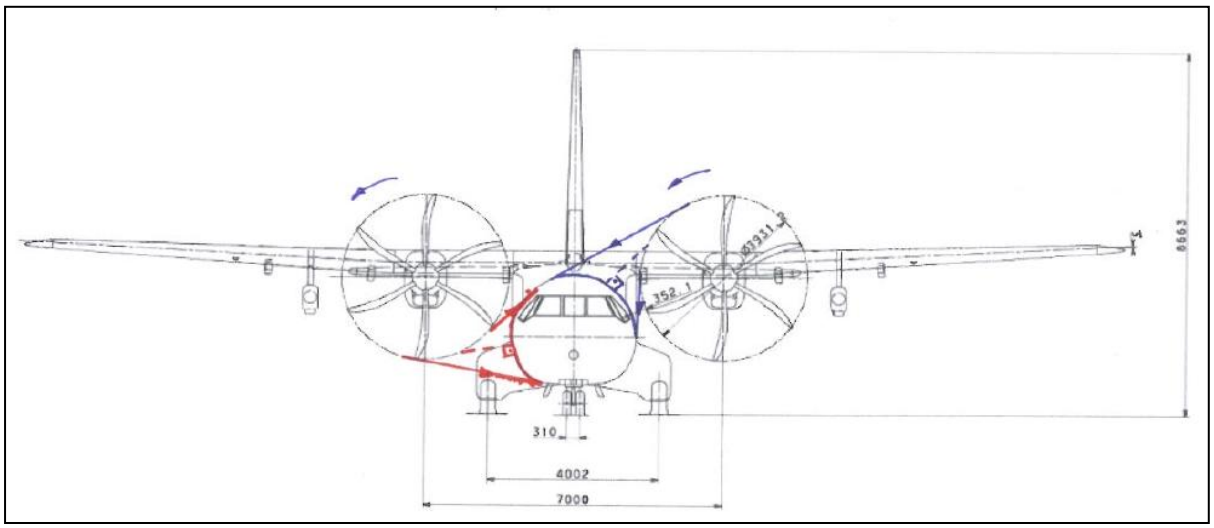

Figure 1.5. *Propeller blade release trajectory analysis [7]*

Impact due to hailstones is also a typical situation during a flight, and with the ice formed on leading edges are the two most important ice impacts on an aircraft structure. Image sequence in Figure 1.6 corresponds with a test campaign of Airbus Military (EADS-CASA) carried out of University Carlos III of Madrid [8].

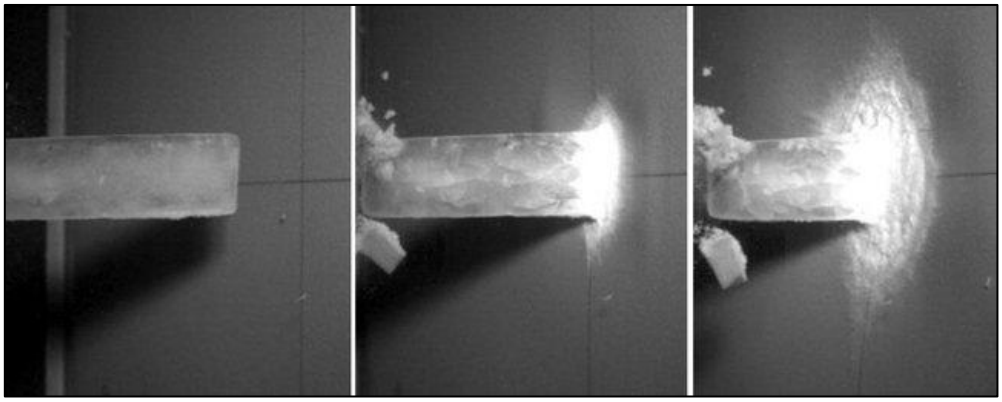

Figure 1.6 *Ice impact sequence [8]*

1.2. Protection concepts in aeronautics

To protect the aircraft there are different types of concepts depending on the required functionally. Sometimes it is not necessary to protect the whole aircraft structure and shields are designed to protect specific zones of the aircraft. These kinds of protection can be classified into three categories:

- "Stand alone" systems protection: independent shield for particular protection of systems, fuel and hydraulic pipes [4]. These shields may be monolithic laminates of high performance fibres that will protect specific aircraft areas from engine fragments.

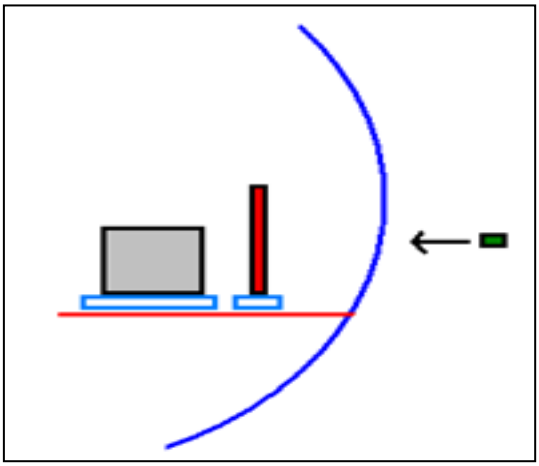

Figure 1.7. *Stand alone protection (in red) [4]*

- System protection attached to existing structure: protection for fuel tanks and fuselage slides. In this case, zones to protect are larger and need a different type of shield; hence a protection attached to the structure is the most suitable option [4].

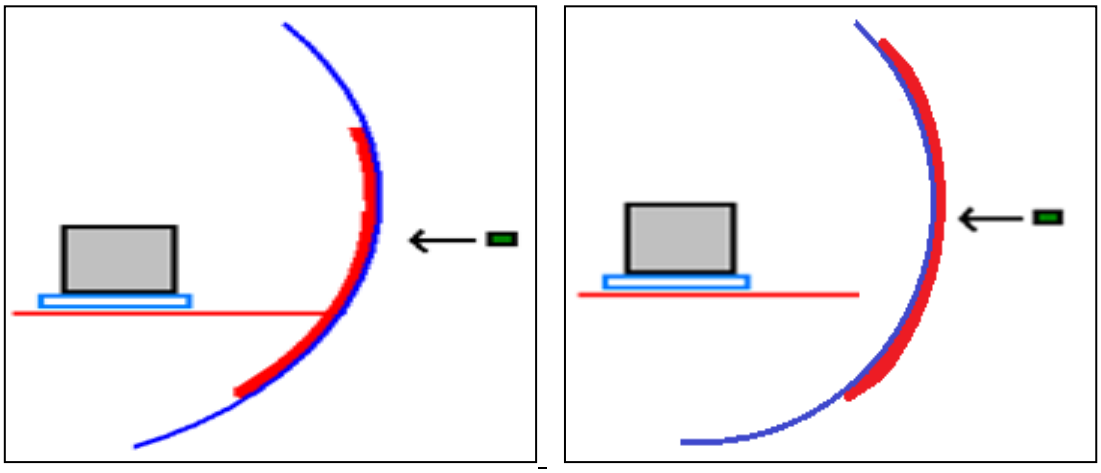

Figure 1.8. *Protection attached to structure (in red) [4]*

- Hybrid armours (multifunctional laminates): aircraft protections which combine structural materials, like carbon fibre reinforced polymers, with impact protection materials, made of high performance organics fibres like aramids, polyethylene and PBO. This combination of materials improves the mechanical characteristics of laminate given structural resistance (carbon fibres) and impact performance (aramid, polyethylene and PBO fibres) in a single monolithic laminate [1].

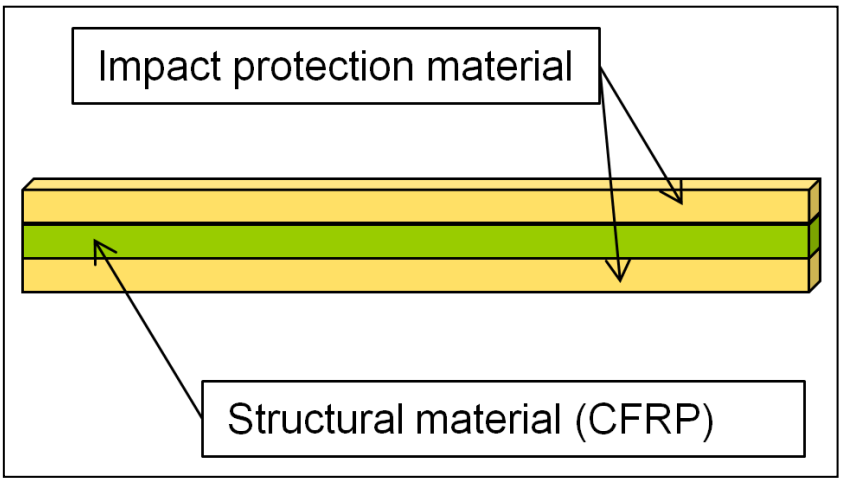

Figure 1.9. *Hybrid armour configuration [1]*

The same types of protections are suitable for gas turbine fragments and ice impacts depending on the required functionality, although the minimum thickness required to stop each type of impact is completely different. In the current work, protections designed are "stand alone", but it is also common to use protections attached to fuselage for ice impacts. These shields are a kind of protective "scarf" around the fuselage in propeller aircrafts.

CHAPTER II. IMPACTS ON COMPOSITES

2.1. Introduction

The scope of the project is focused on shields made of monolithic panels of high performance organic fibres. To obtain a proper material numerical model, it is important to know correctly properties of: protections or shields (in this case composite materials) and projectiles (or impactors).

This chapter presents the principles of composite materials and the different parts of them: fibres and matrix. There are several types of fibres that can be used for impact protection; this project is focused in two of them: aramid and polyethylene fibres. They can be assembled in several ways, providing different composite materials configurations to impact protection.

Then the impact response of this type of materials and typical failure mechanisms will be presented.

At the end of this chapter some semi-analytical models are presented in order to predict penetration and ballistic limit of protections. With these models it is possible to size protections of approximate thickness and areal density necessaries to stop given impactors.

2.2. Composite materials for impact protection

2.2.1. Introduction

Composites are created by the combination of two or more materials, on a macroscopic scale, to form a new material with enhanced properties that are superior to those of the individual constituents [9].

Fibre Reinforced Polymeric (FRP) is a composite material made of a polymeric matrix reinforced with fibres. Fibres and matrix both play critical roles in the composite materials, *fibres* provide strength and stiffness and *matrix* protects and transfers load between fibres [9].

Two main composite materials are studied in this project:

- Aramid fibre composite laminate (**Kevlar 29**) with two different types of matrix:
  - Polyvinyl butyral.
  - Vynilester.

- Polyethylene fibre composite laminate (**Dyneema HB2**) with one type of matrix:
  - Polyethylene.

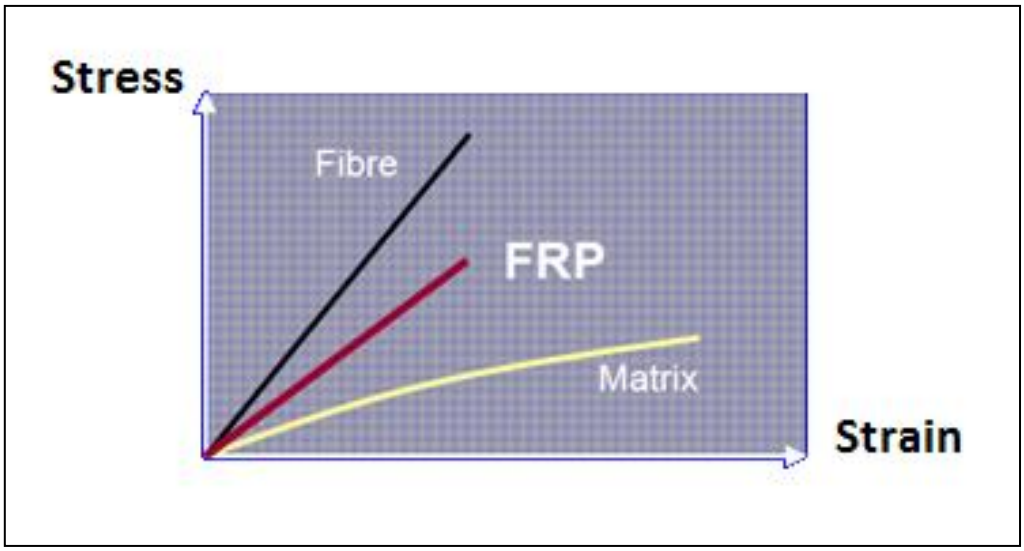

Figure 2.1. *Fibre Reinforced Polymers = fibre + matrix [9]*

Figure 2.1 shows how the Young's modulus of the composite results from a combination of fibres and matrix ones

2.2.2. Fibres

Composite materials for impact protection are manufactured with high performance fibres. These fibres have unique properties which set them apart from other man-made fibres used for industrial applications.

High performance fibres are engineered for particular purposes and uses that require specific characteristics. For impact protection in aeronautics and in other different fields, some of these properties are [10] [11]:

- High stiffness.
- High ultimate strength.
- High strain to failure.
- Low density.
- High sound speed (high modulus and low density).
- Low variation of strength between individual fibres.
- Stability during handling.
- Large length to diameter ratio.

There are several types of fibres with good properties for impacts. Typical high performance fibres are: glass, carbon, aramid, high weight molecular polyethylene (HWMPE), poly-phenylenebenzobisoxazole (PBO) and M5. Table 2.1 summarizes and compare the main characteristics and mechanical properties of high performance fibres.

Fibres	Fibre type	Density (g/cm^3)	Longitudinal tensile modulus E (GPa)	Longitudinal tensile strength σ (MPa)	Elongation at rupture (%)
Kevlar 29	aramid	1.44	70	2920	3.60
Kevlar 49	aramid	1.44	112	3000	2.40
Kevlar 149	aramid	1.47	179	3450	2.00
Kevlar KM2	aramid	1.47	83	3400	3.55
Twaron	aramid	1.45	120	3500	2.50
Dyneema SK75	polyethylene	0.97	110	3500	3.30
Spectra 1000	polyethylene	0.97	113	2570	3.10
Zylon AS	PBO	1.54	180	5800	3.50
Zylon HM	PBO	1.56	270	5800	2.50
E-Glass	glass	2.60	22	3500	4.70
Carbon	carbon	1.75	227	3800	1.76
M5	M5	1.70	271	5800	1.40

Table 2.1. *Main properties of typical high performance fibres [10] [11] [12] [13] [14] [15] [16]*

Data given in Table 2.1 are normally obtained with classical longitudinal tensile test. The properties for different type of fibres may vary significantly. Some fibres have high tensile modulus, but elongation at rupture is lower than others. Depending on the fibre type, the ballistic performance will be different too. Figure 2.2 shows a ballistic performance comparison of different fibres.

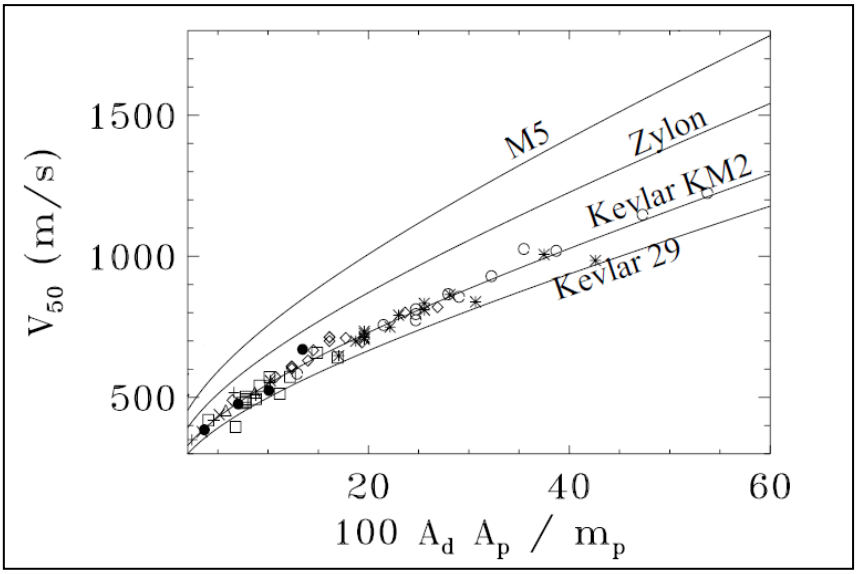

Figure 2.2. *Ballistic limit for different high performance fibres [11]*

In this plot, ballistic limit versus some parameters is represented [11]. Ballistic limit (V_{50} or V_b) is defined as the maximum velocity at which the projectile, in an impact event, is stopped by the protections. The other parameters are:

- A_d: composite areal density.
- A_p: projectile presented area.
- m_p: projectile mass.

Therefore, composite materials made of organic fibres have better behaviour (stop projectiles at higher velocities), if its mass per surface (A_d) and the projectile presented area are high. If projectile mass is higher, at same speed, kinetic energy will be higher too, so ballistic limit will be lower because protections must absorb more energy. Finally, the plot shows that:

- M5 has better impact performance than Kevlar and Zylon.
- Kevlar KM2 has higher modulus than Kevlar 29 and its impact behaviour is also better.
- The higher is the elastic modulus, the better impact performance has the fibre.

2.2.2.1. Aramid

Aramid fibres consist of long molecular chains of poly-paraphenylene terephthalamide [10]. There are two different aramid fibres trademarks: Kevlar and Twaron. Kevlar was developed by DuPont in 1965 and a few years later Twaron was developed by Azko [17].

Aramid fibres posses a crystallographic structure with a monoclinic unit cell (Figure 2.3) and its cristallinity is higher than 90%, which gives to the fibre high stiffness [10].

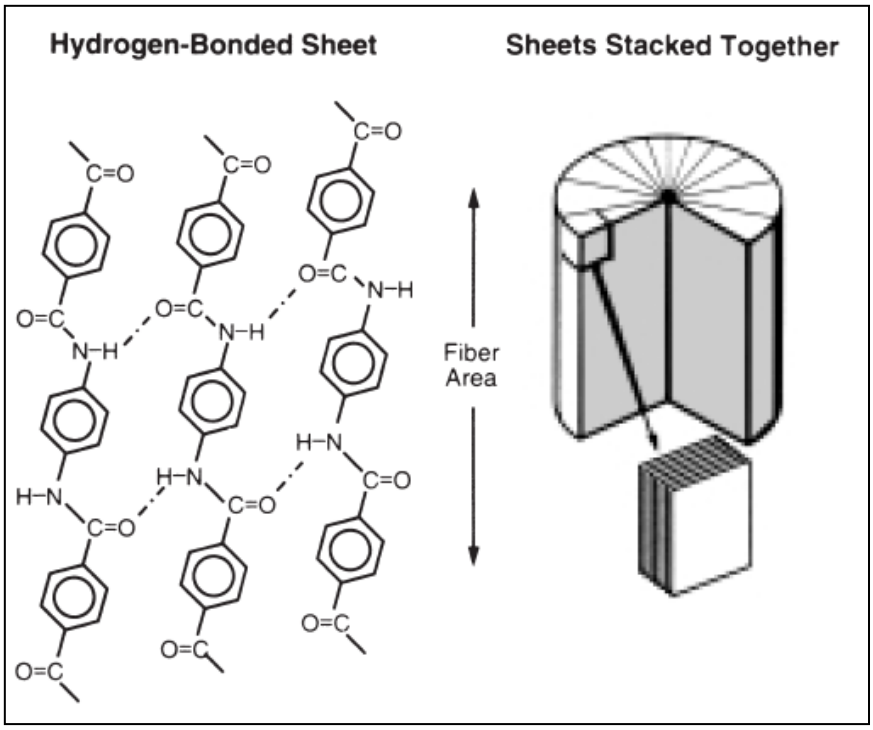

Figure 2.3. *Kevlar crystallographic structure [14]*

Fibres are produced in a solution extruder where the molecular orientation is quenched into place. By controlling the extruding conditions, different strength fibres are obtained [10]. For example, for Kevlar, several types of filaments could be manufactured:

- **Kevlar 29:** all purpose.
- **Kevlar 129:** high tenacity.
- **Kevlar 49:** high modulus.
- **Kevlar 149:** ultra high modulus.

TABLE II-1. Typical Properties of Du Pont KEVLAR® 29 and 49 yarns

Property	Unit	KEVLAR 29	KEVLAR 49
YARN			
Type	denier	1,500	1,140
	(dtex)	(1,670)	(1,270)
	# of filaments*	1,000	768
Density	lb/in.³	0.052	0.052
	(g/cm³)	(1.44)	(1.44)
Moisture Levels			
As Shipped**	%	7.0	3.5
Equilibrium from Bone-Dry Yarn***	%	4.5	3.5
TENSILE PROPERTIES			
Straight Test on Conditioned Yarns†			
Breaking Strength	lb	76.0	59.3
	(N)	(338)	(264)
Breaking Tenacity	g/d	23.0	23.6
	(cN/tex)	(203)	(208)
	psi	424,000	435,000
	(MPa)	(2,920)	(3,000)
Tensile Modulus	g/d	555	885
	(cN/tex)	(4,900)	(7,810)
	psi	10.2×10^6	16.3×10^6
	(MPa)	(70,500)	(112,400)
Elongation at Break	%	3.6	2.4
Resin Impregnated Strands††			
Tensile Strength	psi	525,000	525,000
	(MPa)	(3,600)	(3,600)
Tensile Modulus	psi	12.0×10^6	18.0×10^6
	(MPa)	(83,000)	(124,000)

Property	Unit	KEVLAR 29	KEVLAR 49
THERMAL PROPERTIES			
Shrinkage			
In Water at 212°F (100°C)	%	<0.1	<0.1
In Dry Air at 351°F (177°C)	%	<0.1	<0.1
Shrinkage Tension			
In Dry Air at 351°F (177°C)	G/D	<0.1	<0.2
	(cN/tex)	(0.88)	(1.77)
Specific Heat			
At 77°F (25°C)	cal/g x °C	0.34	0.34
	(J/kg x K)	(1,420)	(1,420)
At 212°F (100°C)	cal/g x °C	0.48	0.48
	(J/kg x K)	(2,010)	(2,010)
At 356°F (180°C)	cal/g x °C	0.60	0.60
	(J/kg x K)	(2,515)	(2,515)
Thermal Conductivity,	BTU x in./(h x ft² x °F)	0.3	0.3
	[W/(m x K)]	[0.04]	[0.04]
Decomposition Temperature in Air†††	°F	800-900	800-900
	(°C)	(427-482)	(427-482)
Recommended max. Temperature Range for Long-Term Use in Air	°F	300-350	300-350
	(°C)	(149-177)	(149-177)
Heat of Combustion	BTU/lb	15,000	15,000
	(Joule/kg)	(35×10^6)	(35×10^6)
Poisson's Ratio			0.36

Table 2.2. *Typical mechanical and thermal properties of Kevlar 29 and Kevlar 49 [14]*

The environmental conditions may modify aramid fibres properties [14]:

- *Chemical agents:* fibres are chemically stable under a wide variety of exposure conditions, but certain acids, bases and sodium hypochlorite can cause degradation particularly over long periods of time and high temperatures.

- *PH:* at neutral PH 7, the filament tenacity remains unchanged at a temperature of 65 ºC for more than 200 days. However if the PH is not neutral the filament loss tenacity. Acid conditions cause more degradation than basics (Figure 2.4).

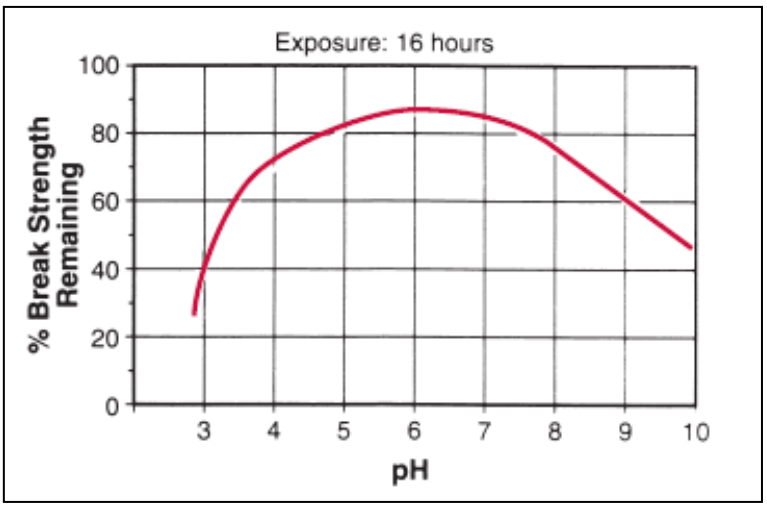

Figure 2.4. *Hydrolytic stability of Kevlar at 154 ºC [14]*

- *Water:* relative humidity has a significant effect on the rate of moisture absorption. The higher relative humidity, the faster fibres absorb. However, tensile properties are unaffected by moisture content.

- *Temperature:* aramid does not melt, it discomposes at relatively high temperatures, from 427 ºC to 482 ºC. Decomposition temperatures vary with the rate of temperature rise and the length of exposure (Figure 2.5).

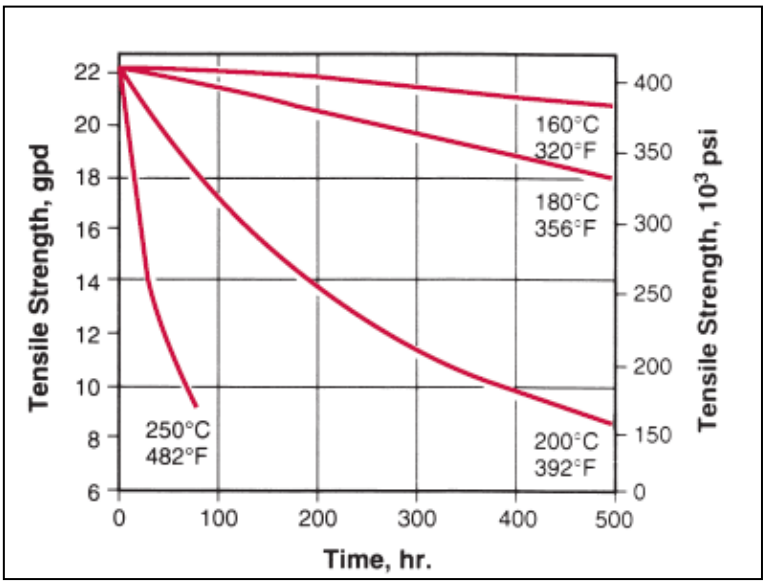

Figure 2.5. *Effect of elevated temperatures on tensile strength of Kevlar 29 [14]*

- *UV light:* like other polymeric materials, aramid fibres are sensitive to UV (ultraviolet) light. Unprotected filaments tend to discolour from yellow (original colour) to brown after long exposure. Prolonged exposure to UV light can also cause loss of mechanical properties, depending on exposure time, radiation intensity and product geometry.

2.2.2.2. Ultra High Molecular Weight Polyethylene (UHWM-PE)

Ultra High Weight Molecular Polyethylene (UHWM-PE) is also known as High Modulus Polyethylene (HMPE) or High Performance Polyethylene (HPPE). It is composed of extremely long chains, with molecular weight numbering in the millions [10]. Long chain serves to transfer load more effectively to the polymer backbone by strengthening intermolecular interactions. This, results in a very tough material, with one the highest impact strength of any thermoplastic currently made [18].

There are two principal polyethylene fibres trademarks: Dyneema and Spectra developed by DSM and by Honeywell respectively [17]. DSM patented a new method in 1979 called *gel spinning*. In this process, the long, flexible and entangled molecules are dissolved in a solvent from 2-15% concentrations and mixed via an extruder, helicon mixer other mixing systems (Figure 2.6) [18].

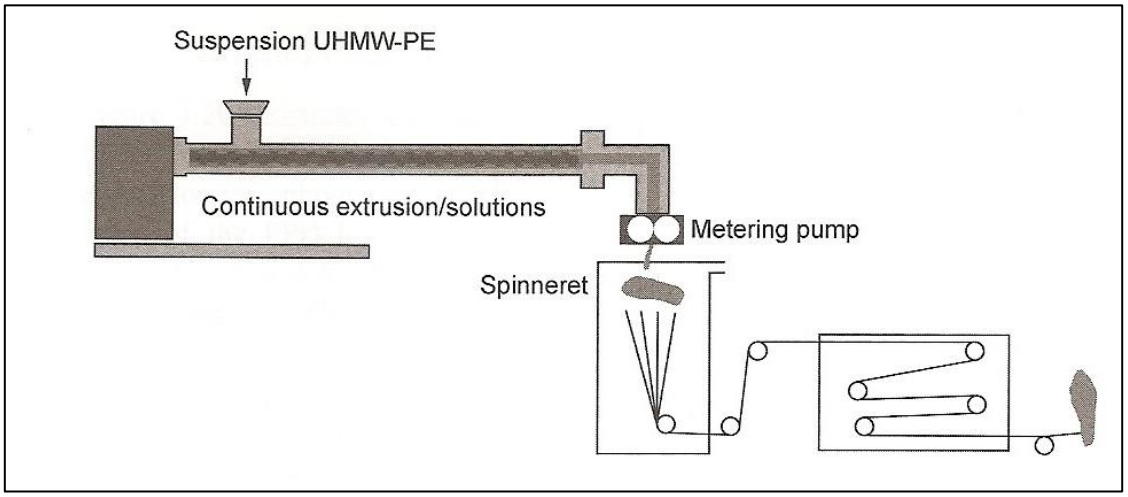

Figure 2.6. *Scheme of gel spinning process [18]*

Polyethylene fibres are highly resistant to corrosive chemicals, with exception of oxidizing acids. They have extremely low moisture absorption, very low coefficient of friction, are self lubricating, and are highly resistant to abrasion. When the fibres are formed, the polymer chains can attain a parallel orientation greater than 95% and a level of cristallinity up to 85%, which gives to fibres high stiffness [18].

The temperature also affects on polyethylene fibres. Melting temperature is about 150 ºC and is not advisable to use them at temperatures exceeding 80 - 100 ºC for longs periods of time. Polyethylene fibres become brittle at temperatures below -150 °C [10].

PHYSICAL PROPERTIES								
(Nominal)	Spectra® fiber 1000							
Weight/Unit Length (Denier) (Decitex)	215 239	275 306	375 417	435 483	650 722	1300 1444	1600 1778	2600 2888
Ultimate Tensile Strength (g/den) (Gpa)	38 3.25	36 3.08	35 3.00	34.5 2.95	36 3.08	35 3.00	35.5 3.02	34 2.91
Breaking Strength (lbs.)	18	22	29	33	52	100	123	195
Modulus (g/den) (Gpa)	1320 113	1320 113	1200 103	1180 101	1175 101	1150 98	1170 99	1135 97
Elongation (%)	2.9	3.1	3.1	3.2	3.5	3.3	3.5	3.5
Density (g/cc) (lbs/in³)	0.97 0.035	0.97 0.035	0.97 0.035	0.97 0.035	0.97 0.035	0.97 0.035	0.97 0.035	0.97 0.035
Filament/tow	60	60	60	120	120	240	240	480
Filament (dpf)	3.6	4.6	6.3	3.6	5.4	5.4	6.67	5.4

Table 2.3 *Mechanical properties of a polyethylene fibre (Spectra 1000) for different weight per length [15]*

Table 2.3 shows mechanical properties of a polyethylene fibre for different weight per length. This magnitude is typically measured with *Deniers*, which is the fibre mass in grams per 9000 meters.

2.2.2.3. Glass

Glass fibres are the oldest and most familiar high performance fibre. These fibres are formed when thin strands of silica-based (SiO_2) are extruded into fibres with small diameters suitable for processing. At 1713ºC, most of the molecules can move about freely. Glass fibre, unlike other fibres for ballistic protection is an amorphous solid; hence, its properties are maintained along and across the fibre.

These fibres are relatively inflexible and they can be found in a wide range of end uses such as insulations, fire resistant fabrics and reinforcing materials for plastic composites. Moisture is absorbed and can generate microscopic cracks and surface defects [10] [18].

2.2.2.4. Carbon

Carbon fibres can be engineered for strength and stiffness to reinforce composite; or, in other forms, improve electrical conductivity, thermal conductivity, and thermal and chemical resistance of textile materials.

A common method to produce carbon filaments is the oxidation and thermal pyrolysis of polyacrylonitrile (PAN). The carbon can become further enhanced, as high modulus (graphitizing) or high strength carbon (carbonization), by heat treatment processes. Carbon fibres are of common use in aeronautics industry for structural proposes due to the high strength to density ratio [10].

2.2.2.5. PBO

PBO is a high performance fibre based on repeating aromatic structures. PBO exhibits very good tensile strength and high modulus, which are useful for reinforcing applications. Currently Toyobo is the company which commercialises PBO fibres with the trade name Zylon (p-phenylene-2, 6-benzobisoxazole) [12].

2.2.2.6. M5

M5 is a high performance organic fibre produced by Magellan Systems and DuPont. This fibre is based in poly-diimidazo-pyridinylene-dihydroxy-phenylene having a covalent bonding in fibre direction and hydrogen bonded network in lateral direction. M5 has very good properties (high modulus, tensile and compressive strength) and furthermore is stable under UV, heat and humidity, with 40% to 60% less weight than aramids [10] [11].

2.2.3. Matrix

The primary function of the matrix (also called resin) is to transfer stresses between the reinforcing fibres. It acts as a glue to hold the fibres together, and protect the fibres from mechanical and environmental damage. Resins are divided into two major groups known as *thermoplastic* and *thermoset* [10].

- ***Thermoplastic resins*** become soft when heated, and may be shaped or moulded while in a heated semi-fluid state and become rigid when cooled [23]. Typical thermoplastic resins are: polyethylene, polypropylene and polyvinyl butyral.

- ***Thermosetting resins*** are usually liquids or low melting point solids in their initial form. When used to produce finished goods, these thermosetting resins are cured by the use of a catalyst, heat or a combination of both. Once cured, solid thermoset resins cannot be converted back to their original liquid form [23]. Most common thermoset resins used in the composites industry are unsaturated polyesters, epoxies and vinylesters.

Here it will only be described resins used in material models treated in the project: vynilester, polyvinyl butyral and polyethylene.

2.2.3.1. Vinylester

Vinylesters were developed to combine the advantages of epoxy resins with the better handling/faster cure, which are typical for unsaturated polyester resins. These resins are produced by reacting epoxy resin with acrylic or methacrylic acid. This provides an unsaturated site, much like that produced in polyester resins when maleic anhydride is used. The resulting material is dissolved in styrene to yield a liquid that is similar to polyester resin. Vinylesters are also cured with the conventional organic peroxides and offer mechanical toughness and excellent corrosion resistance.

2.2.3.2. Polyvinyl butyral

Polyvinyl butyral (or PVB) is a resin usually used for applications that require strong binding, optical clarity, adhesion to many surfaces, toughness and flexibility. It is prepared from polyvinyl alcohol by reaction with butyraldehyde [23].

2.2.3.3. Polyethylene

Polyethylene is a thermoplastic polymer consisting of long chains produced by combing the ingredient monomer ethylene; the name comes from the ingredient and not the actual chemical resulting. The ethylene actually converts to ethane as it takes its place in a polymer and straight sections of the polymer are the same structure as the simple chain hydrocarbons, e.g., propane, decane and other straight single-bonded carbon chains. As with any polymer, the structure of the resulting substance defies molecular description due to cross branching of the chains [23] [17].

2.2.4. Configurations for shield design with organic fibres materials

Once the properties of two components of a composite material (fibres and matrix) are presented, it is time to assemble them. There are different ways of assembling components when shields are designed.

First of all, it is necessary to know that each fibre has a very small diameter, for example Kevlar 29 fibre has a diameter of 12 μm and Spectra 900 fibre 38 μm [16]. Therefore, they need to be entangled or twisted into a ***yarn*** of fibres, which could be defined as a continuous strand of fibres suitable for knitting or weaving to form a textile fabric [10]. Finally, yarns are assembled between them with different configurations; hence armours could be classified as: woven fabrics and non-woven fabrics.

2.2.4.1. Woven fabrics

Woven fabric consists of two sets of interlacing yarns which lie perpendicular to one another. The yarns can be interlaced in many different ways to produce numerous weave designs and each weave has different mechanical properties [19]. Depending on directions, there are two types of yarns (Figure 2.7) [10]:

- ***Warp***: yarns that run in parallel to the longer dimension.
- ***Weft (or fill)***: yarns that cross transversally the other ones.

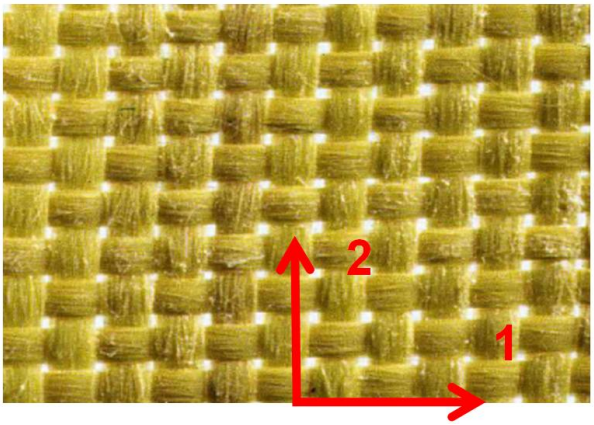

Figure 2.7. *Warp (1) and weft (2) directions on a woven fabric [9]*

There are three basic weaves from which all other weaves are derived:

1. **Plain weave** is considered the simplest of the three weaves (Figure 2.8 left). In a plain weave odd warp threads operate over one and under one filling thread, and even warp threads reverse this order, to under one, over one. Another configuration which derivate of a plain weave is the *basket weave* (Figure 2.8 right); in this case two or more yarns are grouped together in both warp and weft directions and alternately interlaced over and under each other [19].

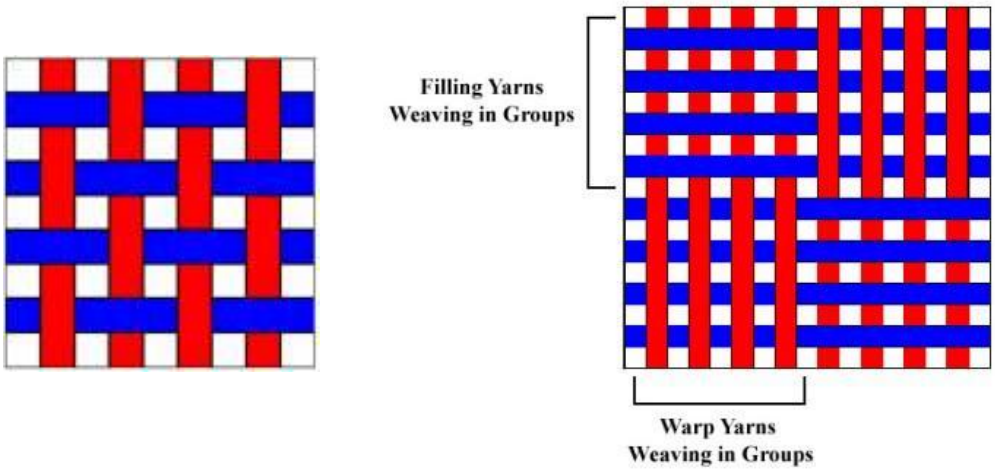

Figure 2.8. *Two different woven fabrics: plain weave (left) and basket weave 4x4 (right) [19]*

2. **Twill weaves** repeat on two or more warp and filling yarns. Twill weaves have a distinctive diagonal line on the surface of the fabric (Figure 2.9 left) [19].

3. **Satin weave** is notable for its smooth surface created by the relatively long warp yarn floats, in this case one warp runs over three or more weft yarn and under one weft yarn [20]. Figure 2.9 right, shows a 5-harness satin weave, where one warp runs over five weft yarns.

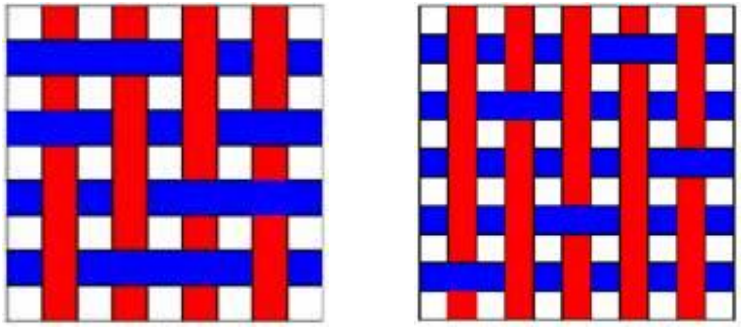

Figure 2.9. *Two different woven fabrics: twill weave (left) and 5-harness satin weave (right) [19]*

2.2.4.2. Non-woven fabrics

Non-woven fabrics are made by the interlocking of fibres by a suitable combination of mechanical work, chemical action, moisture and heat without weaving or knitting. For example, the fibres could be held together by an adhesive agent or by fusing of self-contained thermoplastic fibres [10]. There are two main non-woven fabrics:

1. **Felts** interlock fibres by a combination of chemical action and heat [10]. An example is shown in figure 2.10.

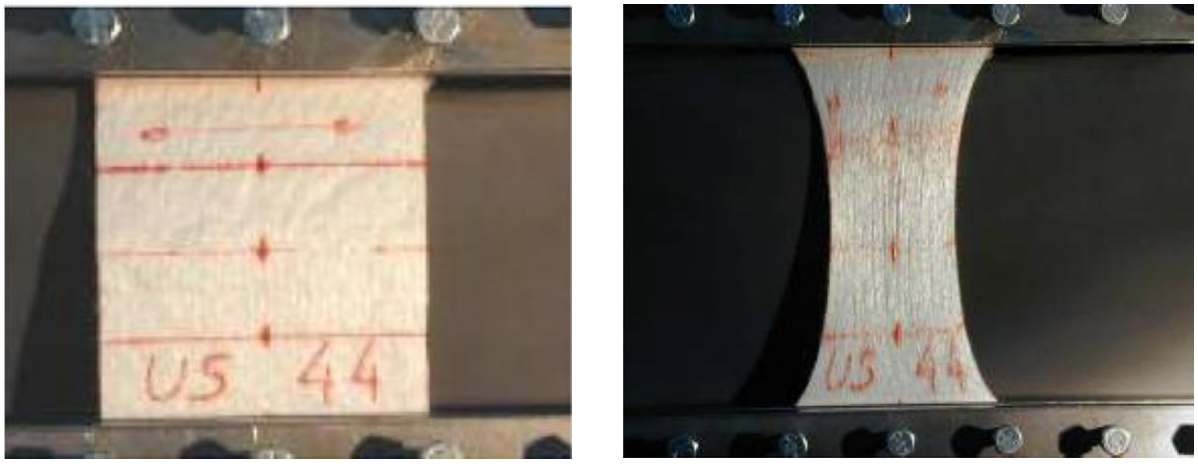

Figure 2.10. *Examples of polyethylene felt [21]*

2. **A filament lay-up composite** is a very significant type of ballistic resistance structure. Although these structures are neither woven nor knitted, and they normally are called non-woven, they also fit the definition of a fibre-matrix composite [18].

   In the filament lay-up structure, all of the fibres are lined parallel to each others as in the beaming operation for woven fabric. A binder is the applied to form the structure into a continuous resin-fixed web of aligned fibres. The resin holds the fibres spacing for further processing. A web of similarly constructed filaments is aligned at 90 degree to form a continuous roll. The 0 degree and 90 degree webs are further consolidated to form a cross plied unidirectional roll product. The roll product developed by this technology is a patented process [18].

The two most typical unidirectional non-woven fabrics in the ballistic protection are Dyneema UD and Spectra Shield. Both of them are made of polyethylene fibres, although some unidirectional fabrics made of aramid fibres can be also found. All these products consist of a roll product of two or four unidirectional plies, cross-plied at 0/90 degrees and sandwiched or not in a thermoplastic film [20].

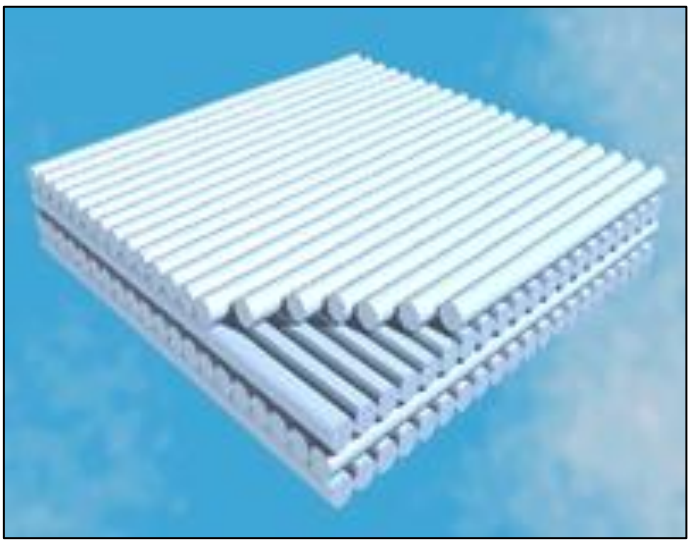

Figure 2.11. *Scheme of Dyneema UD [12]*

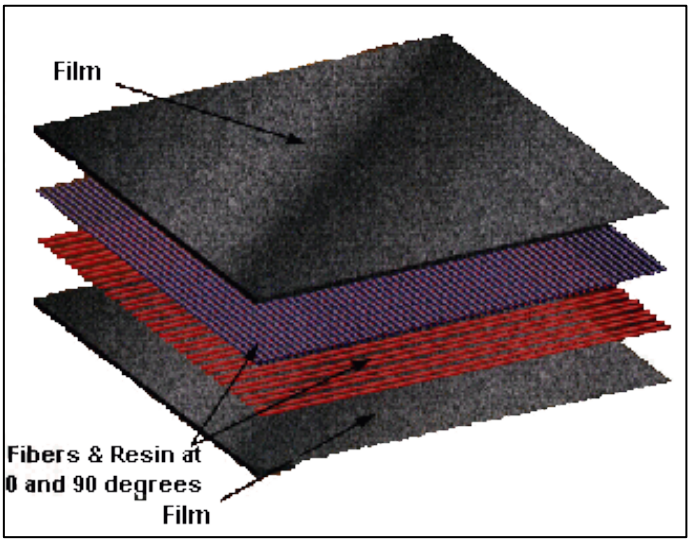

Figure 2.12. *Scheme of Spectra Shield [15]*

2.3. Material response to impact

During an impact event, the target response is a combination of *global* and *local* reactions. The relative contributions from these two reactions are generally determined by a multitude of factors including [18]:

- Strike velocity.
- Projectile properties.
- Target size.
- Boundary conditions

Typically, strike velocity is considered to be the most significant factor to determine the transition between locally dominated and globally dominated response. The range of strike velocities from global to local dominated response covers quasi-static loading at the low end and hyper-velocity impacts at the high end, with typical behaviour being a superposition of both [18]. Figure 2.13 shows material response of high and low velocity impact.

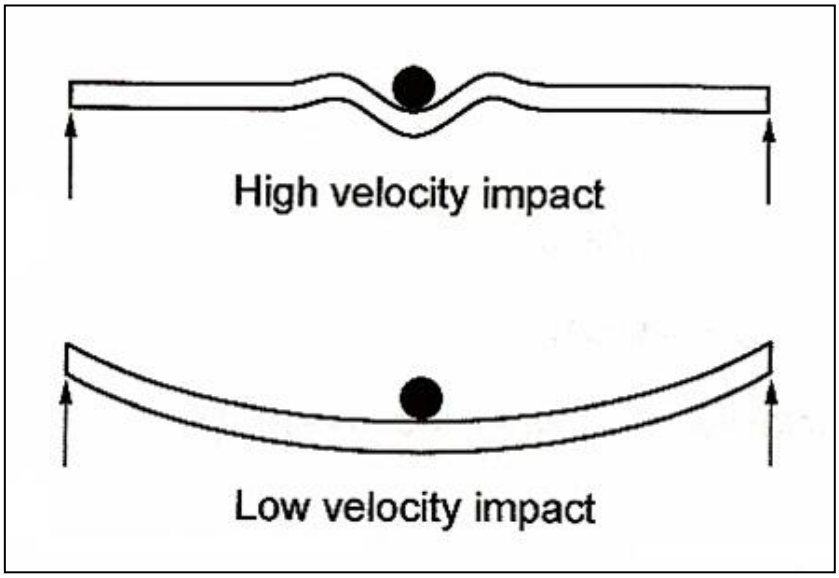

Figure 2.13. *Schematic representation of impact response under high velocity impact and low velocity impact [18]*

In **global response**, global energy absorbing mechanisms are usually dominant in low-velocity impacts events, where there is ample time for the projectile energy to be transferred and spread through a large area of the target. In such cases, the impact event is long enough for the elastic waves (flexural and shear) generated in the target to propagate and reach the boundaries of the target. It is now generally accepted that a longitudinal strain wave, travelling at the speed of sound in the material, is generated in a fabric yarn upon impact. This wave stretches the yarns and causes the material move in-plane towards the impact point. A deformation cone is also created, with a wave front that travels al much lower speed than the longitudinal wave [18].

Examples of quasi-static impact are tools dropped on a structural component during maintenance. In these cases penetration or perforation is rarely experienced. However, damage can still be present and quite often will be below the surface and difficult to detect visually (Figure 2.14c).

Local response refers to the behaviour of the target within close proximity to the projectile contact point. As strike velocities increase, a target panel will exhibit increasing amounts of locally dominated response.

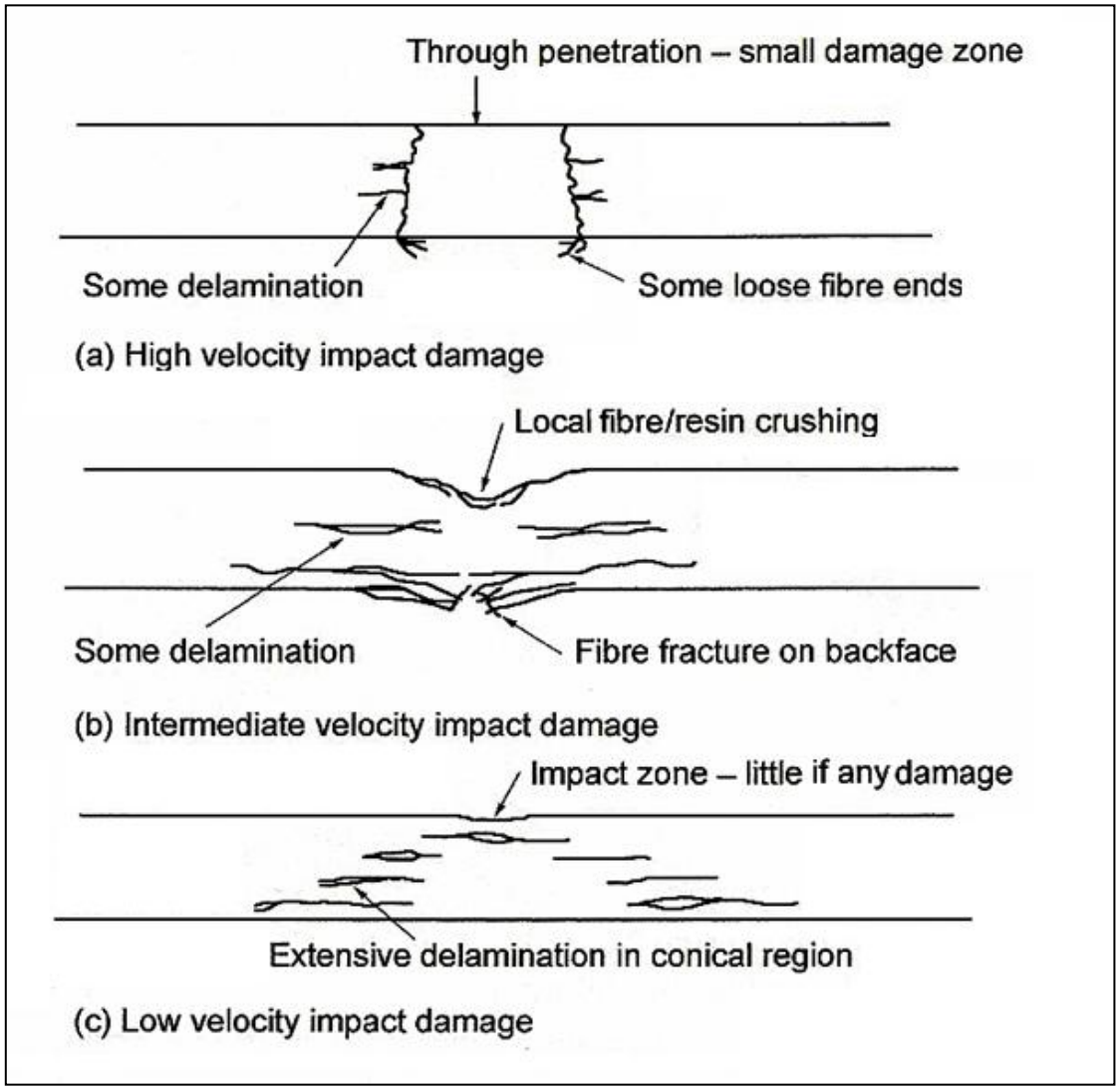

Figure 2.14. *Failure modes in laminated composites resulting from various impact velocities [18]*

Various failure mechanisms are covered next in approximately the order in which they may occur during a penetration event from low to high impact velocities [18].

Matrix cracking / delamination

Two types of matrix cracks have been identified which occur during both static and dynamic impacts. In practically all cases it has been concluded that these cracks serve as the initiation mechanisms for delamination, which is one of the most energy absorbing mechanisms in laminates [18].

1. *Transverse shear cracks* develop slightly away from the impact point at approximately 45º. This is due to the superposition of interlaminar shear stress and transverse normal stress (Figure 2.15 left).

2. *Bending cracks* appear in the bottom layers of the laminate, and are caused by the high in-plane tensile stresses induced by the bending of the plate (Figure 2.15 right).

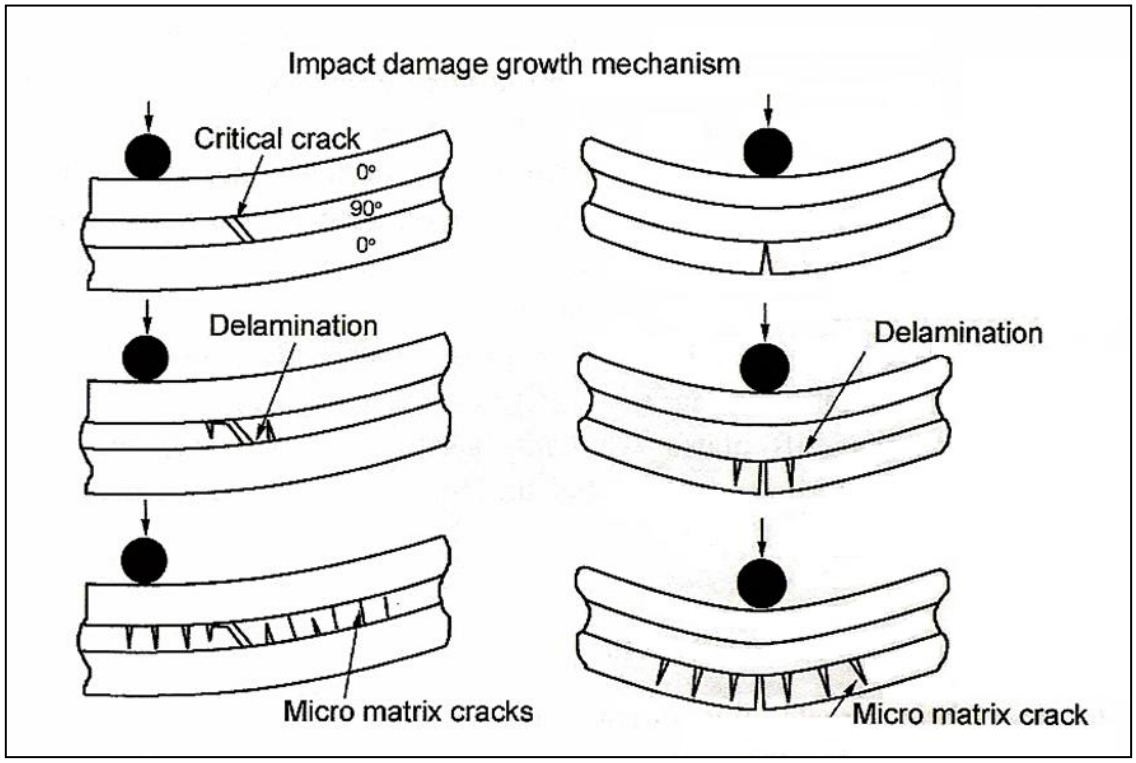

Figure 2.15. *Schematic description of two types of matrix cracks seen in laminated composites [18]*

Fibre breakage or petal formation

Increased bending beyond what causes delamination ultimately results in tensile fibre breakage at the backface of the panel, also referred to as fibre fracture petal, a term borrowed from metal failure modes [18].

Shear plugging

In high velocity impacts on hard and soft composites, the projectile may perforate the first few layers of the target upon impact. This phenomenon occurs more often with projectiles that have sharp edges, or when initial strain in the yarns exceeds their failure threshold.

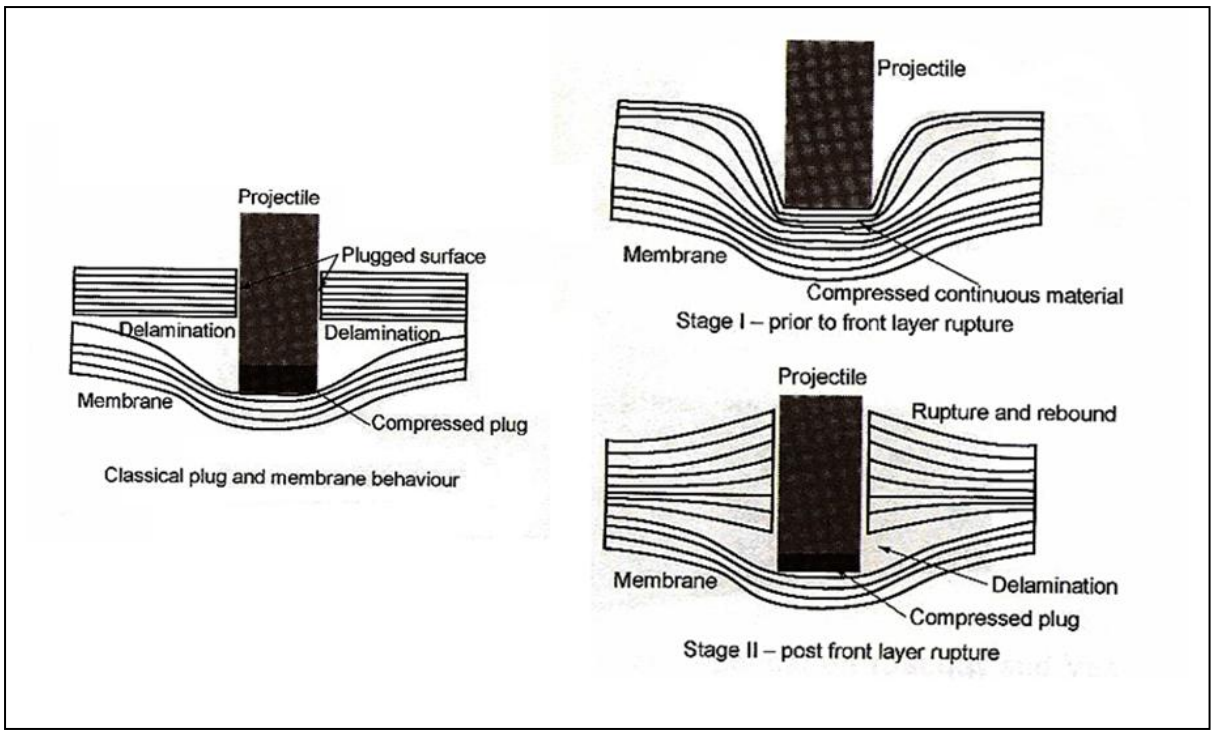

Figure 2.16. *Shear plugging [18]*

Hole expansion or Wedge through

In dry fabrics targets, this mechanism occurs when the projectile perforates the layers of the target by pushing the yarns aside. In general, the hole created by the projectile upon perforation of the target is usually smaller than its diameter, reinforcing the belief that there is always a certain amount of hole expansion present during perforation. This effect it is clearly shown in Figure 7.17, where the hole diameter (L) created during the first penetration stage, boxed in red, is smaller than the projectile diameter (D).

The energy absorbed through this mechanism is mainly in the form of the compression of the yarns around the projectile and the dissipated energy is due to the existing friction between yarns. However, the presence of this mode of perforation versus shear plugging in dry fabrics and laminates is highly affected by the projectile nose shape [18].

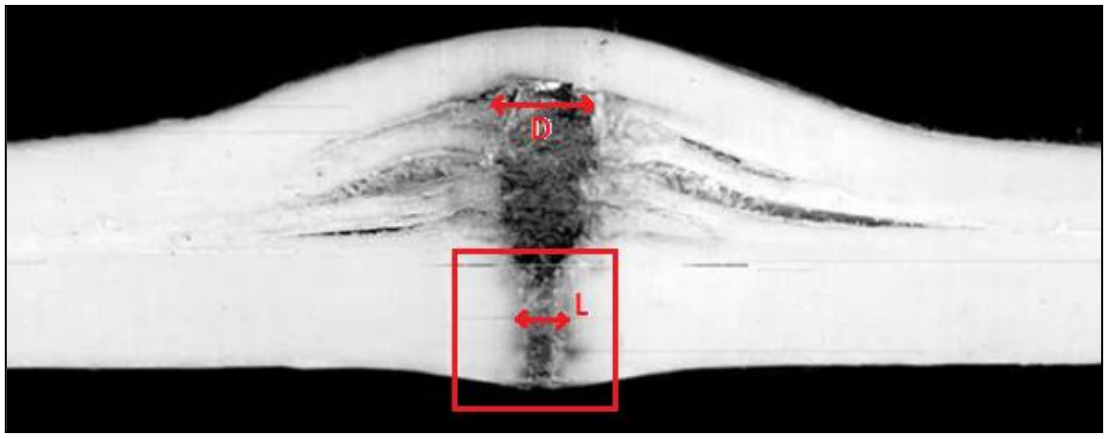

Figure 2.17. *Hole expansion [35]*

Hole friction

The final mechanism, common to all projectile types and most material systems is friction and it is the energy required to push the projectile through the crater created by either hole expansion or plugging. The frictional load is related to the length of penetrator in contact with the panel, the in-plane compressive stresses acting on the penetrator and the coefficient of friction between penetrator and composite [18]. Direction of frictional loads (red arrows) are opposite to the projectile motion (blue arrow), as it is shown in Figure 2.18.

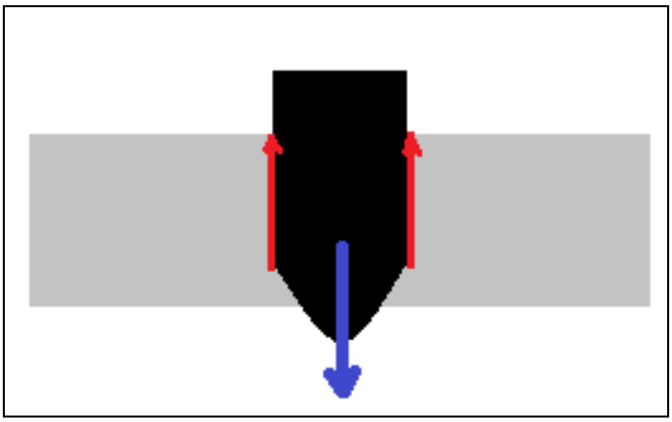

Figure 2.18. *Hole friction*

2.3.1. Key parameters of impact behaviour in composites

- ***Fibre type:*** each fibre type has different performance to impact. Materials with high energy absorption characteristics are considered ideal. High performance fibres and yarns commonly used in practice today are glass, aramid, PBO and polyethylene [18]. A comparison of materials for ballistic application is shown in Figure 2.19.

  In Figure 2.19 the sonic velocity is plotted versus the specific energy absorption capability of several polymeric fibres. Sonic velocity is $V_s = \sqrt{E/\rho}$, so ratio between stiffness and density is represented with this parameter. High performance fibres must fulfil some requirements like: high stiffness and low density. Hence the higher is the sonic velocity, better is the fibre.

  Finally, for impact applications, the best high performance fibres are at the upper right corner of the plot.

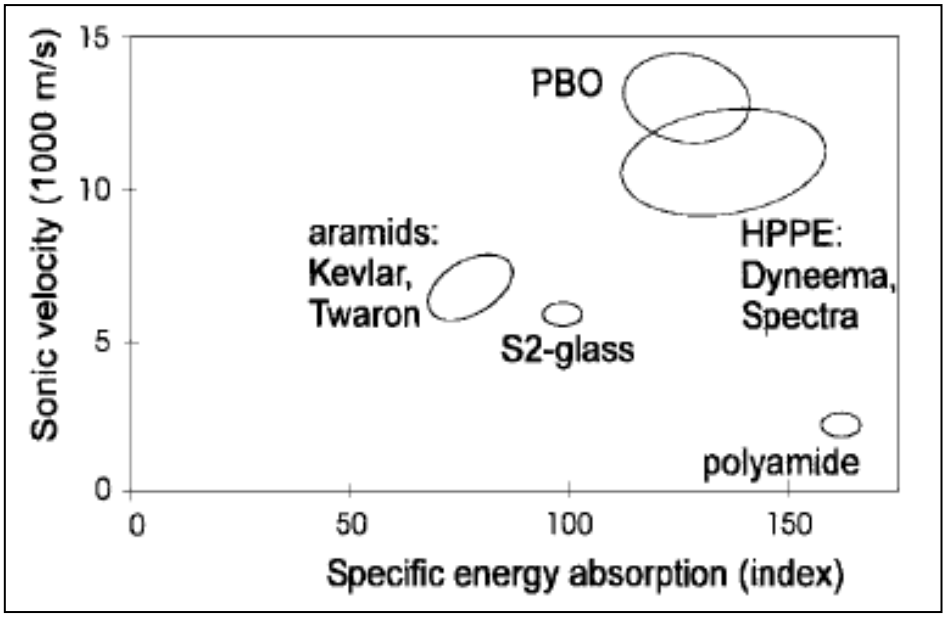

Figure 2.19. *High performance polymeric fibres [35]*

- ***Yarn structure:*** high performance yarns are typically made from filaments assembled together by twisting or entangling. It is known that twisting the yarns alter modulus and strength [18]. Manufacturing process must be done properly or yarn properties could be worse than properties of a single fibre.

- ***Strain rate sensitivity / temperature dependence:*** mechanical properties of high performance polymers are sensitive to the rate of loading and temperature, owing to relaxation and creep mechanisms [18].

  The influence of strain rate in different types of materials has been widely studied. For example, Chocron *et al.* [22] study the influence of strain rate on the mechanical properties of aramid and polyethylene woven fabric composites from tensile measurements provided by a Hopkinson bar and conventional testing machines. Experimental data obtained, show that:

  - *Tensile strength* increases continuously with strain rate, showing differences in the polyethylene composites between static and dynamic tests (six orders of magnitude in strain rate) near 60%. In the aramid composites the increase is also significant, but to a lesser extent.
  - *Failure strain* follows the opposite tendency, although the failure strain maintains similar values in slow and intermediate tests, showing a marked decrease at high strain rates.

  The stress-strain curve also depends on the strain rate; the general tendency is that dynamic stress-strain curves are more linear than the static ones and the elastic modulus increase with the strain rate. Figure 2.20 shows stress-strain curves at different strain rates for several composite materials.

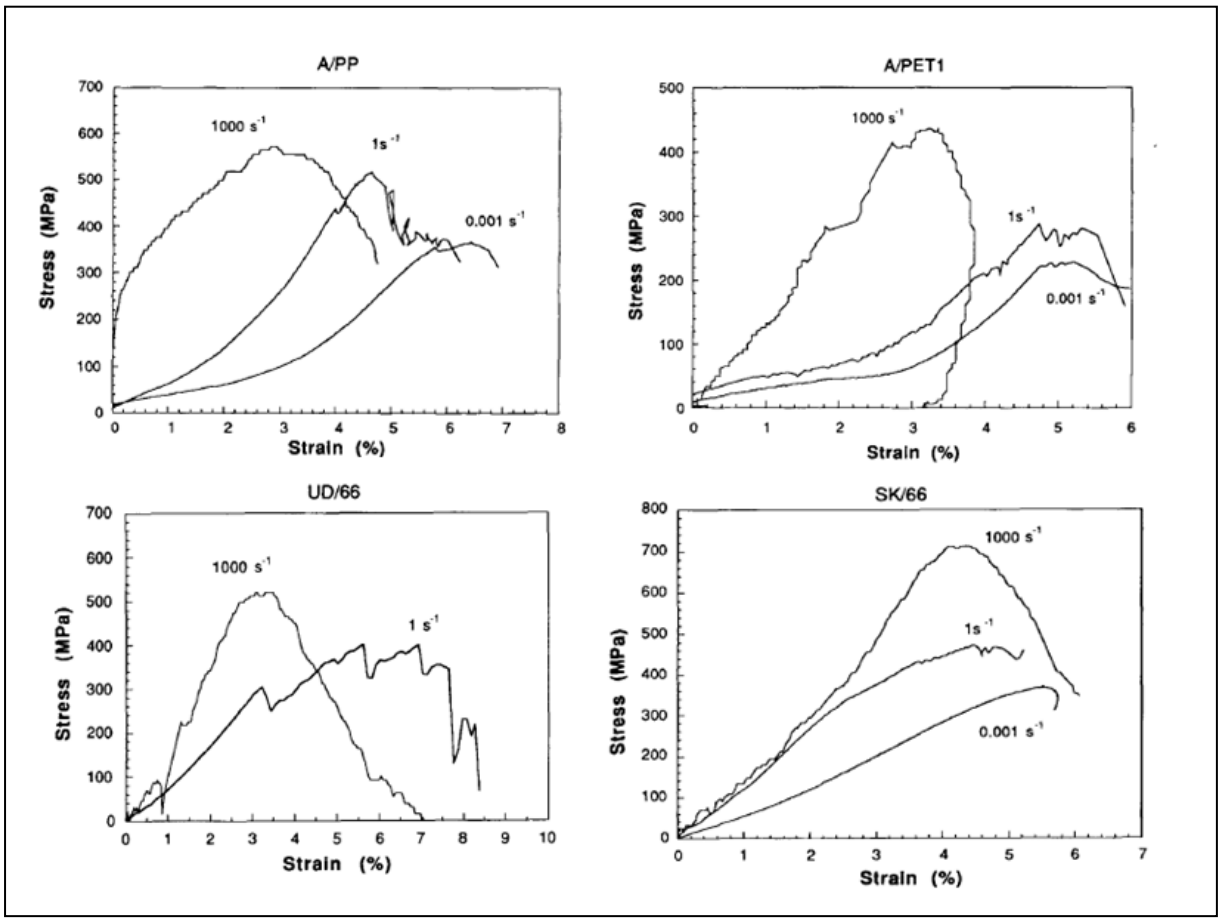

Figure 2.20. *Stress - strain curves at different strain rates for different composite materials [22]:*

- woven aramid / polypropylene (A/PP)
- woven aramid / polyethylenterftalate (A/PET)
- unidirectional polyethylene (UD/66)
- woven polyethylene (SK/66)

Xuesen [24] did also some experiments with aramid organic fibres (Twaron CT716) and fibre behaviour at different strain rates is in close agreement with data previously presented by Chocron *et al.* [22]. Elastic modulus and tensile strength increase continuously with the strain rate, as shown in Figure 2.21.

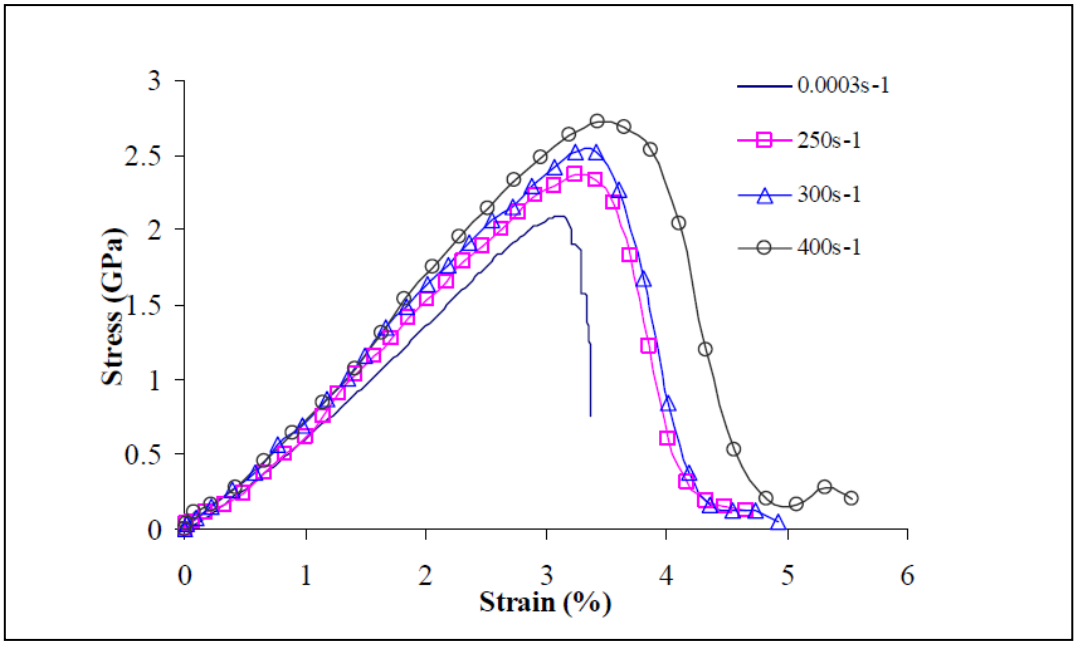

Figure 2.21. *Stress - strain curves of Twaron yarns at various strain rates [20]*

This behaviour of the fibres is the reason why these kinds of materials, which have been studied in the current project, are suitable for impact protection. During an impact event strain rate is high and at high strain rates is when organic fibres show the best performance.

- ***Fibre configuration:*** the most typical configurations used in soft and hard composites are unidirectional or fabric. Woven fabrics exhibit enhanced interlaminar fracture toughness [18].

- ***Lay-up and resin:*** when adding resin to a fabric to form a composite material there are two competing mechanisms for impact performance:

  - *Decrease the sound speed* in the fabric and, consequently also degrades the impact properties.

  - *Increase the number of yarns involved in the impact* hence improving the impact properties.

  Therefore for small threats (which require less areal densities) fabric without resin performs better than fabrics and for larger threats (which require high areal densities) composite with resin performs better than fabrics [10].

2.4. Bullets and fragments

In the current work two different bullets are used to develop the validation activities based on bibliography. For deformation tests a 9 mm Full Metal Jacket (FMJ) bullet is used and for penetration tests a Fragment Simulating Projectile (FSP) 1.1 g weight is used.

2.4.1. Full Metal Jacket bullet

A full metal jacket (or FMJ) is a bullet consisting of a soft core (usually made of lead) encased in a shell of harder metal, such as gilding metal, cupronickel or less commonly a steel alloy. The most common shell material is a copper alloy with approximately 70% copper and 30% zinc. This shell can extend around the entire bullet, or often just the front and sides with the rear left as exposed lead (a bullet that is completely enclosed by the shell is alternatively termed a total metal jacket round) [18].

The jacket allows for higher muzzle velocities than bare lead without depositing significant amounts of metal in the bore. It also prevents damage to bores from steel or armour-piercing core materials [18].

Figure 2.22. *9 mm Full Metal Jacket Bullets [17]*

The complete specifications of this bullet are:

- *Round length:* 29.28 mm
- *Case length:* 19.35 mm
- *Rim diameter:* 9.94 mm
- *Bullet diameter:* 9 mm
- *Bullet weight:* 7.45 g
- *Muzzle velocity:* 396 m/s
- *Muzzle energy:* 584 J
- *Core material:* lead
- *Shell material:* cartridge brass (alloy copper = 70% Cu + 30% Zn)

2.4.2. Fragment Simulating Projectiles

Fragments are generated when a bomb, grenade or artillery shell explodes. Since these explosive devices are made of hardened steel, fragments generated from explosions have variety of shapes and sizes and travel at different velocities respectively [18].

As the name indicates, fragment simulating projectiles (or FSPs) "simulate" a variety of features of fragments. These features are shape, size, geometry, cutting, penetrating and entanglement properties of large, medium and small fragments generated when a hardened steel device explodes [18]. Depending on calibre, FSP are classified according to Table 2.4

FSP Type	Diameter (mm)	Flat (mm)	Ref. Length (mm)	Weight (g)	Rockwell hardness
Calibre .22	5.39	2.54	6.35	1.1	30
Calibre .30	7.52	3.45	8.64	2.8	30
Calibre .50	12.57	5.69	14.73	13.4	30
20 mm	20.00	9.27	22.86	53.8	30

Table 2.4. *Different types of FSP [25]*

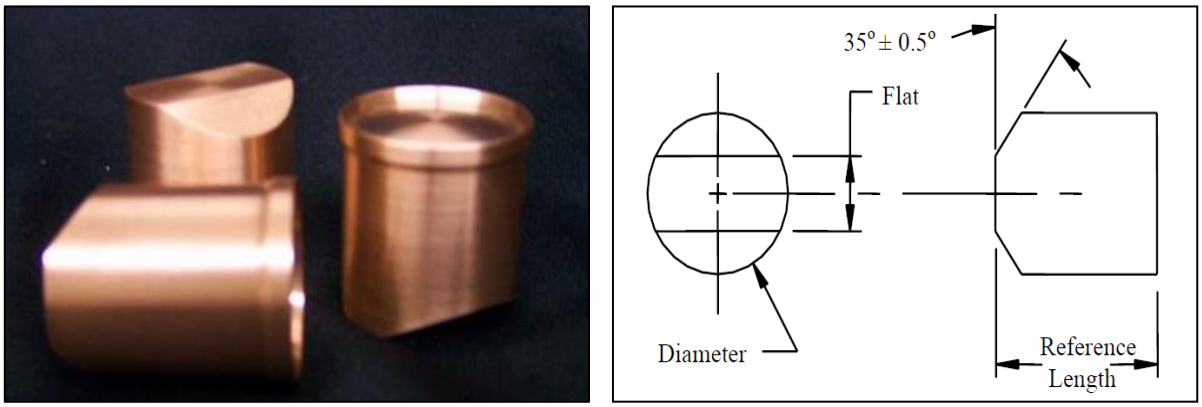

Figure 2.23. *Fragment Simulating Projectiles: real image (left) [17] and scheme (right) [25]*

FSPs are manufactured from cold rolled, annealed steel conforming to composition 4337H and 4340H. FSPs are classified as follows [25]. For the simulations done in this work, a FSP calibre .22 (1.1g weight) is used for penetration test according with standards NATO SATANG 2920, MIL-STD-662F and with data found in bibliographic research.

2.5. Standards and specifications

The standards and specifications are essential elements for the armour design and describe the guidelines for ballistic threads, testing equipment, physical conditions and procedures to test armour under the same specific conditions. The main reason for ballistic test standards is: better understanding of short and long-term behaviour of ballistic protections [18]. Standards and specifications of different countries are slightly different between them, but they keep more similarities than differences. Table 2.5 presents the most common standards.

Standard Name	Agency	Scope	Threats
NIJ 0108.01 Ballistic Resistant Protective Materials	US National Institute of Justice	Applicable to all ballistic resistant materials intended to provide protection against gunfire (no body armour and ballistic helmets)	Small calibre handguns to high-powered or armour-piercing rifles
NIJ 0101.04 Ballistic Resistance of Personal Body Armor	US National Institute of Justice	To establish minimum performance requirements for the ballistic resistance of personal body armour intended to protect torso against gunfire	Small calibre handguns to high-powered or armour-piercing rifles
NIJ 0106.01 Standard for Ballistic Helmets	US National Institute of Justice	To establish minimum performance requirements for helmets intended to protect head against gunfire	Handguns
EN 1063 Security Glazing. Testing and Classification of Resistance Against Bullet Attack	European Committee for Standardization	Specifies performance requirements and test methods for the classification of the bullet-resistance of glass	Small calibre handguns to high-powered or armour-piercing rifles
CEN prEN ISO 14876 Bullet Resistance and Knife Stab Resistance of Body Armor	European Committee for Standardization	Specifies performance requirements for bullet resistance and knife stab resistance of body armour	Handguns, rifles and shotguns
AS/NZS 2343 1997 Bullet Resistance Panels and Elements	Joint Technical Committee MS/43 (Australia and New Zealand)	Specifies requirements for bullet-resistant panels and elements according to their performance in preventing penetration by projectiles	Handguns, rifles and shotguns
Russia-GOST R 50744-95 Armor Clothes, Classification and General Technical Requirements	State Standardization Committee of Russian Federation	Specifies performance requirements and test methods for the ballistic resistance of armour clothes	Small calibre handguns to high-powered or armour-piercing rifles
NATO STANAG 4569 Protection Levels for Logistic and Light Armoured Vehicles	North Atlantic Treaty Organization	Describes the system qualification and acceptance procedure for determining the protection level of logistic and light armoured vehicles for artillery threats	Rifles and heavy guns
MIL-STD-662F V_{50} Ballistic Test for Armor	US Department of Defence	Provides general guidelines to determine the V_{50} ballistic limit of armour. Applicable to any type of armour	Handguns, rifles and heavy guns

Table 2.5. *List of the most utilized ballistic standards [20]*

2.6. Semi-analytical models. Predicting penetration and ballistic limit

One of the most important issues encountered in the study of penetration mechanisms under ballistic impact is the determination of the critical velocity above which a projectile will perforate a target. This particular property is commonly termed as ***ballistic limit (V_b)*** and it is very important in the design of protective systems against ballistic impact. Ballistic limit is also based on a statistical concept: ***ballistic limit velocity (V_{50})*** is defined as the velocity at which the projectile, striking a specified protection with zero yaw and obliquity, has a 50% chance of perforating the target [41].

In order to predict the behaviour of laminate composites (woven and unidirectional), some analytical and empirical models have been studied. Each model has particular hypothesis and restrictions which defines its application range.

Here, some key notes are given to understand properly how these models work and their application range.

2.6.1. Lambert and Jonas model

The deterministic approach to ballistic limits is an outgrowth of attempts to determine projectile performance during penetration trough development of models based on conservation laws and assumptions about the mechanical behaviour of the system. Much unpleasantness in modelling has been historically avoided by taking the penetrator to be nondeforming or rigid. Lambert and Jonas (1976) have observed that this approach generally leads to a form of the type [27]:

$$V_r = \begin{cases} 0, & 0 \le V_s \le V_l \\ a\left(V_s^p - V_l^p\right)^{1/p}, & V_s > V_l \end{cases} \qquad (2.1)$$

where

- V_r : projectile residual velocity
- V_s : projectile striking velocity
- V_l : limit velocity or ballistic limit

Mathematical structure described by Lambert and Jonas, on the basis of experimental and analytical analysis, seems appropriate for representing residual velocity as a function of striking velocity (and of projectile-target characteristics) for long rods impacting single-plate targets of rolled-homogeneous armour (RHA).

For a given projectile-target situation, the following notation is used:

- M : penetrator mass [g]
- L : penetrator length [cm]
- D : penetrator diameter [cm]
- T : target thickness [cm]
- ρ : target density [g/cm^3]

- θ : incidence angle
- V_l : limit velocity or ballistic limit (or an estimation) [m/s]
- V_r : penetrator residual velocity [m/s]
- V_s : penetrator striking velocity [m/s]

Equations are provided for predicting the parameters *a*, *p* and V_l in the context of the "standard" general form used to encompass V_s and V_r of Equation 2.1.

i). Ballistic limit (V_l): Equation 2.2 shows the relation obtained by Lambert and Jonas between ballistic limit and other parameters that are involved in the impact event

$$\frac{MV_l^2}{D^3} = \alpha \left(\frac{T}{D}\right)^c f(z) \tag{2.2}$$

solving equation 2.2, ballistic limit estimation is

$$V_l = \sqrt{\alpha \left(\frac{L}{D}\right)^c f(z) \frac{D^3}{M}} \tag{2.3}$$

where

- k : constant (e.g. *k = 1*, recovers the length trough the target of the projectile line of fire)
- $z = \frac{T(sec\theta)^k}{D}$
- $f(z) = z + e^{-z} - 1$

ii). Empirical parameter (a): a new relation to calculate parameter *a* is shown in Equation 2.4.

$$a = \frac{M}{M + M'/3} \tag{2.4}$$

where:

- M' : approximately (exactly in the case of normal impact) the mass of target material projected in front of the penetrator

iii). Projectile parameter (p): traditional rigid-penetrator theory almost invariably leads to a model corresponding to Equation 2.1 with *p* fixed at 2. Such models have been highly successful in instances where the penetrator suffers little or no deformation. Lambert and Jonas therefore requires *p* to be sensitive effective target thickness in calibers (i.e. to $z = T/D(sec\theta)^k$. A simple appropriately behaved function that was found to be effective is:

$$p = 2 + \frac{z}{3} \tag{2.5}$$

2.6.2. Navarro model

Navarro [30] [31] developed an analytical model of composite panel subjected to impact loading. First of all, the behaviour of single fibre subject to transverse impact is studied. Applying the one-dimensional elastic wave theory, it can be shown two travelling waves start to propagate from the impact point (Figure 2.24): *longitudinal* and *transverse* waves.

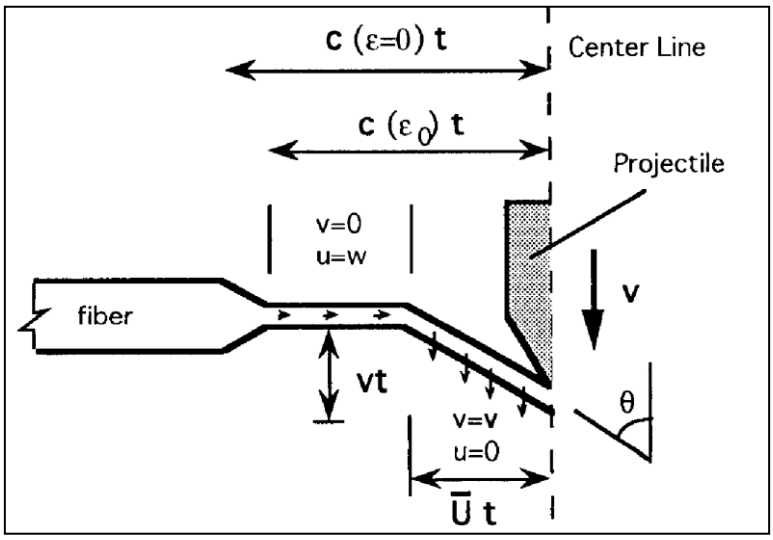

Figure 2.24. *Scheme of a projectile impacting in a single fibre [30]*

The decelerating force *F*, exerted by the fibre on the impactor, can be calculated as follows [30]:

$$F = 2\sigma S_f cos\theta \tag{2.6}$$

where:

- σ : normal stress acting on the fibre cross-section
- S_f : fibre cross-section area
- θ : angle formed between the part of the fibre affected by the transverse wave propagation and the projectile direction

Assuming a linear elastic behaviour for the fibre material, the fibre stress could be computed simply as the product of the fibre's Young modulus (*E)* and the fibre strain (*ε)*.

When a set of *n* identical parallel fibres are impacted by an impactor the motion equation can be written stating Newton's second law as follows (equation 2.7):

$$-2\frac{ES_f n}{m_p}\frac{\varepsilon z}{l} = \frac{d^2 z}{dt^2} \tag{2.7}$$

being m_p the projectile mass, and *z* and *l* respectively, the projectile advance and the actual fibre length affected at time *t* by the transverse wave.

2.6.3. Chocron *et al.* model

The analytical model developed by Chocron *et al.* [32] subdivides a very complex phenomenon, like high velocity impact on composites, into more simple and understandable problems. Assuming a brittle matrix is added to the fabric and that tensile waves reflecting from the rear of the armour break the matrix during the impact, it is possible to build a simple set of ordinary differential equations.

Based on an analytical model for impact on a yarn developed by Smith in 1958, Chocron *et al.* developed an analytical model for impact onto a fabric. The equation of motion of the projectile can be written following the Newton's second law and assuming that: the fabric behaviour is unidirectional even if it is woven, the strain is uniform for all layers under the projectile and only yarns in direct contact with the projectile contribute to its slowing down. Hence, the force can be explicitly written as:

$$F_y = E \cdot \varepsilon \cdot n \cdot S \cdot n_l \cdot cos\theta \tag{2.8}$$

where:

- F_y : component of the force in the direction of motion
- E : Young's modulus of the yarns
- ε : the strain of the fabric under the projectile
- n : number of yarns in direct contact with the projectile
- S : section of the yarn
- n_l : number of layers of the fabric

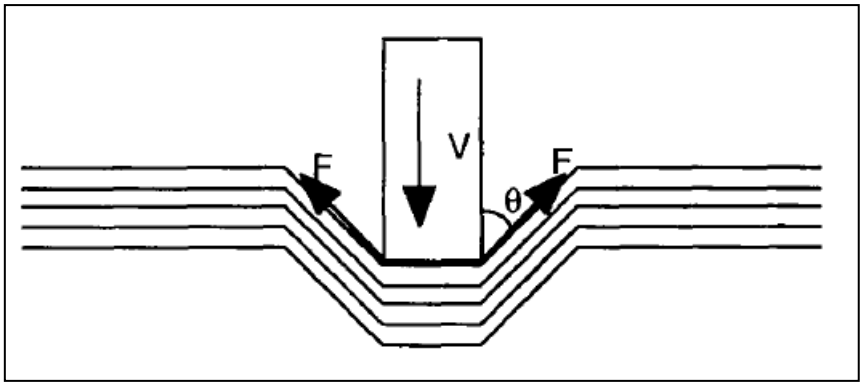

Figure 2.25. *Sketch of the impact of a projectile onto a fabric [32]*

The last step is the failure criterion. Energy absorbed by the fabric when full perforation occurs should be constant independently of the impact velocity. This hypothesis together with the energy equation which states that the energy lost by the projectile during the impact has to be equal to the energy distributed in the fabric:

$$\frac{1}{2}M_p(V_s^2 - V_r^2) = \frac{1}{2}n \cdot n_1 \cdot S \cdot E \cdot c \int_0^t \varepsilon^2(t)dt \tag{2.9}$$

allows the adoption of a new failure criterion where the unknown is the time of failure of the fabric:

$$\frac{M_p V_{50}^2}{n \cdot n_1 \cdot S \cdot E \cdot c} = \int_0^{t_{vs}} \varepsilon^2(t)dt = R \tag{2.10}$$

where:

- R : failure constant, only dependent on the configuration
- t_{vs} : time of the failure
- V_{50} : ballistic limit
- V_s : strike velocity
- V_r : residual velocity

The constant R must be obtained experimentally for one reference configuration (called R_0) whilst for other configurations (called configurations *i*) its value can be analytically found in the following manner:

$$R_i = R_0 \frac{(M_p)_i}{(M_p)_0} \frac{n_0}{n_i} \frac{(n_l)_0}{(n_l)_i} \frac{(V_{50}^2)_i}{(V_{50}^2)_0} \tag{2.11}$$

2.6.4. Bless and Hartman model

The analytical model developed by Bless and Hartman [33] is based in their experience with glass fibre reinforced plastic. After examination of the post-test appearance of targets impacted at just above ballistic limit reveals that there is a region which appears to have experienced compressive failure and expulsion of sheared fibres, followed by a region dominated by tensile failure and shearing of fibres. So, there are two principal physical mechanisms that can be postulated for defeat of composite targets:

- Shear failure around the periphery of the penetration cavity.
- Compressive flow around the penetrator.

Final equation proposed by the authors was:

$$V_{LP} = \frac{T_{pl}}{D_p} \sqrt{\frac{\pi \cdot \tau_{tr}}{g_c \cdot \rho_{pr}}} \tag{2.12}$$

where:

- V_{LP} : ballistic limit
- T_{pl} : plate thickness
- D_p : projectile diameter
- τ_{tr} : effective transverse (trough the thickness) strength of the composite
- g_c : projectile shape factor (equal to 0.86 to fragments simulating projectiles)
- ρ_{pr} : density of the projectile

2.6.5. Caprino *et al.* model

Caprino *et al.* model [34] belongs to the empirical models for predicting the ballistic limit. Empirical approaches remark effect of parameters such as projectile diameter and laminate thickness on quantities of interest such as the penetration energy or the ballistic limit.

It has been studied that the most effective parameters in penetration energy *(U_p)* are: fibre areal weight and the impactor diameter (D_t). According to some researchers, the penetration energy for a given laminate linearly increases with increasing *t* (i.e. areal weight). However, recent data demonstrate that this is not the case and instead of linearly increasing, U_p increase more than linearly with the thickness. Some examples could be that the dependence of the penetration energy on *t* for CRFP laminates are well described by a power law having exponent 1.5, or an exponent of 1.35 for GRP.

Finally, the effect of both the thickness and the impactor diameter could be modelled by power laws having practically the same exponent; it is suggested the following empirical relationship:

$$U_p = K\left(t \cdot V_f \cdot D\right)^{\alpha} \tag{2.13}$$

where:

- U_p : penetrator energy
- t : laminate thickness
- V_f : fibre volume fraction
- D : diameter of the projectile
- K, α : laminate material parameters to be determined from the experimental data

Caprino shows in his work some values for the material parameters (Table 2.6). In particular, characteristics of CFRP (Carbon Fibre Reinforced Polymer), GRP (Glass Reinforced Polymer) and PC (poly-carbonate).

Material	K (J/mm$^{2\alpha}$)	α
CFRP	0.49	1.40
GRP	0.90	1.30
PC	0.35	1.42

Table 2.6. *Values of the constants α and K for some materials [34]*

The similarity of α values raises the question whether this parameter is actually material dependent, or rather it can be considered a constant of general applicability. This is investigated but experimental results showed that the scatter in the experimental data does not allow to judge which of them is the most efficient in predicting penetration energy. Therefore, the assumption of a single α value having a general applicability cannot be rejected.

2.6.6. Jacobs and Van Dingenen model

The model developed by Jacobs and Van Dingenen [35] is empirical and based on the phenomenological description of the impact processes. It considers the projectile deformation.

When stopping a bullet, two aspects have to be considered: the change of penetration mode and the deformation of the bullet. The first layers are penetrated without significant deformation of the projectile; while the last layers are penetrated partially or not penetrated at all. It is assumed that after deformation the bullet again behaves as a non-deformable projectile, with a larger strike face. The assumptions of this model are that energy of is absorbed in three stages:

1. First penetration. Non-deformable projectile at initial strike face area. Experimental tests did reveal a relation between some parameters: areal density of the composite material, strike face area of impactor and energy absorbed during impact by composite. Relation is shown in Equation 2.14.

$$\frac{E_{abs1}}{S_1} = AD_1 \times C \tag{2.14}$$

where:

- E_{abs1} : absorbed energy during stage 1 [J]
- S_1 : strike face area in stage 1 [mm^2]
- AD_1 : areal density of the ballistic package in stage 1 [kg/m^2]
- C : ballistic material related constant (it is the slope of the curve when the ratio between the energy and the strike face area versus the areal density is represented, Figure 2.26) [$J \cdot m^2/mm^2 \cdot kg$] or [$10^6 \cdot m/s$].

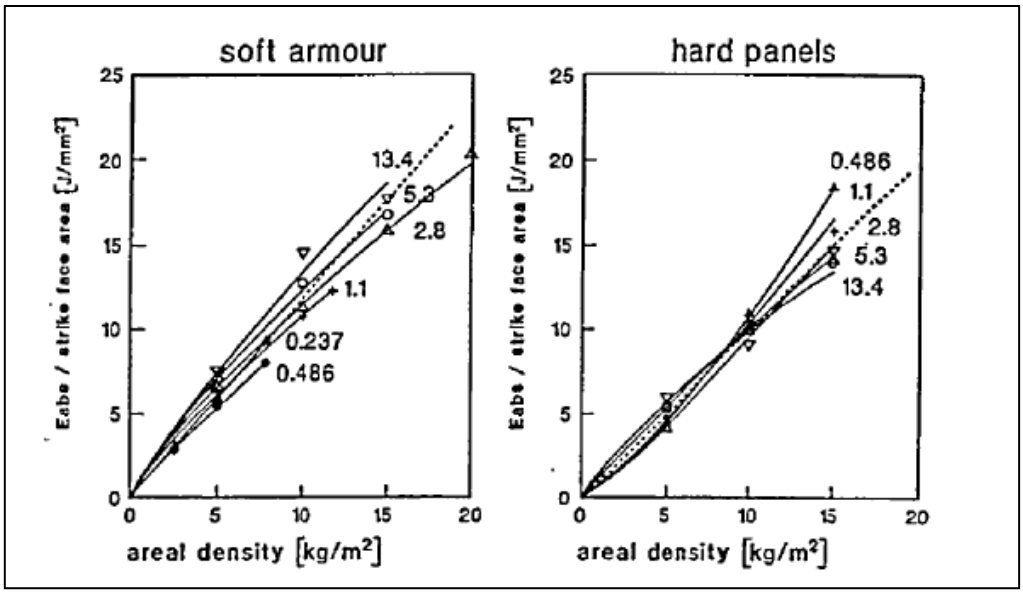

Figure 2.26. *Normalised energy absorption versus areal density [35]*

2. Deformation of the bullet. In the deformation stage the bullet deforms instantaneously, a process wherein a fraction of its energy (E_{absB}) is absorbed. This energy is assumed to be constant for a given bullet and independent from its velocity.

3. Second penetration. Non-deformable projectile at larger strike face area. In the third stage the bullet behaves again like a non-deformable projectile (but with the larger strike face area, S_2) and the areal density (AD_2) corresponds with the laminate plies that have not been penetrated yet.

$$\frac{E_{abs2}}{S_2} = AD_2 \times C \tag{2.15}$$

where:

- E_{abs2} : absorbed energy during stage 2 [J]
- S_2 : strike face area in stage 2 [mm^2]
- AD_2 : areal density of the ballistic package in stage 2 [kg/m^2]

At ballistic limit for the complete system, the total kinetic energy of the bullet will be exactly consumed in the package. In the model the energy that remains after the two first stages, will also corresponds with the ballistic limit for the deformed bullet in the last part of the ballistic package, therefore:

$$E_p = E_{abs1} + E_{absB} + E_{abs2} \tag{2.16}$$

substituting

$$\frac{1}{2} m_p {V_b}^2 = C \cdot AD_1 \cdot S_1 + E_{absB} + C \cdot AD_2 \cdot S_2 \tag{2.17}$$

considering some factors to simplify equation (e.g. $S_1 = f_{s1} \cdot S$).

$$\frac{1}{2} m_p {V_b}^2 = C \cdot AD \cdot S \cdot (f_{s1} f_{AD1} + f_{s2} f_{AD2}) + E_{absB} \tag{2.18}$$

Finally, ballistic limit may be calculated as:

$$V_b = \sqrt{{}^{2}/_{m_p} \left[C \cdot AD \cdot S \cdot (f_{s1} f_{AD1} + f_{s2} f_{AD2}) + E_{absB} \right]} \tag{2.18}$$

In order to calculate for a bullet either the V_b at a given areal density or the areal density at a given velocity, one extra datum is needed. The two strike face areas can be measured, C is a material related constant (that can be measured using FSPs), the total energy absorbed in the three stages is equal to the kinetic energy and the sum of the areal densities AD_1 and AD_2 is the total areal density of the package.

Remark that *f* parameters introduced in Equation 2.18 are non-dimensional.

2.6.7. Van Gorp *et al.* model

Van Gorp *et al.* [36] developed a semi-empirical model to predict the protection offered by Dyneema (polyethylene fibres) against known threat from shrapnel. The model is based on the measurements of V_b values for different FSPs versus areal density. A simple relation of energy absorption and the surface area of the strike face of the fragment is derived.

The presented model is similar to the model of Jacobs and Van Dingenen [35] (DSM co-workers) and is based on the same assumptions, but in this case the authors presented simpler equations and specific for one type of impactor: FSP.

The model is based on the findings of Figure 2.26. This figure (same used in Jacobs and Van Dingenen model) shows for FSPs the relation between the energy absorption and the surface area of strike face of the fragment on the one hand and the areal density on the other. As a first estimate, this relation is linear and independent of the size of the fragment. So the following equations can be derived:

$$\frac{E_{abs}}{S} = AD \times C \tag{2.19}$$

$$E_{abs} = \frac{0.5 \cdot W \cdot {V_{50}}^2}{1000} \tag{2.20}$$

where:

- E_{abs} : absorbed energy [J]
- S : surface area of the strike face area of the FSP [mm^2]
- AD : areal density of the armour [kg/m^2]
- W : FSP weight [g]
- C : material constant [$J \cdot m^2/mm^2 \cdot kg$] or [$10^6 \cdot m/s$]
- V_{50} : ballistic limit [m/s]

The FSPs as defined by NATO STANAG 2920 have a constant relation between weight, diameter and strike face area (being *D* the projectile diameter in mm)

$$W = 0.007 \cdot D^3 \tag{2.21}$$

$$S = 0.785 \cdot D^2 \tag{2.22}$$

A combination of these equations results in the following simple formulas for the protection model (with *K* material related constant)

$$V_{50} = C \cdot AD^{0.5} \cdot W^{-1/6} \tag{2.23}$$

In the paper some material constants values (C) are given for different kinds of material, for example, some of them are the following:

- Soft Dyneema: 227 $J \cdot m^2/mm^2 \cdot kg$
- Hard Dyneema: 207 $J \cdot m^2/mm^2 \cdot kg$

2.6.8. Wen model

Wen [37] presented a projectile-target interaction model that predicts penetration and perforation of FRP laminates. It is assumed that the mean pressure (σ) applied normally to the surface of the projectile can be decomposed into two parts: one part is the cohesive quasi-static resistive pressure (σ_s) due to the elastic-plastic deformations of the laminate material and the other is the dynamic resistive pressure (σ_d) arising from velocity effects.

Finally, the equation presented by Wen for penetration of FRP is:

$$V_b = \frac{\pi\beta\sqrt{\rho_t\sigma_e}D^2T}{4G}\left[1+\sqrt{1+\frac{8G}{\pi\beta^2\rho_tD^2T}}\right] \qquad (2.24)$$

where:

- V_b : ballistic limit
- β : shape parameter (depends on projectile nose)
- ρ_t : laminate density
- σ_e : laminate resistive pressure trough the thickness
- D : projectile diameter
- T : laminate composite
- G : projectile mass

Depending on the projectile shape two different values of parameter β can be defined:

1. Conical nosed projectiles

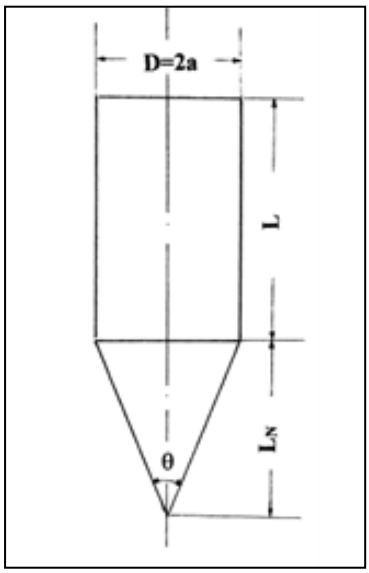

These kinds of projectiles are characterized by nose angle (θ) and by a parameter that depends on it:

$$\beta = 2\sin\left(\theta/_2\right) \qquad (2.25)$$

Flat faced projectiles are a specific case of conical nosed projectiles with a con angle of 180º.

Figure 2.27. *Conical nosed projectile geometry [37]*

2. Ogival nosed projectiles

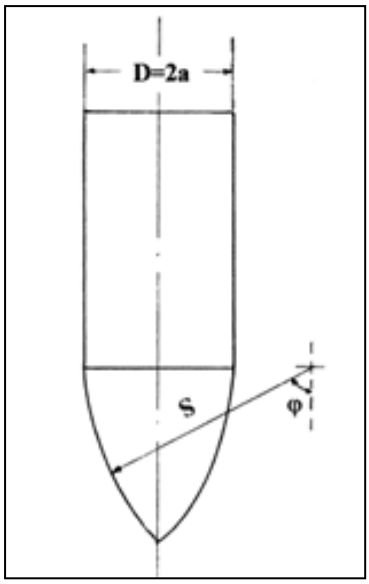

These kinds of projectiles are characterized by calibre radius head (ψ) and by a parameter that depends on it:

$$\psi = {}^{s}/_{2a} \tag{2.26}$$

$$\beta = {}^{3}/_{4\psi} \tag{2.27}$$

A hemispherical-ended projectile can be seen as the special case of an ogival nosed projectile with $\psi = 0.5$.

Figure 2.28. *Ogival nosed projectile geometry [37]*

2.6.9. Song and Egglestone model

Song and Egglestone [27] derived a complex relationship between the ballistic limit and areal density of relatively thin flexible composites in the following equation:

$$V = \gamma(A_d)^{\delta} \tag{2.28}$$

where A_d is the areal density of the laminate and γ and δ are constants closely related to the material properties as well as the laminate configurations of target. The empirical relationship of Equation 2.28 was used to fit curves of Figure 2.29.

Although the data shown in Figure 2.29 are the result of complicated treatment of several parameters, it illustrates the importance of them for optimization of composite protections.

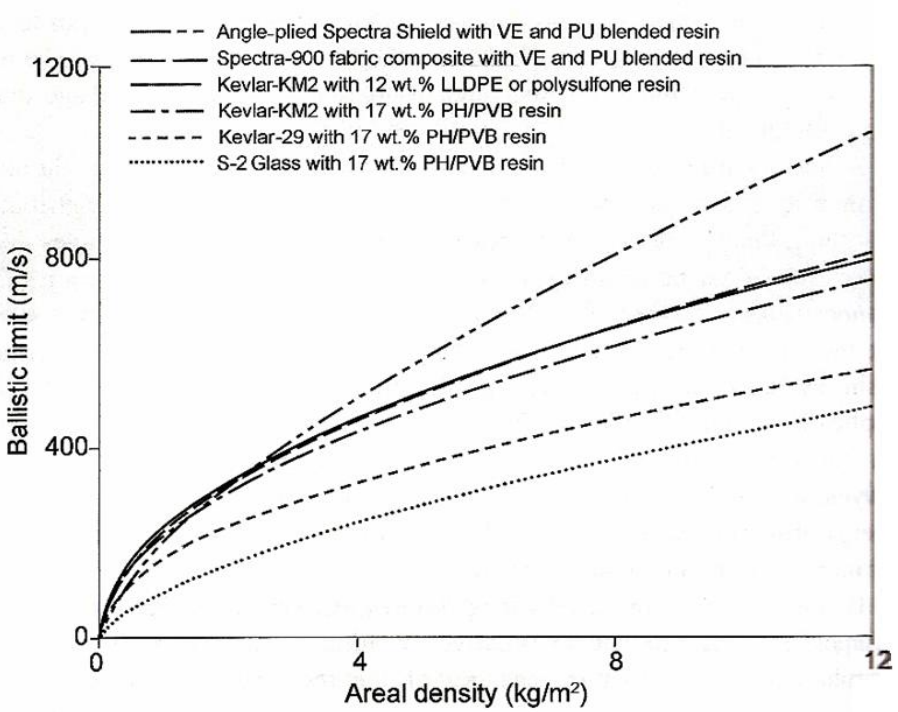

Figure 2.29. *Ballistic limit versus areal density with an FSP 1.1g impactor [27]*

Spectra shield shows better performance than Spectra fabric composite. This result illustrates the importance of the effect of configuration of reinforcement fibres. The differences between fibres can also see in S-2 Glass / PH-PVB, Kevlar 29 / PH-PVB and Kevlar KM2 / PH-PVB. The effect of resin types and contents are also shown in Kevlar KM2 composites.

	S-2 Glass / PH-PVB	Kevlar 29 / PH-PVB	Kevlar KM2 / PH-PVB	Kevlar KM2 / LLDPE	Spectra 900	Spectra shield
γ	98.81	157.59	216	234	223	200
δ	0.64	0.56	0.502	0.492	0.518	0.67

NOTE: PH-PVB: Phenolic Polyvinyl Butyral and LLDPE: Linear Low Density Polyethylene

Table 2.7. *Values of constants for different fibre reinforcements and resin systems [27]*

Table 2.8 presents a summary of some semi-analytical models considering input data and some notes related to applicability. From all models studied, only five of them are used due to simplicity of formulation and available data in literature. Constants of materials for each semi-analytical model are written in red.

MODEL	EQUATION	INPUT		OUTPUT	NOTES
		Material constants	Properties of composite and impactors		
BLESS and HARTMAN [33]	$V_{LP} = \frac{T_{pl}}{D_p}\sqrt{\frac{\pi \cdot \tau_{tr}}{g_c \cdot \rho_{pr}}}$	τ_{tr}	T_{pl}, D_p, g_c, ρ_{pr}	V_{LP}	- Constant material is the trough thickness shear stress. - Impactor is considered with high stiffness.
CAPRINO [34]	$U_p = K\left(t \cdot V_f \cdot D_t\right)^{\alpha}$	K	T, D_t, α, M, V_f	$U_p \rightarrow V_b$	- Simple model for low velocity impacts. - Constant is the dimensional value K. - α may be fixed at 1.4
JACOBS and VAN DINGENEN [35]	$V_b = \sqrt{{}^{2}/_{m_p}\left[C \cdot AD \cdot S \cdot (f_{s1}f_{AD1} + f_{s2}f_{AD2}) + E_{absB}\right]}$	C	E_{abs}, E_{absB}, AD, m_p, S	V_b	- Consider deformation of the bullet. - Impactor stiffness may be controlled by *f* parameters and by E_{absB}. - E_{absB} and *f* parameters may be assumed or extrapolated by data found in bibliography - Constant is the dimensional value C.
VAN GORP [36]	$\frac{E_{abs}}{S} = AD \times C$	C	AD, S	$E_{abs} \rightarrow V_b$	- Impactor is considered with high stiffness. - Simple equation. - Easy to find available data. - Constant is the dimensional value C.
WEN [37]	$V_b = \frac{\pi\beta\sqrt{\rho_t\sigma_e}D^2T}{4G}\left[1 + \sqrt{1 + \frac{8G}{\pi\beta^2\rho_t D^2 T}}\right]$	σ_e	ρ_t, D, T, G, β	V_b	- Many composite and impactor parameters have been considered. - Impactor is considered with high stiffness. - Constant material is the laminate resistive pressure trough the thickness.

Table 2.8. *Summary of some semi-analytical models*

CHAPTER III. NUMERICAL SIMULATIONS

3.1. Introduction

In this chapter, impact numerical simulations were done using PamCrash, a commercial non-linear explicit FE code. Every numerical simulation requires the definition if the next factors:

- ***Impactor:*** is the solid fragment that hits against panel protections. In first simulations, this impactor is an FMJ bullet and FSP. In next chapter, in aeronautical applications, the impactors are gas turbine fragments and ice slices.

- ***Initial velocity:*** impactors travel at different velocities until impact against protections.

- ***Protection (or shield):*** element designed specifically to protect an area from an impact. In this project, protections studied are based on laminate of organic fibres.

- ***Boundary conditions:*** are defined at protection panel sides. Normally four edges of panels are fixed. In most of cases developed in PamCrash, quarter models have been simulated due to symmetry, hence symmetric conditions were also defined.

- ***Contact:*** between impactor and protections. In addition a self-contact is defined to avoid some problems like the material inter-penetration.

The main goal of this chapter is to define two material models for two types of fibres: aramid and polyethylene. To obtain and validate numerical material models, an extensive bibliographic research has been done. First the models are presented and then explained the validation activities performed to decide which material model is more suitable to every application.

3.2. Numerical models of protection laminates

3.2.1. Types of models

When doing computer numerical simulations, the modelling of composite materials can be developed in different ways. A normal classification from global to detailed models may be following:

i). Homogeneous model: properties of the entire composite material are taken into account without considering the specific properties of fibres and matrix. The composite is modelled as an homogeneous material. The properties of the laminate are considered, as if was a one phase material. In this kind of modelling two types of models can be done:

- *Isotropic model*: properties uniforms in all directions.

- *Orthotropic model*: properties uniform in the laminate plane, but different in the out-of-plane direction.

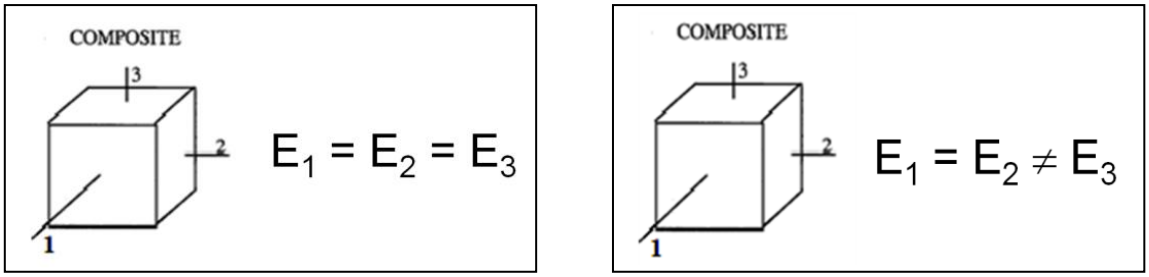

Figure 3.1. *Isotropic material (left) and orthotropic material (right)*

ii). Non homogeneous model. Ply model: in this case, when representing the material, it is considered as heterogeneous material. Each ply of the material is represented independently. Plies can have very different properties, defined by fibres direction.

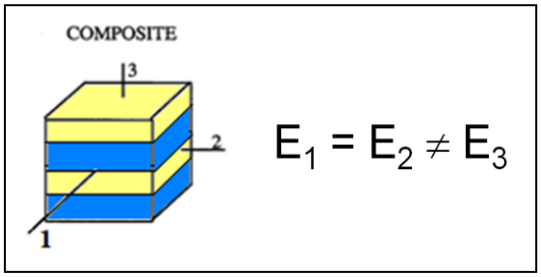

Figure 3.2. *Ply model*

iii). Fibre-matrix. Ply model: is a heterogeneous material model in which the material properties are calculated by superimposing the effects of matrix and fibres. Figure 3.3 shows how fibres and matrix properties are introduced independently.

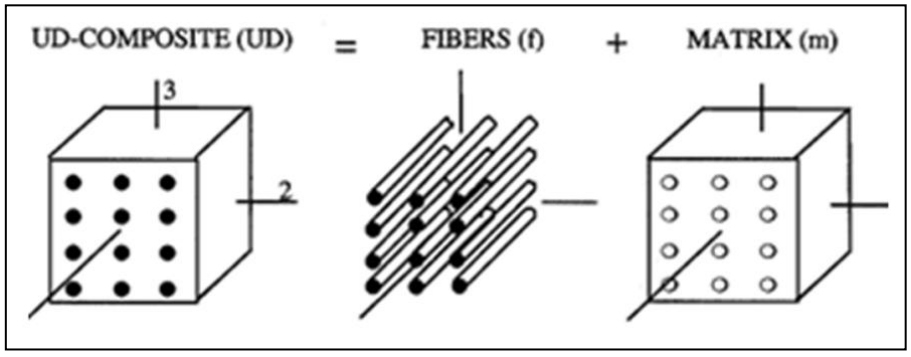

Figure 3.3. *Fibre-matrix model [43]*

Two main references have been studied in order to obtain the necessary information to develop material models in PamCrash for aramid and polyethylene composite materials:

- Colakoglu *et al.* [38] [39] [40] performed experimental tests and numerical simulations on Kevlar 29 / polyvinyl butyral woven composite and on Dyneema HB2 unidirectional composite. The model presented is a homogeneous isotropic elastic-plastic model.

- Silva *et al.* [41] did numerical simulations based on experimental test using Kevlar 29 / vynilester woven composite. The model presented is a homogeneous orthotropic model.

When representing the elements of the composite plates, shell or solid elements may be used. As a general rule, shell elements are more suitable for representing low thickness laminates, while solid elements allow good description of penetration and erosion thick laminates:

- *Shell elements:* low thickness (≤ 2 mm).
- *Solid elements:* high thickness (> 4 mm).

3.2.2. Isotropic homogeneous model

Colakoglu *et al.* [38] [39] [40] present in their study a bi-linear elastic-plastic model to describe the performance of the composite materials. The objective of this study was to investigate the ballistic performances of two different polymer matrix composites used as light ballistic armour. Backside deformation and penetration speed were analyzed experimentally and numerically. Composite materials were:

- *Kevlar 29 / polyvinyl butyral*. It is a woven fabric, hence the elastic modulus of the lamina is the same in principal directions ($E_1 = E_2$). Composite specimens are manufactured at 160°C under 6.5 MPa pressures for a total pressing time of 15 min [39].

- *Dyneema (UHMWPE UD-HB2)*. Every lamina of Polyethylene has 0º and 90º fibre layers on it. Therefore, the elastic modulus of the lamina is also the same in principal directions ($E_1 = E_2$). Polyethylene fibre composite specimens are manufactured at 125°C under 20 MPa pressures for a total pressing time of 30 min [39].

The specimens were first subjected to tension test to obtain mechanical properties. The results are shown in the Table 3.1.

MATERIALS	Modulus (GPa)	Density (kg/m^3)	Tensile Strength (Pa)	Failure Strain (%)
Kevlar 29	9	1160	$450 \cdot 10^6$	9
Dyneema HB2	19.5	900	$650 \cdot 10^6$	7

Table 3.1. *Mechanical properties of composites [39]*

Once characterize the properties of the materials composite the author exposes the following homogeneous isotropic elastic plastic models:

- Kevlar 29 / polyvinyl butyral is taken to be elastic, with E = 9 GPa and ν = 0.08, up to a stress of 450 MPa, and after which is to be perfectly plastic [39].

- Dyneema HB2 is taken to be elastic, with E = 19.5 GPa and ν = 0.3, up to a stress of 650 MPa, and after which is to be perfectly plastic [39].

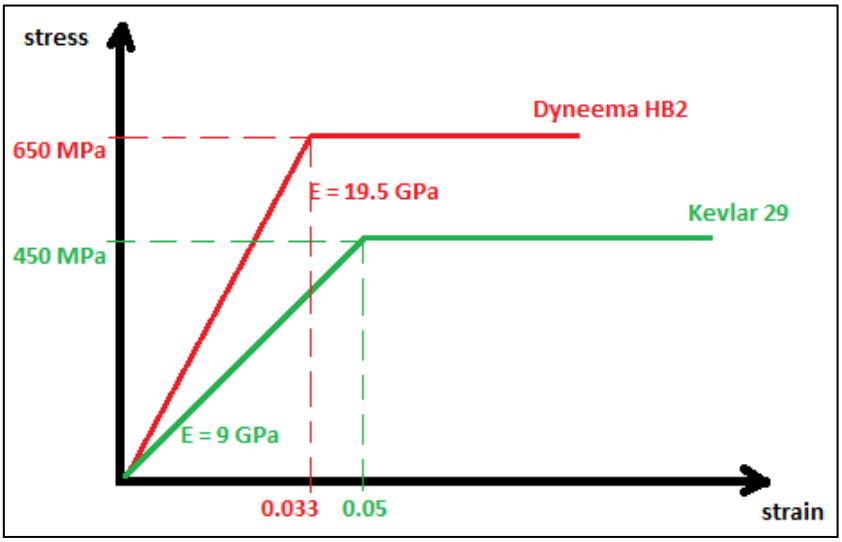

Figure 3.4. *Stress versus strain. Scheme of composite materials properties*

PamCrash has a material type which represents an isotropic elastic-plastic material: ***material type 16*** (MAT 16), isotropic elastic plastic with failure. The input parameters of this material for the two different composites are:

MATERIALS	Density (kg/m^3)	G (Pa)	K (Pa)	Yield stress (Pa)
Kevlar 29	1160	$4.17 \cdot 10^9$	$3.57 \cdot 10^9$	$450 \cdot 10^6$
Dyneema	900	$7.5 \cdot 10^9$	$16.25 \cdot 10^9$	$650 \cdot 10^6$

Table 3.2. *Input PamCrash parameters for material type 16*

An alternative method for defining an isotropic material is by defining a ***material type 30*** (MAT 30), unidirectional composite bi-phase. This material makes reference to a ply, in which all the properties are defined. In this case *Ply type 0* is used, which is the most suitable for using a degenerate orthotropic model, in which all the properties of the material are defined into matrix and a proportion of 0 % of fibre is given.

The advantage of MAT 30 respect to MAT 16 is that a damage law may be defined, and therefore stiffness reduction may be controlled.

Input parameters for MAT 30 are shown in Table 3.3.

MATERIALS	Kevlar 29	Dyneema HB2
E_1 (Pa)	$9 \cdot 10^9$	$19.5 \cdot 10^9$
E_2 (Pa)	$9 \cdot 10^9$	$19.5 \cdot 10^9$
E_3 (Pa)	$9 \cdot 10^9$	$19.5 \cdot 10^9$
G_{12} (Pa)	$4.17 \cdot 10^9$	$7.5 \cdot 10^9$
G_{23} (Pa)	$4.17 \cdot 10^9$	$7.5 \cdot 10^9$
G_{13} (Pa)	$4.17 \cdot 10^9$	$7.5 \cdot 10^9$
ν_{12}	0.08	0.3
ν_{23}	0.08	0.3
ν_{13}	0.08	0.3

Table 3.3. *Input PamCrash parameters for material type 30*

Properties in the elastic range are the same for both isotropic materials, MAT 16 and MAT 30. To be sure that the behaviour of the two types of materials is the same, two test have been done: *tensile test* and *flexion test* in elastic range. Tests were done with a square plate of 300 mm x 300 mm with a thickness of 8 mm (same measures used in Colakoglu *et al.* experiments). The properties of the Kevlar 29 are taken as example.

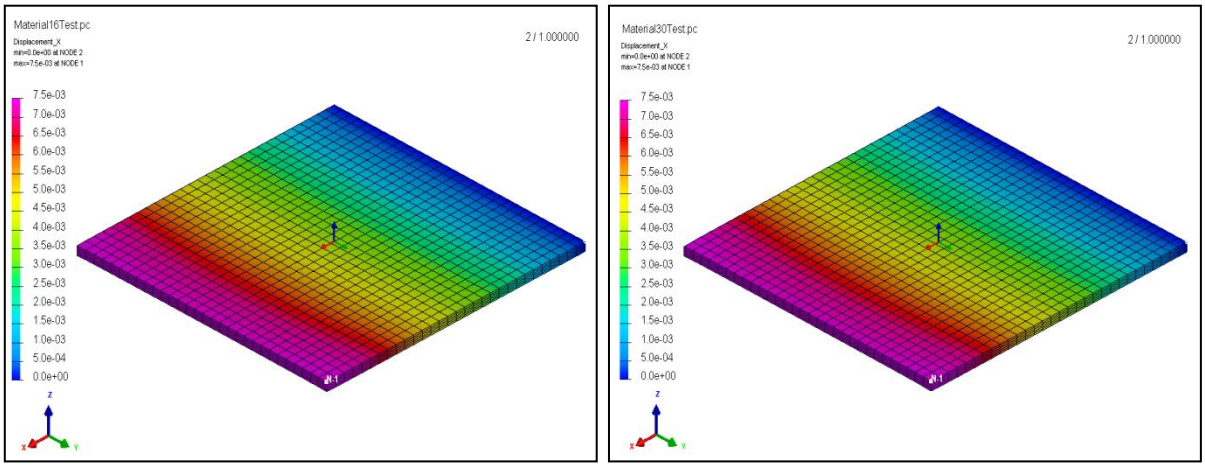

Figure 3.5. *Tensile test of Kevlar 29: MAT 16 (left) and MAT 30 (right)*

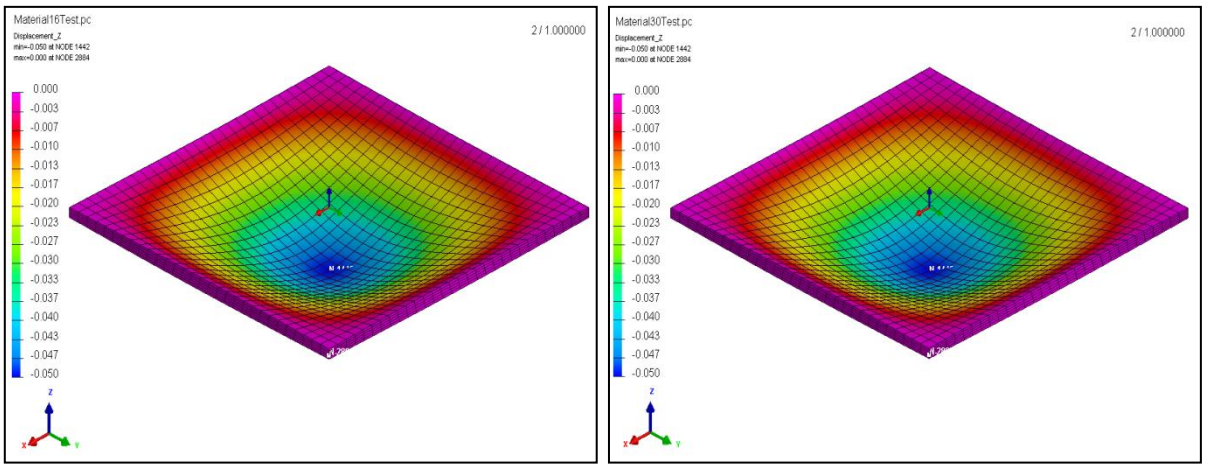

Figure 3.6. *Flexion test of Kevlar 29: MAT 16 (left) and MAT 30 (right)*

Displacements for both material models are the same as expected, being the maximum displacement in tensile test of 7.5 mm (for a load of 225 MPa) and maximum vertical displacement equal to 50 mm (for a load of 50 GPa). Displacement values are in accordance to Hook's law for tensile test and to Navier analytic model for flexion test.

3.2.3. Orthotropic homogeneous model

The orthotropic homogeneous model presented in this work is based in the studies made by Silva *et al.* [41]. In this paper, the experiments were done with Kevlar 29 / vynilester laminates plates. In order to obtain the values of the mechanical material characteristics for numerical simulation, Ernst-Mach Institute was engaged to perform quasi-static tensile tests.

No. of tests	Loading direction	Strain gauge	Results
3	Tensile 0–22° (in-plane)	22 and 23 on surface (two channels)	$E_{22\ machine} = 8075.95$ MPa $E_{22\ gauge} = 6311.69$ MPa $\nu_{23} = 0.216$
3	Tensile 45°–22° (in-plane)	one channel in loading direction	$E_{45°} = 3074.9$ MPa $\nu_{45°} = 0.77$ $G_{23} = 1540.54$ MPa
3	Tensile 0–22° sample too thin	22 and 13 through thickness (two channels)	ν_{13} not possible to measure
4	Compression 11	one channel circumferential	$E_{11} = 239.2$ MPa ν_{13} not possible to measure

Table 3.4. *EMI's orthotropic elastic properties [41]*

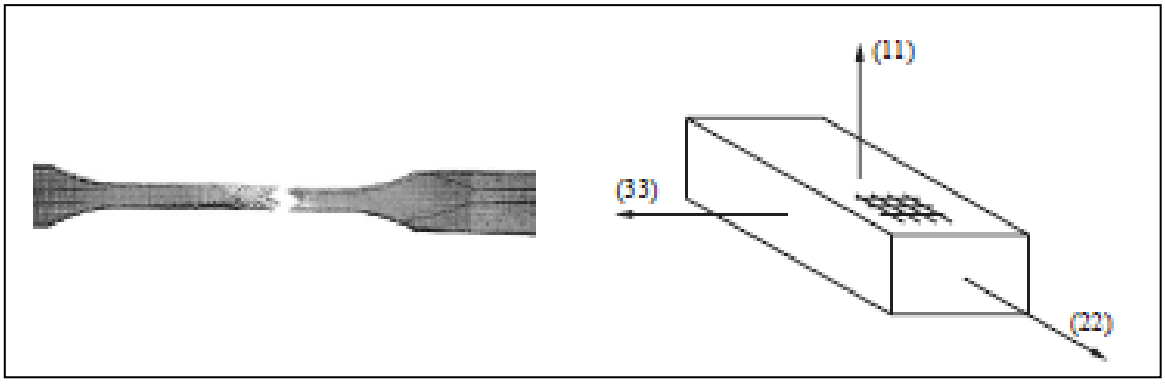

Figure 3.7. *Uniaxial static tension test [41]*

MAT 30 of PamCrash is the best choice to represent orthotropic homogeneous material. It allows to introduce different properties in the different directions of the material. Table 3.4 presents some experimental information for Kevlar 29 laminates, but not all needed (properties in plans 12 and 13. That is the reason why some suppositions must be made.

- ***Shear modulus in planes 12 and 13 (G_{12} and G_{13}).*** It is assumed that trough thickness, main properties are matrix ones. Matrix is an isotropic material and if Young's modulus and Poisson's ratio are defined, it is possible to define the missed properties. Matrix is made of vynilester and this kind of resin presents a Young's modulus of 2 GPa and a Poisson's ratio of 0.35 [46]. Therefore the final properties used in the composite material are:

$$G_{12} = G_{13} = \frac{E}{2(1+\nu)} = \frac{2 \cdot 10^9}{2(1+0.35)} = 0.74\ GPa$$

- ***Poisson's ratio in planes 12 and 13 (v_{12} and v_{13})***. At first, it is possible thinking, that same Poisson's ratio of the matrix could be also used, but composite materials are characterized for being orthotropic, and most of them being isotropic transversely (these kinds of materials are those that have the same properties in one plane and different properties in the direction normal to this plane). These materials must fulfil some requirements, where all the elements of the stiffness matrix must be positive.

  Silva *et al.* [36] proposed a value of Poisson's ratio of 0.115.

Input parameters for an orthotropic material type 30 are shown in Table 3.5:

MATERIALS	Kevlar 29
E_1 (Pa)	$0.24 \cdot 10^9$
E_2 (Pa)	$6.311 \cdot 10^9$
E_3 (Pa)	$6.311 \cdot 10^9$
G_{12} (Pa)	$0.74 \cdot 10^9$
G_{23} (Pa)	$1.54 \cdot 10^9$
G_{13} (Pa)	$0.74 \cdot 10^9$
ν_{12}	0.115
ν_{23}	0.216
ν_{13}	0.115

Table 3.5. *Input PamCrash parameters for material type 30*

3.3. Validation activities

Finally, three models for Kevlar and two models for Dyneema HB2 have been prepared. To tune up models, some numerical simulations were performed in order to determine material parameters as strain for element elimination which will match experimental results.

Composite	MAT 16 isotropic	MAT 30 isotropic	MAT 30 orthotropic
Kevlar 29	X	X	X
Dyneema HB2	X	X	-

Table 3.6. *Initial models prepared before validation tests*

Then, final material models are checked with experimental data extracted from Colakoglu [38] and Silva [41] papers. Numerical validation has been done with penetration tests and deformation tests.

3.3.1. Comparison with experimental and numerical results from Colakoglu *et al.* work

Colakoglu *et al.* [38] performed two kind of ballistic tests: ***deformation test*** and ***penetration test***, where the backside deformation and penetration speed are analyzed. In these cases, 20-layered 300 mm x 300 mm Kevlar 29 / polyvinyl Butyral and Dyneema HB2 composite plate specimens were used. The thicknesses of Kevlar 29 and Dyneema HB2 plates are 8 and 5.6 mm respectively.

- ***Deformation test.*** Plates were conditioned at different temperatures: 0 °C, 15 °C and 30 °C for 24 h before ballistic tests and the experiments were run immediately. NIJ-0101.04 ballistic test setup and ORM 55 model (Oehler Research Model) velocity-meter were used to measure experimental ballistic performance.

  Tests were carried out to obtain ballistic deformation using MP5 automatic pistol barrel and 9 mm Full Metal Jacket bullets. Firings were performed from 15 m distance to the front face of the specimens, at least 50 mm from the edges, and also at least 80 mm away from any damaged areas of previous shots. The shots were carried out at 90 ± 1 degrees to the specimen. The composite plate was fixed from all four edges and a paste was placed to the backside of the composite plate to measure total back face deformations, elastic plus plastic. The standards of National Institute of Justice are followed in these experiments [26].

- ***Penetration test.*** Ballistic penetration tests were performed in 50% relative moisture and at 23°C temperature conditions. They were carried out to both composite materials using FSP striker according to NATO STANAG 2920. The mass of the projectile is 1.1 g. 10 firings shots against 20-layered plate specimens of each material in order to determine the ballistic limit statistically.

In addition to experimental test, numerical simulations of ballistic tests were carried out using the nonlinear FE program Abaqus. The numerical model had two main parts:

- ***Impactor*** was modelled according with the geometry shown in Figure 3.8 for each type of projectile: FMJ bullet and FSP 1.1 g. Density is adjusted so that the impacting mass is ensured to be the same as the one in the experiments.

- ***Protection material*** was modelled as square plate and with solid elements, with the following characteristics:

  - Size: 300 mm x 300 mm
  - Kevlar 29 plate: thickness of 8 mm and density of 1160 kg/m^3
  - Dyneema HB2: thickness of 5.6 mm and density of 900 kg/m^3
  - Mesh of solid elements: 1.25 mm at central region and 10 mm for the rest
  - Thickness of solid elements: around 1.5 mm along all composite plate
  - Boundary conditions: four edges fixed

  Central region of the mesh plate is shown in Figure 3.9.

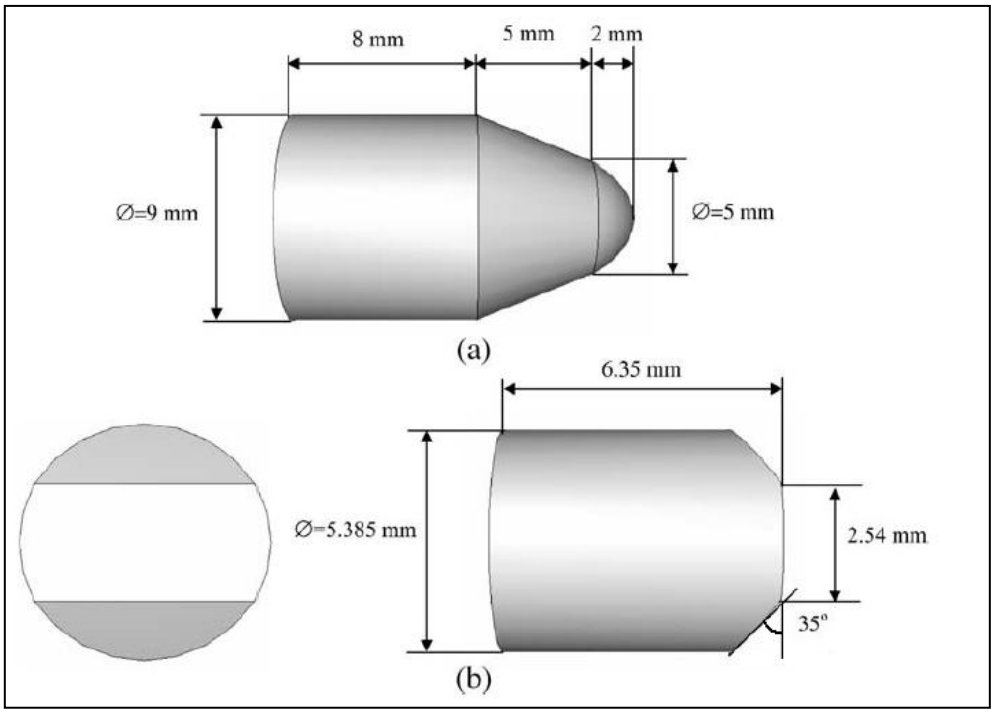

Figure 3.8. *Projectile models used in numerical simulations: FMJ bullet (a) and FSP 1.1g (b) [38]*

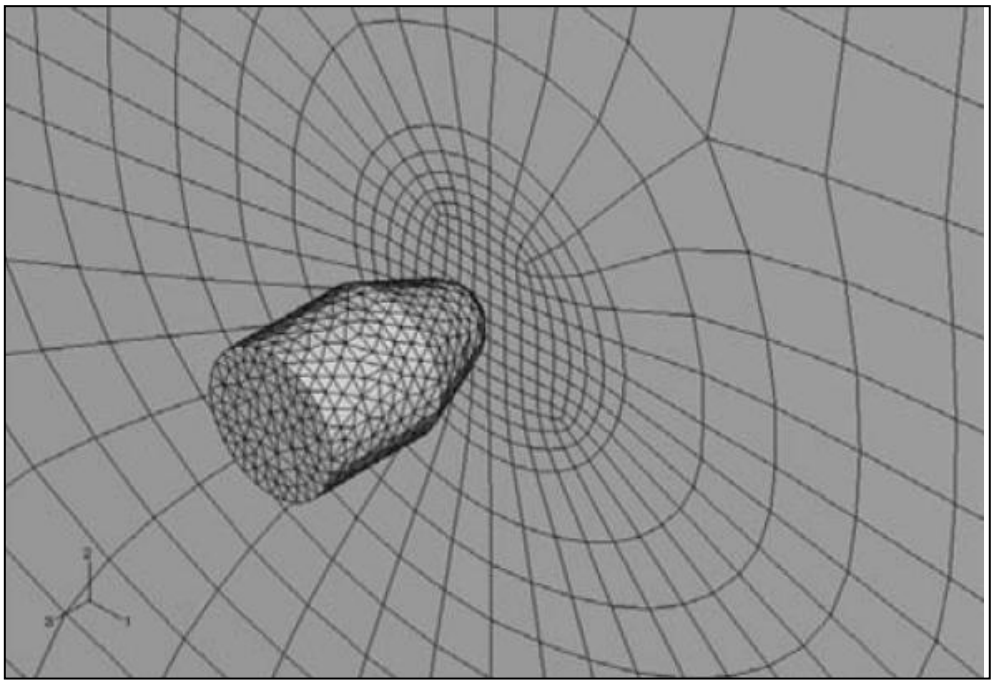

Figure 3.9. *Mesh detail of plate central zone [38]*

Same mesh and conditions have been simulated during PamCrash simulations, in order to compare the material models. Simulations made by Colakoglu *et al.* were made with a complete Abaqus model while PamCrash simulations of this project used quarter model for reducing simulation time.

3.3.1.1. Penetration tests

Parameters for ballistic penetration test for both composite materials are:

- Ballistic limit: 680 m/s for Kevlar 29 and 480 m/s for Dyneema HB2
- Areal density: 9.28 kg/m^2 for Kevlar 29 and 5.04 kg/m^2 for Dyneema HB2
- Thickness: 8 mm for Kevlar 29 and 5.6 mm for Dyneema HB2

Plate mesh used is shown in figures 3.10 and 3.11. The same mesh used by authors in [38] has been selected for these studies.

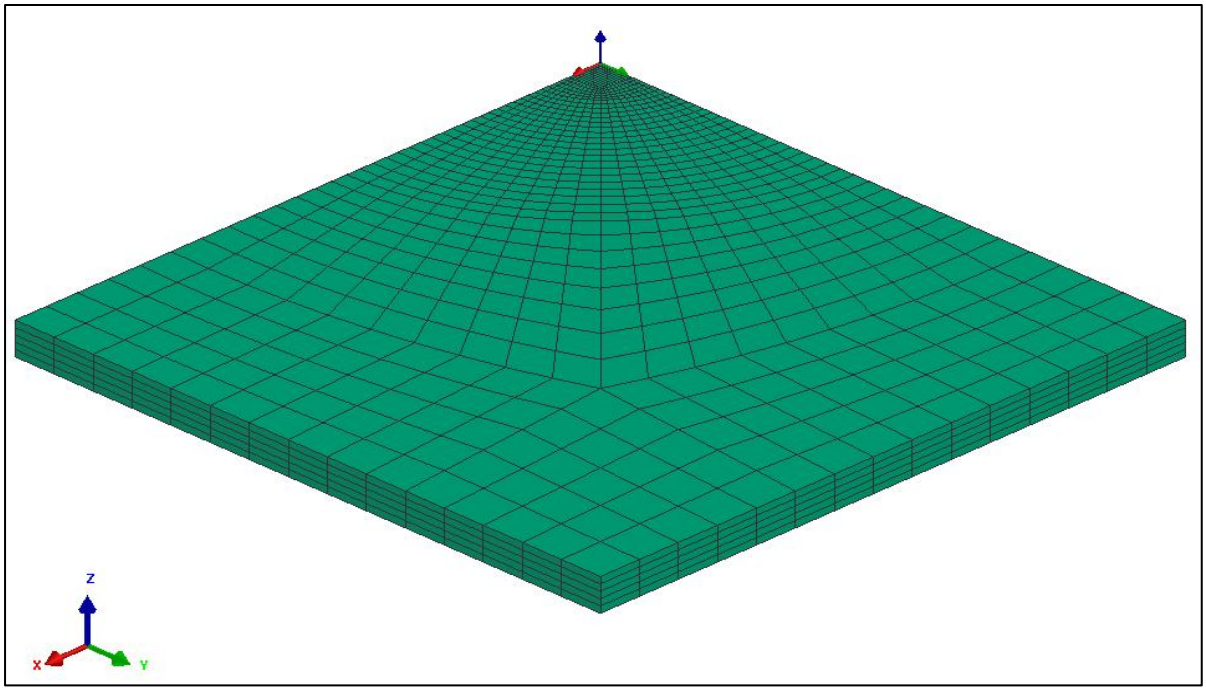

Figure 3.10. *Plate mesh isometric view (8 mm thickness plate)*

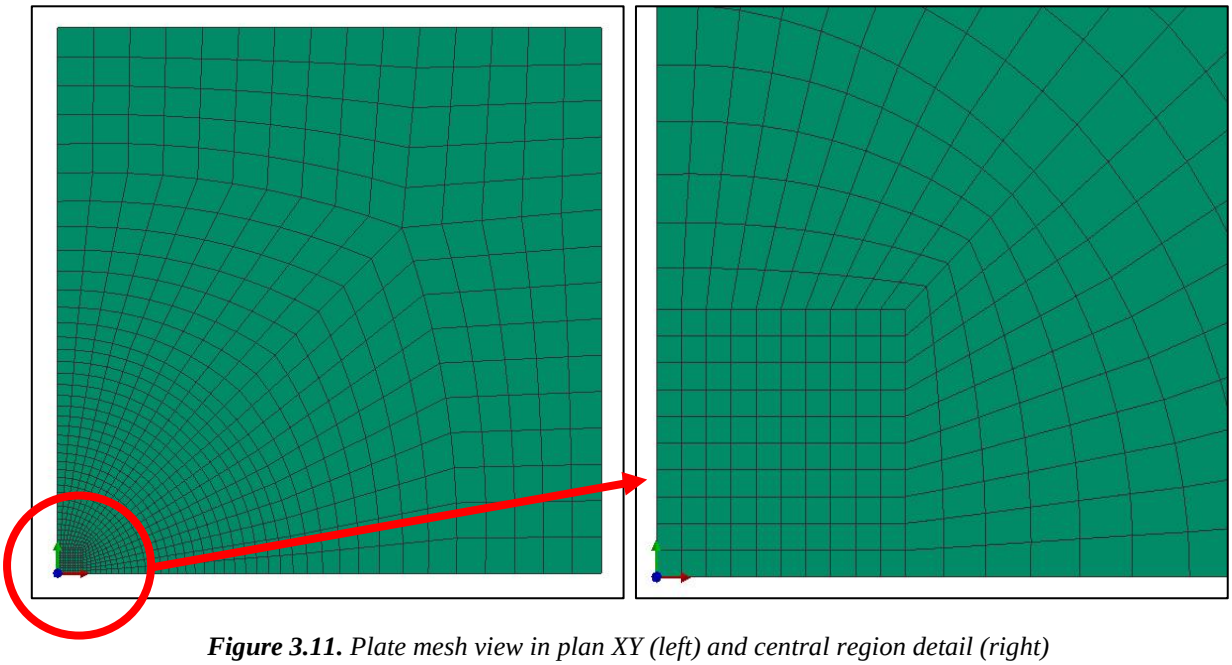

Figure 3.11. *Plate mesh view in plan XY (left) and central region detail (right)*

Bullet has been modelled as a steel isotropic material of Young´s modulus of 160 GPa and a Poisson's ratio of 0.44 [38]. In comparison, bullet stiffness is much higher than plate stiffness. Figure 3.12 shows FSP geometry and mesh at different views.

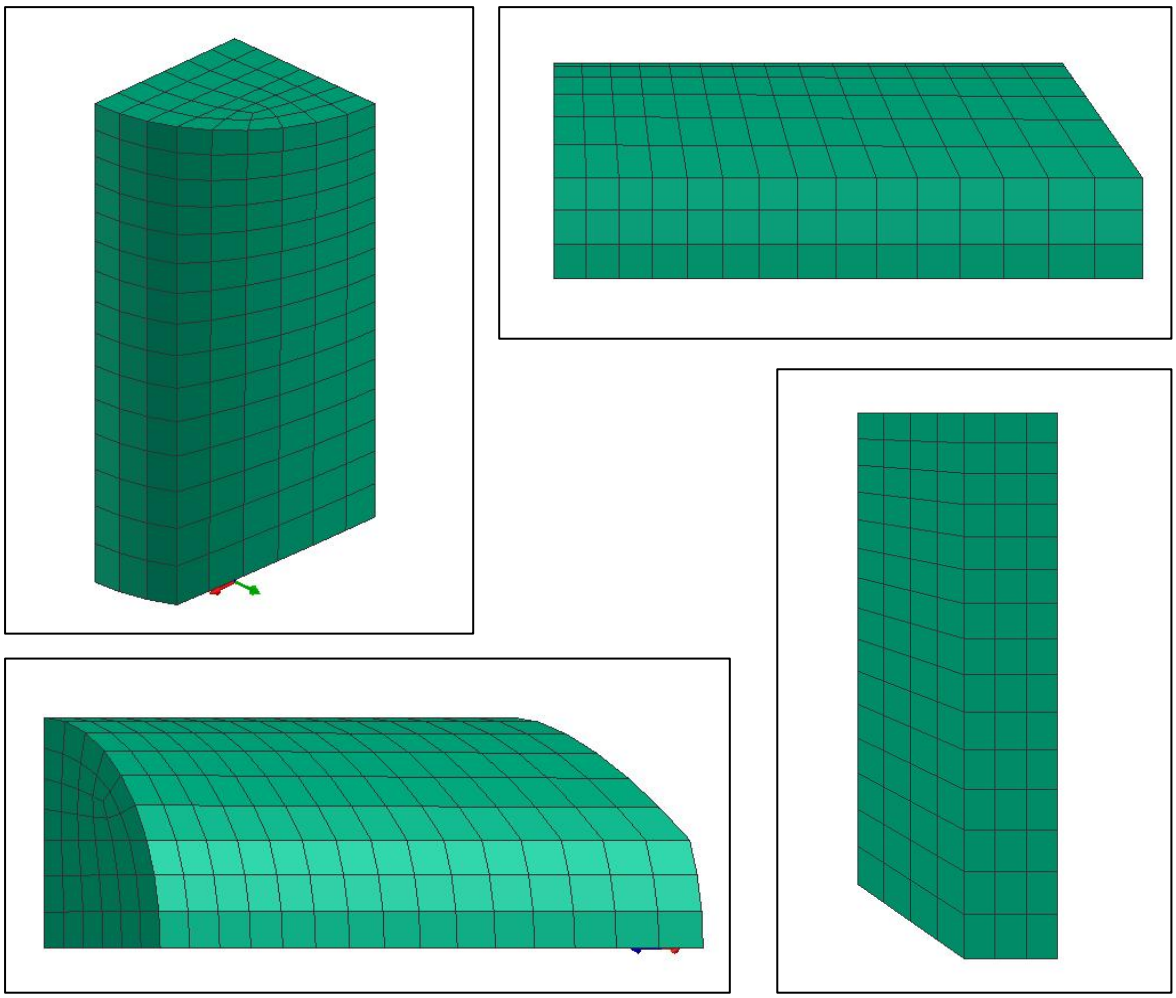

Figure 3.12. *Fragment Simulating Projectiles 1.1g mesh at different views*

The approach to match ballistic limits from numerical simulations to experimental data was:

- For isotropic elastic-plastic models (MAT 16) → variation of the maximum strain at element elimination.
- For orthotropic and isotropic homogeneous models (MAT 30) → variation of material damage law and strain at element elimination.

Finally for Kevlar 29 composite three final models are presented:

MATERIALS	Density (kg/m^3)	G (Pa)	K (Pa)	Yield stress (Pa)	Limit plastic strain (-)
Kevlar 29	1160	$4.17 \cdot 10^9$	$3.57 \cdot 10^9$	$450 \cdot 10^6$	1.8

Table 3.7. *Input PamCrash parameters for isotropic homogeneous Kevlar 29 with material type 16*

MATERIAL	Kevlar 29
E_1 (Pa)	$9 \cdot 10^9$
E_2 (Pa)	$9 \cdot 10^9$
E_3 (Pa)	$9 \cdot 10^9$
G_{12} (Pa)	$4.17 \cdot 10^9$
G_{23} (Pa)	$4.17 \cdot 10^9$
G_{13} (Pa)	$4.17 \cdot 10^9$
ν_{12}	0.08
ν_{23}	0.08
ν_{13}	0.08
$\varepsilon_{plastic\ limit}$	0.5

Damage function	ε_i	ε_1	ε_u	d_1	d_u
Equivalent shear strain	0.0312	0.0575	0.0795	0.02	0.25
Volumetric strain	1	2	3	0	0

Table 3.8. *Input PamCrash parameters (up) and damage law (down) for isotropic homogeneous Kevlar 29 with material type 30*

MATERIAL	Kevlar 29
E_1 (Pa)	$6.311 \cdot 10^9$
E_2 (Pa)	$6.311 \cdot 10^9$
E_3 (Pa)	$0.24 \cdot 10^9$
G_{12} (Pa)	$1.54 \cdot 10^9$
G_{23} (Pa)	$0.74 \cdot 10^9$
G_{13} (Pa)	$0.74 \cdot 10^9$
ν_{12}	0.216
ν_{23}	0.115
ν_{13}	0.115
$\varepsilon_{plastic\ limit}$	$0.24 \cdot 10^9$

Damage function	ε_i	ε_1	ε_u	d_1	d_u
Equivalent shear strain	0.1656	0.8	1.0	0.1	0.8416
Volumetric strain	1	2	3	0	0

Table 3.9. *Input PamCrash parameters (up) and damage law (down) for orthotropic homogeneous Kevlar 29 with material type 30*

Figure 3.13 shows PamCrash simulations of penetration test for Kevlar 29 with the three different material models developed above. Because every material model was tuned up with penetration test, the ballistic limit is the same in numerical simulations and in experimental data (680 m/s). However, beyond this limit the behaviour of three material models is in close agreement, within the whole range of speeds.

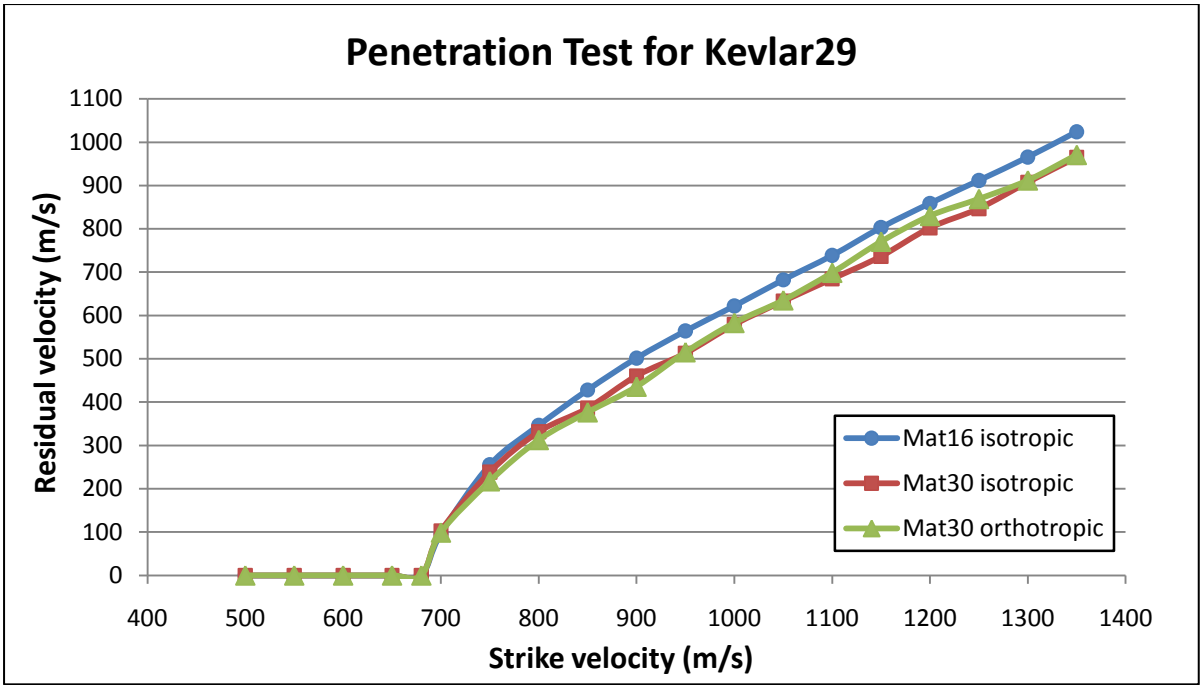

Figure 3.13. *Residual velocity versus strike velocity. 8 mm thickness Kevlar 29 plate with different material models*

Two impact sequences are shown in Figure 3.14. On the left side, velocity is below the ballistic limit; therefore the impactor is stopped by the protections and rebounds on it. Meanwhile, on the right side, velocity above the ballistic limit, thus the impactor fully perforates the protection.

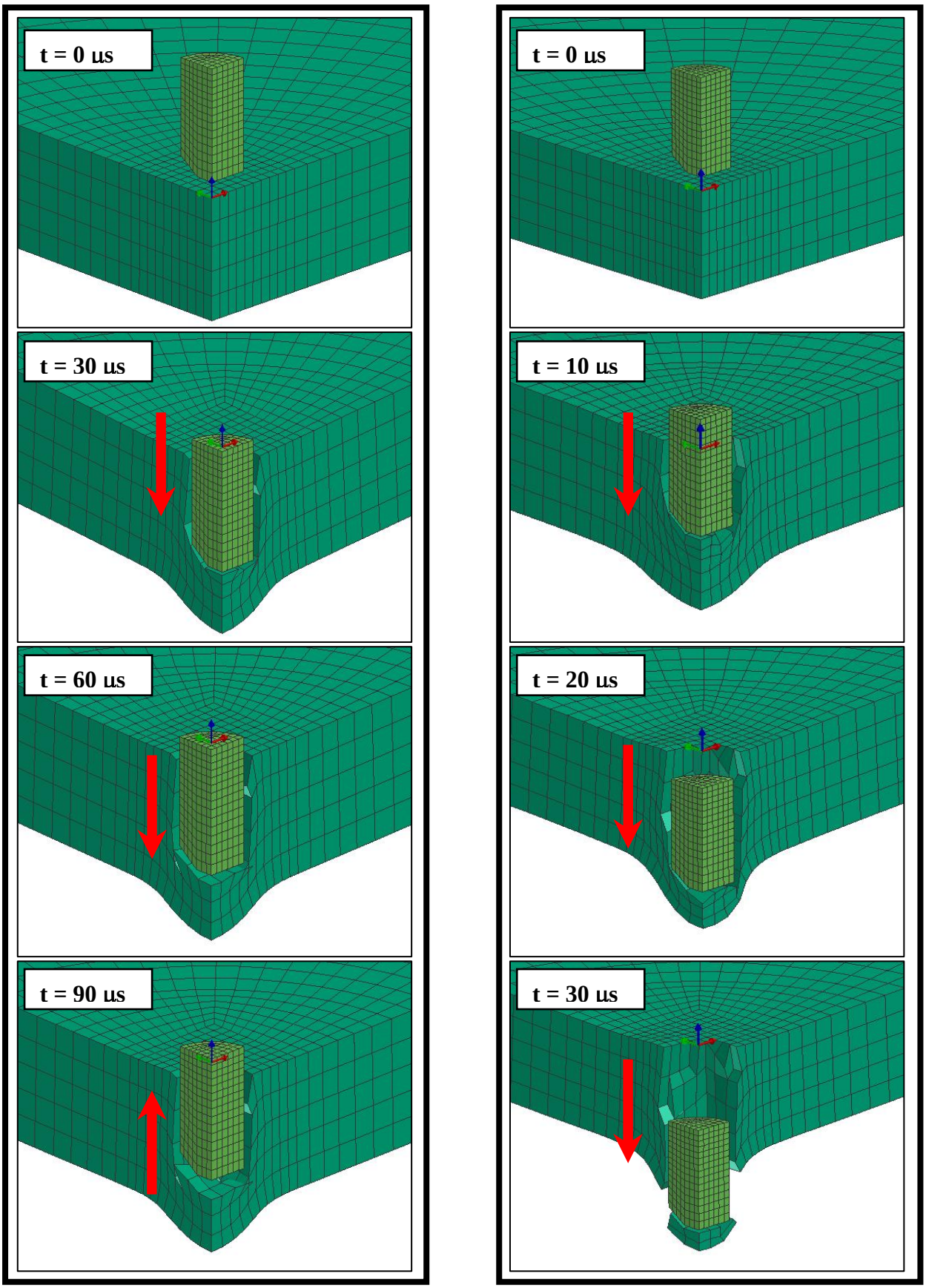

Figure 3.14. *Penetration test sequence for an initial velocity of 600 m/s (left) and 800 m/s (right) with Kevlar 29 composite modelled with isotropic material type 16*

For Dyneema HB2 composite two final models were prepared:

MATERIALS	Density (kg/m^3)	G (Pa)	K (Pa)	Yield stress (Pa)	Limit plastic strain (-)
Dyneema HB2	900	$7.5 \cdot 10^9$	$19.5 \cdot 10^9$	$650 \cdot 10^6$	0.52

Table 3.10. *Input PamCrash parameters for isotropic homogeneous Dyneema HB2 with material type 16*

MATERIAL	Dyneema HB2
E_1 (Pa)	$19.5 \cdot 10^9$
E_2 (Pa)	$19.5 \cdot 10^9$
E_3 (Pa)	$19.5 \cdot 10^9$
G_{12} (Pa)	$7.5 \cdot 10^9$
G_{23} (Pa)	$7.5 \cdot 10^9$
G_{13} (Pa)	$7.5 \cdot 10^9$
ν_{12}	0.3
ν_{23}	0.3
ν_{13}	0.3
$\varepsilon_{plastic\ limit}$	0.5

Damage function	ε_i	ε_1	ε_u	d_1	d_u
Equivalent shear strain	0.019	0.0375	0.052	0.02	0.632
Volumetric strain	1	2	3	0	0

Table 3.11. *Input PamCrash parameters (up) and damage law (down) for isotropic homogeneous Dyneema HB2 with material type 30*

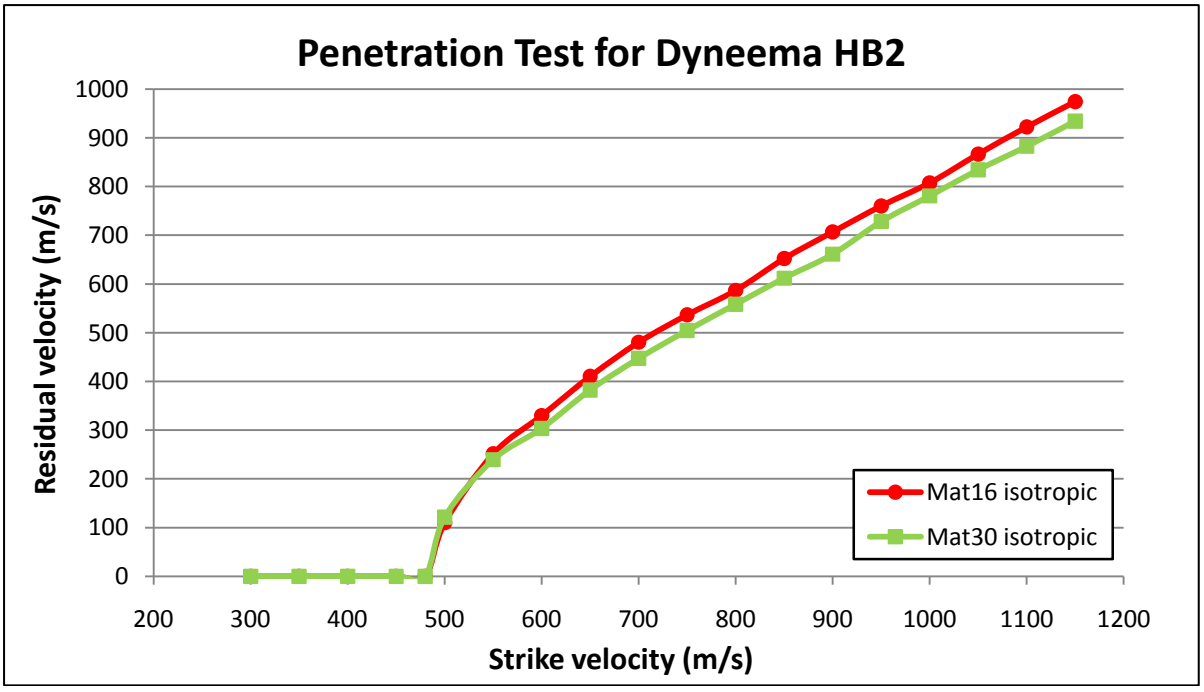

Figure 3.15. *Residual velocity versus strike velocity. 5.6 mm thickness Dyneema HB2 plate with different material models*

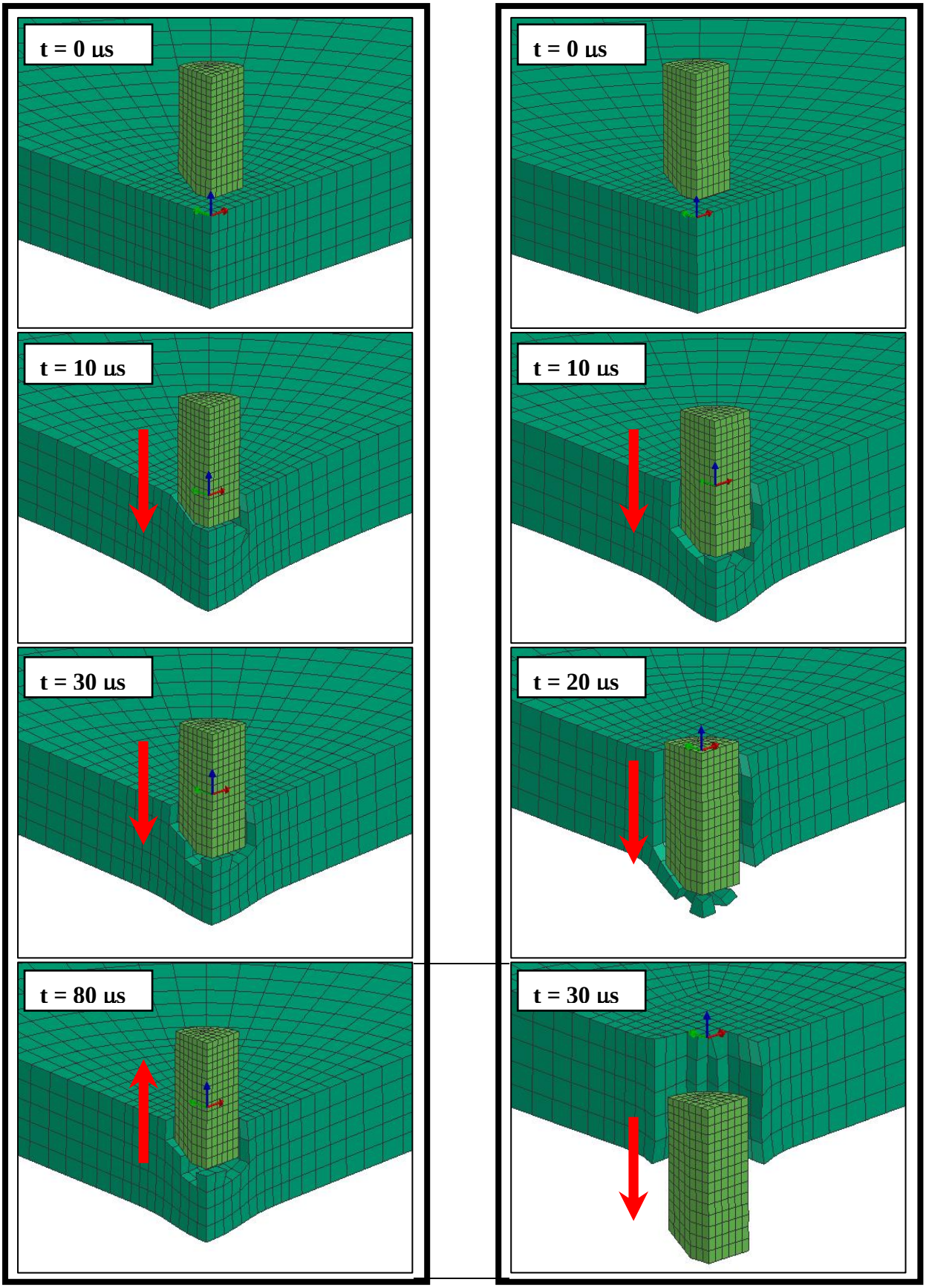

Figure 3.16. *Penetration test sequence for an initial velocity of 400 m/s (left) and 600 m/s (right) with Dyneema HB2 composite modelled with isotropic material type 16*

As it was seen before in Kevlar 29 case, a ballistic limit of 480 m/s can be clearly seen and how over this limit the material behaviour is in close agreement (Figure 3.15). Two impact sequences are shown in Figure 3.16. On the left side, velocity is below the ballistic limit; therefore the impactor is stopped by the protections and rebounds on it. Meanwhile, on the right side, velocity above the ballistic limit, thus the impactor fully perforates the protection.

3.3.1.2. Deformation tests

In the deformation tests the backside deformation is measured. The back face deformation, both elastic and plastic, is measured from the paste, which is placed at the backside of the composite plates.

For these kinds of experiments a FMJ bullet was used according with the geometry shown in Figure 3.8. The FSP is made of steel and is characterized by its high stiffness, but during the impact a FMJ bullet deforms highly up to reach mushroom final shape. This happen because its core is made of lead and has a brass, being much more deformable than a steel bullet.

The FMJ bullet is modeled with a Johnson-Cook model, which is a model for metals subjected to large strains, high strain rates and high temperatures [47]. This model was also used by Tham *et al.* [48] in numerical impact simulations. Bullet is completely modeled with brass properties and then density is adjusted to ensure the total bullet weight.

Material input parameters for Johnson-Cook model and bullet mesh are shown in Table 3.12 and in Figure 3.17 respectively. Elastic modulus and Poisson's ratio are obtained from bibliography [13] while the rest of parameters are taken from Johnson-Cook's paper [47].

Material	Description				Constitutive constants for: $\sigma = [A + Be^n][1 + C\ln\varepsilon][1 - T^m]$				
	E (GPa)	v	Specific Heat (J/kgK)	Melting Temp. (K)	A (MPa)	B (MPa)	n	C	m
Brass	110	0.37	385	1189	112	505	0.42	0.009	1.68

Table 3.12. *Input parameters for brass Johnson-Cook model*

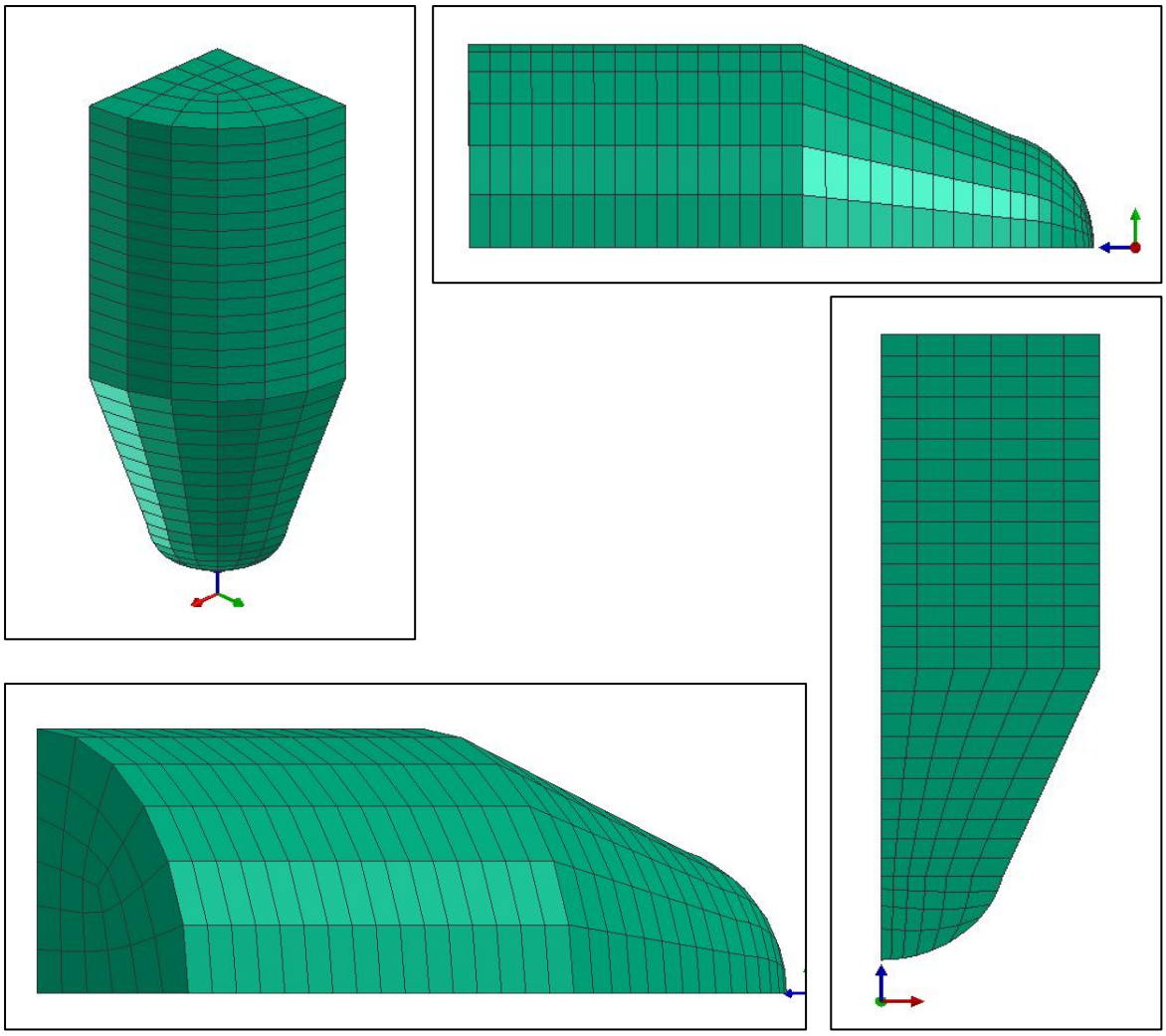

Figure 3.17. *FMJ bullet mesh at different views*

Figures 3.18 and 3.19 show results obtained from experimental and numerical back face deformations, divided by the areal density and the thickness of the plates for Kevlar 29 / polyvinyl butyral composite and Dyneema HB2 laminate composite, respectively. The plots show the following curves:

- Published numerical simulations performed by Colakoglu *et al.* (Abaqus).
- Published experimental data at different temperatures performed by Colakoglu *et al.*
- Numerical simulations done with PamCrash in Airbus Military (EADS-CASA), with all the material models developed above.

For ***Kevlar 29*** the back face deformation simulations did with PamCrash are in agreement with the experimental and numerical values (Figure 3.18). Numerical simulations of deformation test with PamCrash were done for the three models of Kevlar 29 prepared and at same speed values published. At some velocities, values of deformation cannot be measured because the bullet penetrates completely the composite plate:

- MAT 16 isotropic: all values measured except the last one.
- MAT 30 isotropic: only values measured at two first velocities values.
- MAT 30 orthotropic: bullet fully penetrates composite at whole range of velocities.

Errors measured for the three models of Kevlar 29 are:

- MAT 16 isotropic: *minimum error* of 6 % at 422 m/s between numerical simulations with Abaqus and PamCrash and *maximum error* of 21 % at 396 m/s between experimental data at 15 ºC and numerical simulations with PamCrash.
- MAT 30 isotropic: *minimum error* of 0.96 % at 352 m/s between experimental data at 15 ºC and numerical simulations with PamCrash and *maximum error* of 39 % at 396 m/s between experimental data at 15 ºC and numerical simulations with PamCrash.
- MAT 30 orthotropic: bullet fully penetrates composite at whole range of velocities, so there are no errors measured.

As the striker speed increases the back face deformation also increases. The matching between experimental and numerical results is better with MAT 16 isotropic than with MAT 30. Therefore MAT 16 isotropic is selected as the best approach for modelling Kevlar 29.

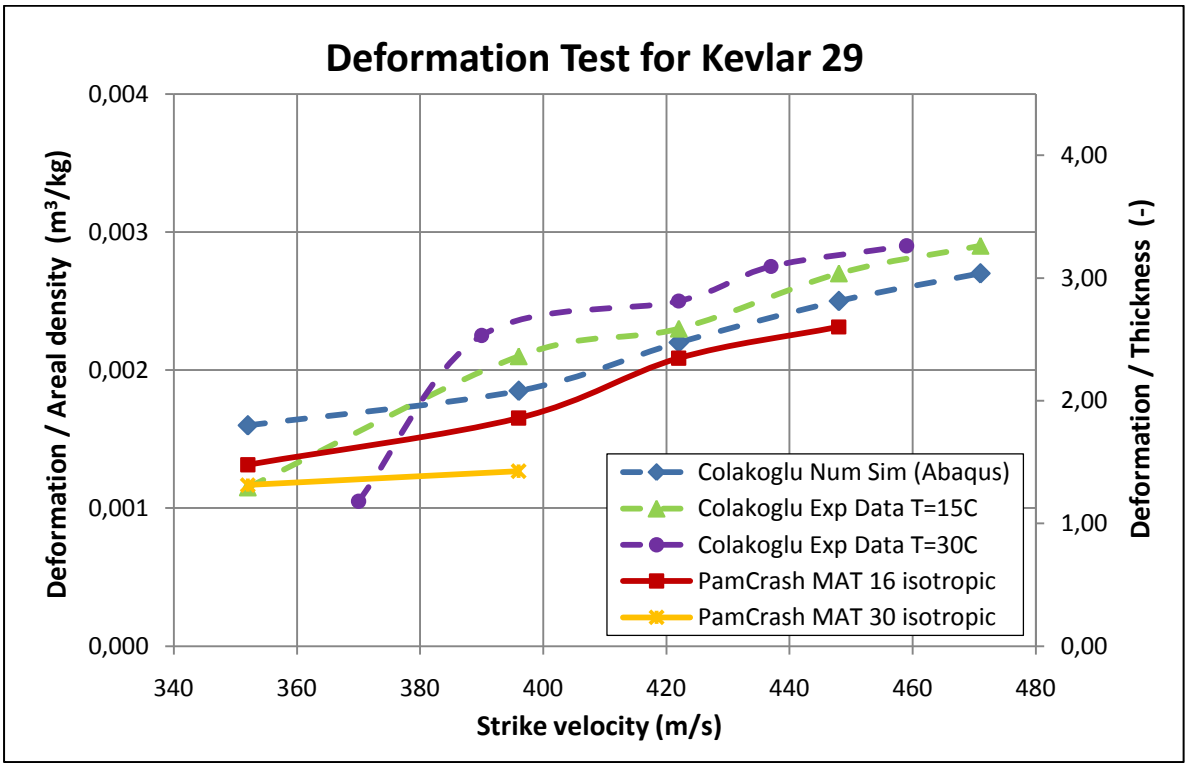

Figure 3.18. *Backface deformation of Kevlar 29 versus initial striker speed*

Deformation tests on ***Dyneema HB2*** composite shows good agreements between both numerical codes (Abaqus and PamCrash), on the other hand comparing with experimental data, whereas at lower initial striker velocity, deformation is in agreement, at higher initial striker velocities, values are lower than the experimental ones.

Errors measured for the two models of Dyneema HB2 are:

- MAT 16 isotropic: *minimum error* of 9 % at 352 m/s between numerical simulations with Abaqus and PamCrash and *maximum error* of 38 % at 396 m/s between experimental data at 15 ºC and numerical simulations with PamCrash.
- MAT 30 isotropic: bullet fully penetrates composite at whole range of velocities, so there are no errors measured.

Like in the case of Kevlar 29, the matching between experimental and numerical results is better with MAT 16 isotropic than with MAT 30. Therefore MAT 16 isotropic is selected as the best approach for modelling Dyneema HB2.

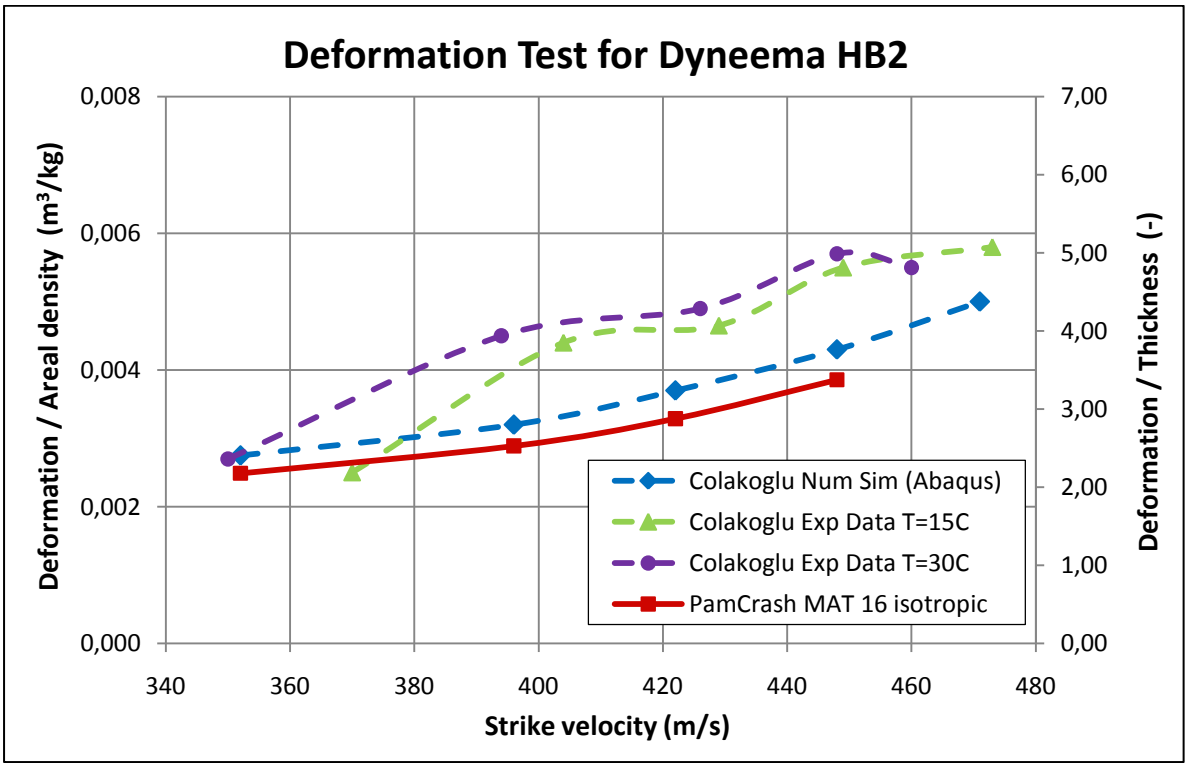

Figure 3.19. *Backface deformation of Dyneema HB2 versus initial striker speed*

Two impact deformation tests sequences are shown in Figure 3.20. On the left side, material model is Kevlar 29 and on the right side material model is Dyneema HB2. Both tests are made at same speed, 352 m/s.

To obtain maximum vertical displacement during deformation test simulations, the composite protection oscillated up to reach maximum value, so in addition an example of the complete sequence is shown in Figure 3.21. Vertical displacement contour plot in mm are printed.

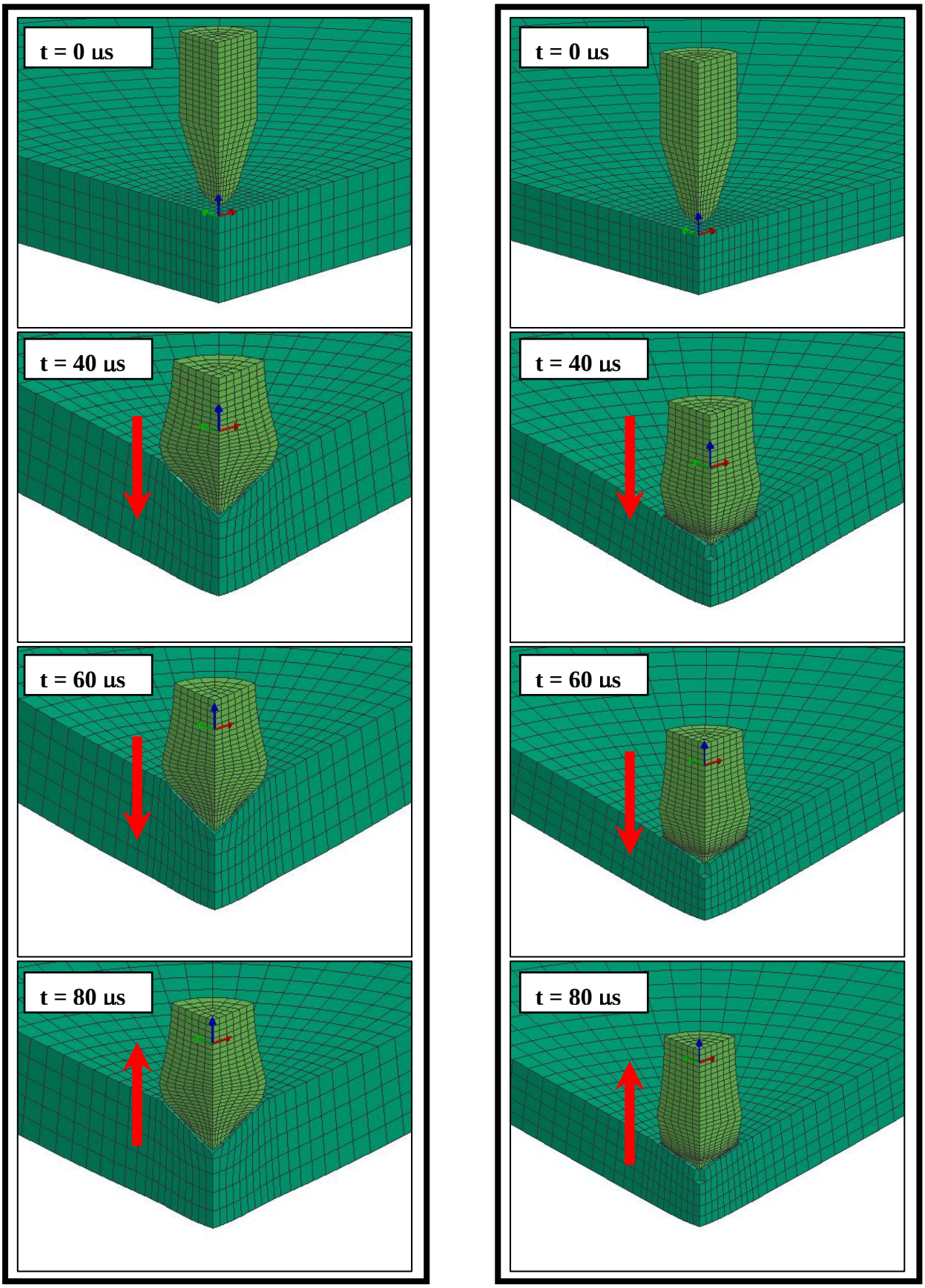

Figure 3.20. *Deformation test sequence for an initial velocity of 352 m/s with Kevlar 29 (left) and with Dyneema HB2 (right) modelled with isotropic material type 16*

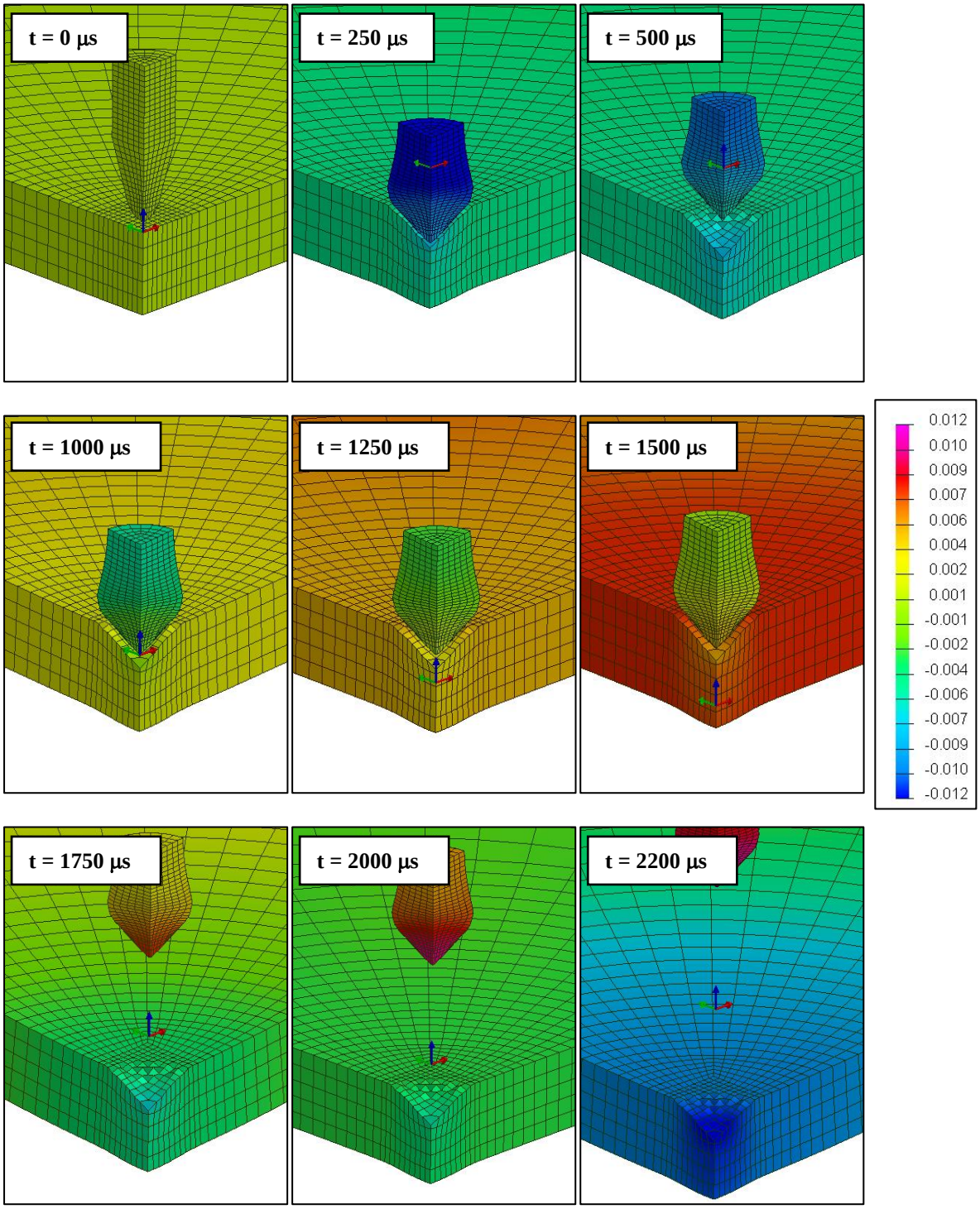

Figure 3.21. *Vertical displacement in mm. Contour plot of deformation test sequence for an initial velocity of 352 m/s with Kevlar 29*

3.3.2. Comparison with experimental and numerical results from Silva *et al.* work

In their study Silva *et al.* [41] performed some numerical simulations and experimental tests. In order to obtain the ballistic performance and ballistic limit value, a series of ballistic tests were performed on Kevlar 29 laminates plates at the Navy School in Lisbon. The plates were made from prepreg fabric impregnated with vynilester resin and cured using the manufacturer's curing conditions.

- Impactor of the ballistic test was a ***Fragment Simulating Projectile (FSP)***. The velocity of the fragment was varied to achieve three perforations and three partial penetrations within a small velocity dispersion range of, typically, 38 m/s. The six velocities were then averaged to derive V_{50} as illustrated in Figure 3.22. Finally experimental results indicate a ballistic limit of 324.3 m/s.

- ***Protection panel*** in the ballistic experimental tests was a 400 x 400 mm^2 Kevlar 29 / vynilester plate, firmly clamped on the edges. Its 2 mm thickness corresponds to seven layers. The experimental locations chosen for projectile impact were selected so as to minimise the effects of previous impact damage and sufficiently far from the boundaries.

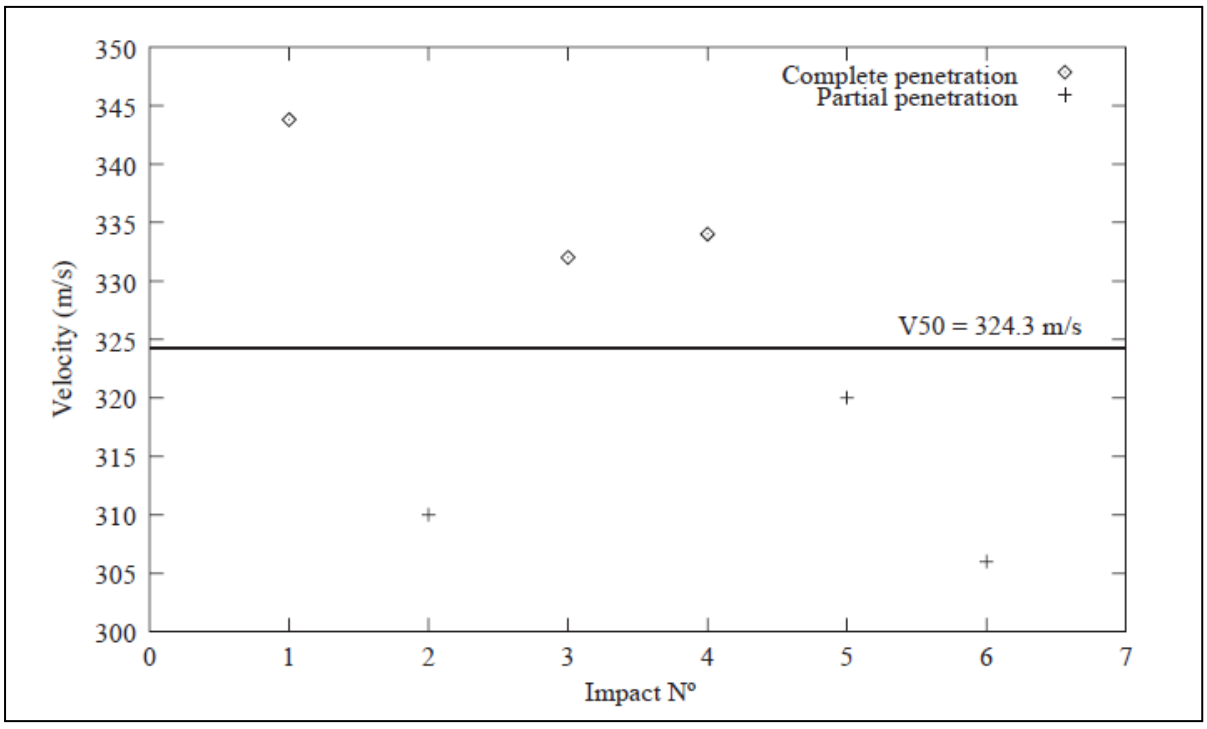

Figure 3.22. *Data point used to determine ballistic limit [41]*

A set of numerical simulations was done in order to predict the ballistic limit and compare it with experimental results. The projectile in numerical simulations is a 4340 steel FSP bullet, modelled using a Johnson-Cook strength model, including strain and strain rate hardening and thermal softening effects. The geometry and mesh are shown in Figure 3.8 (b) and Figure 3.12 respectively, and the input material parameters in Table 3.13.

Material	Description				Constitutive constants for: $\sigma = [A + Be^n][1 + C ln\varepsilon][1 - T^m]$				
	E (GPa)	v	Specific Heat (J/kgK)	Melting Temp. (K)	A (MPa)	B (MPa)	n	C	m
4340 steel	210	0.3	477	1793	792	510	0.34	0.014	1.03

Table 3.13. *Input parameters for steel 4340 Johnson-Cook model [42]*

Silva *et al.* [41] performed a set of numerical simulations using the non-linear FE code LS-Dyna. Strike velocity was raised between 290 m/s to 360 m/s, and the ballistic limit was 320 m/s, in close agreement to the experimental value of 324.3 m/s.

Analogous simulations have been performed in this project considering numerical models for Kevlar 29 (Table 3.6, 3.7 and 3.8) and PamCrash as code. These simulations provide a ballistic limit of 340 m/s, 6 % higher than test, but still in good agreement.

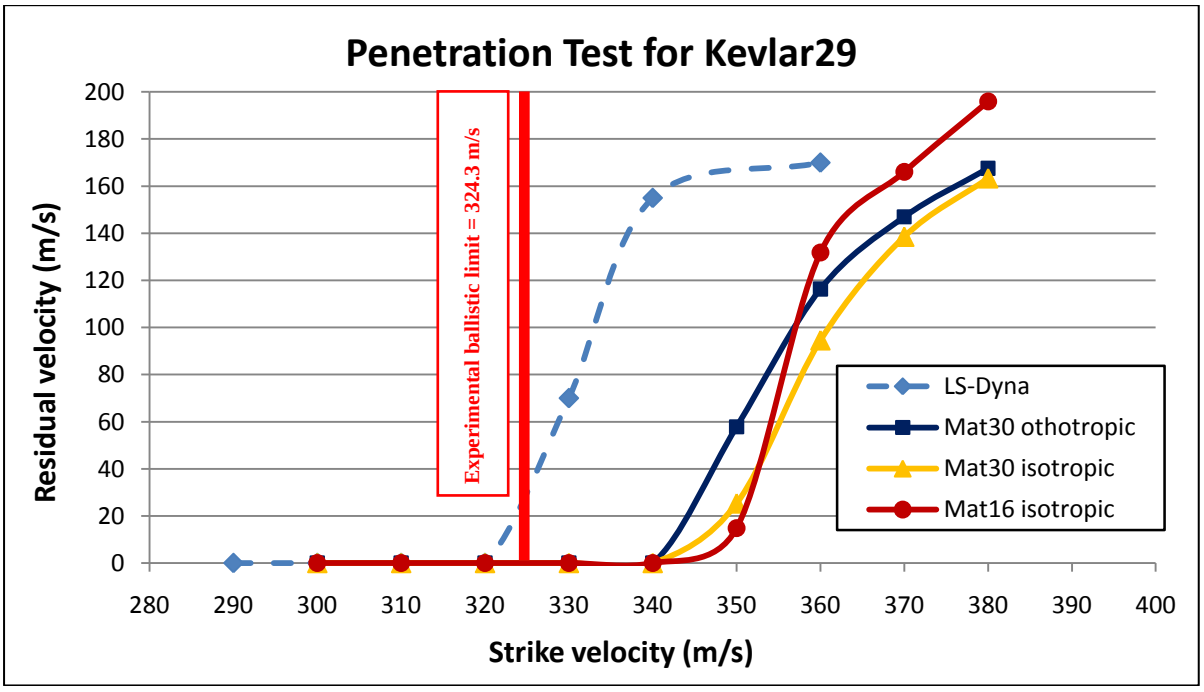

Figure 3.23. *Residual velocity versus strike velocity. 2 mm thickness Kevlar 29 plate with different material models*

3.4. Numerical models proposed for protections materials using PamCrash

The numerical models proposed in this project using PamCrash are able to reproduce experimental ballistic limits coming from two independent sources: Colakoglu *et al.* [39] and Silva *et al.* [41]. This fact strengths confidence on these models for protection design applications.

Once all the developed models have been checked with alternative numerical simulations and experimental results, one can conclude that the material models with the best behaviour are the ones modelled as a homogeneous isotropic model with a material type 16 elastic-plastic. For all material models ballistic limit is tuned up in penetration test, so in this aspect there are no evidences to favour the selection of one material model or other. However in the deformation test, data obtained from numerical simulations reveals that isotropic materials modelled with material type 16 have a better behaviour.

Two models of solid elements are proposed: one for woven Kevlar 29 with a thermosetting resin, and the other for Dyneema HB2 that is an unidirectional composite laminate with layers plied up at 0 and 90 degrees. Properties of these two materials are summarized in Table 3.13

MATERIALS	Density (kg/m^3)	G (Pa)	K (Pa)	Yield stress (Pa)	Limit plastic strain (-)
Kevlar 29	1160	$4.17 \cdot 10^9$	$3.57 \cdot 10^9$	$450 \cdot 10^6$	1.8
Dyneema HB2	900	$7.5 \cdot 10^9$	$16.25 \cdot 10^9$	$650 \cdot 10^6$	0.52

Table 3.14. *Properties of final numerical models adopted with solid elements*

However, when modelling thin laminates (lower than 1 or 2 mm), solid elements may present difficulties in numerical simulations, and ***shell elements*** are more suitable. The next step is to obtain material models for shells with equivalent behaviour to those obtained for solid elements.

In PamCrash the isotropic elastic-plastic material model for shell elements is ***material type 102*** (MAT 102). Two exercises for comparison of MAT 16 (elastic-plastic for solids) and MAT 102 (elastic-plastic for shells) were proposed.

- ***Flexion test without element elimination:*** a load over plastic limit is introduced and then maximum displacement is measured. For shell material the maximum vertical displacement measured was 29 mm and for solid material was 32 mm (Figure 3.24), in a Kevlar 29 laminate. Thus MAT 16 and MAT 102 are equivalent in the elastic range.

- ***Flexion test with element elimination:*** limit plastic strain limit for element elimination is tuned up, until composite plate breaks at the same time with the same load. Example shown in figure 3.25 corresponds to Dyneema HB2.

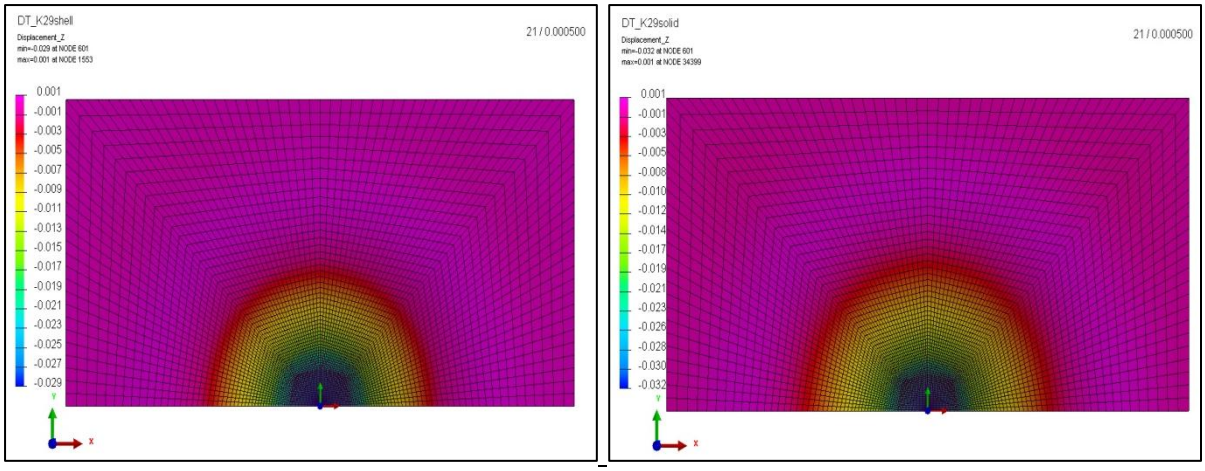

Figure 3.24. *Maximum vertical displacement for shell material model (left) and for solid material model (right)*

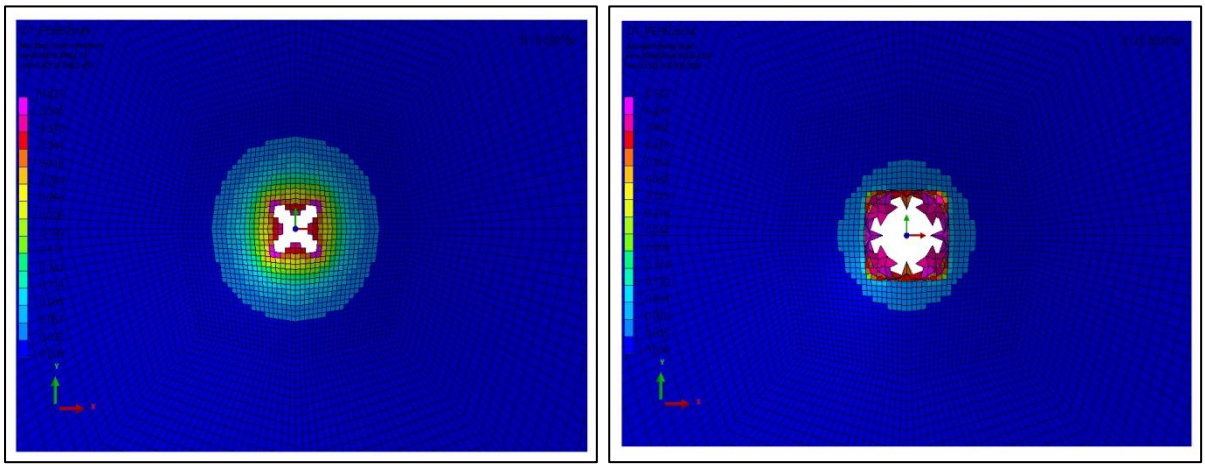

Figure 3.25. *Plastic strain for shell material model (left) and for solid material model (right)*

Finally, the two models developed for modelling composite protections with shell elements are summarized in Table 3.14. The elastic and plastic properties are the same to those of solid elements (Table 3.13). The only change is the maximum strain at rupture that is tuned up, in both cases, to experimental data published by Colakoglu *et al.* [39] and Silva *et al.* [41].

MATERIALS	Density (kg/m^3)	G (Pa)	K (Pa)	Yield stress (Pa)	Limit plastic strain (-)
Kevlar 29	1160	$4.17 \cdot 10^9$	$3.57 \cdot 10^9$	$450 \cdot 10^6$	0.447
Dyneema HB2	900	$7.5 \cdot 10^9$	$16.25 \cdot 10^9$	$650 \cdot 10^6$	0.420

Table 3.15. *Properties of final numerical models adopted with shell elements*

All these materials models are suitable for prediction of ballistic limit in composite protection panels of Kevlar 29 and Dyneema HB2.

CHAPTER IV. APPLICATIONS

4.1. Introduction

Several semi-analytical and numerical models have been studied along the current project in Chapter II and III respectively. The main objective of these models is predicting ballistic limits of protection laminates.

This chapter presents two direct aeronautical applications for predicting the ballistic limits and design of protections made with composite materials:

- Protection designed against small metallic fragments coming from Uncontained Engine Rotor Failure (UERF).

- Protections designed against ice fragments coming from propeller ice release.

Both applications are a current field of research of Airbus Military (EADS-CASA) within Research & Technology Programs like CLEAN SKY (EU founded program) and DEPLA (Spain founded program).

The protection laminates studied were made of aramid and polyethylene fibres. While the impactors were of three types:

Low size metallic impactor

- Diameter = 14.32 mm
- Strike face area = 161 mm^2
- Mass = 8.4 g
- Density = 7850 kg/m^3
- Velocity = 585 m/s
- Energy = 1437 J

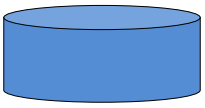

High size metallic impactor

- Diameter = 23.00 mm
- Strike face area = 415 mm^2
- Mass = 74 g
- Density = 8096 kg/m^3
- Velocity = 479 m/s
- Energy = 8489 J

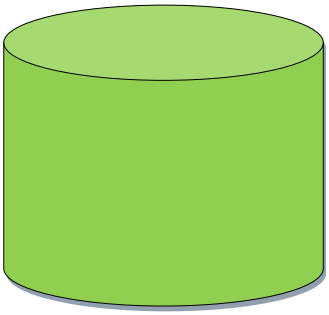

Ice impactor

- Thickness = 6.5 mm
- Diameter = 18.00 mm*
- Strike face area = 254 mm^2
- Mass = 35 g
- Density = 917 kg/m^3
- Velocity = 150 m/s
- Energy = 394 J

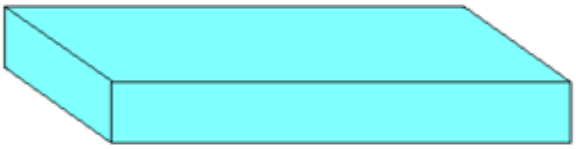

***NOTE:** equivalent diameter of the frontal area.

4.2. Design of protections with semi-analytical models for small metallic and ice impactors

Semi-analytical ballistic impact models have been studied to predict the ballistic limit (V_b or V_{50}) in different composite materials. Once known the hypotheses and restrictions of the models, it would be interesting to do a predetermination of the composite plate dimensions (thickness, areal density and number of plies) to be able to stop certain projectiles: small metallic and ice fragments.

Models proposed depend on some constants which are different for each composite, stack sequence, configuration (woven or non-woven), manufacturing process... Without particular experimental information, these constants have been calculated from data obtained from published work and numerical simulations. To calculate constants of materials the procedure is:

- Semi-analytical models studied, proposed some equations to estimate ballistic limit of composite materials. Equations depends on:
    - Density of composite materials.
    - Composite thickness.
    - Mass of impactor.
    - Shape of impactor (mainly strike face area and diameter).
    - Constants of material.

- Without experimental test, it is necessary to obtain data from ballistic test published in literature. Researchers provide enough information to calculate the constants:
    - Ballistic limit of protection materials.
    - Full properties of impactors (for penetration tests the most common projectile used is a FSP of 1.1 g).
    - Geometry and characteristics of protection material.

- With all necessary information, it is possible to calculate constant of protection materials for each semi-analytical model.

- Once constants are calculated they are used to size protection materials against the three impactors presented in the current work with equations proposed by semi-analytical models.

This calculation procedure may be summarized in two main steps: constants of materials calculation and sizing of protection materials. A scheme to a better understanding is presented in Figure 4.1.

From all models studied in Chapter II, only five of them are used next due to simplicity of formulation and available data in literature:

- Bless and Hartman
- Caprino
- Jacobs and Van Dingenen
- Van Gorp
- Wen

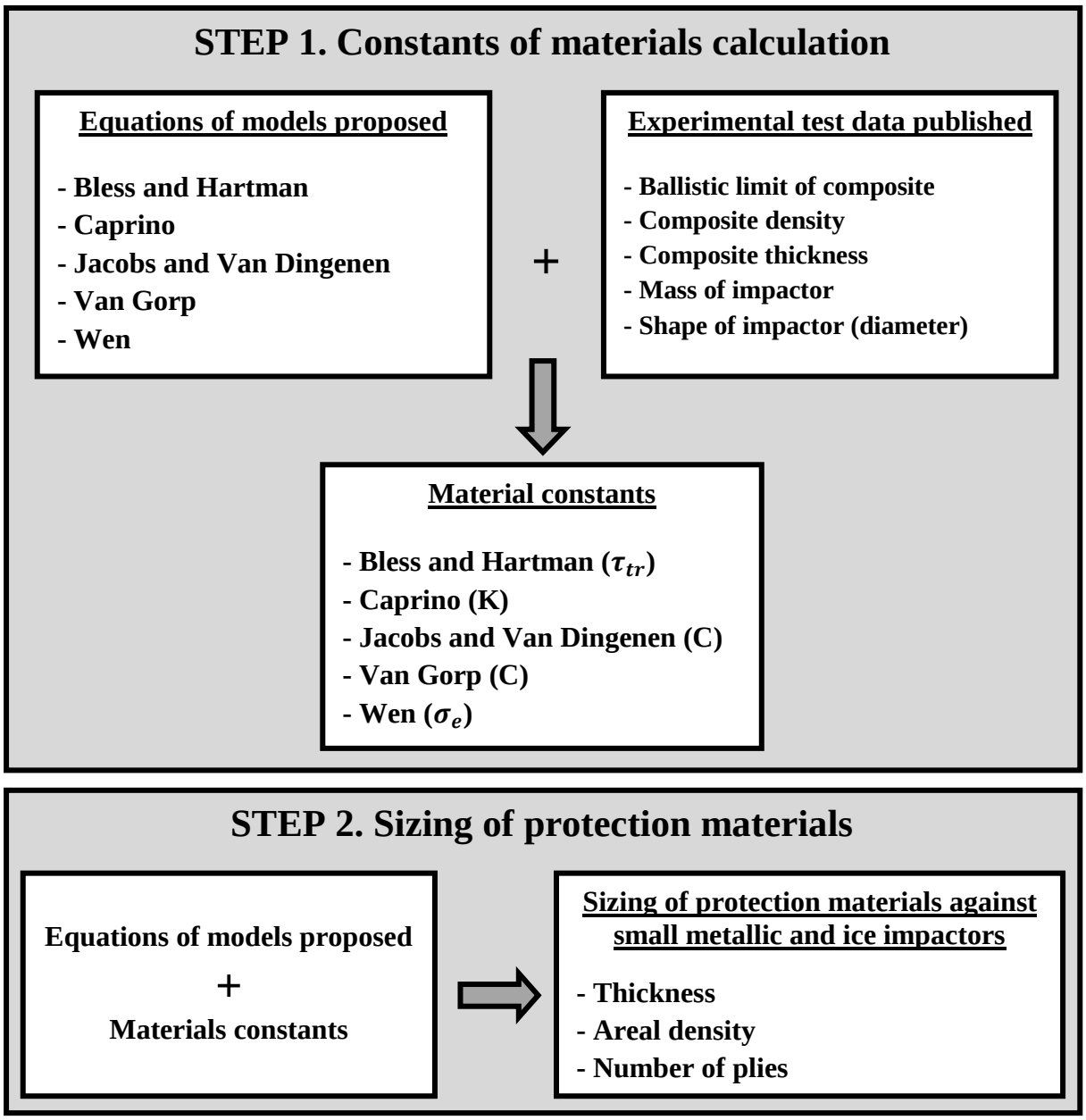

Figure 4.1. *Scheme of calculation procedure for sizing protection materials with semi-analytical models*

In this project two types of fibres are studied: aramid and polyethylene fibres. For each one there are two different papers to work with:

Aramid fibres:
- Silva *et al.* [41] - ballistic tests and numerical simulations with Kevlar 29.
- Justo [48] - ballistic test with Kevlar 129.

Polyethylene fibres:
- Lee *et al.* [49] - ballistic tests with Spectra 900 and two kinds of resins.
- Colakoglu *et al.* [39] - ballistic test and with Dyneema HB2.

Next sections present constants of materials for each semi-analytical model and dimensions for protections panels are presented. To see complete calculations go to appendix A2.

4.2.1. Aramid fibres

Silva *et al.* [41] performed a series of ballistic test on Kevlar 29 laminates plates made from prepreg fabric impregnated with vynilester resin and cured using the manufacturer's curing conditions.

The target in the ballistic experimental tests was plates of 400 x 400 mm^2 firmly clamped on the edges with 2.4 mm thickness that corresponds to seven layers. Several targets with same dimensions were impacted by a fragment simulating projectile (FSP) of 1.1 g weight with a knowing diameter of 5.4 mm (FSP geometry is clearly studied in Chapter II). Ballistic limit measured is 324.3 m/s. Density of composite is 1400 kg/m^3, of the matrix is 1180 kg/m^3 [49] and the density of Kevlar 29 fibres is 1440 kg/m^3. Some additional parameters are needed before start calculation:

$$\rho_l = \rho_f \cdot V_f + \rho_m \cdot V_m \rightarrow 1400 = 1440 \cdot V_f + 1180 \cdot (1 - V_f) \rightarrow V_f = 0.85$$

$$AD = \rho_l \cdot t = 1400 \cdot 2.4 \cdot 10^{-3} = 3.36 \ {}^{kg}/_{m^2}$$

$$7 \ plies = 2.4 \ mm \ thickness \ \leftrightarrow \ 1 \ ply \approx 0.35 \ mm \ thickness$$

With all the necessary data it is possible to begin with the application of the semi-analytical ballistic models:

STEP 1. Constants of materials calculation

Constants of semi-analytical models	Constants values
Bless and Hartman (τ_{tr})	1144 MPa
Caprino (K)	2.01 $J/mm^{2\alpha}$
Jacobs and Van Dingenen (C)	0.75 Jm^2/mm^2kg
Van Gorp (C)	0.75 Jm^2/mm^2kg
Wen (σ_e)	548 MPa

Table 4.1. *Material constants values calculated for Kevlar 29*

STEP 2. Sizing of protection materials

Fibre type	aramid fibre		
Commercial name	Kevlar 29 / vynilester		
Configuration	woven fabric		
	AD (kg/m^2)	**T (mm)**	**# Plies**
Bless - Hartman	17.33	12.38	35
Caprino	12.6	9	26
Jacobs - Van Dingenen	3.7	2.64	8
Van Gorp	11.9	8.5	25
Wen	7.95	5.68	16

Table 4.2. *Semi-analytical models. Protection design of Kevlar 29 for low size metallic impactor*

Fibre type	aramid fibre		
Commercial name	Kevlar 29 / vynilester		
Configuration	woven fabric		
	AD (kg/m^2)	**T (mm)**	**# Plies**
Bless - Hartman	23.16	16.54	47
Caprino	27.86	19.9	57
Jacobs - Van Dingenen	9.87	7.05	20
Van Gorp	27.3	19.5	55
Wen	20.62	14.73	42

Table 4.3. *Semi-analytical models. Protection design of Kevlar 29 for high size metallic impactor*

Fibre type	aramid fibre		
Commercial name	Kevlar 29 / vynilester		
Configuration	woven fabric		
	AD (kg/m^2)	**T (mm)**	**# Plies**
Bless - Hartman	1.9	1.36	4
Caprino	4	2.84	8
Jacobs - Van Dingenen	1.38	0.99	3
Van Gorp	2.1	1.48	5
Wen	2.67	1.91	6

Table 4.4. *Semi-analytical models. Protection design of Kevlar 29 for ice impactor*

Justo [48] studied in his thesis the ballistic performance of several composite materials. In his experiments, one the parameters measured was the ballistic limit, according to NATO STANAG 2920. The specimen of experiments was a plate of 400 mm x 400 mm with an areal density of 5.01 kg/m^2 and with a ballistic limit measured of 487 m/s.

Composite materials are made of aramid fibre Kevlar 129 in a phenolic matrix, being the resin volume fraction 12%. Complete properties of laminates are shown ext in Table 4.5.

Tecido			Matriz	Pré-impregnado	
Fibra	Número de fios [/cm]	Massa específica [kg/m^2]	Tipo	Massa específica [kg/m^2]	Percentagem de resina [%]
Kevlar® 129 3140 dtex	6,4 x 6,4	0.400-0.410	Fenólica PHF modificada	0.455	12
Processamento					
Meio de conformação	Pressão [MPa]	Temperatura [°C]	Tempo [*min*]	Espessura final [*mm/camada*]	
Prensa de pratos quentes	1	165	10	0.45	

Table 4.5. *Properties of fibres, matrix and final laminate of Kevlar 129 [48]*

The density of Kevlar 129 laminate is measured according to standard ISO 1183:1987 (E) using water as immersion liquid at 18 ºC. The final value of laminate density is 1078 kg/m^3. Fibre density of Kevlar 129 is 1470 kg/m^3. Some additional parameters are needed before start calculation:

$$V_f = 1 - V_r = 1 - 0.12 = 0.88$$

$$AD = \rho_l \cdot t \rightarrow t = \frac{AD}{\rho_l} = \frac{5.01}{1078} = 4.65\ mm$$

$$1\ ply = 0.45\ mm\ thickness$$

Another way to calculate ply thickness could be:

$$t = \frac{\rho_{sf}}{V_f \cdot \rho_f} \rightarrow t = \frac{0.410}{0.88 \cdot 1470} = 0.32\ mm$$

There is a slightly difference between theoretical value of ply thickness (0.32 mm) and real value given by author (0.45 mm) but this difference is perfectly explained by the effect of manufacturing process. A value of 0.45 mm thickness for each ply is taken.

STEP 1. Constants of materials calculation

Constants of semi-analytical models	Constants values
Bless and Hartman (τ_{tr})	687 MPa
Caprino (K)	1.71 J/mm$^{2\alpha}$
Jacobs and Van Dingenen (C)	1.14 Jm^2/mm^{2}kg
Van Gorp (C)	1.14 Jm^2/mm^{2}kg
Wen (σ_e)	557 MPa

Table 4.6. *Material constants values calculated for Kevlar 129*

STEP 2. Sizing of protection materials

Fibre type	aramid fibre		
Commercial name	Kevlar 29 / phenolic		
Configuration	woven fabric		
	AD (kg/m^2)	**T (mm)**	**# Plies**
Bless - Hartman	17.23	15.98	36
Caprino	10.5	9.74	22
Jacobs - Van Dingenen	2.44	2.26	6
Van Gorp	7.83	7.26	17
Wen	6.1	6.58	14

Table 4.7. *Semi-analytical models. Protection design of Kevlar 129 for low size metallic impactor*

Fibre type	aramid fibre		
Commercial name	Kevlar 29 / phenolic		
Configuration	woven fabric		
	AD (kg/m^2)	**T (mm)**	**# Plies**
Bless - Hartman	23	21.33	49
Caprino	23.24	21.56	49
Jacobs - Van Dingenen	6.5	6.02	14
Van Gorp	17.94	16.65	38
Wen	17	15.73	36

Table 4.8. *Semi-analytical models. Protection design of Kevlar 129 for high size metallic impactor*

Fibre type	aramid fibre		
Commercial name	Kevlar 29 / phenolic		
Configuration	woven fabric		
	AD (kg/m^2)	**T (mm)**	**# Plies**
Bless - Hartman	1.9	1.76	4
Caprino	3.31	3.07	7
Jacobs - Van Dingenen	0.9	0.83	2
Van Gorp	1.36	1.26	3
Wen	2.11	1.96	5

Table 4.9. *Semi-analytical models. Protection design of Kevlar 129 for ice impactor*

4.2.2. Polyethylene fibres

Lee *et al.* [49] study the penetration failure mechanisms of armour fibre composites. The study utilized material systems based on the plain-weave fabric of Spectra 900 oriented polyethylene: 5-ply fabric-reinforced composite laminate (≈1.5mm thick). Two different types of resins, vynilester (Dow Derakane 411-45) and aliphatic ester type polyurethane (Mobay Dispercoll E-585) were used as matrixes for Spectra fabric-reinforced composites. The resin contents of final composites were approximately 25% with density of 1180 kg/m^3. Density of Spectra fibre is 970 kg/m^3.

The composite panels were prepared by pressing prepreg plies between two flat aluminium plates. Relying on a programmable press, the temperature was raised at a constant rate from room temperature to the cure temperature where it remained for a fixed period of time. The respective levels of heating rate, cure temperature, cure time, cooling rate, and pressure were: 11°C/min, 116°C, 20 min, 11°C/min, 3.83 MPa (555 psi) for Spectra fabric composites. The cured composite panels were then removed from the press at room temperature.

Some additional parameters are needed before start calculation:

$$\rho_l = \rho_f \cdot V_f + \rho_m \cdot V_m = 970 \cdot 0.75 + 1180 \cdot 0.25 = 1023 \ {}^{kg}/_{m^3}$$

$$AD = \rho_l \cdot t = 1023 \cdot 1.5 \cdot 10^{-3} = 1.53 \ {}^{kg}/_{m^2}$$

$$5 \ plies = 1.5 \ mm \ thickness \ \leftrightarrow \ 1 \ ply \approx 0.3 \ mm \ thickness$$

One type of projectile was used in ballistic tests: fragment-simulating steel projectile (FSP) of 1.1 gram mass and 5.6 mm diameter. It is possible to see the projectile dimensions in figure below. The density of the projectile is 7850 kg/m^3.

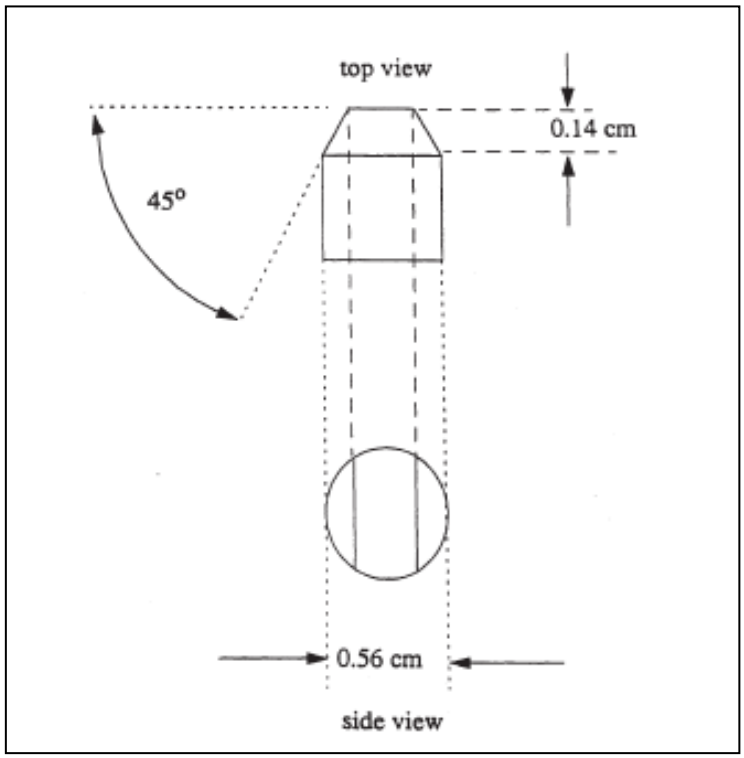

Figure 4.2. *FSP used to evaluate the armour system [49]*

At impact velocity, when a full penetration occurs, it is reached the ballistic limit. Lee *et al.* shows in their paper the energy absorption for full penetration of 5-ply laminates of Spectra fabric-reinforced composite with the two kinds of resin. With vynilester resin the energy absorption is 30.07 J and with polyurethane is 25.95 J, so ballistic limit for both composites can be calculated as:

$$E_p = \frac{1}{2} m_p {V_p}^2 \begin{cases} V_{pVE} = \sqrt{\dfrac{2 \cdot 30.07}{1.1 \cdot 10^{-3}}} = 234 \ {}^{m}/_{s} \\ V_{pPU} = \sqrt{\dfrac{2 \cdot 25.95}{1.1 \cdot 10^{-3}}} = 217 \ {}^{m}/_{s} \end{cases}$$

With all the necessary data, it is possible to begin with the application of the ballistic models for a predetermination of the dimensions:

STEP 1. Constants of materials calculation

Constants of semi-analytical models	Constants values	
	Vynilester matrix	Polyurethane matrix
Bless and Hartman (τ_{tr})	1640 MPa	1410 MPa
Caprino (K)	2.28 J/mm$^{2\alpha}$	1.98 J/mm$^{2\alpha}$
Jacobs and Van Dingenen (C)	0.8 Jm^2/mm^{2}kg	0.7 Jm^2/mm^{2}kg
Van Gorp (C)	0.8 Jm^2/mm^{2}kg	0.7 Jm^2/mm^{2}kg
Wen (σ_e)	550 MPa	470 MPa

Table 4.10. *Material constants values calculated for Spectra 900 with vynilester and polyurethane*

STEP 2. Sizing of protection materials

Fibre type	polyethylene fibre		
Commercial name	Spectra 900 / vinylester		
Configuration	plain woven fabric		
	AD (kg/m^2)	**T (mm)**	**# Plies**
Bless - Hartman	10.58	10.34	35
Caprino	9.52	9.31	31
Jacobs - Van Dingenen	3.47	3.39	11
Van Gorp	11.17	10.91	34
Wen	6.45	6.3	21
Fibre type	polyethylene fibre		
Commercial name	Spectra 900 / polyurethane		
Configuration	plain woven fabric		
	AD (kg/m^2)	**T (mm)**	**# Plies**
Bless - Hartman	11.41	11.15	37
Caprino	10.53	10.29	34
Jacobs - Van Dingenen	3.97	3.88	13
Van Gorp	12.75	12.46	42
Wen	7.16	7	24

Table 4.11. *Semi-analytical models. Protection design of Spectra 900 for low size metallic impactor*

Fibre type	polyethylene fibre		
Commercial name	Spectra 900 / vinylester		
Configuration	plain woven fabric		
	AD (kg/m^2)	**T (mm)**	**# Plies**
Bless - Hartman	14.13	13.81	46
Caprino	21.07	20.60	69
Jacobs - Van Dingenen	9.25	9.04	30
Van Gorp	25.57	24.99	84
Wen	16.47	16.10	54
Fibre type	polyethylene fibre		
Commercial name	Spectra 900 / polyurethane		
Configuration	plain woven fabric		
	AD (kg/m^2)	**T (mm)**	**# Plies**
Bless - Hartman	15.23	14.89	50
Caprino	23.30	22.78	76
Jacobs - Van Dingenen	10.57	10.33	35
Van Gorp	29.22	28.56	95
Wen	18.41	18.00	60

Table 4.12. *Semi-analytical models. Protection design of Spectra 900 for high size metallic impactor*

Fibre type	polyethylene fibre		
Commercial name	Spectra 900 / vinylester		
Configuration	plain woven fabric		
	AD (kg/m^2)	**T (mm)**	**# Plies**
Bless - Hartman	1.17	1.14	4
Caprino	3.01	2.94	10
Jacobs - Van Dingenen	1.29	1.26	4
Van Gorp	1.94	1.89	7
Wen	2.05	2.00	7
Fibre type	polyethylene fibre		
Commercial name	Spectra 900 / polyurethane		
Configuration	plain woven fabric		
	AD (kg/m^2)	**T (mm)**	**# Plies**
Bless - Hartman	1.26	1.23	4
Caprino	3.32	3.25	11
Jacobs - Van Dingenen	1.47	1.44	5
Van Gorp	2.22	2.17	8
Wen	2.35	2.30	8

Table 4.13. *Semi-analytical models. Protection design of Spectra 900 for ice impactor*

Colakoglu *et al.* [39] study ballistic properties of polymer matrix composite made of polyethylene fibres: Dyneema HB2. Every lamina of polyethylene manufactured by Dyneema Company has 0° and 90° fibre layers on it, therefore, the elastic modulus of the lamina is the same in principal directions for this materials ($E_1 = E_2$). Composite specimens were manufactured at 125°C under 20 MPa pressures for a total pressing time of 30 min.

For the ballistic test 20-layered plate specimens are used and the thickness polyethylene plates are 5.6 mm respectively. Penetration test is carried out using a FSP of 1.1 g according to NATO STANAG 2920 (Figure 4.3). Ballistic limit of specimens of Dyneema HB2 is V_{50} = 480 m/s and an areal density of 5.04 kg/m^2, therefore density of laminate is 900 kg/m^3. In this paper, there is no enough information to obtain fibre volume fraction, hence Caprino model cannot be used here.

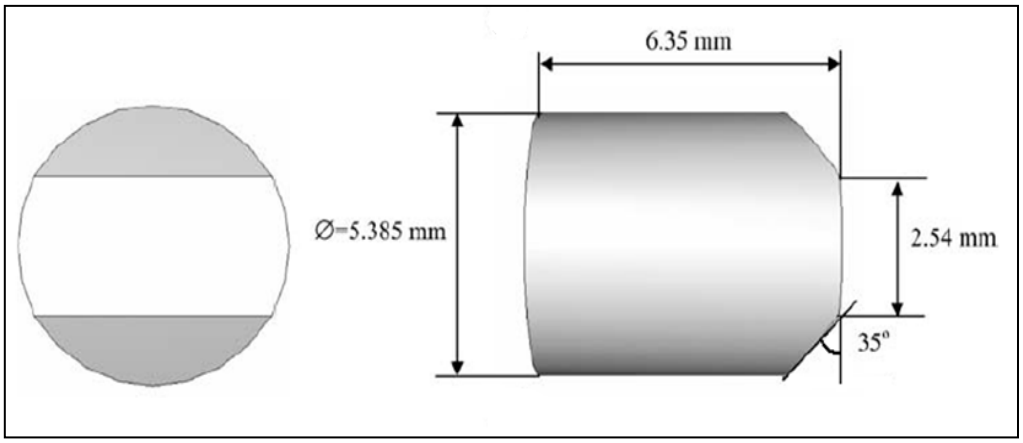

Figure 4.3. *1.1g FSP according to NATO STANAG 2920 [39]*

STEP 1. Constants of materials calculation

Constants of semi-analytical models	Constants values
Bless and Hartman (τ_{tr})	456 MPa
Caprino (K)	-
Jacobs and Van Dingenen (C)	1.1 Jm^2/mm^{2}kg
Van Gorp (C)	1.1 Jm^2/mm^{2}kg
Wen (σ_e)	500 MPa

Table 4.14. *Material constants values calculated for Dyneema HB2*

STEP 2. Sizing of protection materials

Fibre type	polyethylene fibre		
Commercial name	Dyneema UHMWPE UD-HB2		
Configuration	unidirectional [0°/90°/0°/90°]n		
	AD (kg/m^2)	**T (mm)**	**# Plies**
Bless - Hartman	17.65	19.61	70
Caprino	-	-	-
Jacobs - Van Dingenen	2.53	2.81	10
Van Gorp	8.11	9.01	32
Wen	4.73	5.25	19

Table 4.15. *Semi-analytical models. Protection design of Dyneema HB2 for low size metallic impactor*

Fibre type	polyethylene fibre		
Commercial name	Dyneema UHMWPE UD-HB2		
Configuration	unidirectional [0°/90°/0°/90°]n		
	AD (kg/m^2)	**T (mm)**	**# Plies**
Bless - Hartman	23.57	26.19	94
Caprino	-	-	-
Jacobs - Van Dingenen	6.73	7.47	28
Van Gorp	18.6	20.66	74
Wen	20.76	23.06	82

Table 4.16. *Semi-analytical models. Protection design of Dyneema HB2 for high size metallic impactor*

Fibre type	polyethylene fibre		
Commercial name	Dyneema UHMWPE UD-HB2		
Configuration	unidirectional [0°/90°/0°/90°]n		
	AD (kg/m^2)	**T (mm)**	**# Plies**
Bless - Hartman	1.94	2.16	8
Caprino	-	-	-
Jacobs - Van Dingenen	0.94	1.04	4
Van Gorp	1.41	1.56	6
Wen	2.55	2.83	11

Table 4.17. *Semi-analytical models. Protection design of Dyneema HB2 for ice impactor*

4.2.3. Conclusions extracted from design of protections with semi-analytical models

After sizing of protection materials with the five semi-analytical models previously selected it is possible to conclude:

- Dimensions obtained with Jacobs and Van Dingenen model are very low for both composite of organic fibres and for three types of impactors. This model allows considering the stiffness of the projectile by using some parameters, but without more extensive studies it is impossible to know properly these factors.

- Caprino model is a semi-analytical model validated with experimental data for low velocity impact. The value of the constant α was estimated at 1.4 according with some values found in Caprino's works [34], but there is no data for aramid and polyethylene fibres.

- Dimensions obtained with Bless and Hartman model, Wen model and Van Gorp model are in close agreement between them, however the Van Gorp model presents the most simple equation.

- Finally and considering all of these aspects, the semi-analytical model presented by Van Gorp, seems to be the most suitable for sizing protection panels against impacts. In next chapter this model was used to propose an analytical expression according with numerical simulations performed with PamCrash.

- Values obtained by sizing protections with semi-analytical models have a significantly dispersion range, however it is enough to obtain previous values of protections dimensions for the three types of impactors:

  1. ***Low size metallic impactor:*** aramid fibres ≈ 10 mm / polyethylene fibres ≈ 10 mm
  2. ***High size metallic impactor:*** aramid fibres ≈ 25 mm / polyethylene fibres ≈ 25 mm
  3. ***Ice impactor:*** aramid fibres ≈ 2 mm / polyethylene fibres ≈ 2 mm

4.3. Design of protections with numerical models for small metallic impactors

Two types of impactors have been proposed as small metallic fragments representative as Uncontained Engine Rotor Failure (UERF). The aim of the design is to determine the minimum protection thickness to stop impactors.

In addition, the influence of impactor velocity, the impact angle or boundary conditions have been studied.

4.3.1. Impactors

Two types of small metallic fragments have been prepared for simulations: low size and high size impactors. Figure 4.4 and 4.5 shows FE mesh corresponding to geometrical data presented in section 4.1.

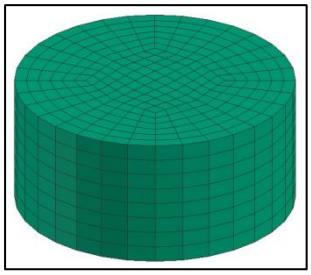

Figure 4.4. *Geometry and mesh of low size impactor*

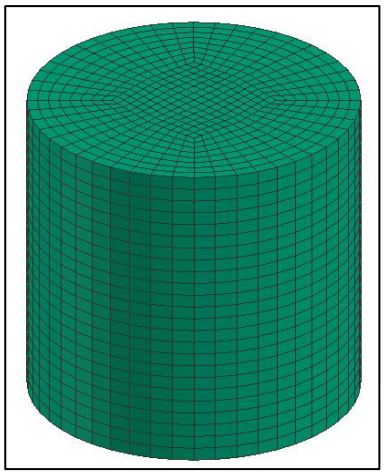

Figure 4.5 *Geometry and mesh of high size impactor*

The material used is steel modelled in PamCrash with a MAT16. The steel material model developed has high stiffness and the effects of the impactor material will likely be negligible.

MATERIAL	G (Pa)	K (Pa)	Yield stress (Pa)	Et (Pa)
Steel	$7.54 \cdot 10^{10}$	$16.30 \cdot 10^{10}$	$720 \cdot 10^{6}$	$1.96 \cdot 10^{11}$

Table 4.18. *Properties of steel for small metallic impactors*

4.3.2. Protection panels

The protection panels have been modelled using MAT 16 of PamCrash with properties validated for Kevlar 29 and Dyneema HB2 (Chapter III). From the application of semi-analytical models, section 4.2, an estimation of thickness is 10 mm for low size - high velocity impactor and 25 mm for high size - high velocity one.

These values are taken as first tentative of protection thickness. Protection panels are flat plates of 350 mm x 350 mm.

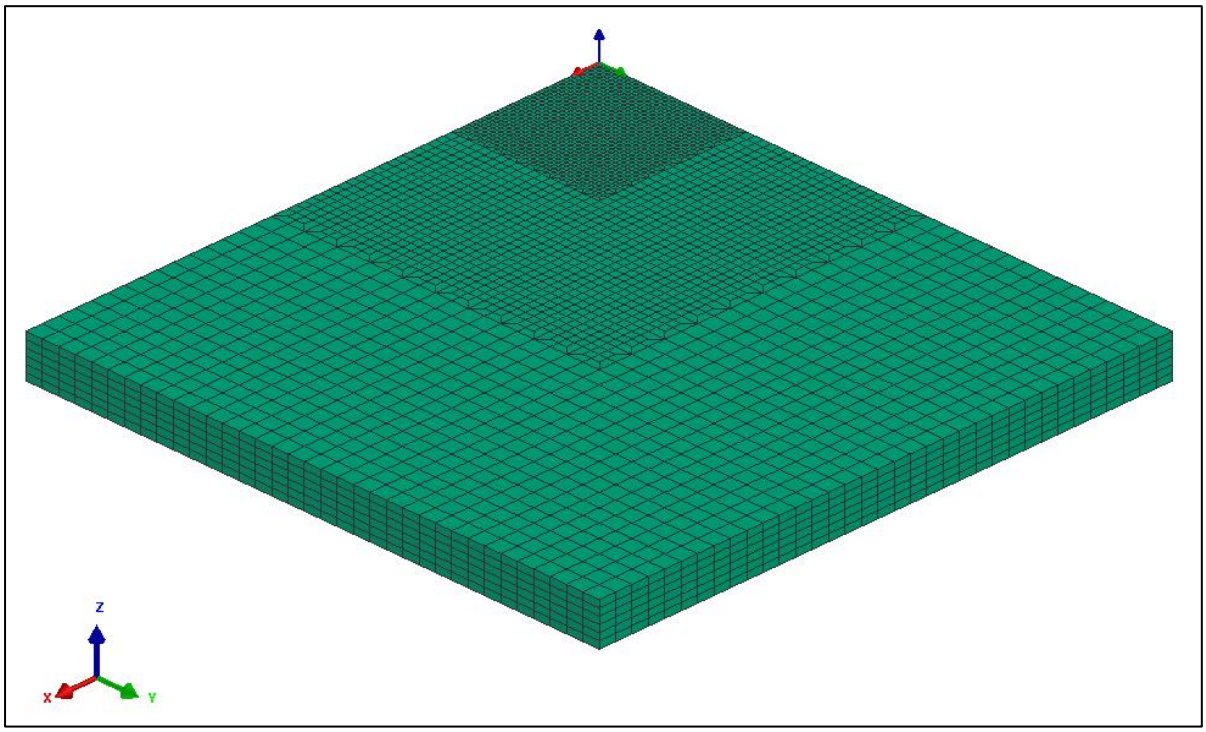

Figure 4.6. *Plate mesh isometric view (12 mm thickness plate)*

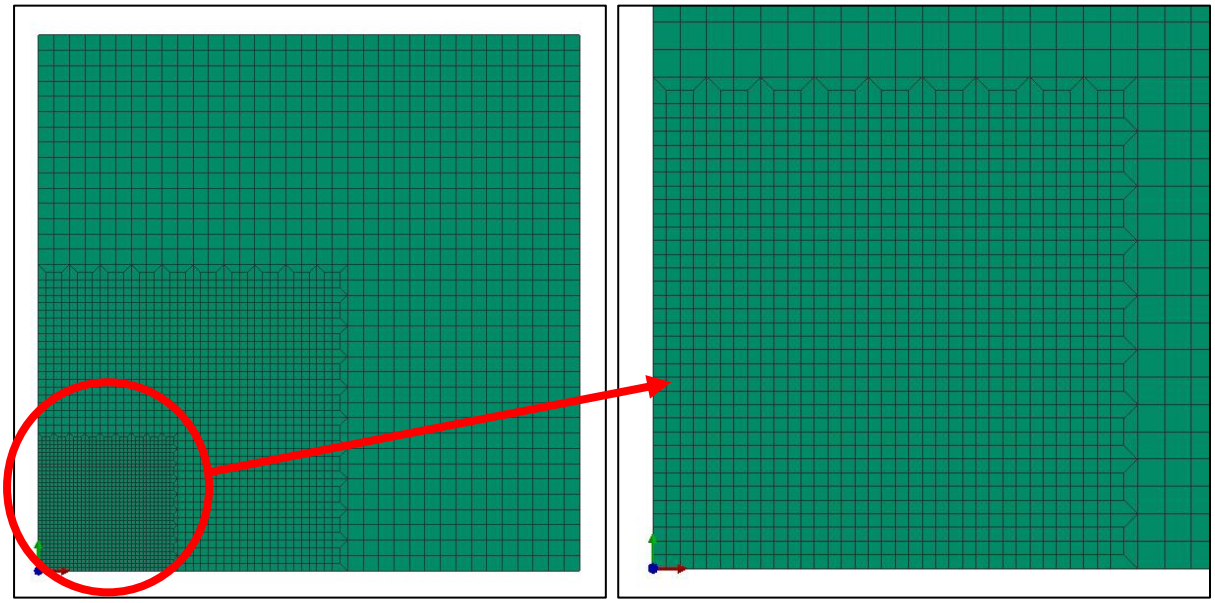

Figure 4.7. *Plate mesh view in plan XY (left) and central region detail (right)*

4.3.3. Curves of design

The design of protections consists in given an impactor type at a certain velocity; determine the minimum thickness of the laminate made of a certain material.

In case of small metallic fragments and protections of Kevlar 29 and Dyneema HB2, the sets of numerical simulations cover thickness between 5 mm up to 30 mm and are summarized in Table 4.19.

For the low size metallic fragment at 585 m/s, designs obtained with numerical simulations are:

- **Kevlar 29 → 8 mm**
- **Dyneema HB2 → 11 mm**

In case of the high size metallic fragment at 479 m/s, designs are:

- **Kevlar 29 → 21 mm**
- **Dyneema HB2 → 30 mm**

These results are in accordance with the ones anticipated by the semi-analytical models of 10 mm for the low size impactor and 25 mm for the high size one. Figure 4.8 shows two sequences of low size fragment impacting a 12 mm Kevlar 29 protection (above design thickness) and high size one impacting a 12 mm Dyneema HB2 protection (below design thickness).

Small metallic 8g impactor			
Kevlar 29		**Dyneema HB2**	
Thickness (mm)	**Perforation**	**Thickness (mm)**	**Perforation**
12	partial perforation	12	partial perforation
10	partial perforation	11	ballistic limit
8	ballistic limit	10	total perforation
7	total perforation	9	total perforation
6	total perforation	8	total perforation
Small metallic 74g impactor			
Kevlar 29		**Dyneema HB2**	
Thickness (mm)	**Perforation**	**Thickness (mm)**	**Perforation**
12	total perforation	12	total perforation
15	total perforation	15	total perforation
20	total perforation	20	total perforation
21	ballistic limit	25	total perforation
22	partial perforation	28	total perforation
23	partial perforation	29	total perforation
25	partial perforation	30	ballistic limit
30	partial perforation	31	partial perforation

Table 4.19. *Minimum thickness necessary to stop impactors for both materials (in red)*

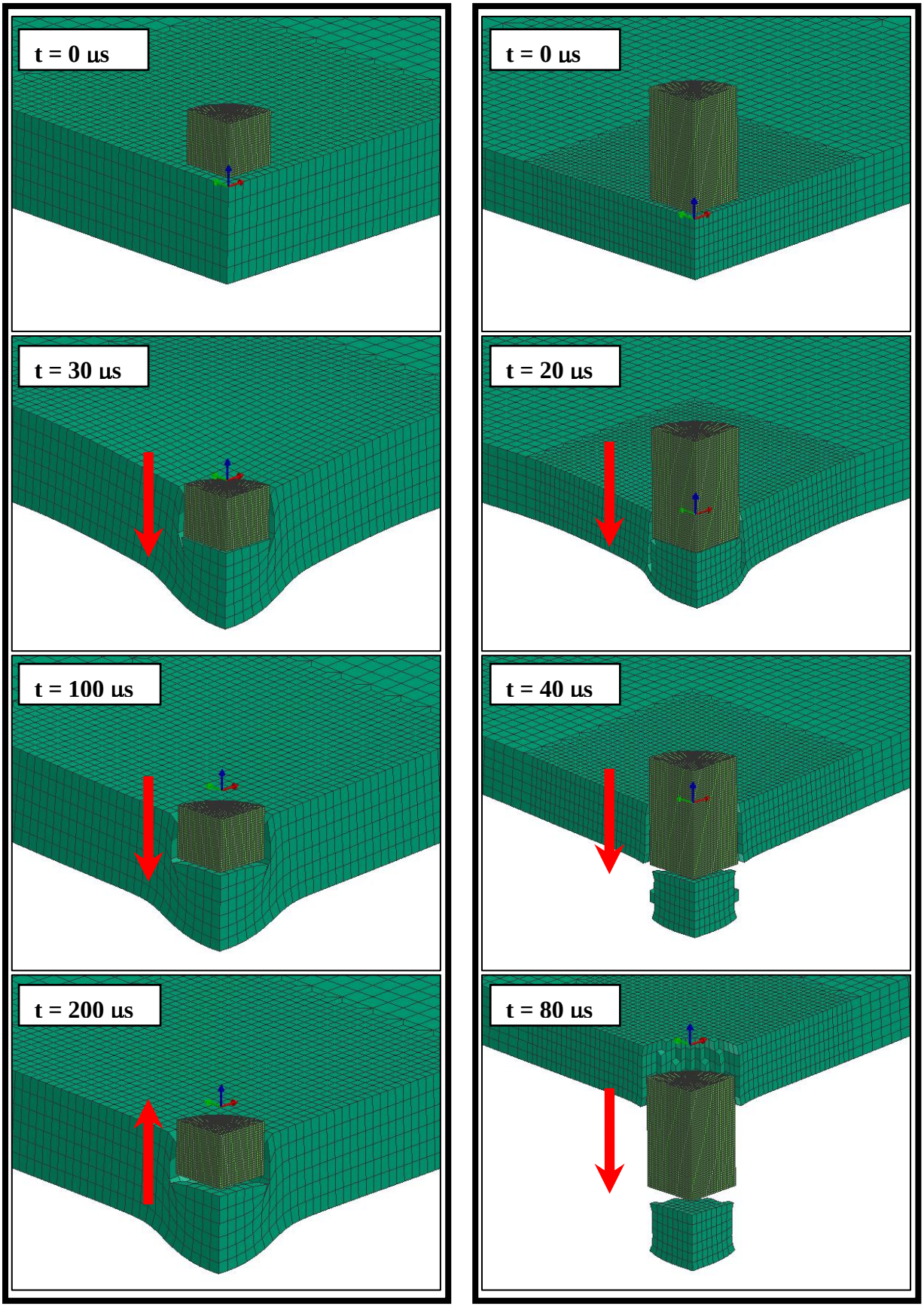

Figure 4.8. *Impact sequence for small metallic 8g impactor against 12 mm thickness protection made of Kevlar 29 (left) and for small metallic 74g impactor against 12 mm thickness protection made of Dyneema HB2 (right)*

A conventional way of representing the impact behaviour of a protection shield is by means of curves representing the impactor residual velocity versus the initial strike velocity. Every curve is valid for a given impactor (mass, shape and stiffness) and for a given protection (material and thickness). The ballistic limit corresponding at every configuration is the maximum initial velocity where residual velocity starts being positive. The design curves of a protection material represent residual velocity depending on laminate thickness. Figure 4.9, 4.10, 4.12 and 4.13 cover impacts of small metallic fragments against Kevlar 29 and Dyneema HB2 protections. Design thicknesses are shown in red lines.

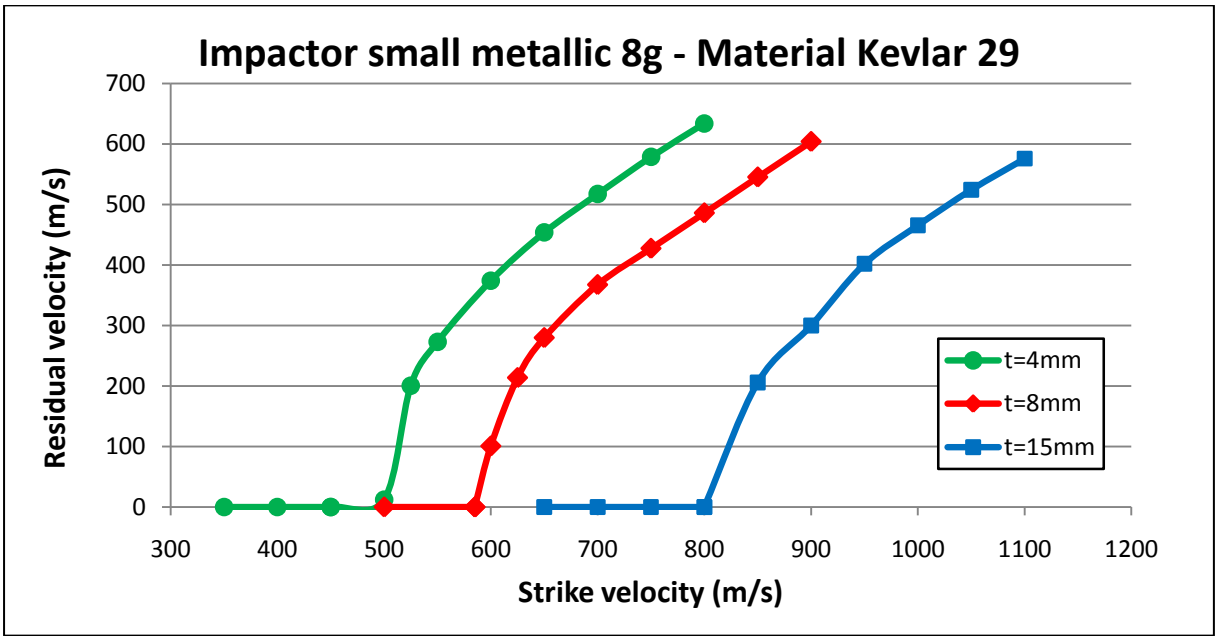

Figure 4.9. *Residual velocity versus strike velocity at various thicknesses for an small metallic impactor of 8g and Kevlar 29 target*

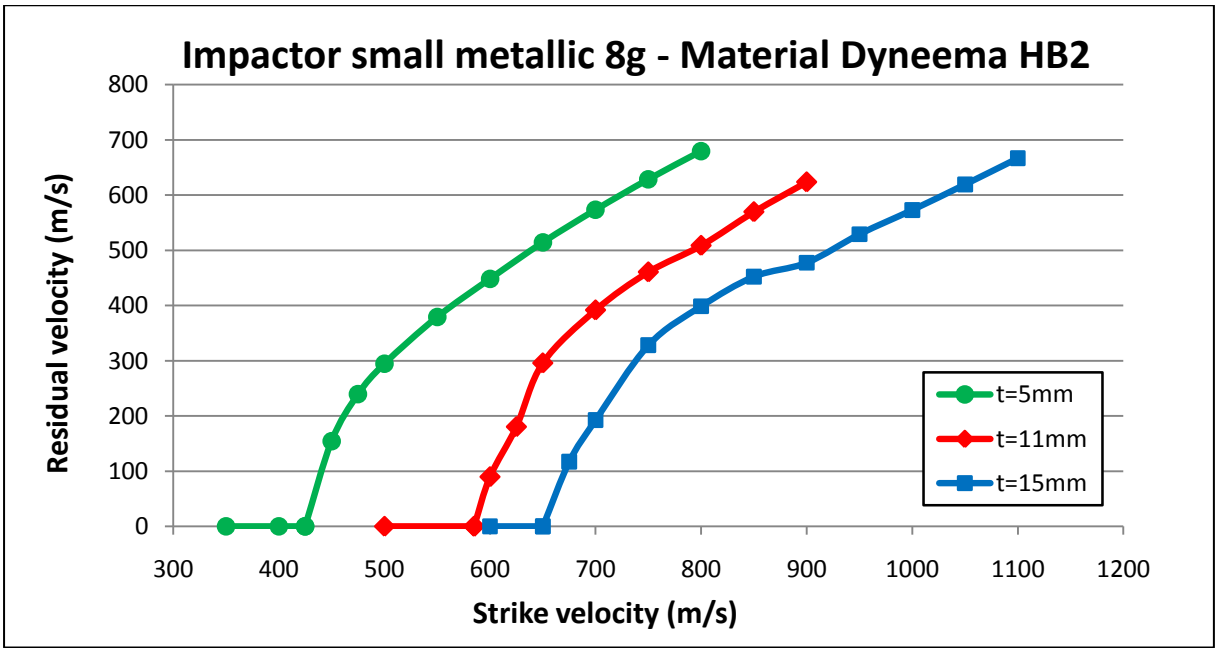

Figure 4.10. *Residual velocity versus strike velocity at various thicknesses for an small metallic impactor of 8g and Dyneema HB2 target*

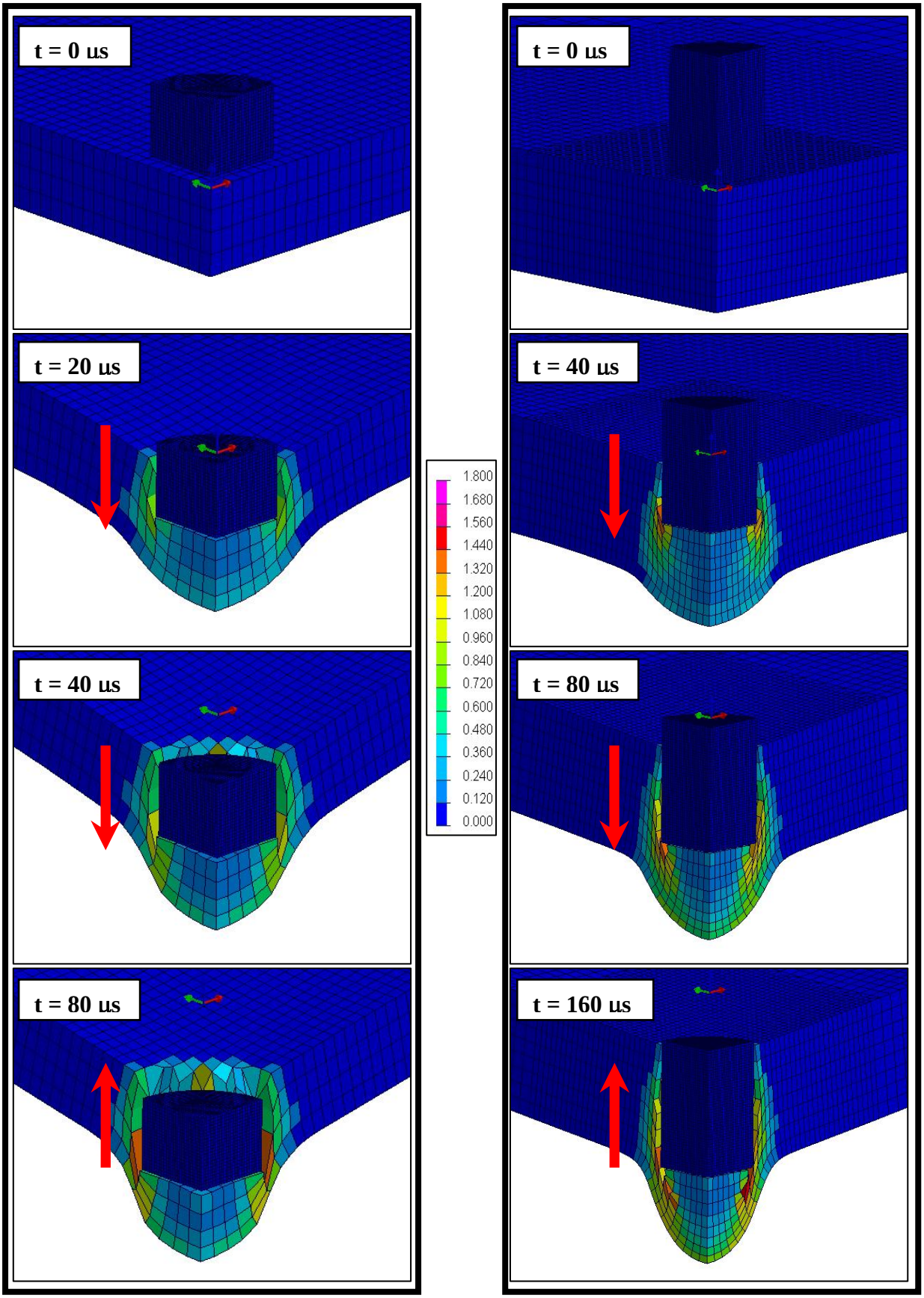

Figure 4.11. *Plastic strain contours: impact sequence for small metallic 8g impactor (left) and for small metallic 74g impactor (right) against protection made of Kevlar 29 at nominal conditions*

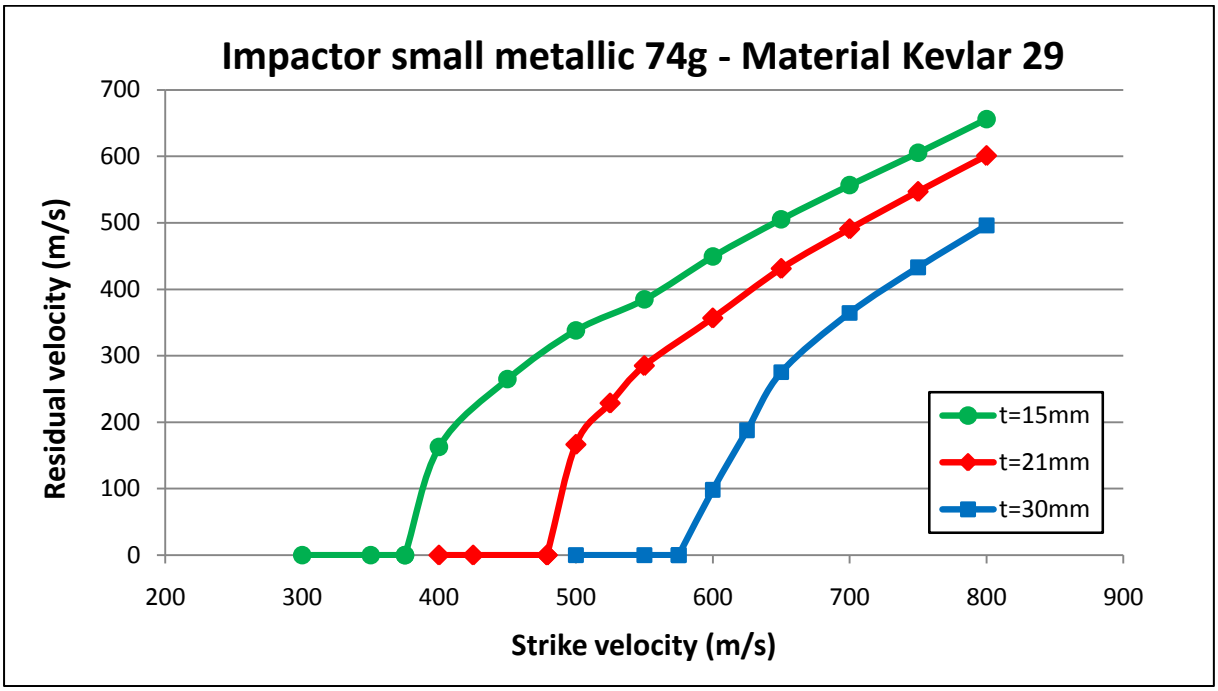

Figure 4.12. *Residual velocity versus strike velocity at various thicknesses for an small metallic impactor of 74g and Kevlar 29 target*

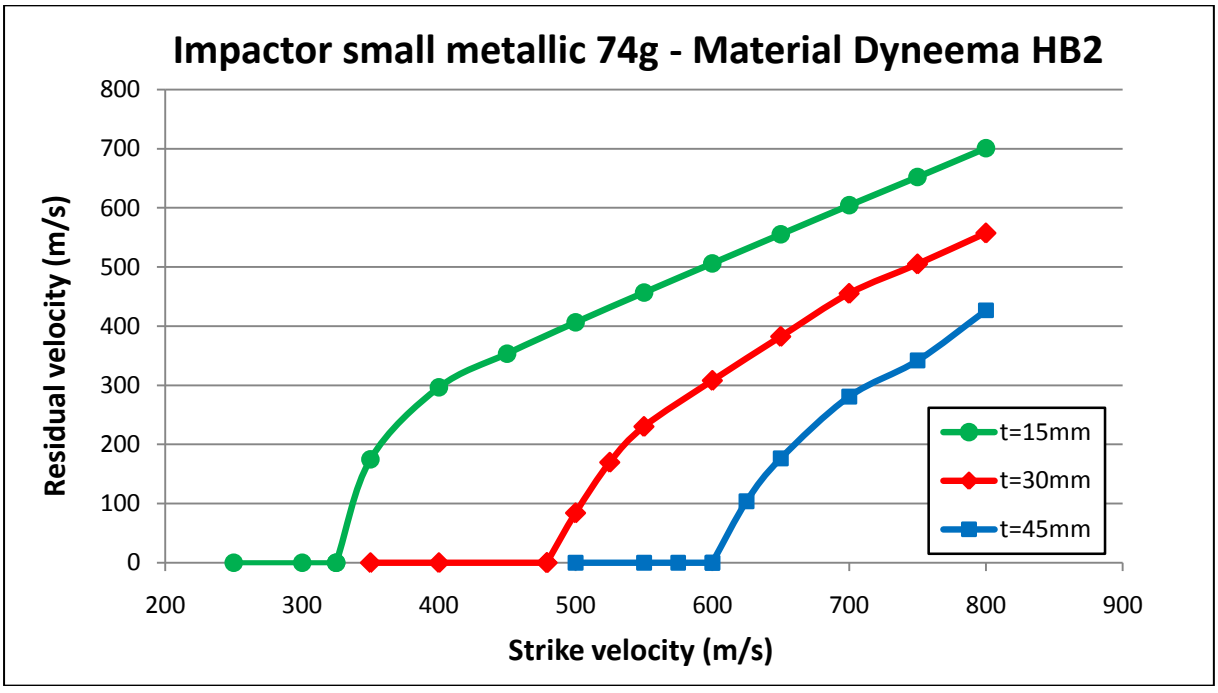

Figure 4.13. *Residual velocity versus strike velocity at various thicknesses for an small metallic impactor of 74g and Dyneema HB2 target*

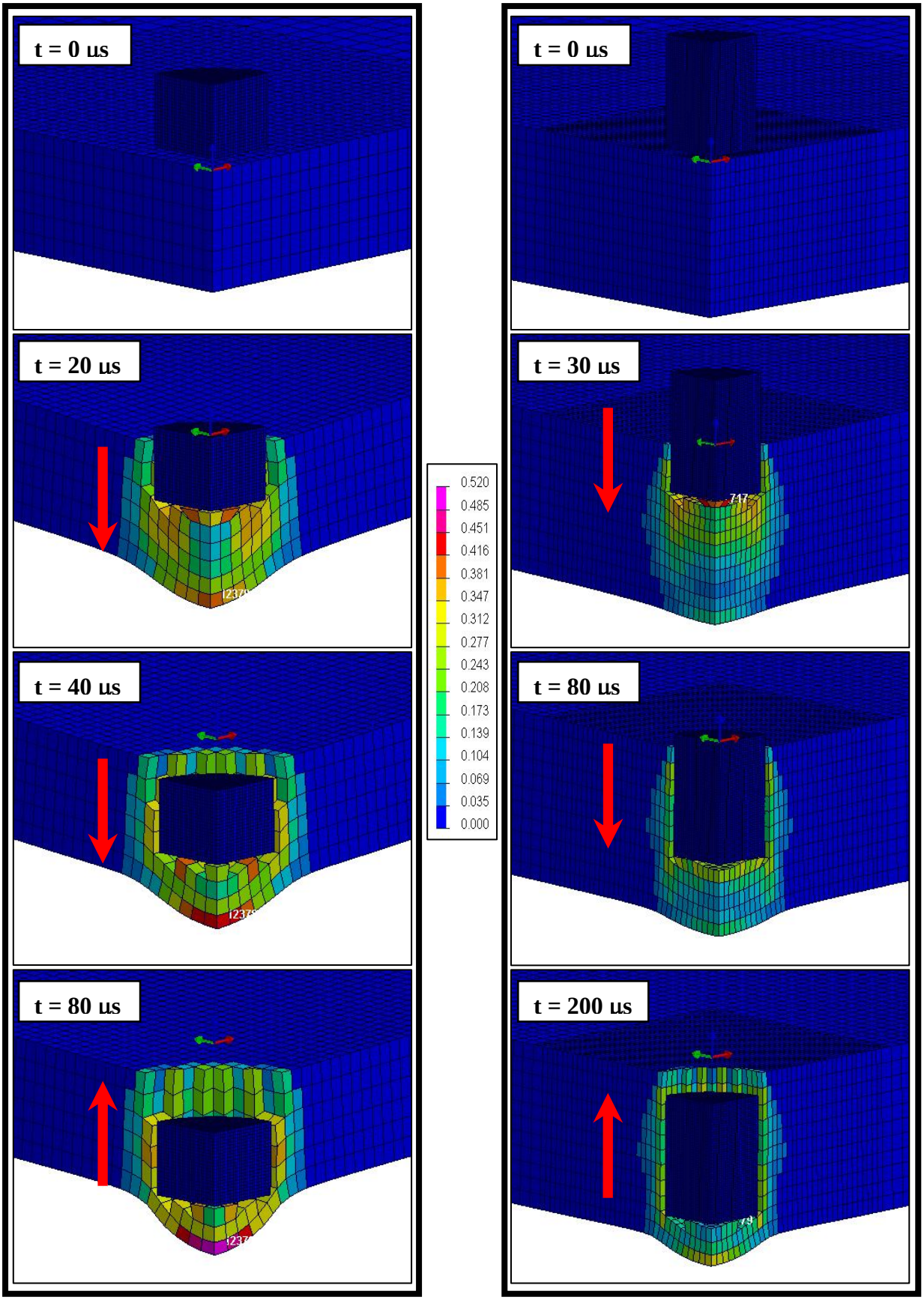

Figure 4.14. *Plastic strain contours: impact sequence for small metallic 8g impactor (left) and for small metallic 74g impactor (right) against protection made of Dyneema HB2*

With the information obtained from the numerical simulations, the semi-analytical model of Van Gorp *el al.* [31] presented in section 2.6.7 may be tuned up. In this model the ballistic limit may be expressed in terms of:

$$V_b = K \cdot \sqrt{\frac{S \cdot t}{m_p}} \qquad (4.1)$$

where:

- t : thickness of composite [m]
- S : surface area of the strike face area of impactor [mm^2]
- m_p : projectile mass [kg]
- K : constant depending on protection material properties and the impactor type [mkg/s^2mm^2].

With set of conditions coming from the numerical simulations, an average value of the constant parameter (K) is calculated.

The value of K may be obtained at every impact configuration. Tables 4.20 and 4.21 show values for the low and high size impactor, and Kevlar 29 and Dyneema HB2 protections.

Results show that dependence of the impactor type is small in comparison to the protection properties.

	V_b (m/s)	m_p (kg)	E_{abs} (J)	S (mm^2)	ρ_{lam} (kg/m^3)	t (m)	AD (kg/m^2)	C (Jm^2/mm^2kg)	K (mkg/s^2mm^2)
Small metallic 8g	450	0.008	810	161	1160	0.004	4.64	1.08	50.16
	585	0.008	1369	161	1160	0.008	9.28	0.92	46.10
	800	0.008	2560	161	1160	0.015	17.4	0.91	46.04
Small metallic 74g	375	0.074	5203	415.5	1160	0.015	17.4	0.72	40.86
	479	0.074	8489	415.5	1160	0.021	24.36	0.84	44.11
	575	0.074	12233	415.5	1160	0.03	34.8	0.85	44.30
							$K_{average}$		**45.26**
							Deviation		**2.79**

Table 4.20. *Material constant for Kevlar 29*

	V_b (m/s)	m_p (kg)	E_{abs} (J)	S (mm^2)	ρ_{lam} (kg/m^3)	t (m)	AD (kg/m^2)	C (Jm^2/mm^2kg)	K (mkg/s^2mm^2)
Small metallic 8g	425	0.008	723	161	900	0.005	4.5	1.00	42.37
	585	0.008	1369	161	900	0.011	9.9	0.86	39.32
	650	0.008	1690	161	900	0.015	13.5	0.78	37.41
Small metallic 74g	325	0.074	3908	415.5	900	0.015	13.5	0.70	35.41
	479	0.074	8489	415.5	900	0.03	27	0.76	36.91
	600	0.074	13320	415.5	900	0.045	40.5	0.79	37.75
							$K_{average}$		**38.19**
							Deviation		**2.19**

Table 4.21. *Material constant for Dyneema HB2*

Reference values for semi-analytical expression based on Van Gorp model are:

$$K_{Kevlar\ 29} = 45.26\ mkg/s^2mm^2 \qquad K_{Dyneema\ HB2} = 38.19\ mkg/s^2mm^2$$

which may be used for design applications for small metallic fragments impacting on Kevlar 29 and Dyneema HB2 protections. This expression is based on model proposed by Van Gorp *et al.* and constant values have been obtained by means of validated numerical simulations.

Comparison of ballistic limit predictions using pure numerical simulations of PamCrash and the expression of Van Gorp (Equation 4.1) are shown for the two types of small metallic fragments.

For low size metallic impactor data of ballistic limit are shown in Figures 4.15 and 4.16. Results are compared, and differences are not higher than 10 % in any case.

Small metallic 8g impactor							
Kevlar 29				Dyneema HB2			
t (mm)	V_b analytic (m/s)	V_b PamCrash (m/s)	Error (%)	t (mm)	V_b analytic (m/s)	V_b PamCrash (m/s)	Error (%)
4	412.72	450	8.28	5	395.23	425	7.00
8	583.67	585	0.23	11	586.22	585	0.21
15	799.23	800	0.10	15	684.56	650	5.05

Table 4.22. *Comparison of ballistic limit calculated with numerical simulations and with analytical expression*

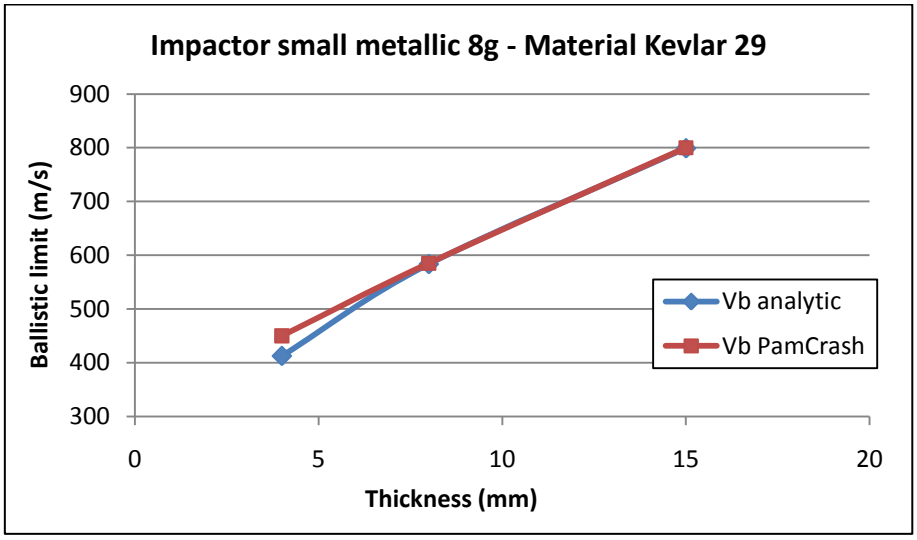

Figure 4.15. *Ballistic limit calculated for Kevlar 29 and small metallic 8g impactor at three different thicknesses*

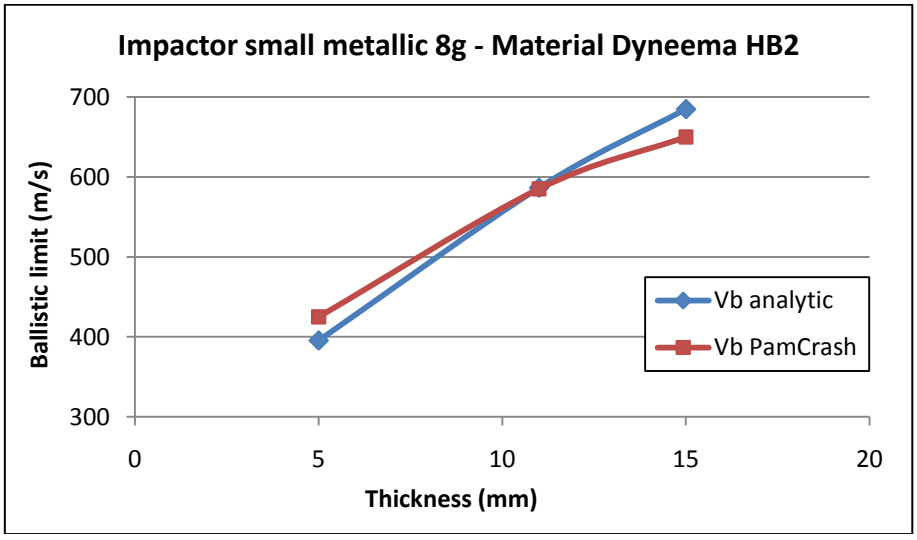

Figure 4.16. *Ballistic limit calculated for Dyneema HB2 and small metallic 8g impactor at three different thicknesses*

Figures 4.17 and 4.18 show ballistic limit data for high size metallic impactors. Results are compared, and differences are not higher than 10 % in any case.

Small metallic 74g impactor							
Kevlar 29				Dyneema HB2			
t (mm)	V_b analytic (m/s)	V_b PamCrash (m/s)	t (mm)	t (mm)	V_b analytic (m/s)	V_b PamCrash (m/s)	t (mm)
15	415.36	375	9.72	15	350.48	325	7.27
21	491.47	479	2.54	30	495.66	479	3.36
30	587.41	575	2.11	45	607.05	600	1.16

Table 4.23. *Comparison of ballistic limit calculated with numerical simulations and with analytical expression*

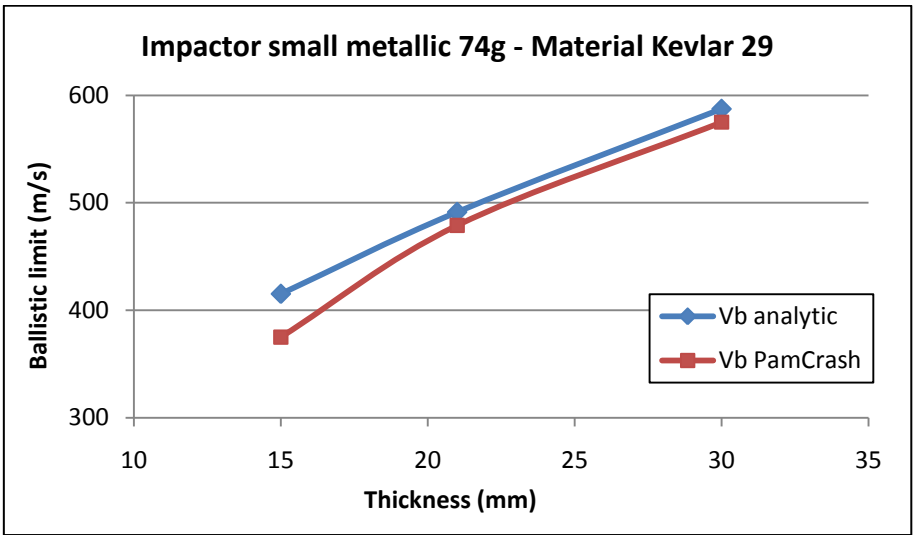

Figure 4.17. *Ballistic limit calculated for Kevlar 29 and small metallic 74g impactor at three different thicknesses*

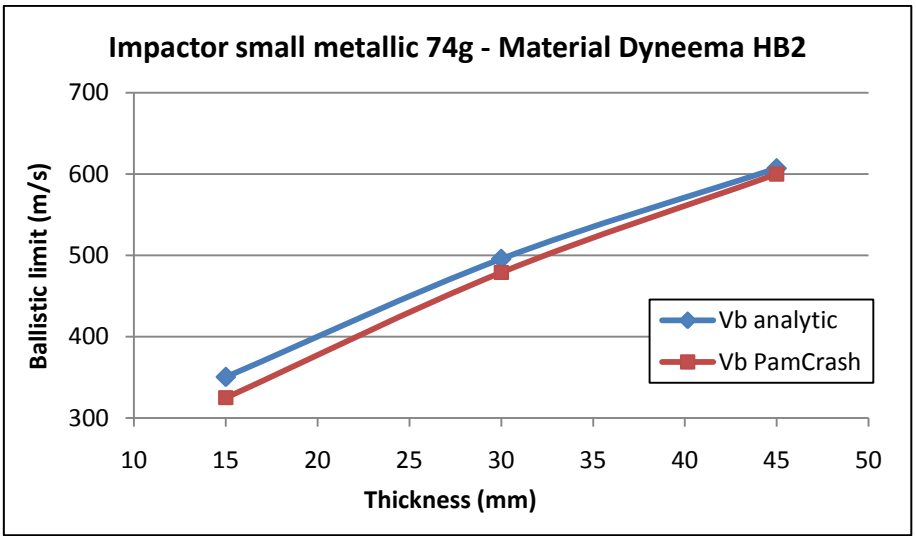

Figure 4.18. *Ballistic limit calculated for Dyneema HB2 and small metallic 74g impactor at three different thicknesses*

4.3.4. Sensitivity analysis

Two sensitivity analyses have been performed by means of numerical simulations next:

- Effect of impactor angle.
- Effect of boundary conditions.

4.3.4.1. Sensitivity to impact angle

Previous numerical simulations were frontal impacts where the angle of impact was 90º. The variation of ballistic limit at several impact angles is studied at nominal thickness for each type of impactor:

- *Low size metallic impactor:* 8 mm for Kevlar 29 and 11 mm for Dyneema HB2
- *High size metallic impactor:* 21 mm for Kevlar 29 and 30 mm for Dyneema HB2

When considering impacts with a certain impact angle. three possibilities mat occur:

- Total penetration
- Partial penetration
- No penetration

In order to estimate ballistic limit variation with impact angle, partial penetration have been considered as total penetration (conservative assumption).

The ballistic limit obtained with numerical simulations for both impactors and both plate materials are summarized in Table 4.24:

Small metallic 8g impactor				**Small metallic 74g impactor**			
K29 t_n = 8 mm		**DyHB2 t_n = 11 mm**		**K29 t_n=21mm**		**DyHB2 t_n=30mm**	
Angle (º)	**V_b (m/s)**	**Angle (º)**	**V_b (m/s)**	**Angle (º)**	**V_b (m/s)**	**Angle (º)**	**V_b (m/s)**
90	585	90	585	90	479	90	479
75	700	75	660	75	560	75	520
60	720	60	720	60	580	60	580
45	800	45	880	45	680	45	680
30	960	30	980	30	880	30	960

Table 4.24. *Ballistic limit at different angles of impact*

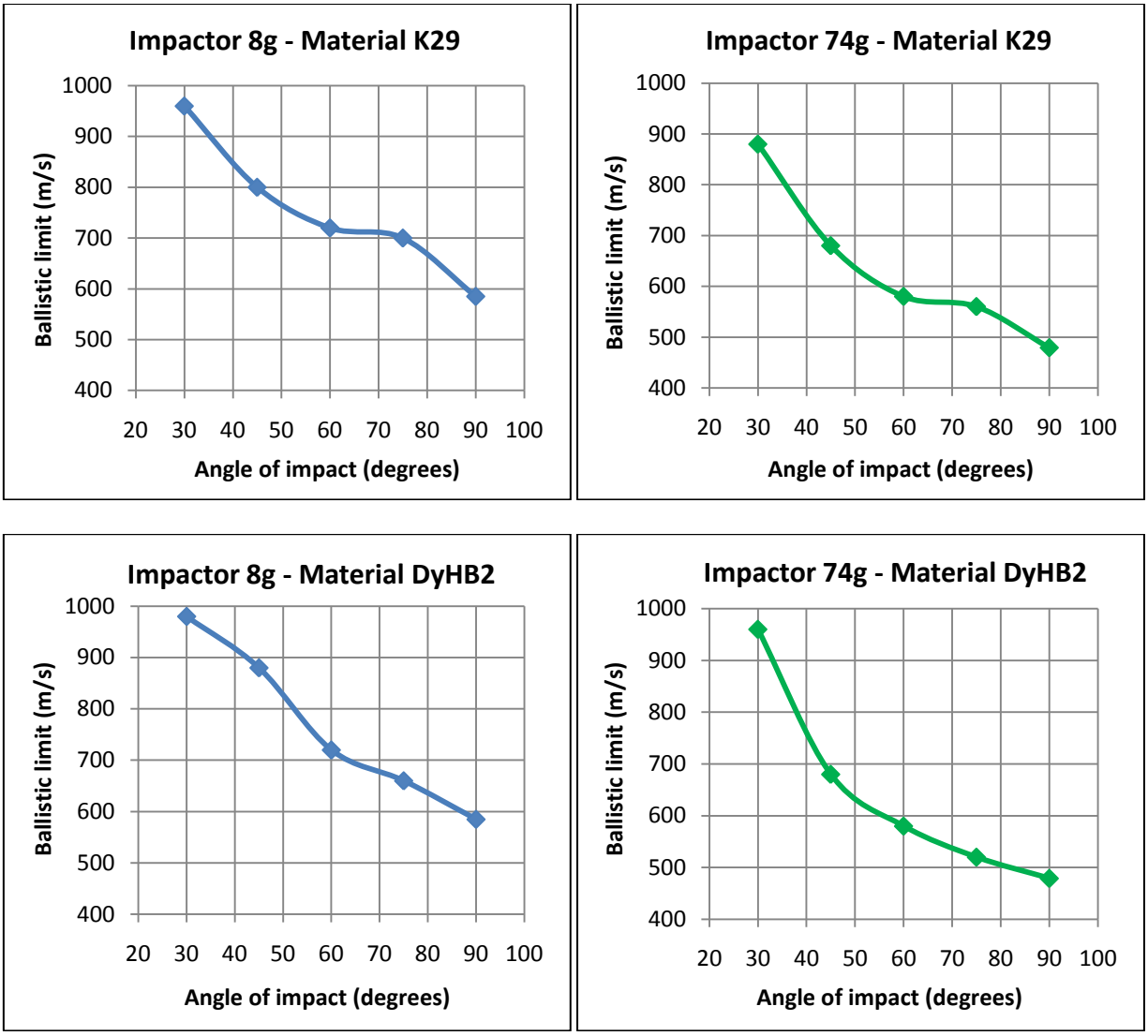

Figure 4.19. *Ballistic limit at different angles of impact*

The main component of the velocity in this case is the component normal to the target ($V_{vertical}$). Therefore, a semi-analytic expression for the ballistic limit that depends on the angle of impact considers the normal velocity to the surface and a coefficient which only depends on the impact angle.

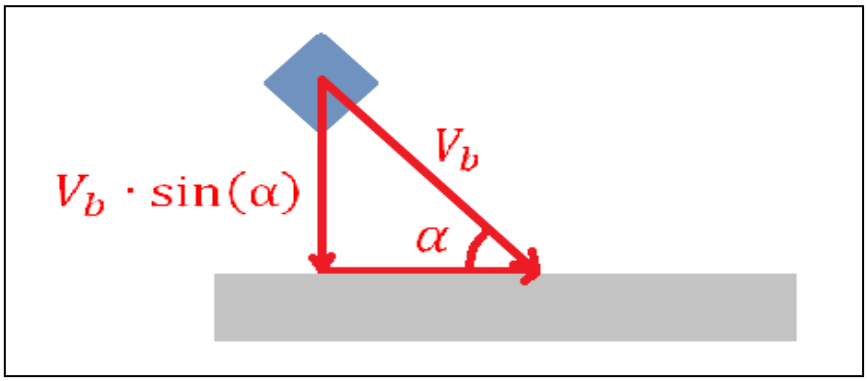

Figure 4.20. *Impact scheme with impact angle*

The speed limit in the case of normal impact is known. Then the ballistic limit for different angles of impact is assumed to be proportional to *sin (α)* and to a constant that depends on the angle of impact. Therefore, the expression could be written as follows:

$$V_{b\alpha} = V_{b90^\circ} \cdot sin(\alpha) \cdot C_i(\alpha) \qquad (4.5)$$

The coefficient *Ci (α)* is independent of the type of material used for target and of the weight and size of the impactor. If the impact angle constant is calculated with data obtained from the simulations, it is possible to check if all constants are the same for the same angle regardless the plate material and impactor weight. The *Ci (α)* coefficient represents the variation of ballistic limit at an impact angle (α) respect to a perpendicular impact condition.

An example of the calculation of a constant *Ci (α)* is presented here and then the rest are summarized in Table 4.25:

- *Target Kevlar 29 plate with 8 mm thickness and small metallic 8g impactor at 90º → V_b = 585 m/s*
- *Target Kevlar 29 plate with 8 mm thickness and small metallic 8g impactor at 75º → V_b = 700 m/s*

$$V_{b\alpha} = V_{b90^\circ} \cdot sin(\alpha) \cdot C_i(\alpha) \rightarrow V_{b75^\circ} = V_{b90^\circ} \cdot sin(75°) \cdot C_i(75°)$$

$$C_i(\alpha) = \frac{V_{b75^\circ}}{V_{b90^\circ} \cdot sin(75°)} \rightarrow C_i(\alpha) = \frac{700}{585 \cdot sin(75°)} \rightarrow C_i(\alpha) = 1.24$$

		Small metallic 8g impactor		Small metallic 74g impactor	
		K29 t=8mm	DyHB2 t=11mm	K29 t=21mm	DyHB2 t=30mm
Angle of impact (º)	90º	1.00	1.00	1.00	1.00
	75º	1.24	1.17	1.21	1.12
	60º	1.42	1.42	1.40	1.40
	45º	1.93	2.13	2.01	2.01
	30º	3.28	3.35	3.67	4.01

		Coefficient C_i (α)	
		Average	Stand. deviation
Angle of impact (º)	90º	1.00	0.00
	75º	1.19	0.04
	60º	1.41	0.01
	45º	2.02	0.07
	30º	3.58	0.29

Table 4.25. *Coefficients of impact angle for both impactors (up) and coefficient average and deviation (down)*

As expected, the coefficient only depends on the angle of impact.

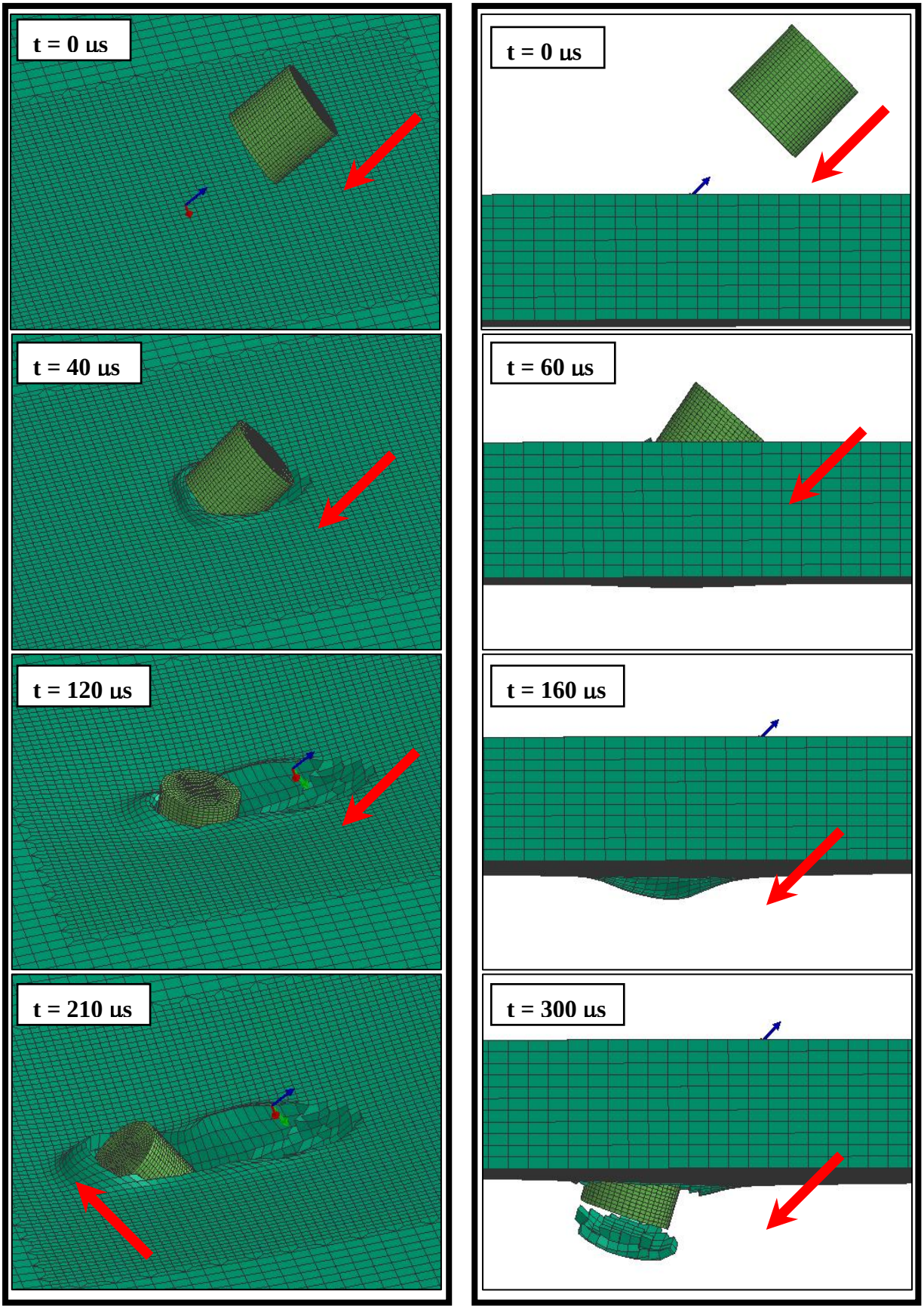

Figure 4.21. *Impact sequence of small metallic 74g impactor with an impact angle of 30º at 840 m/s impacting on Kevlar 29 (left) and small metallic 74g impactor with an impact angle of 45º at 700 m/s impacting on Dyneema HB2 (right)*

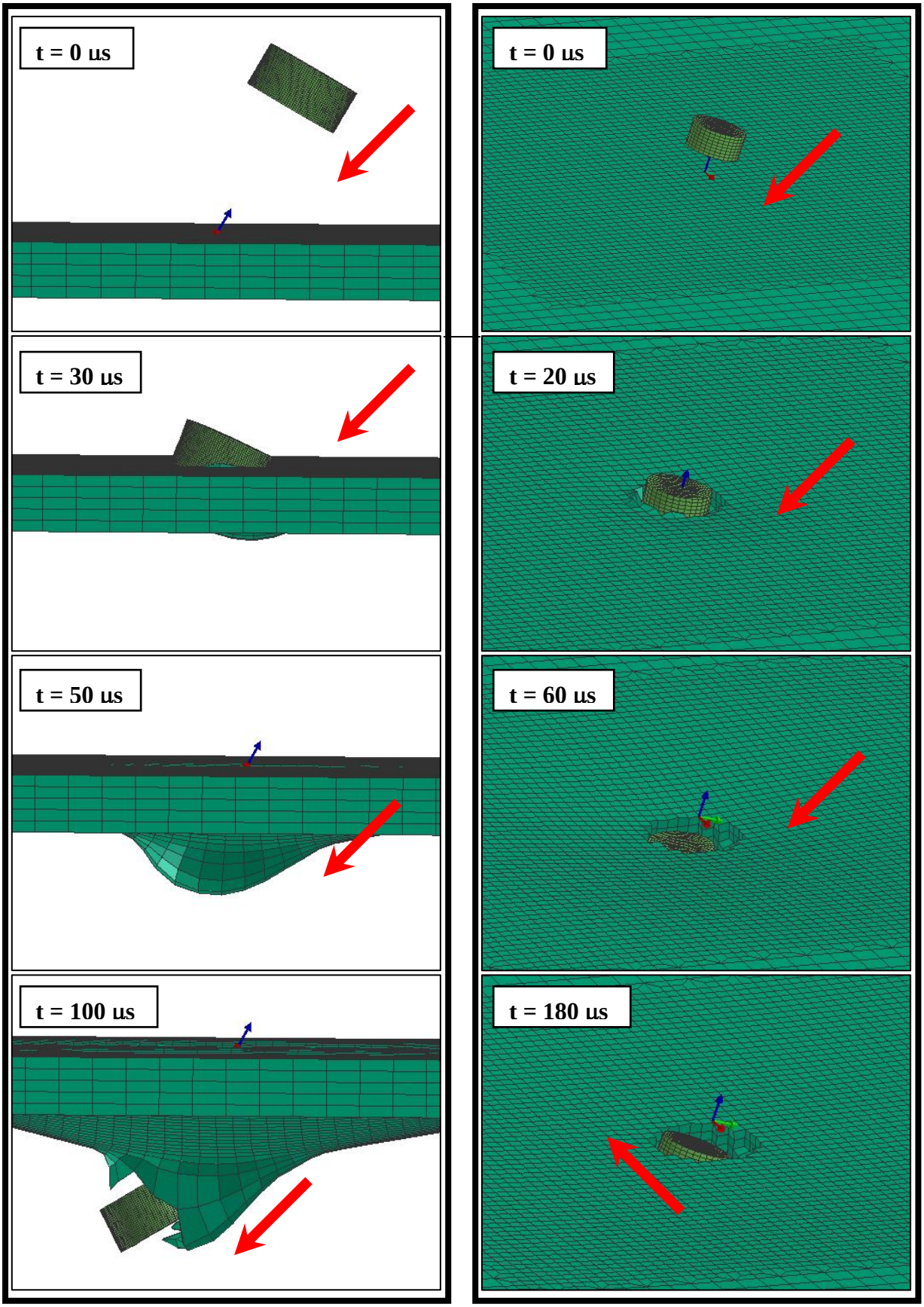

Figure 4.22. *Impact sequence of small metallic 8g impactor with an impact angle of 60º at 800 m/s impacting on Kevlar 29 (left) and small metallic 8g impactor with an impact angle of 75º at 640 m/s impacting on Dyneema HB2 (right)*

4.3.4.2. Sensitivity to boundary conditions

The way in which the protection panels may be attached to the aeronautical structure will be dependent on the structural architecture. Up to know, all simulations performed have considered four edges clamped. However, in certain situations the protection panel attachment may be different.

A right estimation of the sensitivity to boundary conditions can be done by running more cases at the same velocities in the nominal case thickness:

- *Low size metallic impactor:* 8 mm for Kevlar 29
  11 mm for Dyneema HB2
- *High size metallic impactor:* 21 mm for Kevlar 29
  30 mm for Dyneema HB2

Thus, a study of the impact performance when the panels are attached by only two opposite edges is presented:

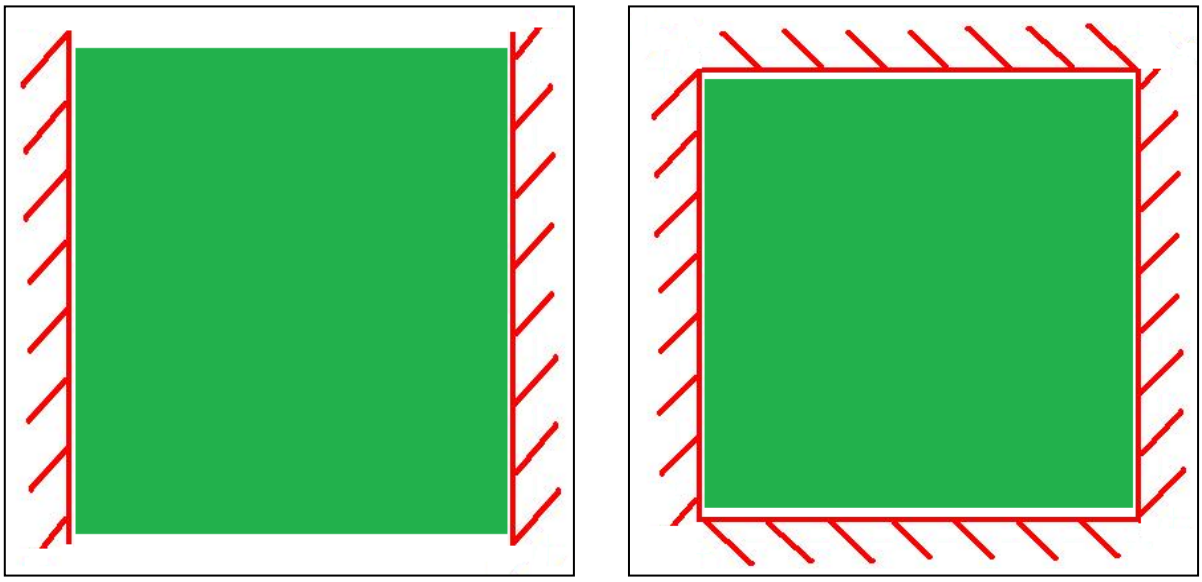

Figure 4.23. *Scheme of boundary conditions with 2 edge fixed (left) and 4 edge fixed (right)*

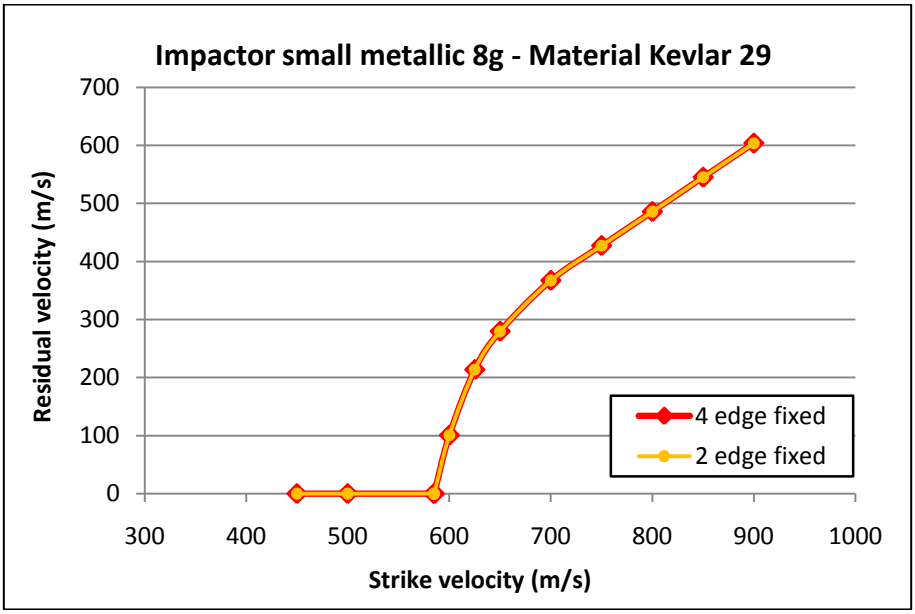

Figure 4.24. *Sensitivity to boundary conditions. Small metallic 8g impactor and Kevlar 29 8 mm thickness plate*

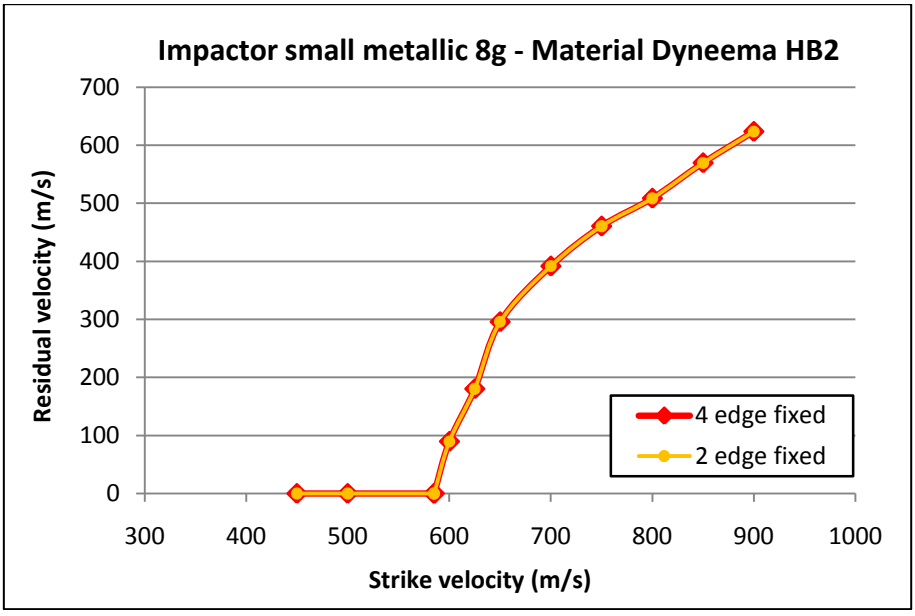

Figure 4.25. *Sensitivity to boundary conditions. Small metallic 8g impactor and Dyneema HB2 11 mm thickness plate*

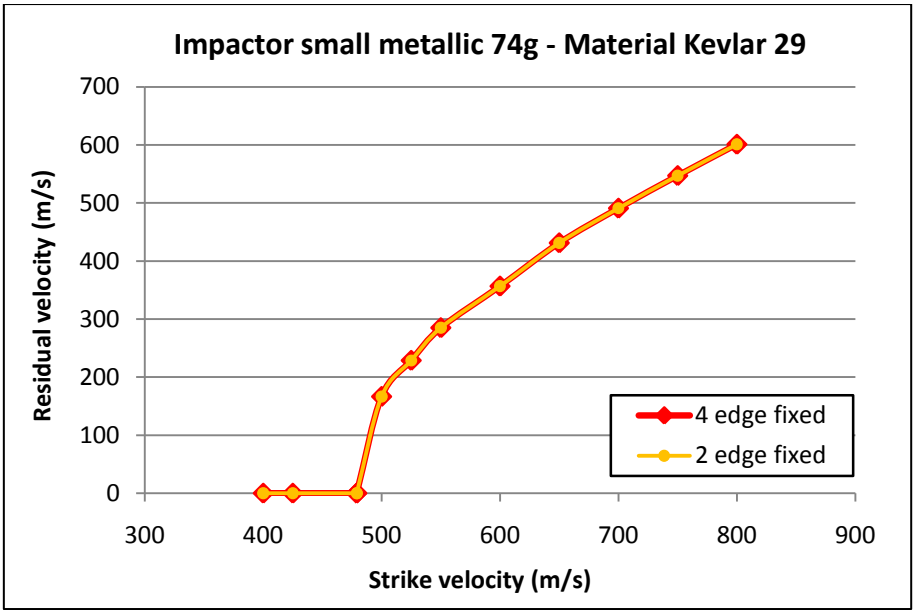

Figure 4.26. *Sensitivity to boundary conditions. Small metallic 74g impactor and Kevlar 29 21 mm thickness plate*

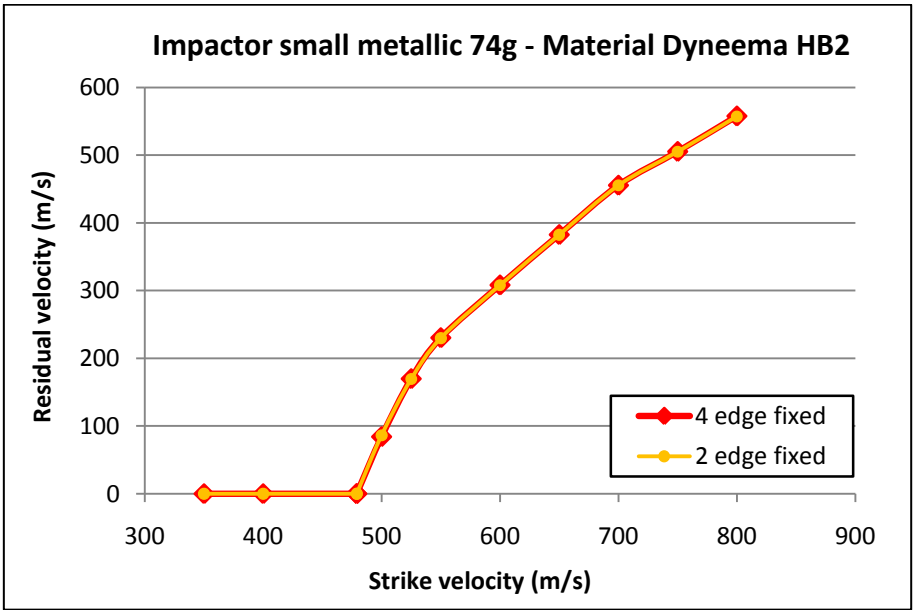

Figure 4.27 *Sensitivity to boundary conditions. Small metallic 8g impactor and Dyneema HB2 30 mm thickness plate*

From study it can be concluded that boundary conditions have no effect in the behaviour of the composite plates. Figures 4.24 to 4.27 show that that curves of 4 edges fixed and 2 edges fixed are completely superposed. Thus ballistic limit is not sensitive to boundary conditions in this type of impacts regarding high velocity small metallic fragments.

4.4. Design of protections with numerical models for ice impactors

The second application of the semi-analytical and numerical models is the design of protection panels against ice impact. In this case, impact velocities are normally lower than in impacts coming from Uncontained Engine Rotor Failure (UERF); and the impactor stiffness and cohesion significantly lower.

The application in this case is to study the impact performance of Kevlar 29 and Dyneema HB2 when impacted by ice. The shape and size of ice are fixed and here it is studied the performance of thin protection laminates.

The numerical model of ice is based on Smooth Particle Hydrodynamics (SPH), and its constitutive model comes from in-house knowledge of Airbus Military (EADS-CASA). The model of ice has been extensively validated in previous industrial works [8].

The protection panels of Kevlar 29 and Dyneema HB2 were prepared using models presented in Chapter III. However, in this case panels are relatively thin and shell elements have been used instead solid ones.

4.4.1. Impactor

Only one type of impactor is used in this set of numerical simulations. Impactor is an ice plate that represents ice release from propeller blades. Complete geometry is shown in Figure 4.28.

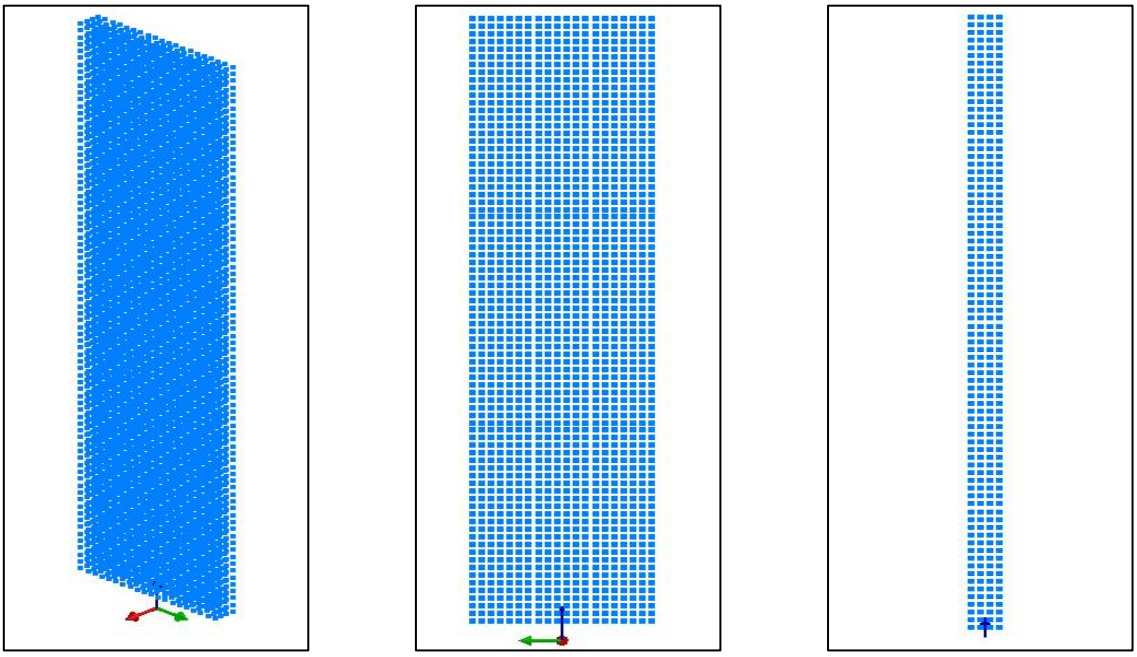

Figure 4.28. *SPH model of ice impactor*

The best approach for ice impactor modelling is by using Smooth Particle Hydrodynamics (SPH) technology. In the SPH approach, particles are defined like individual points interacting to each other using interpolation functions that act only to those particles trapped in certain domain of influence. Localization and information transmission from one particle to another are achieved through the notion of an interpolation distance called the "smoothing length". A particle "P" is said to have a contributing neighbour "N", when particle "N" lies within the sphere of influence of "P". The main problem to tackle when using SPHs is to reproduce the characteristics of a solid material with fluid particles equation of state.

Each SPH particle has its volume, which can be represented as a sphere centred on the particle centre of mass, and then a radius "r" can be deduced for each particle. The smoothing length "h" is defined as a multiple of the radius, by means of the also called, parameter ratio. The particle domain of influence extends well beyond its radius, currently twice the smoothing length [43] [44].

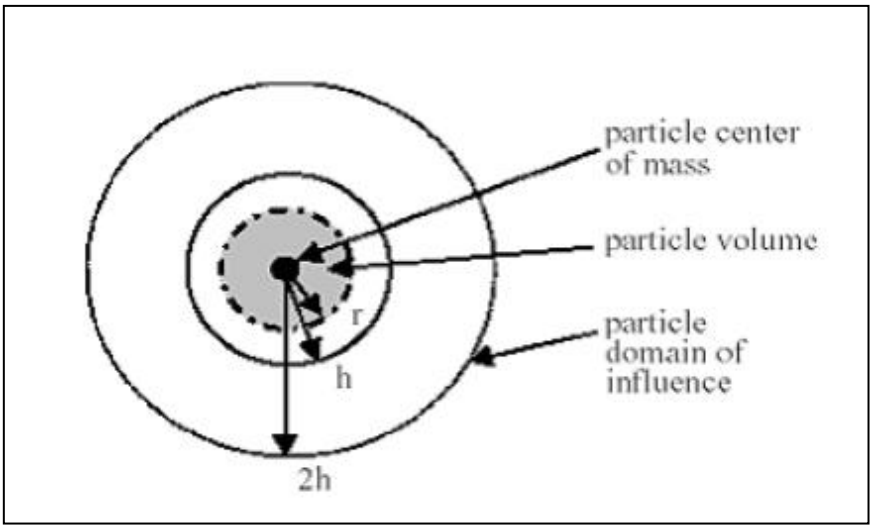

Figure 4.29. *SPH main control parameters [43]*

Ice material characteristics are defined by means of an equation of state (EOS) corresponding Murnaghan model. This is implemented in Pam Crash by means of ***material type 28*** (MAT 28) [43]. This material corresponds to a liquid with an artificially increased compressibility used to perform a certain class of hydrodynamic simulations, where the flow velocities remain well below the physical speed of sound, and where compressibility effects are of minor importance. In such cases, the liquid may be considered more compressible than in reality, which may be achieved using Murnaghan EOS model. The artificial fluid should have a speed of sound still well above the speed of the bulk flow and therefore it creates very small density fluctuations. The pressure for the Murnaghan EOS is given by:

$$p = p_0 + B\left[\left(\rho/\rho_0\right)^{\gamma} - 1\right] \tag{4.1}$$

4.4.2. Protection panels

Nominal protections for ice impact at 150 m/s were initially designed with two thicknesses depending on the protection material:

- *Aramid material:* nominal thickness of 1.1 mm.
- *Polyethylene material:* nominal thickness of 1.6 mm.

For thickness lower than 2 mm the best choice for modelling protection panels are shell elements. Figures 4.30 and 4.31 show the mesh of protection with shell elements. Dimensions of protections are 500 mm x 500 mm in this case.

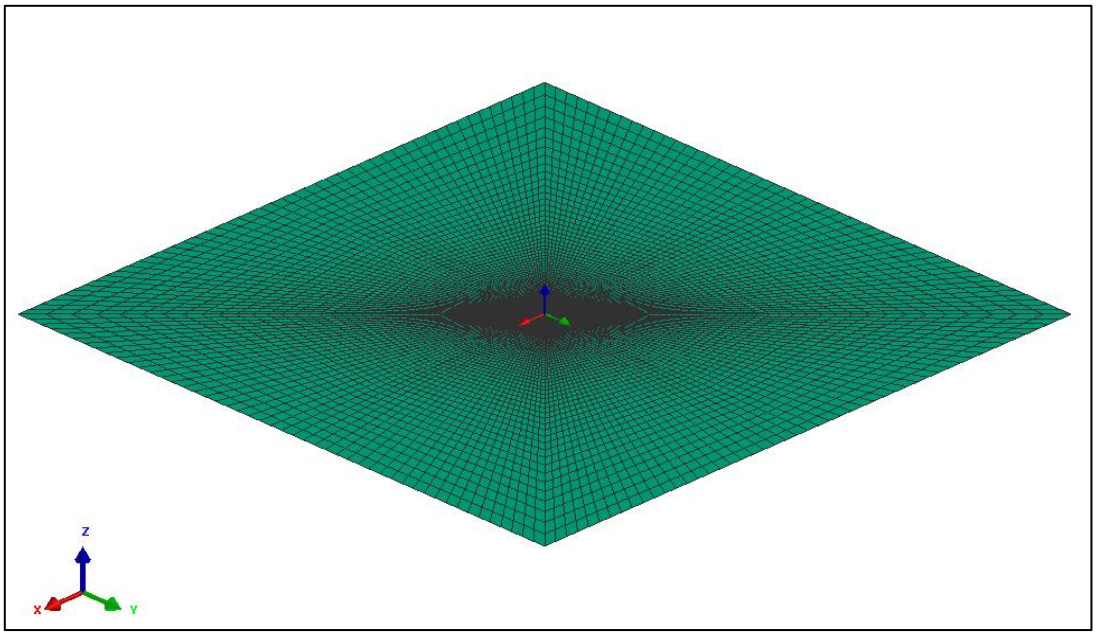

Figure 4.30. *Shell plate mesh isometric view*

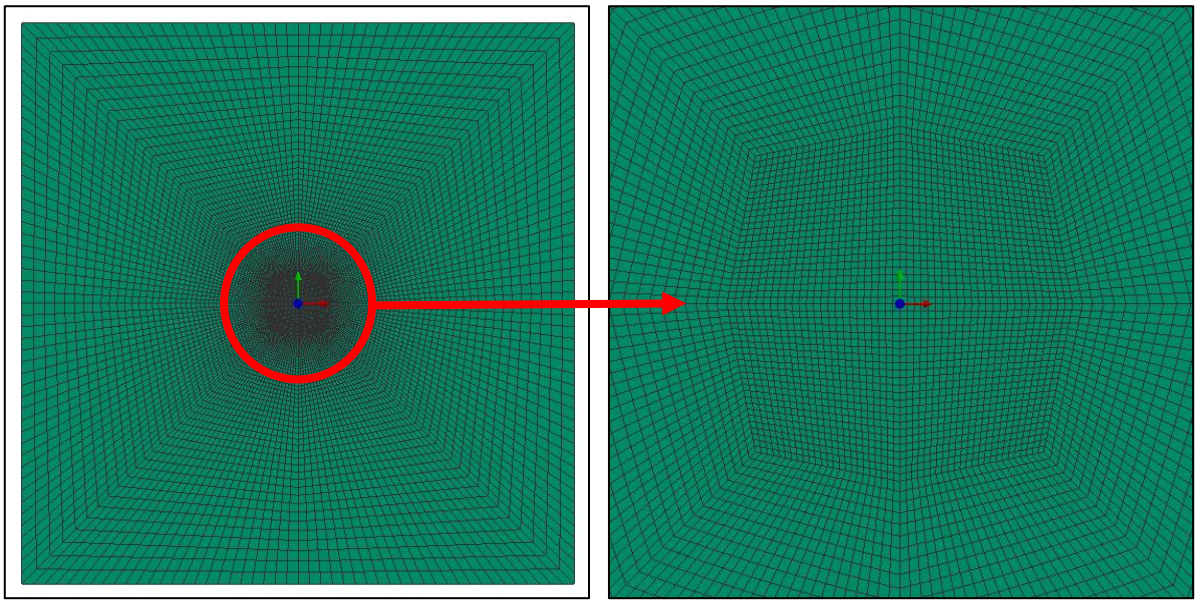

Figure 4.31. *Plate mesh view in plan XY (left) and central region detail (right)*

4.4.3. Curves of design

In the same way that for small metallic fragments, design curves were obtained for ice impactors. These curves relate residual velocity with initial velocity and they depend on the type of impactor, protection material and thickness. Nominal cases are:

- 35 g ice impactor travelling at 150 m/s against 1.1 mm protection panel made of Kevlar 29.
- 35 g ice impactor travelling at 150 m/s against 1.6 mm protection panel made of Dyneema HB2.

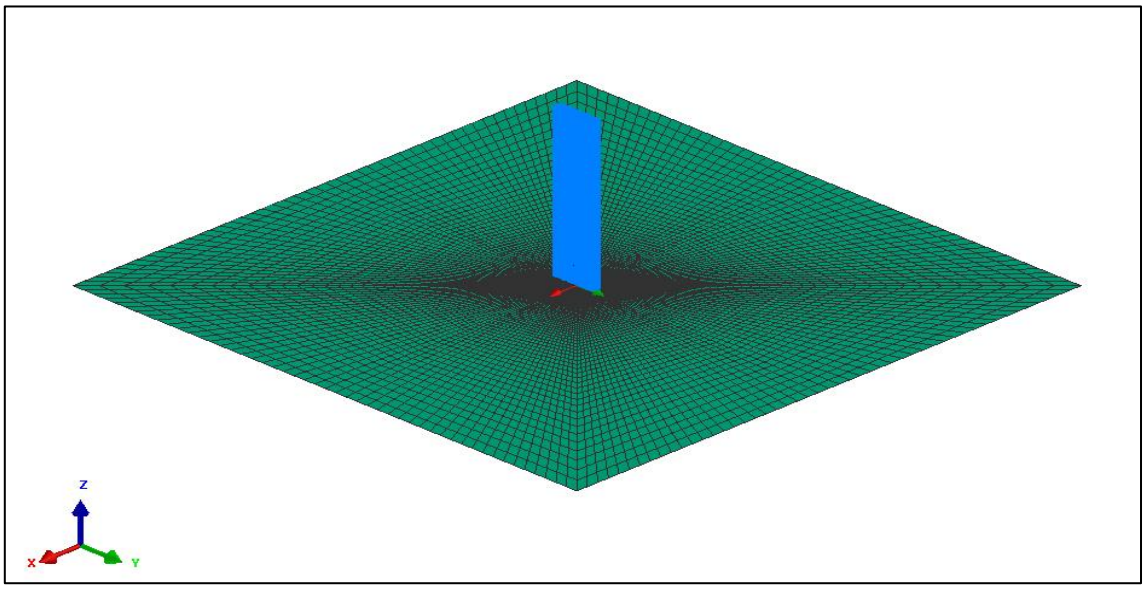

Figure 4.32. *Initial configuration: ice impactor and composite plate*

Numerical simulations for ice impact reveal that nominal thickness for both protection materials is properly designed because panels of Kevlar 29 and Dyneema HB2 stopped ice impactors. Panel of Kevlar 29 presents a ballistic limit of 250 m/s, while panel of Dyneema HB2 a value of 350 m/s, both of them at nominal thickness. So, it is concluded that initial design resists the impact and the thickness could be decreased up to panels of 0.5 mm thicknesses.

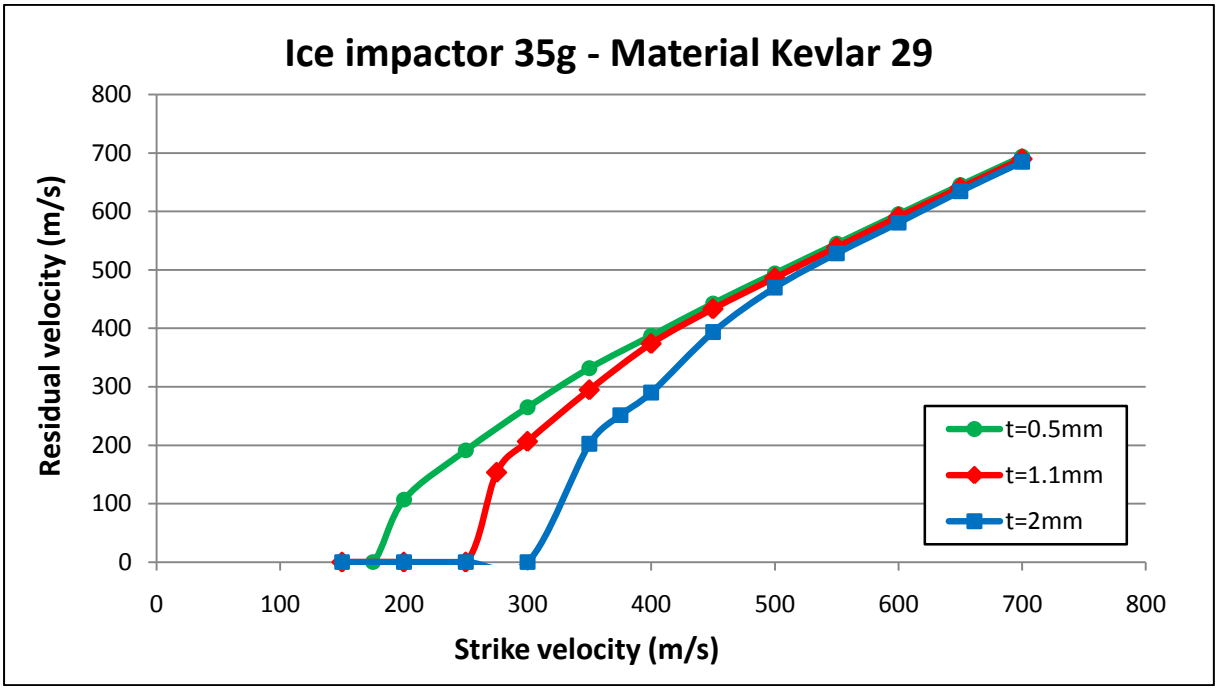

Figure 4.33. *Residual velocity versus strike velocity at various thicknesses for an ice impactor of 35g and Kevlar 29 target*

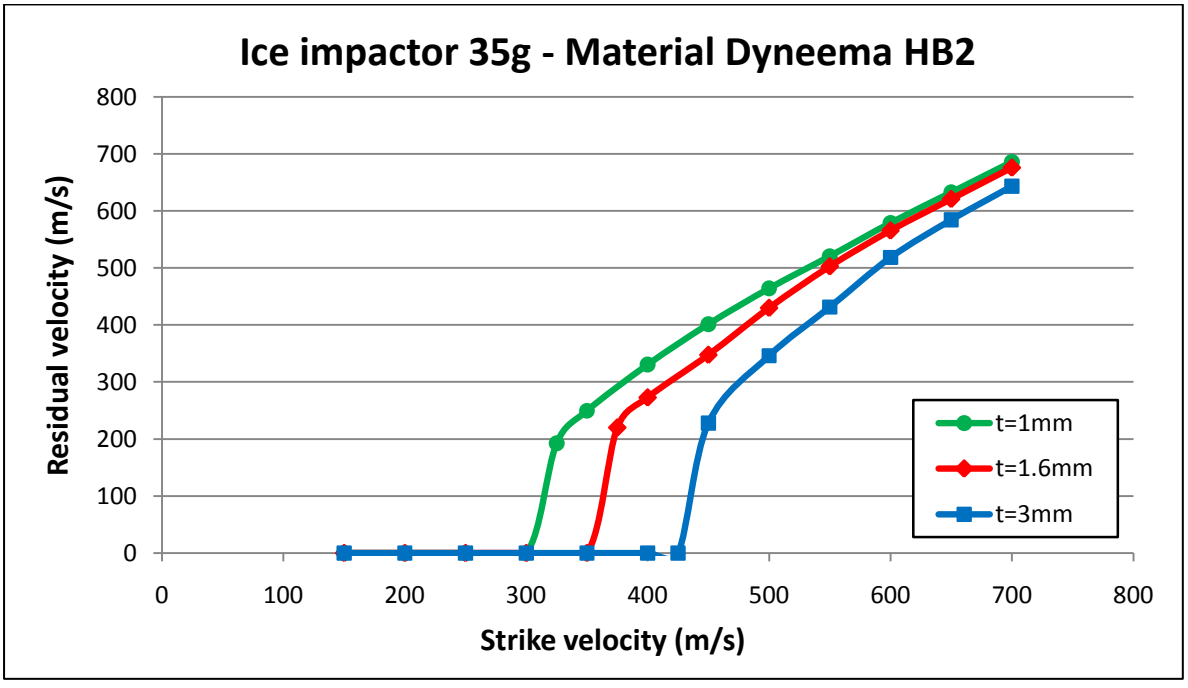

Figure 4.34. *Residual velocity versus strike velocity at various thicknesses for an ice impactor of 35g and Dyneema HB2 target*

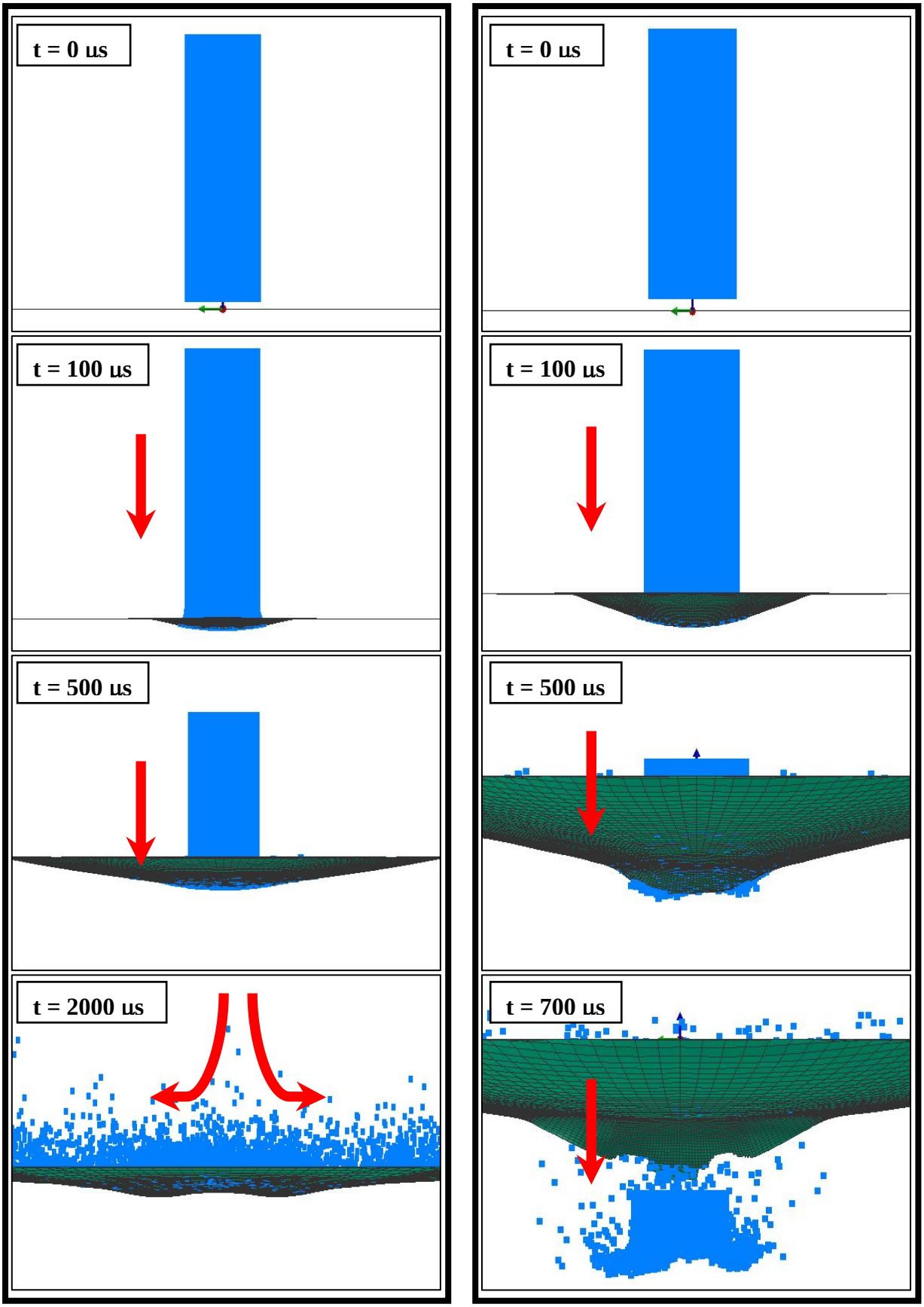

Figure 4.35. *Ice impact sequence for 1.1 mm thickness Kevlar 29 protection at 150 m/s (left) and at 300 m/s (right)*

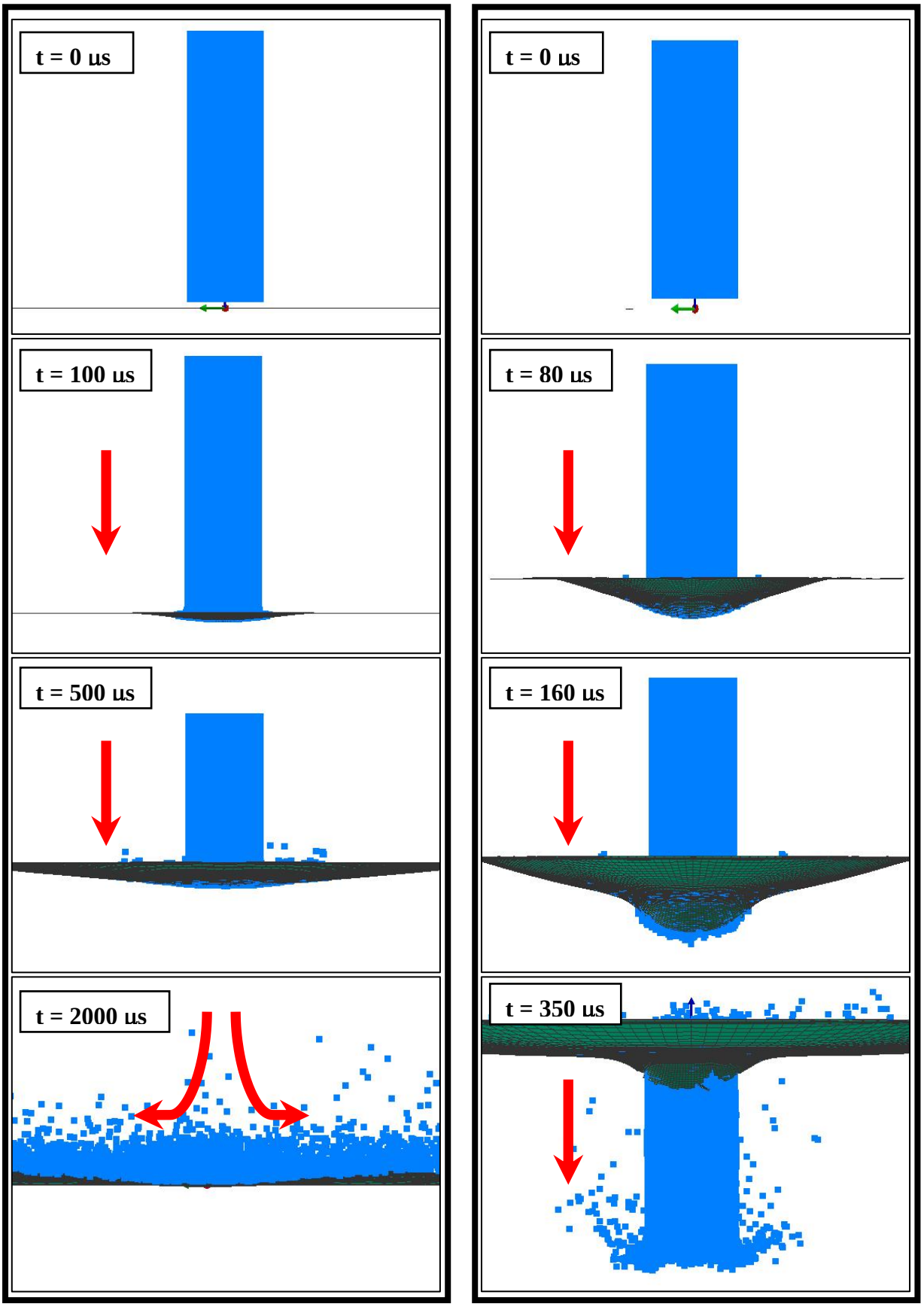

Figure 4.36. *Ice impact sequence for 1.6 mm thickness Dyneema HB2 protection at 150 m/s (left) and at 500 m/s (right)*

Figures 4.35 and 4.36 show the impact sequence at velocities below and above the ballistic limit for Kevlar 29 and Dyneema HB2 respectively. Comparing these sequences with those obtained for the small metallic fragments it is observed that the nature of the impact is different in both cases. Ice impact produce global bending of the protection, while small fragments produce very local effects.

Below and above ballistic limit, marks on panel protection are completely different. Below ballistic limit there is no element elimination and protection is able to stop impactor, but above ballistic limit, impactor perforates protection totally.

Numerical models of materials developed in the current project are elastic-plastic models, therefore in order to determine final damage of protection panel at two different impacts velocities plastic strain is plotted in Figures 4.37 and 4.38.

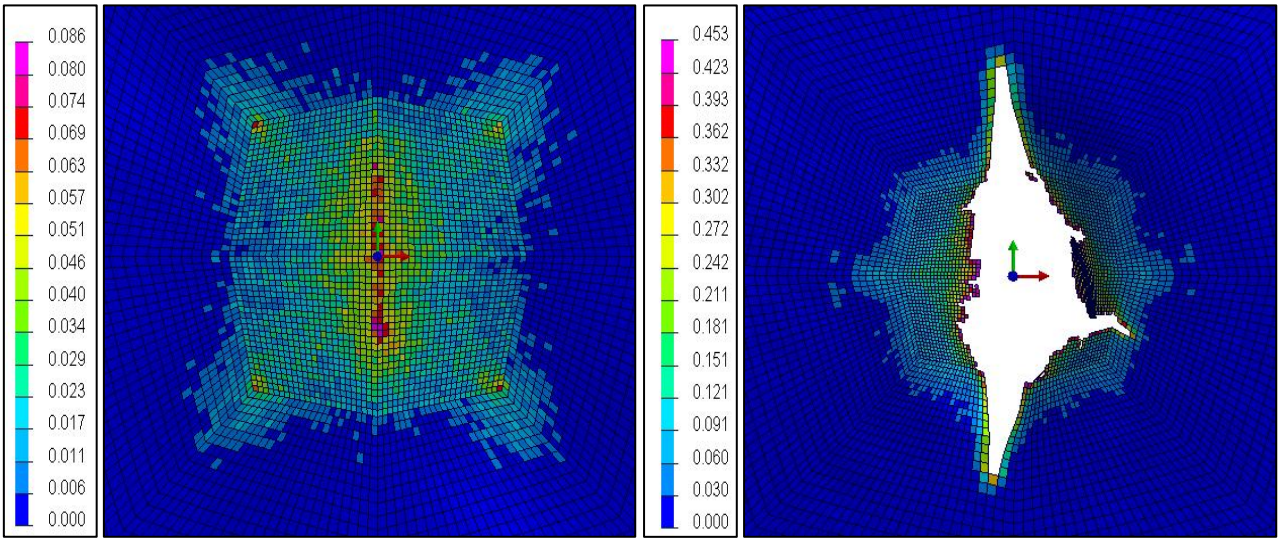

Figure 4.37. *Final mark (plastic strain contours) for 1.1 mm thickness Kevlar 29 at 150 m/s (left) and at 300 m/s (right)*

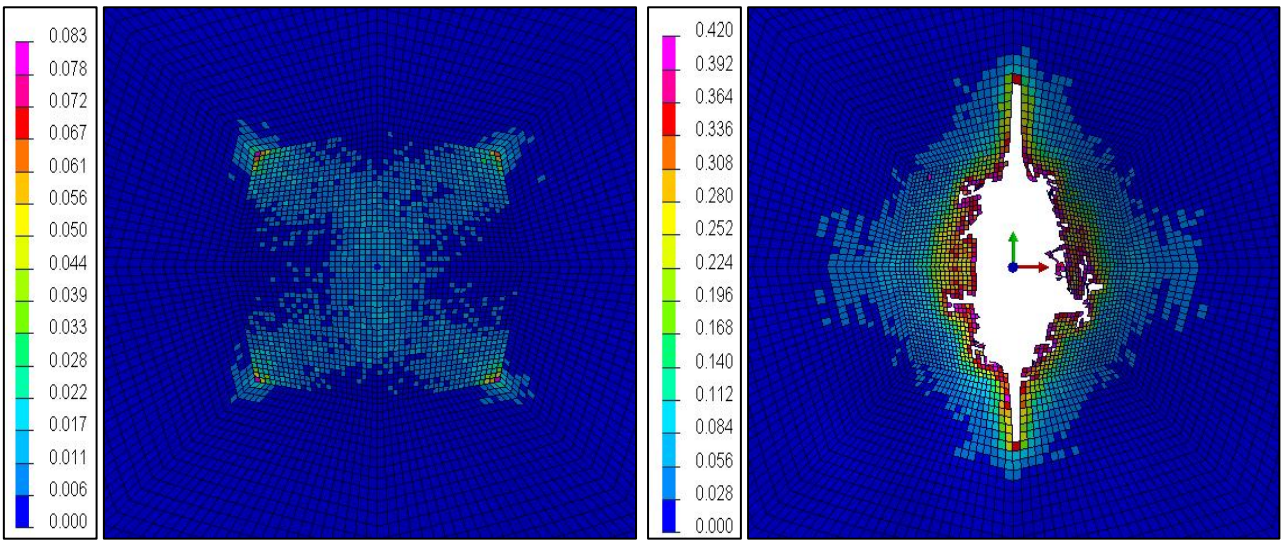

Figure 4.38. *Final mark (plastic strain contours) for 1.6 mm thickness Dyneema HB2 at 150 m/s (left) and at 500 m/s (right)*

Maximum vertical displacement of protections is also measured for the two velocities and in both materials. At 150 m/s is easy to measure vertical displacement due to there is no perforation and central point will reach maximum value. However, at velocities above ballistic limit is more complicated. In these cases, displacement of elements that have not been eliminated is measured. Values are shown in Table 4.26.

Kevlar 29 t =1.1 mm		**Vertical displacement (mm)**	**Dyneema HB2 t =1.6 mm**		**Vertical displacement (mm)**
V = 150 m/s	no perforate	27.8	**V = 150 m/s**	no perforate	18.43
V = 300 m/s	perforate	37.1	**V = 500 m/s**	perforate	26.15

Table 4.26. *Maximum vertical displacements for both materials at two different velocities*

Now, using the same equation (Equation 4.1) based on Van Gorp semi-analytical model, the constants for both protection materials when impacted by ice were calculated:

	V_b (m/s)	m_p (kg)	E_{abs} (J)	S (mm^2)	ρ_{lam} (kg/m^3)	t (m)	AD (kg/m^2)	C (Jm^2/mm^2kg)	K (mkg/s^2mm^2)
ICE	175	0.035	536	254	1160	0.0005	0.58	3.64	91.87
	250	0.035	1094	254	1160	0.0011	1.28	3.37	88.48
	300	0.035	1575	254	1160	0.0020	2.32	2.67	78.75
							$K_{average}$		**86.37**
							Deviation		**5.56**

Table 4.27. *Material constant for Kevlar 29*

	V_b (m/s)	m_p (kg)	E_{abs} (J)	S (mm^2)	ρ_{lam} (kg/m^3)	t (m)	AD (kg/m^2)	C (Jm^2/mm^2kg)	K (mkg/s^2mm^2)
ICE	300	0.035	1575	254	900	0.0010	0.90	6.89	111.4
	350	0.035	2144	254	900	0.0016	1.44	5.86	102.7
	425	0.035	3161	254	900	0.0030	2.70	4.61	91.08
							$K_{average}$		**101.7**
							Deviation		**8.31**

Table 4.28. *Material constant for Dyneema HB2*

Therefore, the Van Gorp model is tuned up by numerical simulations and provides the following expression for ice impact:

$$V_b = K \cdot \sqrt{\frac{S \cdot t}{m_p}} \qquad (4.1)$$

where:

- t : thickness of composite [m]
- S : surface area of the strike face area of impactor [mm^2]
- m_p : projectile mass [kg]
- K : constant depending on protection material properties and the impactor type

$K_{Kevlar\ 29}$ = 86.37 mkg/$s^2$$mm^2$ **$K_{Dyneema\ HB2}$ = 101.7 mkg/$s^2$$mm^2$**

4.4.4. Sensitivity analysis

Two different types of sensitivity analysis will be studied next: effect of impact angle of projectile and effect of boundary conditions.

4.4.4.1. Sensitivity to impact angle

Previous simulations were done with an impact angle of 90º, but now, this angle will be changed from 90º to 30º, with a drop of 15 degrees each time. The variation of ballistic limit at several impact angles is studied at nominal thickness for protection panels made of Dyneema HB2.

During simulations the projectile penetrates completely the target (CP) or it does not penetrate the target (NP). But there is one more option, when the projectile penetrates up to plate backside and it does not cross completely the target. In that case there is partial penetration (PP). To do a safer design, we have considered partial penetrations as complete penetrations of the material.

Geometry of ice impactor is different than geometry of UERF impactors studied in earlier points. In this case, impactor has not a cylindrical shape, so the impact angle might be changed in two different ways (Figure 4.39).

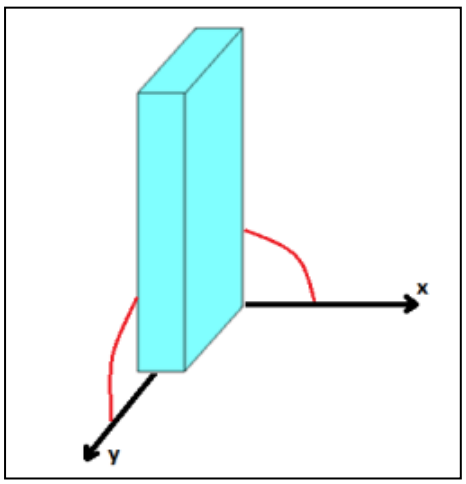

- **Rotate ice impactor to axis X**

- **Rotate ice impactor to axis Y**

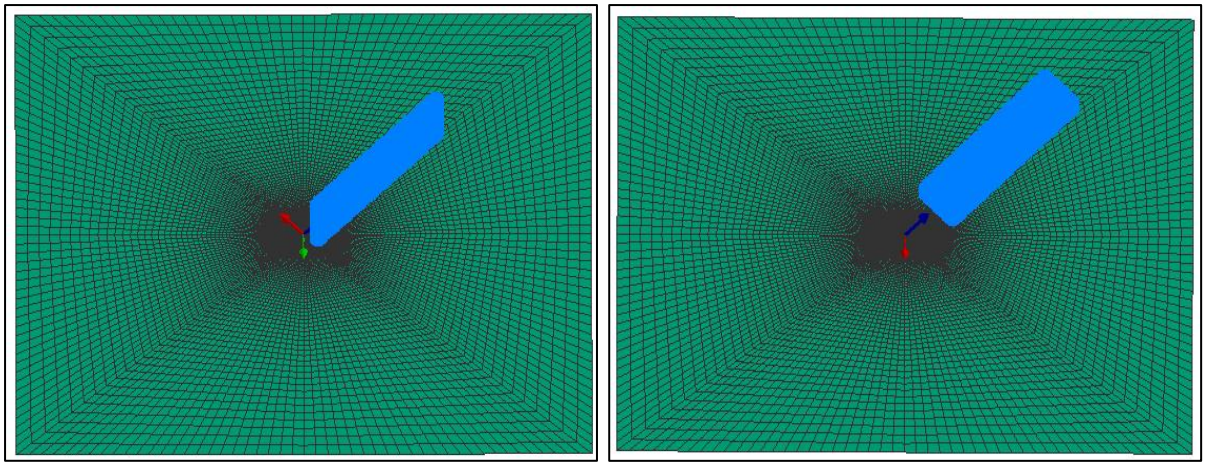

Figure 4.39. *Ice impactor rotated to axis X (left) and to axis Y (right)*

Finally, the ballistic limits obtained with numerical simulations for ice impactor rotated to axis X or Y, and a protection panel made of Dyneema HB2 with l.6 mm thickness are summarized in Table 4.29.

Ice impactor 35g DyHB2 t = 1.6 mm			
Axis X		**Axis Y**	
Angle (º)	**V_b (m/s)**	**Angle (º)**	**V_b (m/s)**
90	350	90	350
75	350	75	350
60	380	60	380
45	480	45	480
30	620	30	620

Table 4.29. *Ballistic limit depending on impact angle*

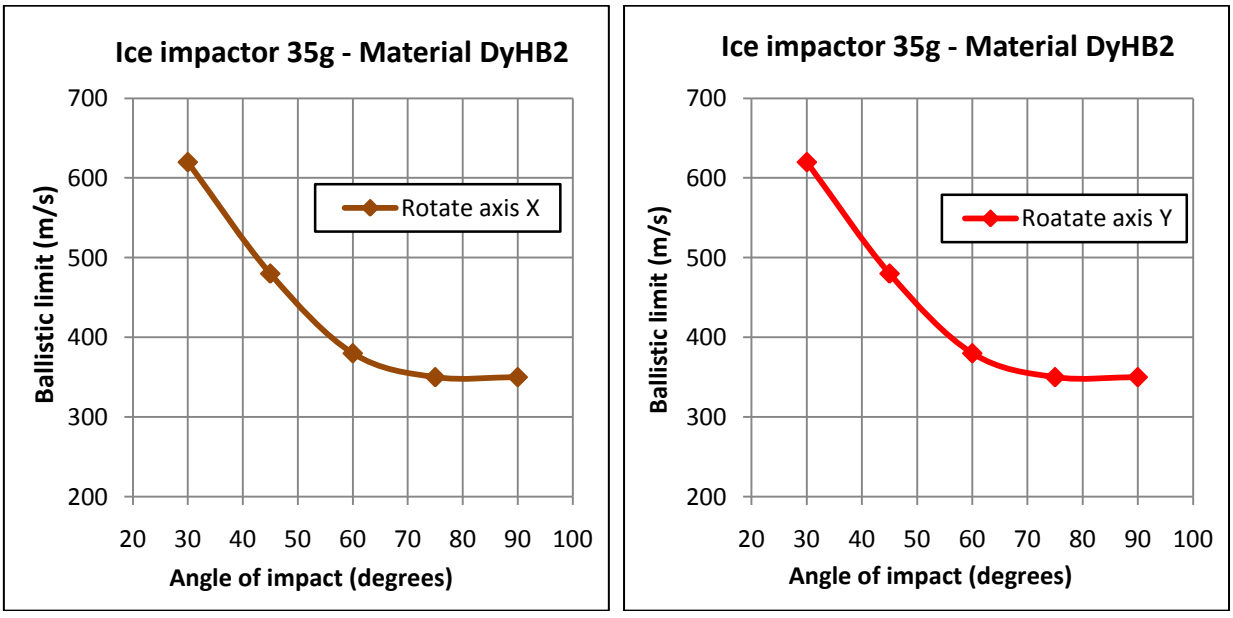

Figure 4.40. *Ballistic limit depending on impact angle*

Now, with same procedure developed with small metallic impactors, it is possible to calculate coefficient $C_i\ (\alpha)$, according with Equation 4.6.

$$V_{b\alpha} = V_{b90^\circ} \cdot sin(\alpha) \cdot C_i(\alpha) \tag{4.6}$$

		Ice impactor 35g DyHB2	
		Axis X	**Axis Y**
Angle of impact (º)	**90º**	1.00	1.00
	75º	1.04	1.04
	60º	1.25	1.25
	45º	1.94	1.94
	30º	3.54	3.54

Table 4.30. *Coefficients of impact angles*

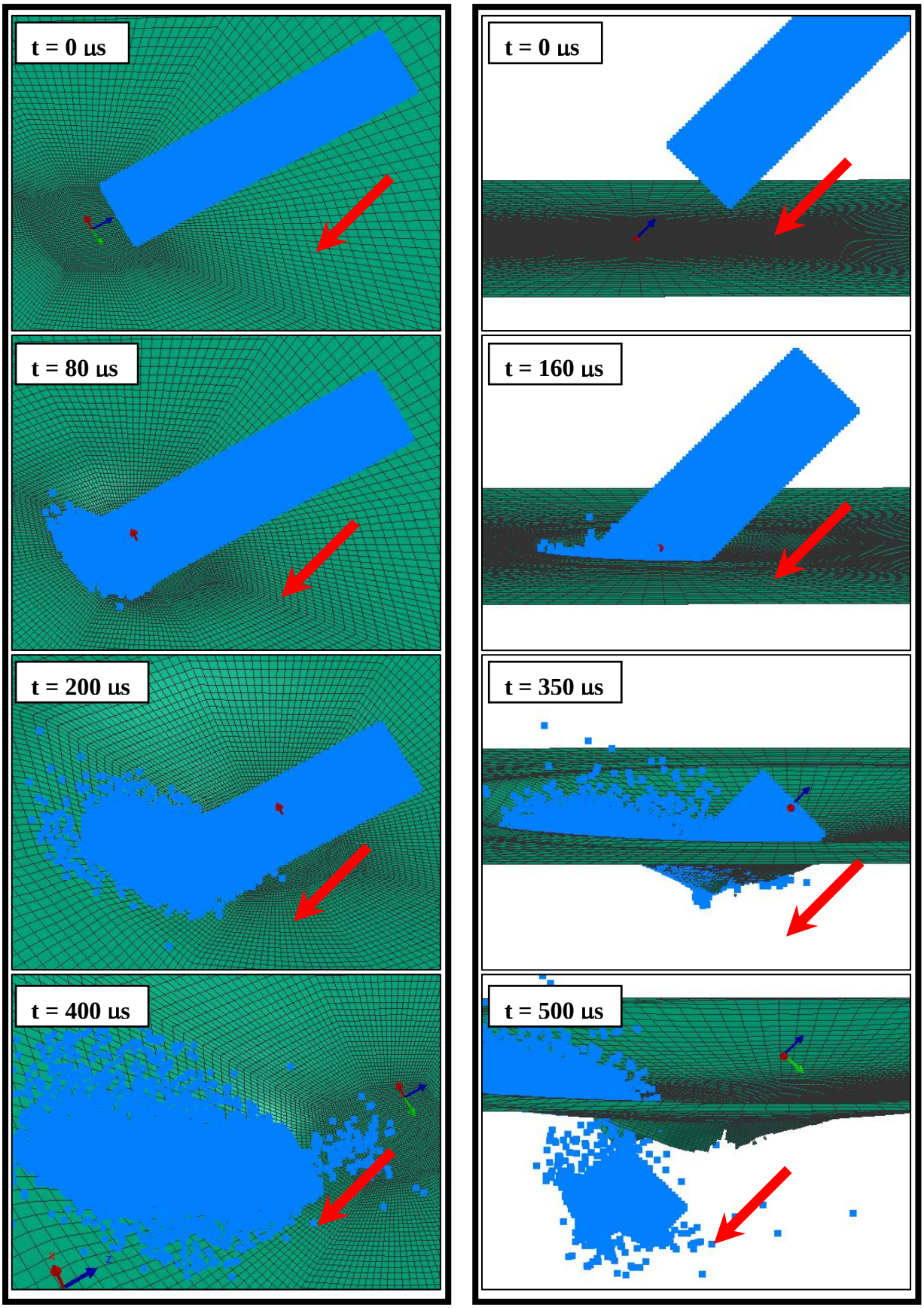

Figure 4.41. *Ice impact sequence for 1.6 mm thickness Dyneema HB2 protection at 550 m/s with impact angle of 30º (left) and at 540 m/s with impact angle of 45º (right)*

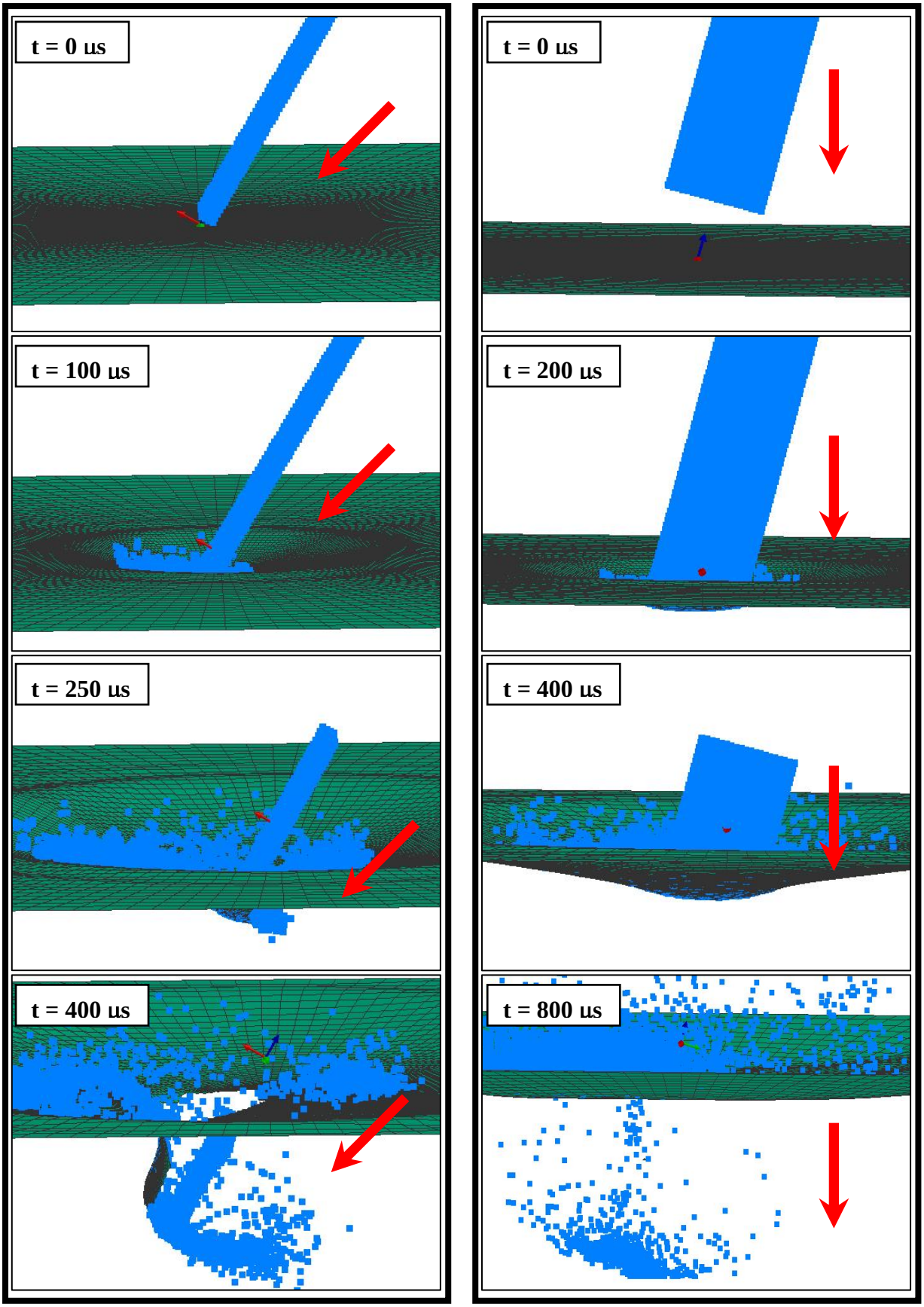

Figure 4.42. *Ice impact sequence for 1.6 mm thickness Dyneema HB2 protection at 460 m/s with impact angle of 60º (left) and at 360 m/s with impact angle of 75º (right)*

4.4.4.2. Sensitivity to boundary conditions

So far the simulations have been performed with the composite plates fixed from all four edges. It is important to estimate the influence of boundary conditions because when the protection panels are installed on the aircraft structure, they may have different behaviour depending on how they are fixed. In this case, ice impactor has not cylindrical shape so there are two different ways of fixing two edges:

- 2 edge fixed in axis X.
- 2 edge fixed in axis Y.

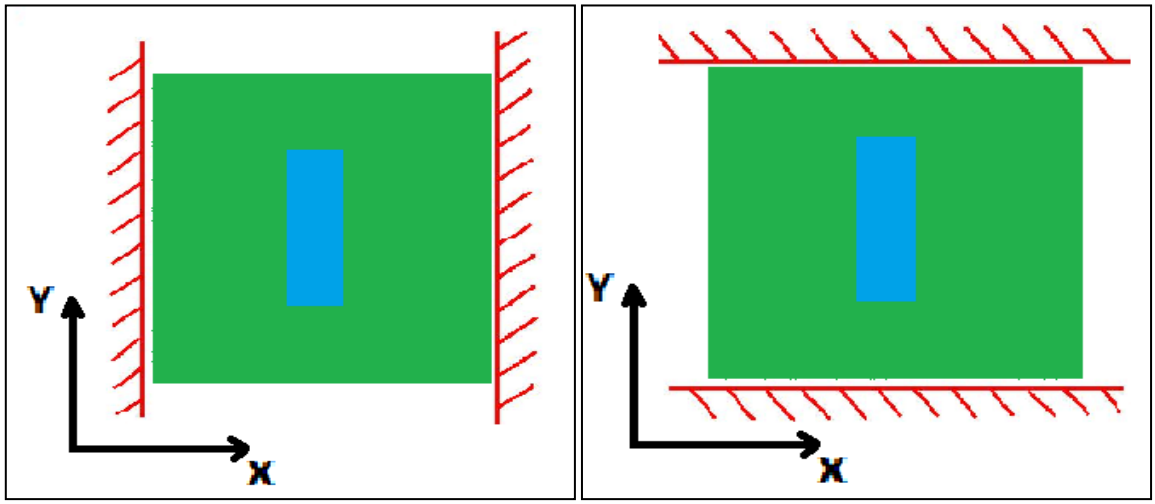

Figure 4.43. *Scheme of fixing 2 edge of axis X (left) and 2 edge of axis Y (right)*

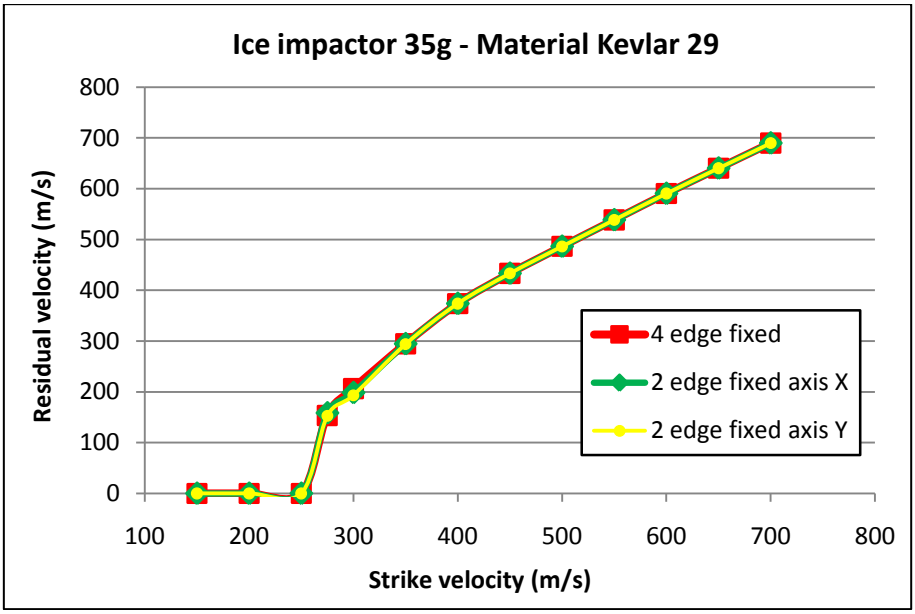

Figure 4.44. *Sensitivity to boundary conditions. Ice impactor 35g and Kevlar 29 1.1 mm thickness plate*

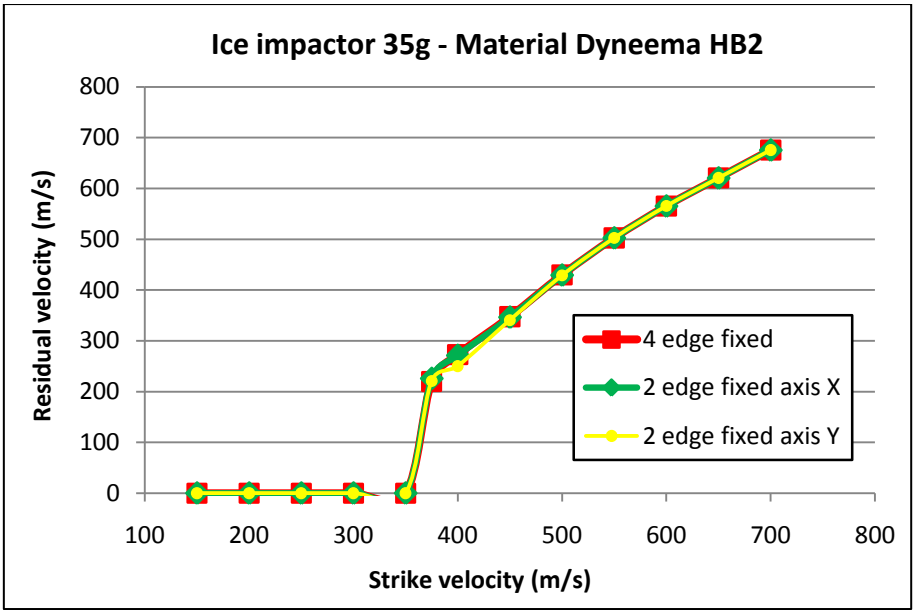

Figure 4.45. *Sensitivity to boundary conditions. Ice impactor 35g and Dyneema HB2 1.6 mm thickness plate*

Boundary conditions have no effect in the behaviour of the composite plates. If figures above are observed, one can see that that curves of 4 edges fixed and 2 edges fixed are completely superposed, except in velocity values near to ballistic limit, where residual velocities with 2 edges fixed are slightly smaller than with 4 edges fixed.

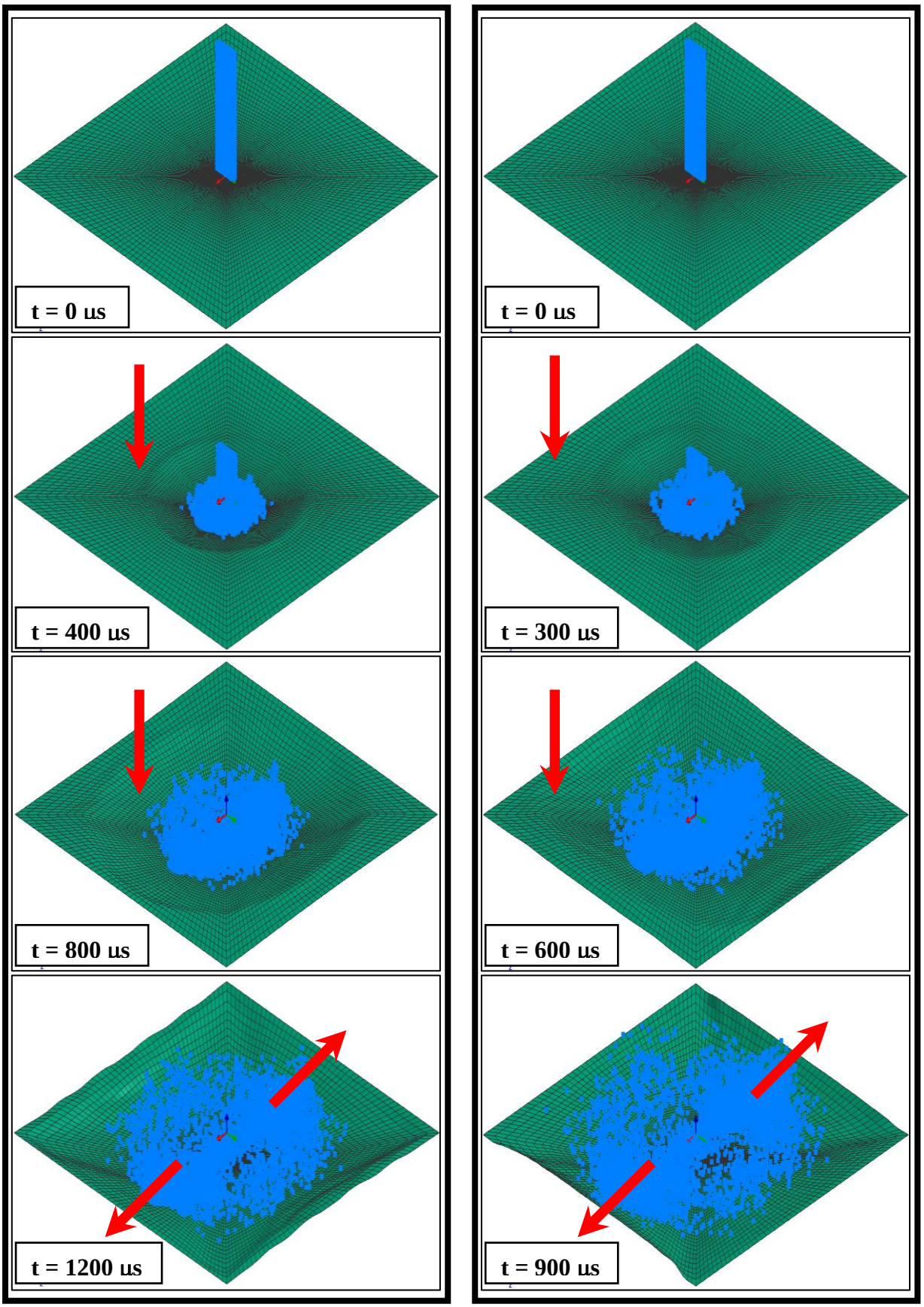

Figure 4.46. *Ice impact sequence at 150 m/s for 1.6 mm thickness Kevlar 29 protection with 2 edges fixed of axis X (left) and for 1.6 mm thickness Dyneema HB2 protection with 2 edges fixed of axis Y (right)*

CONCLUSIONS

This project has been devoted to the study of protection materials for impact applications. In particular the type of protections investigated were aramid and polyethylene composite panels in applications for the aeronautical industry.

The project has been done in collaboration with the Structural Dynamic and Aeroelasticity Department of Airbus Military (EADS-CASA) within the framework of a six-month internship.

The conclusions of the project may be summarized in the following points:

1. The impact performance of protection composite laminates has been analyzed from two points of view:

   - Semi-analytical models proposed in literature.

   - Numerical simulations using non-linear Finite Element Analysis.

2. Within the semi-analytical models found in literature, the model proposed by *Van-Gorp et al.* has been considered as the most suitable for design purposes of protection panels made with aramid and polyethylene fibres.

$$V_b = K \cdot \sqrt{\frac{S \cdot t}{m_p}}$$

   where:
   - V_b : ballistic limit [m/s]
   - S : surface area of the strike face area of the impactor [mm^2]
   - t : thickness [m]
   - m_p : projectile mass [kg]
   - *K* : constant of the material [mkg/s^2mm^2]

3. Two material models for numerical simulations are proposed for Kevlar 29 woven composite material (aramid) and Dyneema HB2 non-woven cross plied composite material (polyethylene).

4. Both models are based on isotropic elastic-plastic with failure materials. They have been extensively validated with experimental and numerical data of published works. The aim of these models is to predict the ballistic limits of protection composite laminates.

5. Numerical simulations have been applied to two aeronautical impactors: small metallic fragments coming from Uncontained Engine Rotor Failure (UERF) and ice impacts coming from propeller ice release in turboprop aircrafts.

   - *Small metallic fragments* is a typical high velocity impact with high-stiffness impactor where protection behaviour is local. In case of low size impactors the minimum thickness required using Kevlar 29 is 8 mm while using Polyethylene HB2 11 mm. Otherwise, for high size impactors the minimum thickness required is 21 mm using Kevlar 29 and 30 mm for Dyneema HB2.

- *Ice impacts* where velocity and impactor stiffness are reduced and protection response is extended to the whole panel. Thicknesses of aramid and polyethylene protections of 1.1 mm and 1.5 mm respectively, are able of stopping the impactor.

6. Numerical simulations have been applied in conjunction of the *Van Gorp* semi-analytical model in order to obtain a set of expressions useful for design. Proposed values of *K* constant for small metallic and ice fragments are:

	ARAMID [mkg/s^2mm^2]	**POLYETHYLENE** [mkg/s^2mm^2]
METALLIC FRAGMENTS	45.26	38.19
ICE FRAGMENTS	86.37	101.70

7. Sensitivity analyses regarding the angle of impact and protection boundary conditions have been performed for both applications:

   - Boundary conditions have no effect in impact performance. Ballistic limits are no modified by considering either four or two edges clamped.

   - The lower the angle impact is the higher the ballistic limit, as expected. For instance, an impact angle reduction of 60º implies an increase of 30% in ballistic limit.

BIBLIOGRAPHIC REFERENCES

[1]. EADS-CASA. IF-T-AAO-10017. "Multifunctional laminates-Impact behaviour of hybrid laminates".

[2]. Airworthiness Regulation FAR25. AMC 20-128A. "Design Considerations for Minimizing Hazards Caused by Uncontained Turbine Engine and Auxiliary Power Unit Rotor Failure".

[3]. International news website. EURONEWS. "Aterrizaje de emergencia de un Airbus A380 de Qantas en Singapur". es.euronews.net

[4]. EADS-CASA. Joint Technology Initiative for Aeronautics and Air Transport. "Composite blade impact on composite aircraft structure", "Metallic fragments on composite blade or aircraft structure" and "Hybrid armour".

[5]. NASA's Glenn Research Center website. www.nasa.gov/centers/glenn/home/index.html

[6]. Williams, F.M. "Measurements of Ice Mechanical Properties". *Army Cold Regions Research and Engineering Laboratory*. Integrated Publishing. www.tpub.com

[7]. EADS-CASA. NT-T-AA0-09007. "Impacts of composite fragment on composite structure. Preliminary numerical simulations".

[8]. Triviño, V.; Pérez-Galán, J.L. and Climent, H. "Ice impact on aeronautical structures". IFASD 2007. July 2007.

[9]. Bank, L.C. "Composites for Constructions: Structural Design with FRP Materials". *Chapter 2*. John Wiley & Sons, 2006.

[10]. Chocron, S. "Impacts research at SwRI. From Fibers to Composites". *Conference at Airbus Military.* Southwest Research Institute (SwRI). 2009.

[11]. Cunniff, P.M. and Auerbach M.A. "High performance M5 fiber for ballistics / structural composites". *Course Mechanical Behaviour of Polymers*. MIT. 2005.

[12]. International website of Toyobo Company. High performance fibres manufacturer: Dyneema and Zylon. www.toyobo.co.jp/e/products

[13]. Online materials information resource. MATWEB. www.matweb.com

[14]. International website of DuPont Company. High performance fibres manufacturer: Kevlar and Nomex. Kevlar Technical Guide. www.DuPont.com

[15]. International website of Honeywell Company. High performance fibres manufacturer: Spectra. www.honeywell.com/spectra

[16]. DOT/FAA/AR-97/53. "Advanced Armor Technology: Application Potential for Engine Fragment Barriers for Commercial Aircraft". *U.S. Department of Transportation. Federal Aviation Administration.*

[17]. http://www.directindustry.es

[18]. Bhatnagar, A. "Lightweight ballistic composites. Military and law-enforcement applications". *Woodhead Publishing in Materials.* Cambridge (England). 2006.

[19]. www.techexchange.com

[20]. Zaera, R. "Ballistic Impacts on Polymer Matrix Composites, Composite Armor, Personal Armor". *Department of Continuum Mechanics and Structural Analysis*. University Carlos III of Madrid. Inside book: Abrate, S. "Impact Engineering of Composite Structures".

[21]. Chocron, S.; Pintor, A.; Gálvez, F.; Roselló, C.; Cendón. D. and Sánchez-Gálvez, V. "Lightweight polyethylene non-woven felts for ballistic impact applications: Material characterization". *Composites - Part B: engineering,* Vol. 39, 2008, pp 1240-1246.

[22]. Chocron, S.; Rodríguez, J.; Martínez, M.A. and Sánchez-Gálvez, V. "High strain rate properties of aramid and polyethylene woven fabrics composites". *Composites - Part B: engineering,* Vol. 27B, 1996, pp 147-154.

[23]. www.mdacomposites.org

[24]. Xuesen, Z. "Numerical analysis of fabric armour under ballistic impact". *PhD Thesis*. National University of Singapore. 2006.

[25]. Department of Defence. "MIL-DTL-46593B - Fragment Simulating Projectiles used in ballistic testing". *U.S. Department of Defence.* August 2008.

[26]. National Institute of Justice. "NIJ standard 0101.04 for Ballistic Resistance of Personal Body Armor. Revision A". *Office of Justice Programs. U.S. Department of Justice.* June 2001.

[27]. Zukas, J.A.; Nicholas, T.; Swift, H.F.; Greszczuk, L.B. and Curran D.R. *Impact Dynamics*. John Wiley & Sons, 1982.

[28]. Abrate, S. "Ballistic impact on composites". *16th International Conference on Composite Materials*, 2008.

[29]. Faik, S. and Witteman, H. "Modelling of impact dynamics: a literature survey". *International ADAMS User Conference*, 2000.

[30]. Navarro, C. "Simplified modelling of the ballistic behaviour of fabrics and fibre-reinforced polymeric matrix composites". *Key Engineering Materials*, Vols. 141-143, 1998, pp. 383-402.

[31]. Navarro, C.; Rodríguez J. and Cortés R. "Analytical modelling of composite panels subjected to impact loading". *Journal de Physique IV. Colloque C8, supplément au Journal de Physique III*, Vol. 4, September 1994.

[32]. Chocron I.S.; Rodríguez J. and Sánchez-Gálvez V. "A simple analytical model for ballistic impact in composites". *Journal de Physique IV. Colloque C3, supplément au Journal de Physique III*, 1997.

[33]. Bless, S.J. and Hartman, D.R. "Ballistic penetration of S-2 glass laminates". *21st International SAMPE Technical Conference*, September 25-28. 1989.

[34]. Caprino, G. and Lopresto, V. "On the penetration energy for fibre-reinforced plastics under low velocity impact conditions". *Composites Science and Technology*, Vol. 61, No. 1, January 2001, pp. 65-73.

[35]. Jacobs, M.J.N. and van Dingenen, J.L.J. "Ballistic protection mechanisms in personal armour". *Journal Materials Science*, Vol. 36, No. 13, 2001, pp. 3137-3142.

[36]. Van Gorp, E.H.M.; van der Loo, L.L.H. and van Dingenen, J.L.J. "A model for HPPE-based lightweight add on armour". *14th International Symposium on Ballistics*, September 26-29. 1993.

[37]. Wen, H.M. "Predicting the penetration and perforation of FRP laminates struck normally by projectiles with different nose shapes". *Composite Structures*, Vol. 49, No. 3, 2000, pp. 321-329.

[38]. Colakoglu, M. "Investigation of the ballistic performance of two different polymer matrix composites". *Key Engineering Materials*, Vols. 348-349, 2007, pp. 241-244.

[39]. Colakoglu, M.; Soykasap, O. and Özek, T. "Experimental and numerical investigations on the ballistic performance of polymer matrix composites used in armor design". *Applied Composite Materials*, Vol. 14, pp. 47-58.

[40]. Colakoglu, M and Soykasap, O. "Ballistic performance of a Kevlar 29 woven fibre composite under varied temperatures". *Mechanics of Composite Materials*, Vol. 46, pp. 35-42.

[41]. Silva, M.A.G.; Cismasiu, C. and Chiorean, C.G. "Numerical simulation of ballistic impact on composite laminates". *International Journal of Impact Engineering*. Vol. 31, 2005, pp. 289-306.

[42]. Silva, M.A.G.; Cismasiu, C. and Chiorean, C.G. "Low Velocity Impact on Laminates Reinforced with Polyethylene and Aramid Fibres".

[43]. ESI Group. "Virtual Performance Solution 2010 - Solver Notes Manual".

[44]. ESI Group. "Virtual Performance Solution 2010 - Explicit Solver Reference Manual".

[45]. ESI Group. "Virtual Performance Solution 2010 - Implicit Solver Reference Manual".

[46]. www.chemyq.com

[47]. Johnson, G.R. and Cook, W.H. "A constitutive model and data for metals subjected to large strains, high strain rates and high temperatures". *In: Proceedings of the 7th international symposium on ballistics*. Hague, Netherlands. 1991.

[48]. Justo, J.M.C.F. "Estudo do Comportamento ao Impacto de Alta Velocidade de Estruturas em Materiais Compósitos". *PhD Thesis*. Universidade do Porto. June 2006.

[49]. Lee, B.L.; Walsh, T.F.; Won, S.T. and Patts, H.M. "Penetration Failure Mechanisms or Armor-Grade Fiber Composites under Impact". *Journal of Composite Materials.* Vol. 35, 2001, pp. 1605-1633.

[50]. Harel, H; Marom, G. and Kenig, S. "Delamination Controlled Ballistic Resistance of Polyethylene/Polyethylene Composite Materials". *Applied Composite Materials.* Vol. 9, 2002, pp. 33-42.

APPENDIX

A1. Project budget

1. **Author:** Alberto Portilla Bullido

2. **Department:** Continuum Mechanics and Structural Analysis

3. **Project description:**

- ***Title:*** Numerical analysis of impact behaviour on aeronautical composite protections
- ***Duration:*** 7 months
- ***Indirect cost rate:*** 20%

4. **Direct cost:**

PERSONAL				
Employee	**Task**	**Hours**	**€ / hour**	**Cost (€)**
Senior engineer	Project tasks planning	4	30	120
	Bibliographic research	6	30	180
	Investigation	8	30	240
	Development of technical notes	10	30	300
	Hours of simulation	14	30	420
Junior engineer	Project tasks planning	2	15	30
	Bibliographic research	54	15	810
	Investigation	112	15	1680
	Material numerical models development	28	15	420
	Validation activities	40	15	600
	Numerical models applications	30	15	450
	Hours of simulation			
	Validation activities	250	15	3750
	Applications	200	15	3000
	Sensitivity studies	200	15	3000
	Development of technical notes	120	15	1800
			TOTAL	16800

EQUIPMENT					
Description	**Cost (€)**	**Percentage of dedication**	**Dedication (months)**	**Depreciation period (months)**	**Input cost (€) ***
CPU computer	450	100	6	60	45
Simulation CPU computer	350	100	6	60	35
Screen	200	100	6	60	20
Keyboard	24	100	6	60	2.40
Mouse	16	100	6	60	1.60
Laptop	500	100	1	60	8.33
				TOTAL	112.33

$$* \frac{A}{B} xCxD$$

A = dedication (months) B = depreciation period (60 months)
C = equipment cost D = percentage of dedication (100%)

SOFTWARE LICENSE			
Software	**License cost (€ / annual)**	**Duration (months)**	**Cost (€)**
Patran	4000	6	2000
PamCrash	5000	6	2500
		TOTAL	4500

OTHER COSTS			
Concept	**Days**	**Unit cost (€)**	**Cost (€)**
Subsistence	115	6	690
		TOTAL	690

5. Cost summary:

CONCEPTS	TOTAL COSTS (€)
Personal	16800
Equipment	112
Software license	4500
Other costs	690
Indirect costs	4420
TOTAL	**26523 Euros**

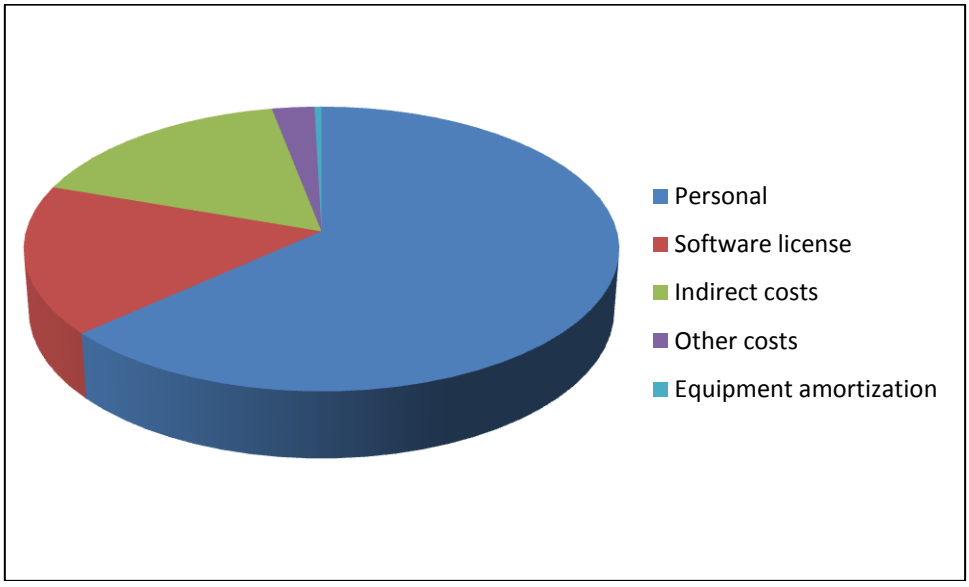

Figure A1.1. *Budget graphic with main costs*

A2. Design of protections with semi-analytical models. Complete calculation

In this appendix, two examples of protection design are shown, one for aramid fibres (data given by Silva *et al.* [41] for Kevlar 29) and other one for polyethylene fibres (data given by Lee *et al.* [49] for Spectra 900). Calculation procedure follows the two main steps:

- **STEP 1.** Constants of materials calculation
- **STEP 2.** Sizing of protection materials

Silva *et al.* [41] performed a series of ballistic test on Kevlar 29 laminates plates made from prepreg fabric impregnated with vynilester resin.

Bless and Hartman model: correction shape factor is equal to 0.86 for FSPs.

$$V_{LP} = \frac{T_{pl}}{D_p}\sqrt{\frac{\pi \cdot \tau_{tr}}{g_c \cdot \rho_{pr}}} \rightarrow 324.3 = \frac{2.4 \cdot 10^{-3}}{5.4 \cdot 10^{-3}}\sqrt{\frac{\pi \cdot \tau_{tr}}{0.86 \cdot 7850}} \rightarrow \tau_{tr} = 1144\ MPa$$

With the values of trough thickness shear stress calculated we can go on. The shape factor is 1 due to the geometry of the impactor is clearly defined.

$$V_{LPLSI} = \frac{T_{pl}}{D_p}\sqrt{\frac{\pi \cdot \tau_{tr}}{g_c \cdot \rho_{pr}}} \rightarrow 585 = \frac{T_{pl}}{14.32}\sqrt{\frac{\pi \cdot 1144 \cdot 10^6}{1 \cdot 7850}} \rightarrow T_{plLSI} = 12.38\ mm$$

$$V_{LPHSI} = \frac{T_{pl}}{D_p}\sqrt{\frac{\pi \cdot \tau_{tr}}{g_c \cdot \rho_{pr}}} \rightarrow 479 = \frac{T_{pl}}{23}\sqrt{\frac{\pi \cdot 1144 \cdot 10^6}{1 \cdot 8096}} \rightarrow T_{plHSI} = 16.54\ mm$$

$$V_{LPII} = \frac{T_{pl}}{D_p}\sqrt{\frac{\pi \cdot \tau_{tr}}{g_c \cdot \rho_{pr}}} \rightarrow 150 = \frac{T_{pl}}{18}\sqrt{\frac{\pi \cdot 1144 \cdot 10^6}{1 \cdot 917}} \rightarrow T_{plII} = 1.36\ mm$$

Caprino model: an α value of 1.4 is assumed. The kinetic energy absorbed by the plate is 57.84 J (a FSP of 1.1 g travelling at 324.3 m/s).

$$U_p = K\left(t \cdot V_f \cdot D_t\right)^{\alpha} \rightarrow 57.84 = K(2.4 \cdot 0.85 \cdot 5.4)^{1.4} \rightarrow K = 2.01\ {}^{J}/_{mm^{2\alpha}}$$

Once we have determined the constant value of the materials, we can define a specific shield thickness to stop the giving impactors.

$$U_{pLSI} = K\left(t \cdot V_f \cdot D_t\right)^{\alpha} \rightarrow 1437 = 2.01(t \cdot 0.85 \cdot 14.32)^{1.4} \rightarrow t = 9\ mm$$

$$U_{pHSI} = K\left(t \cdot V_f \cdot D_t\right)^{\alpha} \rightarrow 8489 = 2.01(t \cdot 0.85 \cdot 23)^{1.4} \rightarrow t = 19.9\ mm$$

$$U_{pII} = K\left(t \cdot V_f \cdot D_t\right)^{\alpha} \rightarrow 394 = 2.01(t \cdot 0.85 \cdot 18)^{1.4} \rightarrow t = 2.84\ mm$$

Jacobs and Van Dingenen model:

i). Calculate C considering non deformable projectiles. In this case deformation energy is equal to zero.

$$S(strike\ face\ area) = \pi R^2 = \pi\left(\frac{5.4}{2}\right)^2 = 22.90\ mm^2$$

$$E_{abs} = S \times AD \times C \ \rightarrow\ C = \frac{E_p}{S \cdot AD} = \frac{57.84}{22.90 \cdot 3.36} = 0.75$$

ii). Apply the analytical model in each specific case, but considering deforming bullets. The values of factors and deformation energy are taken from data of Jacobs and Van Dingenen paper [35].

Low size metallic impactor: deformation energy is 250 J and the factors are

- $f_{s1} = 1$
- $f_{s2} = 4$
- $f_{AD1} = 0.45$
- $f_{AD2} = 0.55$

$$E_{pLSI} = E_{abs1} + E_{absB} + E_{abs2}$$

$$AD_{LSI} = \frac{E_p - E_{absB}}{S \cdot C \cdot (f_{s1}f_{AD1} + f_{s2}f_{AD2})} = \frac{1437 - 250}{161 \cdot 0.75 \cdot (2.65)} = 3.7\ {}^{kg}/_{m^2}$$

High size metallic impactor: deformation energy is 350 J and the factors are

- $f_{s1} = 1$
- $f_{s2} = 4$
- $f_{AD1} = 0.45$
- $f_{AD2} = 0.55$

$$E_{pHSI} = E_{abs1} + E_{absB} + E_{abs2}$$

$$AD_{HSI} = \frac{E_p - E_{absB}}{S \cdot C \cdot (f_{s1}f_{AD1} + f_{s2}f_{AD2})} = \frac{8489 - 350}{415 \cdot 0.75 \cdot (2.65)} = 9.87\ {}^{kg}/_{m^2}$$

Ice impactor: deformation energy is 100 J and the factors are

- $f_{s1} = 1$
- $f_{s2} = 1.5$
- $f_{AD1} = 0.75$
- $f_{AD2} = 0.25$

$$E_{pSI} = E_{abs1} + E_{absB} + E_{abs2}$$

$$AD_{II} = \frac{E_p - E_{absB}}{S \cdot C \cdot (f_{s1}f_{AD1} + f_{s2}f_{AD2})} = \frac{394 - 100}{254 \cdot 0.75 \cdot (1.125)} = 1.38\ {}^{kg}/_{m^2}$$

Van Gorp model: the same constant calculated in Jacobs and Van Dingenen model is used.

$$AD_{SI} = \frac{E_p}{S \cdot C_m} = \frac{1437}{161 \cdot 0.75} = 11.9 \ {}^{kg}/_{m^2}$$

$$AD_{BI} = \frac{E_p}{S \cdot C_m} = \frac{8489}{415 \cdot 0.75} = 27.3 \ {}^{kg}/_{m^2}$$

$$AD_{II} = \frac{E_p}{S \cdot C_m} = \frac{394}{254 \cdot 0.75} = 2.1 \ {}^{kg}/_{m^2}$$

Wen model:

i). To calculate elastic limit of composite in trough-thickness compression, we use the equation for conical nosed projectiles. In this case the FSP is not perfectly conical nosed but we can do an approximation. There is a formulation for truncated-cone-nose projectiles [37] (better formulation for FSP geometry) but it is much more complicated and the analytical expression has two unknown variables (resistive pressure in flat and in cone parts) instead only one unknown variable as in the case of conical nosed projectiles. Hence an approximation for conical nosed projectiles is done:

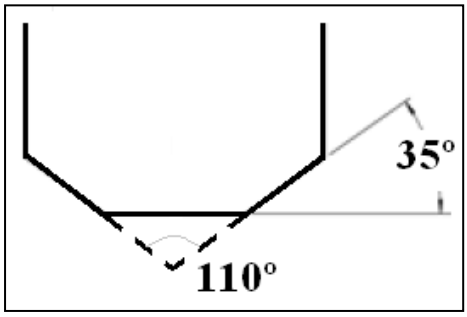

If the FSP were considered as a perfect conical nosed projectile the cone angle was 110º, and if it were considered as a flat faced projectile the angle was 180º. So simplifying, a conical nosed projectile is considered with a cone angle of 125º approximately.

$$\beta = 2\sin({}^{\theta}/_{2}) = 2\sin({}^{125^\circ}/_{2}) = 1.77$$

$$V_b = \frac{\pi\beta\sqrt{\rho_t\sigma_e}D^2T}{4G}\left[1 + \sqrt{1 + \frac{8G}{\pi\beta^2\rho_t D^2 T}}\right] \rightarrow$$

$$\rightarrow 324.3 = \frac{\pi \cdot 1.77\sqrt{1400 \cdot \sigma_e}(5.4)^2(2.4)}{4 \cdot 1.1}\left[1 + \sqrt{1 + \frac{8 \cdot 1.1}{\pi \cdot (1.77)^2 \cdot 1400 \cdot (5.4)^2(2.4)}}\right]$$

$$\rightarrow \sigma_e = 548 \ MPa$$

ii). Now to determine the protection against giving impactors it is necessary to use the equation for flat-faced projectiles, due to impactors are all of them flat-faced.

Low size metallic impactor

$$V_b = \frac{\pi\sqrt{\rho_t \sigma_e} D^2 T}{2G}\left[1 + \sqrt{1 + \frac{2G}{\pi \rho_t D^2 T}}\right] \rightarrow$$

$$\rightarrow 585 = \frac{\pi\sqrt{1400 \cdot \sigma_e} \cdot (14.32)^2 \cdot T}{2 \cdot 8.4}\left[1 + \sqrt{1 + \frac{2 \cdot 8.4}{\pi \cdot 1400 \cdot (14.32)^2 \cdot T}}\right] \rightarrow$$

$$\rightarrow T_{LSI} = 5.68\ mm$$

High size metallic impactor

$$V_b = \frac{\pi\sqrt{\rho_t \sigma_e} D^2 T}{2G}\left[1 + \sqrt{1 + \frac{2G}{\pi \rho_t D^2 T}}\right] \rightarrow$$

$$\rightarrow 479 = \frac{\pi\sqrt{1400 \cdot \sigma_e} \cdot (23)^2 \cdot T}{2 \cdot 74}\left[1 + \sqrt{1 + \frac{2 \cdot 74}{\pi \cdot 1400 \cdot (23)^2 \cdot T}}\right] \rightarrow$$

$$\rightarrow T_{HSI} = 14.73\ mm$$

Ice impactor

$$V_b = \frac{\pi\sqrt{\rho_t \sigma_e} D^2 T}{2G}\left[1 + \sqrt{1 + \frac{2G}{\pi \rho_t D^2 T}}\right] \rightarrow$$

$$\rightarrow 150 = \frac{\pi\sqrt{1023 \cdot \sigma_e} \cdot (18)^2 \cdot T}{2 \cdot 35}\left[1 + \sqrt{1 + \frac{2 \cdot 35}{\pi \cdot 1023 \cdot (18)^2 \cdot T}}\right] \rightarrow$$

$$\rightarrow T_{II} = 1.91\ mm$$

Lee *et al.* [49] study the penetration failure mechanisms of armour fibre composites. The study utilized material systems based on the plain-weave fabric of Spectra 900 oriented polyethylene.

Bless and Hartman model: correction shape factor is equal to 0.86 for FSPs.

$$V_{LPVE} = \frac{T_{pl}}{D_p}\sqrt{\frac{\pi \cdot \tau_{trVE}}{g_c \cdot \rho_{pr}}} \rightarrow 234 = \frac{1.5 \cdot 10^{-3}}{5.6 \cdot 10^{-3}}\sqrt{\frac{\pi \cdot \tau_{trVE}}{0.86 \cdot 7850}} \rightarrow \tau_{trVE} = 1.64\ GPa$$

$$V_{LPPU} = \frac{T_{pl}}{D_p}\sqrt{\frac{\pi \cdot \tau_{trPU}}{g_c \cdot \rho_{pr}}} \rightarrow 217 = \frac{1.5 \cdot 10^{-3}}{5.6 \cdot 10^{-3}}\sqrt{\frac{\pi \cdot \tau_{trPU}}{0.86 \cdot 7850}} \rightarrow \tau_{trPU} = 1.41\ GPa$$

With the values of trough thickness shear stress calculated we can go on. The shape factor is 1 due to the geometry of the impactor is clearly defined.

$$V_{LPLSI} = \frac{T_{pl}}{D_p}\sqrt{\frac{\pi \cdot \tau_{trVE}}{g_c \cdot \rho_{pr}}} \rightarrow 585 = \frac{T_{pl}}{14.32}\sqrt{\frac{\pi \cdot 1.64 \cdot 10^9}{1 \cdot 7850}} \rightarrow T_{plLSI} = 10.34\ mm$$

$$V_{LPLSI} = \frac{T_{pl}}{D_p}\sqrt{\frac{\pi \cdot \tau_{trPU}}{g_c \cdot \rho_{pr}}} \rightarrow 585 = \frac{T_{pl}}{14.32}\sqrt{\frac{\pi \cdot 1.41 \cdot 10^9}{1 \cdot 7850}} \rightarrow T_{plLSI} = 11.15\ mm$$

$$V_{LPHSI} = \frac{T_{pl}}{D_p}\sqrt{\frac{\pi \cdot \tau_{trVE}}{g_c \cdot \rho_{pr}}} \rightarrow 479 = \frac{T_{pl}}{23}\sqrt{\frac{\pi \cdot 1.64 \cdot 10^9}{1 \cdot 8096}} \rightarrow T_{plHSI} = 13.81\ mm$$

$$V_{LPHSI} = \frac{T_{pl}}{D_p}\sqrt{\frac{\pi \cdot \tau_{trPU}}{g_c \cdot \rho_{pr}}} \rightarrow 479 = \frac{T_{pl}}{23}\sqrt{\frac{\pi \cdot 1.41 \cdot 10^9}{1 \cdot 8096}} \rightarrow T_{plHSI} = 14.89\ mm$$

$$V_{LPII} = \frac{T_{pl}}{D_p}\sqrt{\frac{\pi \cdot \tau_{trVE}}{g_c \cdot \rho_{pr}}} \rightarrow 150 = \frac{T_{pl}}{18}\sqrt{\frac{\pi \cdot 1.64 \cdot 10^9}{1 \cdot 917}} \rightarrow T_{plII} = 1.14\ mm$$

$$V_{LPII} = \frac{T_{pl}}{D_p}\sqrt{\frac{\pi \cdot \tau_{trPU}}{g_c \cdot \rho_{pr}}} \rightarrow 150 = \frac{T_{pl}}{18}\sqrt{\frac{\pi \cdot 1.41 \cdot 10^9}{1 \cdot 917}} \rightarrow T_{plII} = 1.23\ mm$$

Caprino model: an α value of 1.4 is assumed

$$U_{pVE} = K\left(t \cdot V_f \cdot D_t\right)^{\alpha} \rightarrow 30.07 = K_{VE}(1.5 \cdot 0.75 \cdot 5.6)^{1.4} \rightarrow K_{VE} = 2.28\ {}^{J}/_{mm^{2\alpha}}$$

$$U_{pPU} = K\left(t \cdot V_f \cdot D_t\right)^{\alpha} \rightarrow 25.95 = K_{PU}(1.5 \cdot 0.75 \cdot 5.6)^{1.4} \rightarrow K_{PU} = 1.98\ {}^{J}/_{mm^{2\alpha}}$$

Once we have determined the constant value of the materials, we are able to define a specific shield to stop the giving impactors.

$$U_{pLSI} = K_{VE}\left(t \cdot V_f \cdot D_t\right)^{\alpha} \rightarrow 1437 = 2.28(t \cdot 0.75 \cdot 14.32)^{1.4} \rightarrow t_{LSI} = 9.31\ mm$$
$$U_{pLSI} = K_{PU}\left(t \cdot V_f \cdot D_t\right)^{\alpha} \rightarrow 1437 = 1.98(t \cdot 0.75 \cdot 14.32)^{1.4} \rightarrow t_{LSI} = 10.29\ mm$$

$$U_{pHSI} = K_{VE}\left(t \cdot V_f \cdot D_t\right)^{\alpha} \rightarrow 8489 = 2.28(t \cdot 0.75 \cdot 23)^{1.4} \rightarrow t_{HSI} = 20.60\ mm$$
$$U_{pHSI} = K_{PU}\left(t \cdot V_f \cdot D_t\right)^{\alpha} \rightarrow 8489 = 1.98(t \cdot 0.75 \cdot 23)^{1.4} \rightarrow t_{HSI} = 22.78\ mm$$

$$U_{pII} = K_{VE}\left(t \cdot V_f \cdot D_t\right)^{\alpha} \rightarrow 394 = 2.28(t \cdot 0.75 \cdot 18)^{1.4} \rightarrow t_{II} = 2.94\ mm$$
$$U_{pII} = K_{PU}\left(t \cdot V_f \cdot D_t\right)^{\alpha} \rightarrow 394 = 1.98(t \cdot 0.75 \cdot 18)^{1.4} \rightarrow t_{II} = 3.25\ mm$$

Jacobs and Van Dingenen model:

i). Calculate C considering non deformable FSPs. In this case deformation energy is equal to zero.

$$S(strike\ face\ area) = \pi R^2 = \pi\left(\frac{5.6}{2}\right)^2 = 24.63\ mm^2$$

$$E_{abs} = S \times AD \times C$$

$$C_{VE} = \frac{E_p}{S \cdot AD} = \frac{30.07}{24.63 \cdot 1.53} = 0.8$$
$$C_{PU} = \frac{E_p}{S \cdot AD} = \frac{25.95}{24.63 \cdot 1.53} = 0.7$$

ii). Apply in specific case, but with penetration by deforming bullets.

Low size metallic impactor: deformation energy is 250 J and the factors are

- $f_{s1} = 1$
- $f_{s2} = 4$
- $f_{AD1} = 0.45$
- $f_{AD2} = 0.55$

$$E_{pLSI} = E_{abs1} + E_{absB} + E_{abs2}$$

$$AD_{VELSI} = \frac{E_p - E_{absB}}{S \cdot C_{VE} \cdot (f_{s1}f_{AD1} + f_{s2}f_{AD2})} = \frac{1437 - 250}{161 \cdot 0.8 \cdot (2.65)} = 3.47\ {}^{kg}/_{m^2}$$
$$AD_{PULSI} = \frac{E_p - E_{absB}}{S \cdot C_{PU} \cdot (f_{s1}f_{AD1} + f_{s2}f_{AD2})} = \frac{1437 - 250}{161 \cdot 0.7 \cdot (2.65)} = 3.97\ {}^{kg}/_{m^2}$$

High size metallic impactor: deformation energy is 350 J and the factors are

- $f_{s1} = 1$
- $f_{AD1} = 0.45$
- $f_{s2} = 4$
- $f_{AD2} = 0.55$

$$E_{pHSI} = E_{abs1} + E_{absB} + E_{abs2}$$

$$AD_{VEHSI} = \frac{E_p - E_{absB}}{S \cdot C_{VE} \cdot (f_{s1}f_{AD1} + f_{s2}f_{AD2})} = \frac{8489 - 350}{415 \cdot 0.8 \cdot (2.65)} = 9.25 \ {}^{kg}/_{m^2}$$

$$AD_{PUHSI} = \frac{E_p - E_{absB}}{S \cdot C_{PU} \cdot (f_{s1}f_{AD1} + f_{s2}f_{AD2})} = \frac{8489 - 350}{415 \cdot 0.7 \cdot (2.65)} = 10.57 \ {}^{kg}/_{m^2}$$

Ice impactor: deformation energy is 100 J and the factors are

- $f_{s1} = 1$
- $f_{AD1} = 0.75$
- $f_{s2} = 1.5$
- $f_{AD2} = 0.25$

$$E_{pII} = E_{abs1} + E_{absB} + E_{abs2}$$

$$AD_{VEII} = \frac{E_p - E_{absB}}{S \cdot C_{VE} \cdot (f_{s1}f_{AD1} + f_{s2}f_{AD2})} = \frac{394 - 100}{254 \cdot 0.8 \cdot (1.125)} = 1.29 \ {}^{kg}/_{m^2}$$

$$AD_{PUII} = \frac{E_p - E_{absB}}{S \cdot C_{PU} \cdot (f_{s1}f_{AD1} + f_{s2}f_{AD2})} = \frac{394 - 100}{254 \cdot 0.7 \cdot (1.125)} = 1.47 \ {}^{kg}/_{m^2}$$

Van Gorp model: the same constants calculated in Jacobs and Van Dingenen model are used (0.8 with matrix of vynilester and 0.7 with matrix of polyurethane)

$$AD_{VELSI} = \frac{E_p}{S \cdot C_{mVE}} = \frac{1437}{161 \cdot 0.8} = 11.17 \ {}^{kg}/_{m^2}$$

$$AD_{PULSI} = \frac{E_p}{S \cdot C_{mPU}} = \frac{1437}{161 \cdot 0.7} = 12.75 \ {}^{kg}/_{m^2}$$

$$AD_{VEHSI} = \frac{E_p}{S \cdot C_{mVE}} = \frac{8489}{415 \cdot 0.8} = 25.57 \ {}^{kg}/_{m^2}$$

$$AD_{PUHSI} = \frac{E_p}{S \cdot C_{mPU}} = \frac{8489}{415 \cdot 0.7} = 29.22 \ {}^{kg}/_{m^2}$$

$$AD_{VEII} = \frac{E_p}{S \cdot C_{mVE}} = \frac{394}{254 \cdot 0.8} = 1.94 \ {}^{kg}/_{m^2}$$

$$AD_{PUII} = \frac{E_p}{S \cdot C_{mPU}} = \frac{394}{254 \cdot 0.7} = 2.22 \ {}^{kg}/_{m^2}$$

Wen model:

i). To calculate elastic limit of composite in trough-thickness compression we use the equation for conical projectiles. In this case the FSP is not perfectly conical nosed but we can do an approximation with cone angle of 125°, therefore:

$$\beta = 2\sin\left({}^{\theta}/_{2}\right) = 2\sin\left({}^{125^\circ}/_{2}\right) = 1.77$$

$$V_{bVE} = \frac{\pi\beta\sqrt{\rho_t\sigma_e}D^2T}{4G}\left[1+\sqrt{1+\frac{8G}{\pi\beta^2\rho_tD^2T}}\right] \rightarrow$$

$$\rightarrow 234 = \frac{\pi\cdot 1.77\sqrt{1023\cdot\sigma_e}(5.6)^2(1.5)}{4\cdot 1.1}\left[1+\sqrt{1+\frac{8\cdot 1.1}{\pi\cdot(1.77)^2\cdot 1023\cdot(15.6)^2\cdot(1.5)}}\right]$$

$$\rightarrow \sigma_{eVE} = 550\ MPa$$

$$V_{bPU} = \frac{\pi\beta\sqrt{\rho_t\sigma_e}D^2T}{4G}\left[1+\sqrt{1+\frac{8G}{\pi\beta^2\rho_tD^2T}}\right] \rightarrow$$

$$\rightarrow 217 = \frac{\pi\cdot 1.77\sqrt{1023\cdot\sigma_e}(5.6)^2(1.5)}{4\cdot 1.1}\left[1+\sqrt{1+\frac{8\cdot 1.1}{\pi\cdot(1.77)^2\cdot 1023\cdot(15.6)^2\cdot(1.5)}}\right]$$

$$\rightarrow \sigma_{eVPU} = 470\ MPa$$

ii). Now to determine the protection against giving impactors it is necessary to use the equation for flat-faced projectiles, due to impactors are all of them flat-faced.

Low size metallic impactor

$$V_b = \frac{\pi\sqrt{\rho_t\sigma_e}D^2T}{2G}\left[1+\sqrt{1+\frac{2G}{\pi\rho_tD^2T}}\right] \rightarrow$$

$$\rightarrow 585 = \frac{\pi\sqrt{1023\cdot\sigma_e}\cdot(14.32)^2\cdot T}{2\cdot 8.4}\left[1+\sqrt{1+\frac{2\cdot 8.4}{\pi\cdot 1023\cdot(14.32)^2\cdot T}}\right] \rightarrow$$

$$\rightarrow T_{VELSI} = 6.3\ mm$$

$$\rightarrow T_{PULSI} = 7\ mm$$

High size metallic impactor

$$V_b = \frac{\pi\sqrt{\rho_t \sigma_e} D^2 T}{2G}\left[1 + \sqrt{1 + \frac{2G}{\pi \rho_t D^2 T}}\right] \rightarrow$$

$$\rightarrow 479 = \frac{\pi\sqrt{1023 \cdot \sigma_e} \cdot (23)^2 \cdot T}{2 \cdot 74}\left[1 + \sqrt{1 + \frac{2 \cdot 74}{\pi \cdot 1023 \cdot (23)^2 \cdot T}}\right] \rightarrow$$

$$\rightarrow T_{VEHSI} = 16.1\ mm$$

$$\rightarrow T_{PUHSI} = 18\ mm$$

Ice impactor

$$V_b = \frac{\pi\sqrt{\rho_t \sigma_e} D^2 T}{2G}\left[1 + \sqrt{1 + \frac{2G}{\pi \rho_t D^2 T}}\right] \rightarrow$$

$$\rightarrow 150 = \frac{\pi\sqrt{1023 \cdot \sigma_e} \cdot (18)^2 \cdot T}{2 \cdot 35}\left[1 + \sqrt{1 + \frac{2 \cdot 35}{\pi \cdot 1023 \cdot (18)^2 \cdot T}}\right] \rightarrow$$

$$\rightarrow T_{VEII} = 2\ mm$$

$$\rightarrow T_{PUII} = 2.3\ mm$$